INSTITUTE

FOR

COSMIC RAY RESEARCH

THE UNIVERSITY OF TOKYO

ANNUAL REPORT
(APRIL 2014 – MARCH 2015)

5-1-5, Kashiwanoha, Kashiwa, Chiba 277-8582, Japan

Telephone: (81) 4-7136-3102
Facsimile: (81) 4-7136-3115
WWW URL: http://www.icrr.u-tokyo.ac.jp/

TABLE OF CONTENTS

PREFACE

This report summarizes the scientific activities of the Institute for Cosmic Ray Research (ICRR) of the University of Tokyo in the Japanese FY 2014.

ICRR is an inter-university research institute for studies of cosmic rays. The headquarters of ICRR is located in Kashiwa, Chiba prefecture, Japan. In order to promote various cosmic-ray-related studies efficiently, ICRR has three research divisions; Neutrino and Astroparticle division, High Energy Cosmic Ray division, and Astrophysics and Gravity division. ICRR has 3 observatories in Japan; Kamioka Observatory (Kamioka underground, Gifu prefecture), Norikura Observatory (2770 meters above sea level, Mt. Norikura, Gifu prefecture), and Akeno Observatory (Yamanashi prefecture), together with 1 research center; Research Center for Cosmic Neutrinos (Kashiwa, Chiba prefecture). Furthermore, Gravitational Wave Project Office has been established in 2011 in order to construct the KAGRA gravitational wave detector. In addition, there are 2 major experimental facilities outside of Japan. They are located in Utah in USA, and Yangbajing in Tibet, China.

Many researchers from various Japanese institutions as well as those from overseas are involved in the research programs of ICRR. It should be noted that most of the scientific outputs from this institute are the results of the collaborative efforts by many scientists from various institutions. In order to produce outstanding results, it is very important to carry out an experiment by an international collaboration composed of top-level researchers all over the world. Hence, most of the experimental collaborations that ICRR is involved are international ones. For example, the number of collaborators in the Super-Kamiokande experiment is about 120; about a half of them are from abroad (USA, Korea, China, Poland, Spain and Canada).

Many exciting scientific activities of ICRR are described in this report. One of the highlights in FY 2014 is the results from the Telescope Array experiment, which observed an excess of highest energy cosmic rays from a particular direction of the Universe. It should be noted that the Super-Kamiokande and T2K (which uses Super-Kamiokande as the far detector) experiments have been continuously producing impressive results on neutrino oscillation physics. Another highlight is the construction of the KAGRA gravitational wave detector, which intends to detect gravitational waves for the first time and open a new field of "gravitational wave astronomy".

As an inter-university research institute, ICRR is reviewed by the top-level researchers in the field. Furthermore, future projects of ICRR are evaluated by a committee composed of top-level researchers from various nearby fields. The report from the ICRR Future Project Evaluation Committee was released in September 2013. The Committee evaluated various possible future projects of ICRR. Several projects have been recommended highly. Among them, joining the CTA project, which is a global TeV gamma ray astronomy project, has been recommended as the top priority ICRR future project. The review report from the External Review Committee, which was released in May 2013 (please see the 2013 Annual Review), also supported joining CTA. ICRR is going to make every endeavor to realize the CTA project as an important international partner of this project.

We hope that this report is useful for the understanding of the current research activities of ICRR. Finally, we appreciate very much the strong support of our colleagues in this research field, the University of Tokyo and the Japanese Ministry of Education, Culture, Sports, Science and Technology. They are indispensable for the continuing, and exciting scientific outcome of ICRR.

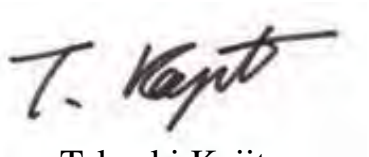

Takaaki Kajita,
Director,
Institute for Cosmic Ray Research,
The University of Tokyo

The ICRR building at Kashiwa, Chiba, Japan.

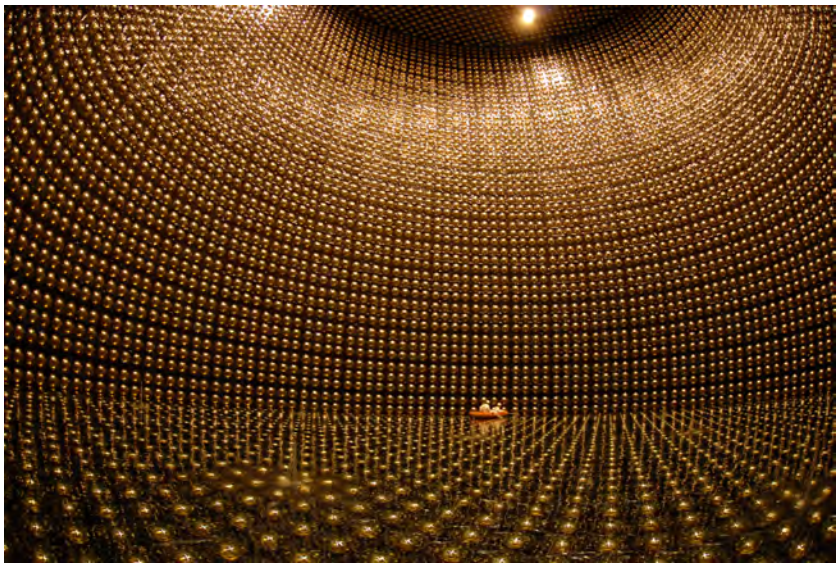

The Super-Kamiokande detector (the photo was taken during pure water fill in 2006).

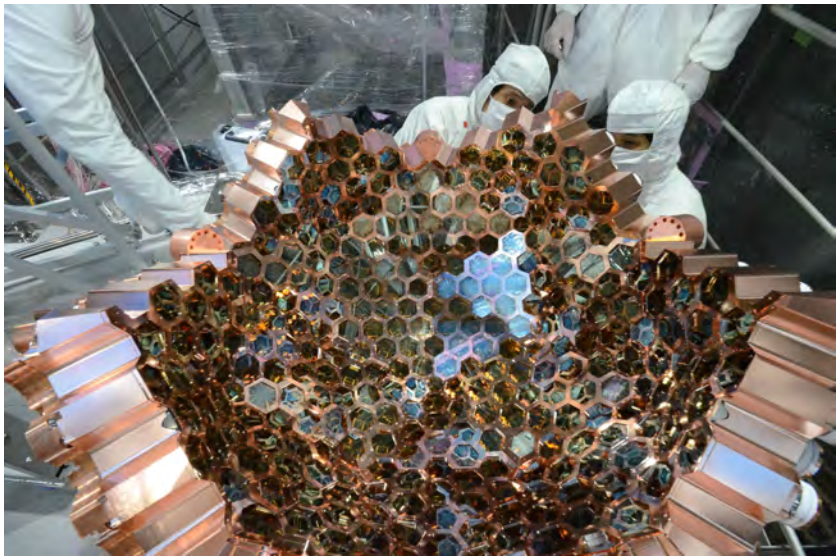

The XMASS detector (the photo was taken during the refurbishment work in 2013).

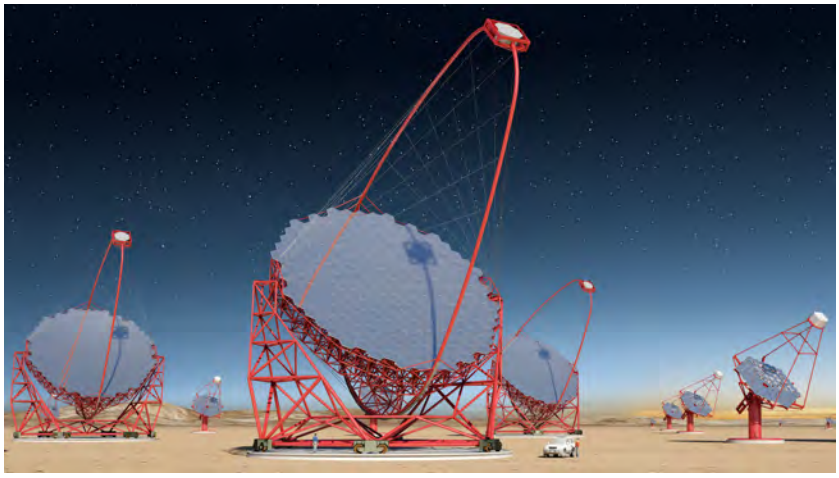

Artist view of the CTA observatory. CTA consists of three types of telescopes, Large Size Telescopes (23m diameter), Mid Size Telescopes (12m) and Small Size Telescopes (4m), and covers the broad energy band from 20GeV to 100TeV.

Tibet-III air shower array (37000 m^2) at Yangbajing, Tibet (4300 m in altitude).

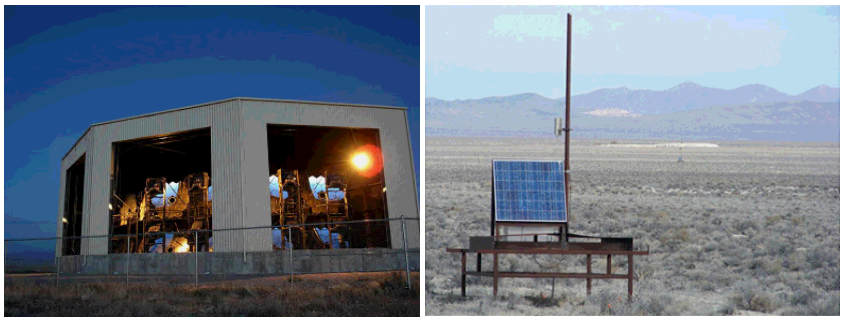

Air fluorescence telescopes (left) and a scintillator surface detector (right) of the Telescope Array experiment in Utah, USA to explore the origin of extremely high energy cosmic rays.

KAGRA X-arm tunnel.

A public lecture held by Research Center for Cosmic Neutrinos.

Organization

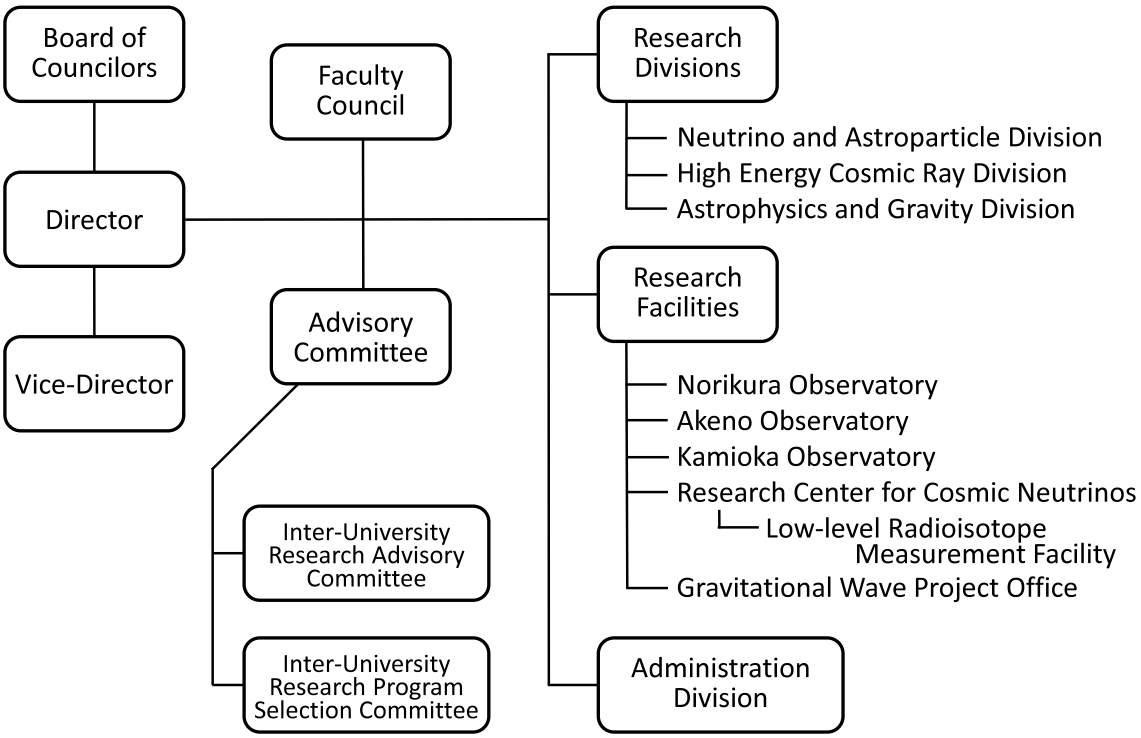

Number of Staff Members (As of May 1, 2014)

	Scientific Staff	Technical Staff	Research Fellows	Administrators and Secretaries	Total
Neutrino and Astroparticle Div.	24	4	1	15	44
High Energy Cosmic Ray Div.	18	11	5	2	36
Astrophysics and Gravity Div.	14	3	5	5	27
Administration	0	0	0	14	14
Total	56	18	11	36	121

FY 2008–2014 Budget

	2008	2009	2010	2011	2012	2013	2014
Personnel expenses	632 000	590 000	576 000	653 000	658 000	687 000	706 000
Non-personnel expenses	1 121 000	1 292 000	1 048 000	1 400 000	1 172 000	1 034 000	1 189 000
Total	1 753 000	1 882 000	1 624 000	2 053 000	1 830 000	1 721 000	1 895 000

(in 1 000 yen)

RESEARCH DIVISIONS

Neutrino and Astroparticle Division

High Energy Cosmic Ray Division

Astrophysics and Gravity Division

NEUTRINO AND ASTROPARTICLE DIVISION

Overview

This division aims to study particle physics with prime interests in physics of neutrinos and proton decay, and astroparticle physics with the use of underground experimental facilities.

Our most important facility is the Super-Kamiokande (SK) detector. It is a 50 kton water Cherenkov detector using 11,129 50 cm-diameter photomultipliers (PMTs) for its inner detector and 1,885 20 cm-diameter PMTs for its outer detector. The data taking of SK started in April 1996. The neutrino oscillations in atmospheric neutrinos were discovered in 1998 and thereby demonstrating that neutrinos have a finite mass. In 2001, the accurate measurements of the ^{8}B solar neutrino flux by SK and SNO discovered that neutrino oscillations are the solution of the solar neutrino problem beyond doubt. After those discoveries, precise measurements of atmospheric neutrinos and solar neutrinos have been performed and they unraveled various phenomena of neutrino oscillations. In the last few years, excess of events induced by ν_τ appearance was observed in atmospheric neutrinos, and the day/night difference of the solar neutrino flux, which is expected from the matter effect of neutrino oscillations, was observed in the precise solar neutrino measurement.

The search for nucleon decay at SK gives the current best limit which strongly constrains the grand unification scenario of particle interactions. SK has been searching for neutrinos from supernovae by two methods, one is a search for burst neutrinos originate from nearby supernovae, another is so-called supernova relic neutrinos, which is an accumulated supernova burst neutrinos from the beginning of the universe.

A high intensity neutrino beam experiment using the J-PARC accelerator (T2K) was started in 2009. The T2K experiment uses the SK detector as the far detector. Electron neutrino appearance (the effect of the mixing angle θ_{13}) and the high precision measurement of oscillation parameters are main physics subjects in T2K. An indication of electron neutrino appearance was found in June 2011, and the significance of the appearance has been greatly improved in 2013. Since 2014, anti-neutrino beam data also has been taken in order to search for CP violation.

Another activity of the Neutrino and Astroparticle division is a multi-purpose experiment using liquid xenon aiming at the detection of cold dark matter, neutrino absolute mass using neutrinoless double beta decay, and low energy solar neutrinos. The construction of a 800 kg liquid xenon detector was completed at the end of 2010 and subsequent commissioning run continued by June 2012. With the commissioning data, low-mass WIMPs, annual modulation of event rate, and axions were studied. Detector refurbishment to reduce the surface background had been performed in 2013 and stable data has been taken in 2014.

In addition to those on-going projects, some R&D projects are also proceeded. GADZOOKS! is a project to add 0.1% of gadolinium into the Super-K tank in order to tag neutrons for $\bar{\nu}_e$ detection. It should enable us to detect supernova relic neutrinos. A feasibility study for GADZOOKS! has been performed using a 200 ton tank which mimics the Super-K detector. The Hyper-Kamiokande (Hyper-K) detector is proposed as a next generation underground water Cherenkov detector. The detector is approximately 20 times larger in volume than Super-K and has discovery potential of leptonic CP violation and proton decays. New photosensor R&D and physics potential studies for Hyper-K has been performed in 2014.

SUPER-KAMIOKANDE

[Project Leader: Masayuki Nakahata]
Kamioka Observatory, ICRR, The University of Tokyo

Search for nucleon decay

Proton decays and bound neutron decays (nucleon decays in general) is the most dramatic prediction of Grand Unified Theories (GUTs) in which three fundamental forces of elementary particles are unified into a single force. Super-Kamio kande (SK) is the world's largest detector to search for nucleon decays. Various nucleon decay modes have been looked for, but we have found no significant signal excess so far. It was pointed out that neutron tagging described in the previous annual report can contribute to reduce atmospheric neutrino background. As a first step, we tried to include it into $p \to e^+\pi^0$ analysis. In addition to them, some of nucleon decay modes which violate baryon and lepton number by two have been newly studied.

A proton decay into one positron and one neutral pion ($p \to e^+\pi^0$) is one of the most popular decay modes. This decay mode is mediated by super-heavy gauge bosons and discovery of the signal would give us the information of the mass of the gauge bosons. To discriminate the signal from the atmospheric neutrino background, we reconstruct the number of particles (Cherenkov rings) and reconstruct the total visible energy corresponding to parent proton mass and total momentum corresponding to the proton's Fermi momentum. The dominant background is charged current single pion productions by atmospheric neutrino interactions. They are often accompanied by neutron in their final state, which are captured by hydrogen and emit 2.2 MeV gamma ray after 200μs. With SK-IV's upgraded electronics it is now possible to record all PMT hit information in the 500μs after an event, and it allows us to identify gamma ray signal from the neutron capture.Originally this technique as been developed to separate neutrino and antineutrino interaction, and it is also

useful for proton decay analysis to reduce background. Details about neutron tag is described in the previous annual report. By applying neutron tagging, we found that background rate could be suppressed from 2.5 events/Megaton·year to 1.4 events/Megaton·year, almost by half. If proton decays in nucleus, nucleon emission could happen when the remaining nucleus is deexcited. The nucleon emission is implemented into proton decay MC based on [1]. As a result, efficiency for $p \to e^+\pi^0$ is reduced by 5%.

Several papers related to nucleon decay search have been published in 2014. $p \to \nu K^+$ is regarded as a dominant decay mode predicted by SUSY-GUTs. In this process, K^+ can not emit Cherenkov light because its momentum is below the Cherenkov threshold. Thus decay products from K^+, $K^+ \to \mu^+\nu, \pi^+\pi^0$, which have characteristic momentum because most of K^+ stop in water, are used for select the events. A 260kt·year exposure of SK has been analyzed and no events have been observed. The lifetime limit for this mode is set to be greater than 5.9×10^{33} year [2].

$n \to \overline{\nu}\pi^0$ and $p \to \overline{\nu}\pi^+$ are motivated by minimal SUSY SO(10) which predicts range of nucleon lifetime as $\tau_{n\to\overline{\nu}\pi^0} = 2\tau_{p\to\overline{\nu}\pi^+} \leq 5.7 - 13 \times 10^{32}$. For $n \to \overline{\nu}\pi^0$, a π^0 can be detected by SK. On the other hand, a π^+ is identified as a μ-like ring in $p \to \overline{\nu}\pi^+$. There are large background from atmospheric ν in single π^0 and single μ-like events, but nucleon decay signals have characteristic momentum. Thus momentum distributions of single π^0 and single μ-like events in 172.8kt·year data are fitted by expected momentum distributions of nucleon decay signal MC and atmospheric ν MC. Data are well described by atmospheric ν MC and lifetime limits with 90% CL are estimated to be 1.1×10^{33} years for $n \to \overline{\nu}\pi^0$ and 3.9×10^{32} years for $p \to \overline{\nu}\pi^+$, respectively, which reject most of predicted range [3]

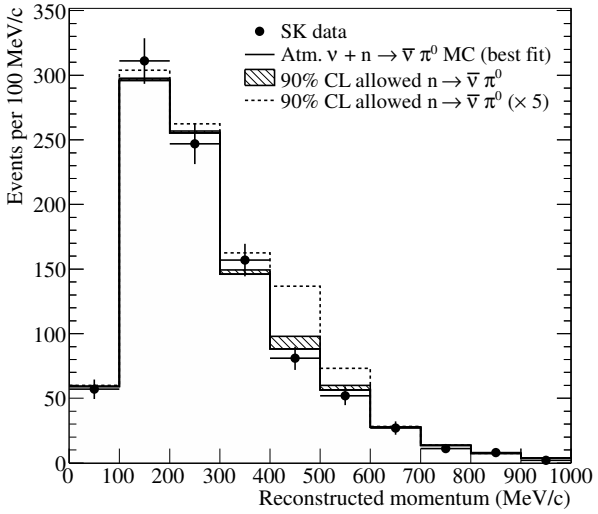

Fig. 1. Reconstructed mometum of single π^0 events of data (blackdots), best fit result of atmospheric neutrino plus $n \to \overline{\nu}\pi^0$ MC (solid line), and 90% C.L. allowed amount of nucleon decay (hatched histogram).

The trilepton nucleon decay modes $p \to e^+\nu\nu$ and $p \to \mu^+\nu\nu$, which are described in the annual report of the last year, violate $|\Delta(B-L)|$ by two units. In the final state, just a e^+-like or μ^+-like ring is detected in these processes, which are suffered from large background comes from atmospheric ν interactions. Momentum distributions of single e-like and μ-like ring from a 273.4kt·year data are fitted by momentum distribution estimated by nucleon decay MC and atmospheric ν MC. There are no excess in data and lower limits on the partial lifetimes of $\tau_{p\to e^+\nu\nu} < 1.7\times10^{32}$ years and $\tau_{p\to\mu^+\nu\nu} < 2.2\times10^{32}$ years are obtained [4].

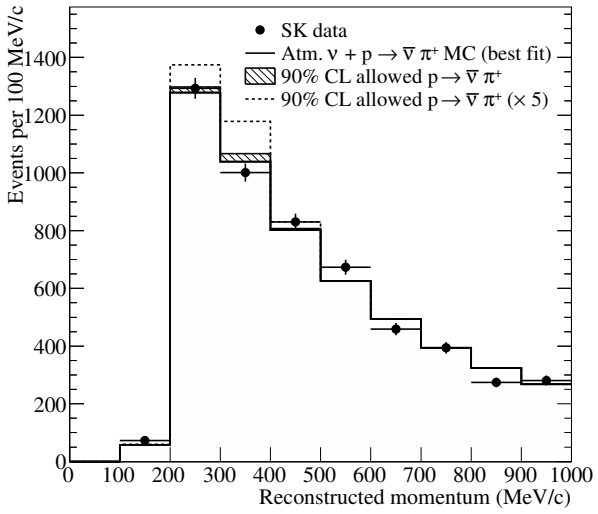

Fig. 2. Reconstructed mometum of single μ events of data (blackdots), best fit result of atmospheric neutrino plus $p \to \overline{\nu}\pi^+$ MC (solid line), and 90% C.L. allowed amount of nucleon decay (hatched histogram).

Dinucleon decay is the name given to the process where the quarks of the two bound nucleons interact to produce a decay. This process could be occurred by the exchange of a heavy particle which is not predicted by the standard model. $pp \to K^+K^+$ provides a sensitive probe of the R-parity-violating parameter λ_{112}". In this process, K^+s can produce Cerenkov rings and they decay with 12 ns lifetime, thus distances between vertices of K^+ decays and K^+s themselves are about 1.3 m. It is assumed in usual event reconstruction that all rings are produced at one vertex. To reconstruct multiple vertex events, vertex of each ring is reconstructed by masking other rings after the usual reconstruction. A boosted decision tree (BDT), which is one of multivariate technique is employed to select candidate events. The most powerfully discriminating BDT input variables are the distance between the reconstructed vertices of the kaon-decay products and the reconstructed momentum of K^+ candidates. In 91.6 kton·year SK-I data, there are no candidate events observed and a lower limit of 1.7×10^{32} years has been placed on the lifetime. A corresponding upper limit on λ_{112}" is estimated to 7.8×10^{-9} [5].

Bibliography

[1] H. Ejiri, Phys. Rev. C **48**, 1442 (1993).

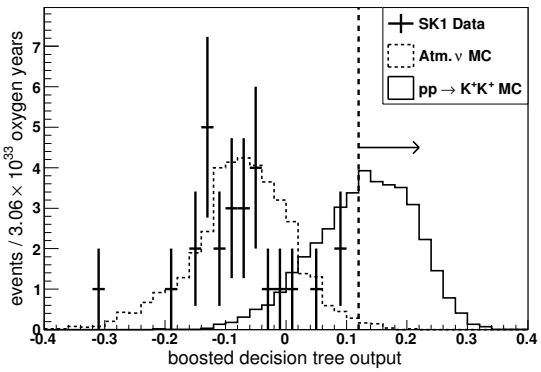

Fig. 3. Final output of the BDT dicision tree. Events to the right of the cut at 0.12 are regarded as signal candidates. All data points are consistent with background and no signal candidates are found in data.

[2] K. Abe *et al.* [Super-Kamiokande Collaboration], Phys. Rev. D **90**, 072005 (2014).

[3] K. Abe *et al.* [Super-Kamiokande Collaboration], Phys. Rev. Lett. **113**, 121802 (2014).

[4] T. Takhistov *et al.* [Super-Kamiokande Collaboration], Phys. Rev. Lett. **113**, 101801 (2014).

[5] M. Litos *et al.* [Super-Kamiokande Collaboration], Phys. Rev. Lett. **113**, 101801 (2014).

Atmospheric neutrinos

Cosmic ray interactions in the atmosphere produce neutrinos via the decay products of secondary hadrons, such as pions and kaons, emerging from these interactions. The atmospheric neutrino flavor ratio, $(\nu_\mu + \bar{\nu}_\mu)/(\nu_e + \bar{\nu}_e)$, is expected to be approximately two based on the structure of the pion decay chain. Though the uncertainty on this ratio is estimated to be only 5 % or less, the absolute scale of the flux for all neutrino species is much less understood and its prediction carries an uncertainty of at least 20 %. It should be noted that despite this uncertainty, above a few GeV where the effects of the geomagnetic field are negligible, the fluxes of upward- and downward-going neutrinos are nearly equal and therefore provide a useful constraint in the study of these neutrinos. Super-Kamiokande has been observing atmospheric neutrinos since 1996 and has accordingly made several important measurements, including the discovery of neutrino oscillations [1, 2].

Three flavor oscillations and the neutrino mass hierarchy

The SK atmospheric neutrino data are described at leading order by two-flavor $\nu_\mu \rightarrow \nu_\tau$ oscillations with maximal mixing (θ_{23}=π/4). However, sub-leading contributions via $\nu_\mu \rightarrow \nu_e$ oscillations induced by the mixing angle θ_{13} as well as the "solar" mixing parameters ($\Delta m^2_{12}, \theta_{12}$) provide the ability to probe currently unknown aspects of the standard neutrino oscillation paradigm, such as the existence of leptonic *CP* violation and the neutrino mass ordering (hierarchy). Understanding these open questions may bring important insight into larger questions, such as the origin and evolution of today's matter-dominated universe.

Several sub-leading oscillation effects are expected to appear in atmospheric neutrinos:

- Resonant enhancement of $\nu_\mu \rightarrow \nu_e$ oscillations due to the effects of matter occur at energies between 2 and 10 GeV and will manifest as an excess of upward-going electron-like events (e-like) in the atmospheric sample.
- This enhancement exists for either ν_e or $\bar{\nu}_e$ depending on the mass hierarchy. Therefore the mass hierarchy can be probed by understanding the relative amount of neutrino and antineutrino interactions in the detector.
- The combination of the solar oscillation parameters and the octant of $\sin^2\theta_{23}$, may enhance or suppress the event rate, and to some extent alter the spectral shape, of Sub-GeV electron-like data the due to $\nu_\mu \leftrightarrow \nu_e$ oscillations they induce.
- The *CP* violating term, δ_{cp}, induces several sub-dominant oscillation effects which are predicted to appear across many of the SK atmospheric neutrino samples.

Super-Kamiokande has studied the effects of these oscillations on atmospheric neutrino data separated into fully-contained (FC) events, partially-contained (PC) events, and upward-going muon topologies. Fully-contained events are characterized by a primary interaction vertex that is located inside the 22.5 kton fiducial volume of the detector and whose visible particles stop within the inner detector. On the other hand, though the primary vertex position of PC events is within the fiducial volume, they are characterized by having at least one charged particle escaping the inner detector and depositing light in the outer detector. In most cases the escaping particle is a muon. Upward-going muons originate from high energy muon-neutrino interactions in the rock surrounding the detector. Since all other particles are lost to interactions in the rock, only the muon is penetrating enough to reach the detector and be identified. The FC sample is separated into electron-like and muon-like (μ-like) subsamples by applying a particle identification algorithm to the most energetic Cherenkov ring of each event. Since PC and upward-going events are predominantly produced by muon neutrinos, no particle identification is applied. Though SK cannot distinguish on an event-by-event basis neutrino and antineutrino interactions, since the effect of the mass hierarchy lies in the difference of their oscillations, statistical separation of multi-GeV electron-like subsamples is performed. A likelihood method designed to enhance the kinematic differences between neutrino and antineutrino interactions is applied to separate the events into ν_e-like and $\bar{\nu}_e$-like subsamples.

The atmospheric neutrino data accumulated during SK-I,-II,-III,and -IV and corresponding to 1489+799+518+1775 days of FC/PC and 1646+828+636+1775 days of upward-going muon data have been analyzed. Zenith angle distributions for six data subsamples are shown in Fig. 4. An oscillation analysis considering all mixing parameters from the PMNS framework, including the *CP* violating term, δ_{cp}, and

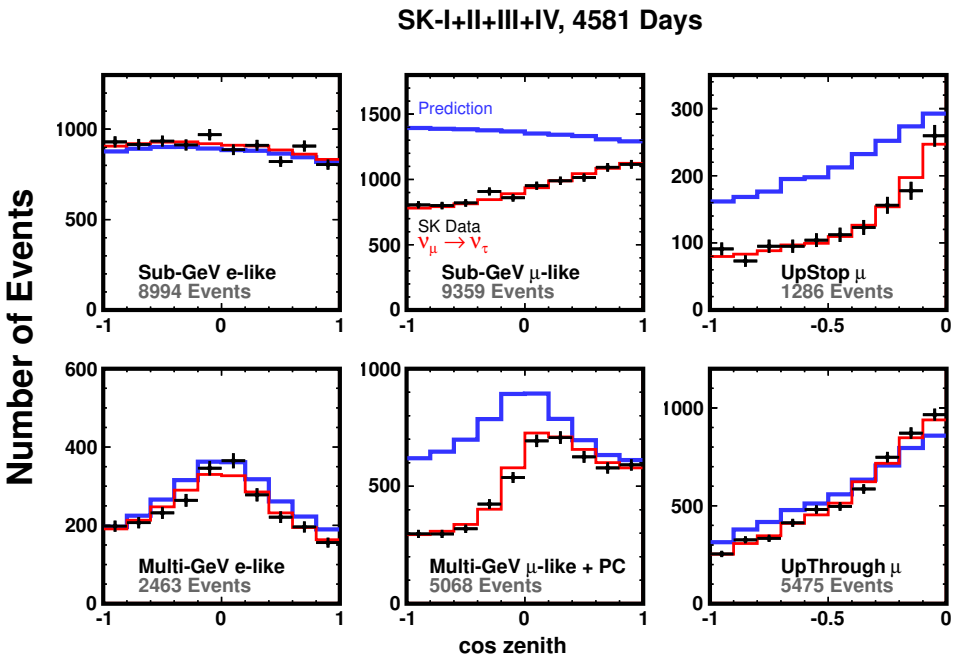

Fig. 4. Zenith angle distributions of SK atmospheric neutrino data. The horizontal axis indicates the cosine of the reconstructed zenith angle ($\cos\theta$ =-1 corresponds to the upward-going direction). The data are shown by the black points with error bars and the MC predictions without oscillations and with two flavor $\nu_\mu \rightarrow \nu_\tau$ oscillations are shown by the blue and red lines, respectively.

the effects of the earth's matter on neutrino propagation, has been performed assuming that θ_{13} is constrained to the measured value from reactor neutrino experiments, $\sin^2\theta_{13}$=0.025. It should be noted, however, that the uncertainty on this measurement is included as a systematic uncertainty in this analysis. Fig. 5 shows the allowed region of the atmospheric mass squared difference (Δm^2_{32}) and θ_{23} parameters obtained from the analysis. Though accelerator experiments such as T2K and MINOS give more stringent constraints, the atmospheric neutrino measurements are consistent with these results. Comparing the minimum absolute χ^2 values between fits to the normal and inverted hierarchy hypotheses indicate that the Super-K data have a weak preference for the normal mass hierarchy, $\Delta\chi^2 = \chi^2_{NH} - \chi^2_{IH}$ = -0.9. In order to improve sensitivity to the mass hierarchy the analysis has been extended to include external constraints from the T2K experiment. T2K is modeled using atmospheric neutrino MC reweighted to the beam spectrum and incorporates publicly available data and systematic error information for the analysis [6, 5]. The modeled T2K data samples are then fit in conjunction with the atmospheric neutrino data including relevant systematic error correlations. In this fit the normal hierarchy preference is strengthened to $\Delta\chi^2 = -1.2$. The best fit oscillation parameters and minimum χ^2 values from these analyses are shown in Table 1. It should be noted that the data show a slight preference for $\delta_{cp} = 220^\circ$ but include $\sin\delta_{cp}$ = 0 at the 90% C.L. in all fits.

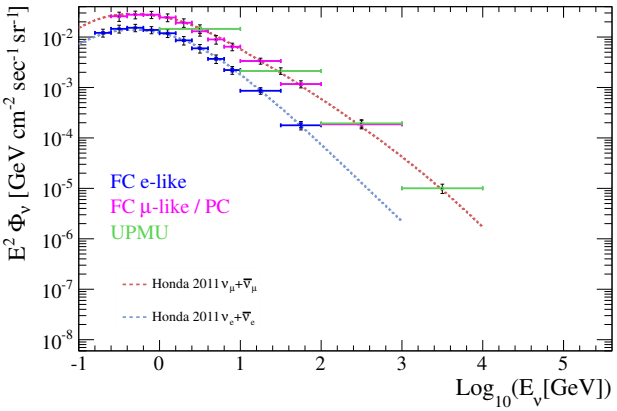

Fig. 6. Super-Kamiokande's measurement of the atmospheric $\nu_e + \bar{\nu}_e$ and $\nu_\mu + \bar{\nu}_\mu$ flux as a function of energy overlaid with model predictions (dashed-lines).

Atmospheric Neutrino Flux Measurement

Measurements of neutrino oscillations like the above and searches for rare processes subject to atmospheric neutrino backgrounds, such a searches for proton decay, are reliant on accurate modeling of the atmospheric neutrino flux. As a result measurements of the flux are a vital tool for establishing the validity of these models. While the computational accuracy and systematic uncertainties present in simulations used to build these flux models have improved dramatically over the last 20 years, atmospheric neutrino flux measurements, particularly at low energies are sparse; The Frejus experiment made the first flux measurements up to 10^4 GeV in 1995 and the cubic-kilometer ice Cherenkov experiments have extended these measurements beyond 10^5 GeV within the last

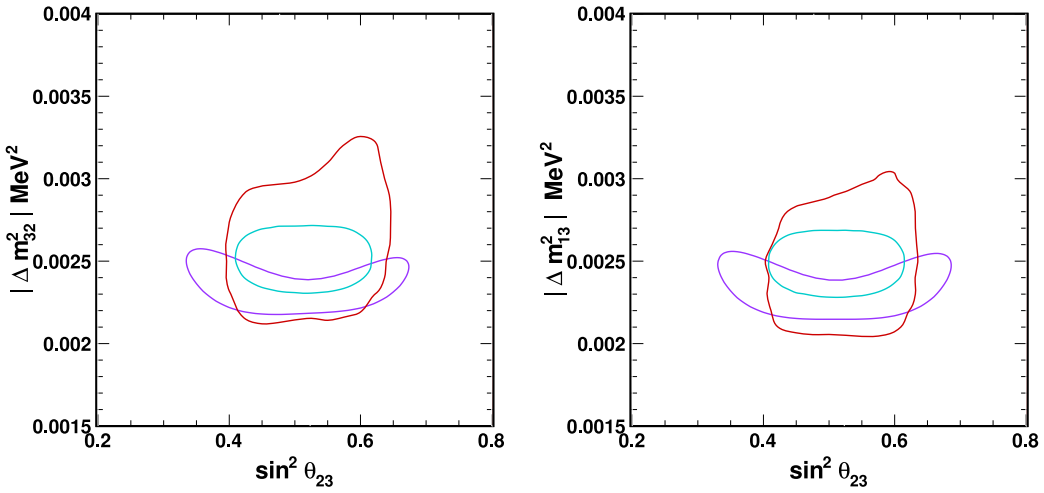

Fig. 5. Allowed regions in the atmospheric mixing plane, $\Delta m^2_{23,31}$ and $\sin^2\theta_{23}$, at the 90% C.L. as measured by Super-Kamiokande atmospheric neutrinos (red), MINOS (purple) [3], and T2K [6] (cyan). Fits to the normal and inverted hierarchy hypotheses are shown in the left and right figures, respectively.

	$\sin^2\theta_{13}$	δ_{CP}	$\sin^2\theta_{23}$	Δm^2_{32} ($\times 10^{-3}$)	χ^2
SK only (NH)	0.025	3.84	0.57	2.6	559.8
SK only (IH)	0.025	3.84	0.57	2.5	560.7
SK+T2K (NH)	0.025	4.19	0.55	2.5	578.2
SK+T2K (IH)	0.025	4.19	0.55	2.5	579.4

Table 1. Best fit oscillation parameters obtained by the three flavor oscillation analysis. Fits are conducted for both the normal (NH) and inverted (IH) hierarchy assumptions for the atmospheric neutrino data ("SK only") and including constraints from the T2K experiment("SK+T2K"). All fits are performed assuming $\sin^2\theta_{13}$=0.025.

five years. With its efficient particle identification and larger size relative to the Frejus experiments, Super-Kamiokande can provide high statistics measurements of both the $\nu_e + \bar{\nu}_e$ and $\nu_\mu + \bar{\nu}_\mu$ flux at energies below 100 GeV, which are inaccessible to current ice Cherenkov detectors, and thereby bridge the gap between existing measurements. The flux measurement at SK is performed using both the FC e-like data, FC μ-like interactions and the PC and upward-going muon data. A Bayesian unfolding technique is used to extract a measurement of the flux as a function of the true neutrino energy based on the reconstructed lepton momentum of the selection data samples. The results are in good agreement with the predictions of modern flux models and are shown in figure 6.

Additionally, the presence of the geomagnetic field enforces a rigidity cutoff on the flux of primary cosmic rays. This cutoff manifests as a suppression of west-going cosmic rays and results in an east-west asymmetry in the flux of these particles, which should also be visible in the atmospheric neutrino flux. At lower energies the effect is expected to be strongest and weaken at higher energies. Though this asymmetry has been previously observed in Super-K's ν_e-dominated e-like samples, it was only seen with marginal significance in the μ-like data. However, in the 15 years since this analysis was performed Super-K has both improved its reconstruction and analysis as well as increased the data sample by a factor of more than six. Figure 7 shows the azimuthal distribution of the FC sub-GeV e-like and μ-like data from a 295 kiloton year exposure of the detector. The azimuthal angle is defined to be the angle measured clockwise from true south to the reconstructed lepton direction. Events reconstructed in the interval 0 to 180 (180 to 360) degrees are defined to west (east)-going. Measurements of the asymmetry of the east-west event rate, $A = (N_{east} - N_{west})/(N_{east} + N_{west})$, yield $A_e = 0.153 \pm (0.015)(\text{stat}) \pm (0.004)(\text{syst})$ for e-like events and $A_\mu = 0.108 \pm (0.014)(\text{stat}) \pm (0.004)(\text{syst})$ for μ-like events. These results indicate a clear observation of an east-west asymmetry with 8σ and 6σ significance, respectively. Note that this is the first confirmation of this effect in the ν_μ flux. Further, it should be pointed out that the data in the figure are in good agreement with the predictions from the flux models.

Search for sterile neutrino

Though the standard three flavor oscillation scheme has been established by a wide range of experiments, there remain "anomalies" which are not consistent in this picture; For example, the LSND experiment observed $\bar{\nu}_e$ appearance over a short baselines, which when interpreted as an oscillation signal suggests a mass difference inconsistent with the results of solar and atmospheric neutrino measurements, $\Delta m^2_s \sim 1\text{eV}^2$ [6]. The MiniBooNE experiment, which was designed to study this anomaly, reported a similar excess of $\bar{\nu}_e$ events [7]. Due to the strong constraint on the number of neutrinos from LEP measurements, the additional neutrino suggested by this

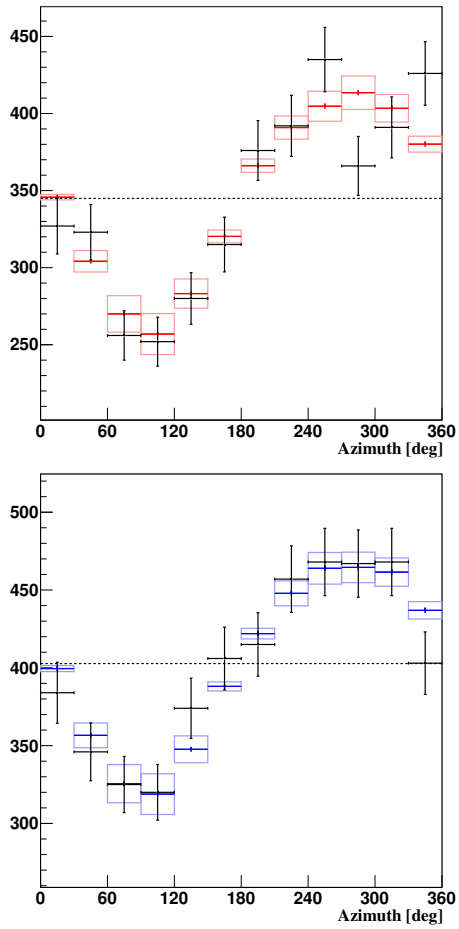

Fig. 7. Azimuthal distributions of e-like (top) and μ-like (bottom) data with reconstructed lepton momentum between 0.4 and 3.0 GeV and reconstructed zenith angle defined by $|cos(\theta)| < 0.6$. The MC prediction with its uncertainty is shown in the colored boxes.

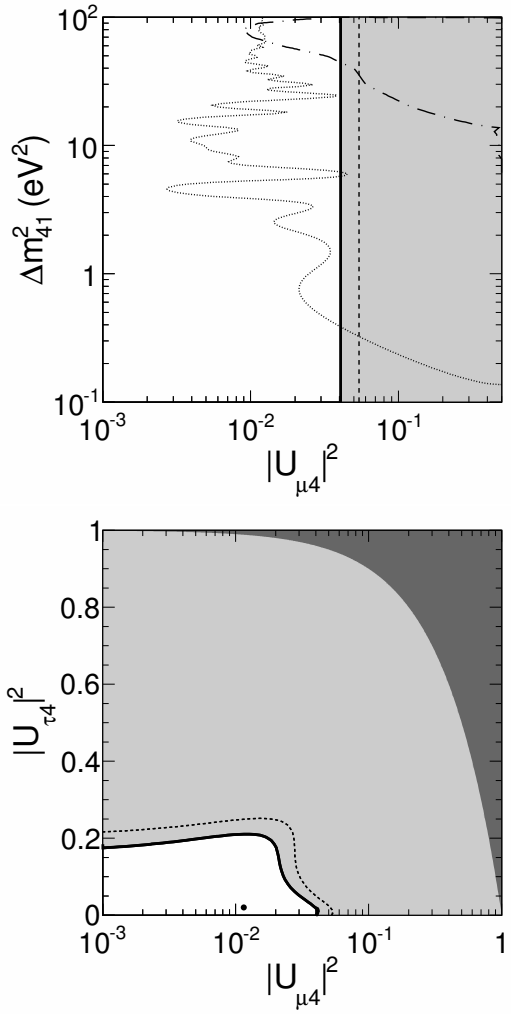

Fig. 8. (Top) Super-Kamiokande's upper limits on $|U_{\mu 4}|^2$ and on $|U_{\mu 4}|^2$ vs $|U_{\tau 4}|^2$ (bottom). The 90% and 95% C.L. limits are shown by the solid and dashed lines, respectively. The light gray region is excluded at 90 % and the dark gray region is disallowed by unitarity.

new mass difference must not participate in weak interactions. These non-interacting neutrinos are therefore called "sterile." If there is indeed a heavy fourth neutrino state, the effects of the extra oscillation channel atop the dominant $\nu_\mu \to \nu_\tau$ oscillations are expected to be visible in the atmospheric neutrino flux.

The atmospheric neutrino data has been fit searching for evidence of these oscillations. However, at large masses atmospheric neutrino oscillations become insensitive to the exact value of the mass splitting and are primarily sensitive to the additional mixing matrix elements between the active and sterile states, $U_{\mu 4}$ and $U_{\tau 4}$. More importantly, the data are insensitive to the precise number of additional sterile neutrinos, a feature unique to atmospheric neutrino studies, so the analysis is performed using a model with only one additional neutrino (the "3+1" model) [9]. The results of two fits, one for $U_{\mu 4}$ with standard matter effects only and one for $U_{\mu 4}$ and $U_{\tau 4}$ including sterile matter effects only, are shown in Fig. 8. Tight constraints on both parameters have been obtained, with $|U_{\mu 4}|^2 < 0.041$ and $|U_{\tau 4}|^2 < 0.18$ at 90% C.L., and a large portion of the allowed region from [9] has been ruled out [14].

Limits on Lorentz invariance violation

Symmetry of physical systems under Lorentz transformations is a fundamental feature of both the Standard Model of particle physics and the General Theory of Relativity. Accordingly, violation of this symmetry, termed Lorentz invariance violation (LIV), would provide striking evidence for new physics and has been the focus of many experiments. Neutrino oscillations are sensitive to two types of LIV phenomena: sidereal effects, in which oscillations are seen to vary as the earth rotates through its sidereal day, and spectral anomalies, which induce oscillation effects whose frequency is proportional to the neutrino pathlength or the product of the neutrino pathlength with its energy. At Super-K LIV is studied within the context of the standard model extension (SME) [12] which introduces a LIV term,H_{LV}, into the standard neutrino Hamiltonian,

$$H = UMU^\dagger + V_e + H_{LV},$$

where U is the PMNS mixing matrix, M is the neutrino mass matrix and V_e is the earth matter potential. Though H_{LV} can have many possible complex coefficients corresponding to higher

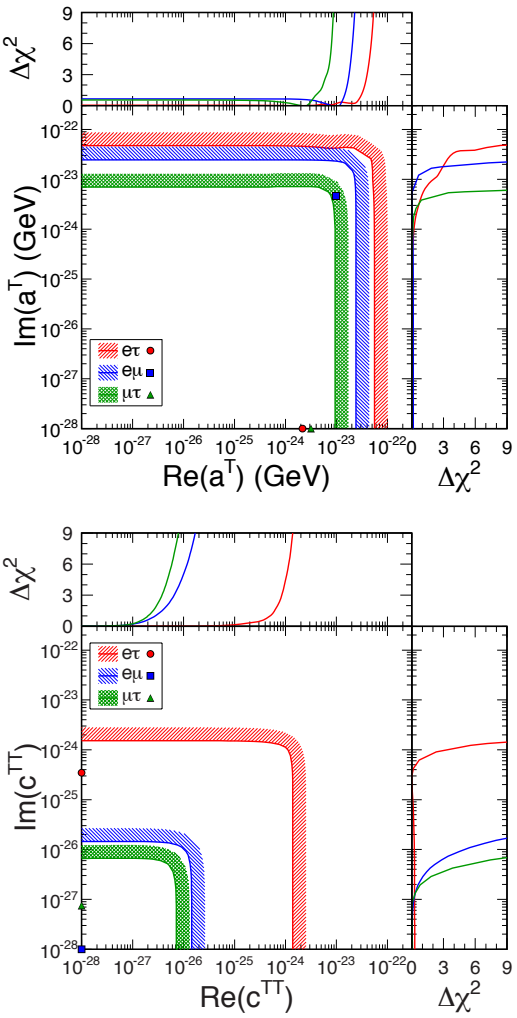

Fig. 9. Contours showing the 95 % confidence level allowed regions for the Lorentz invariance violating parameters $a^T_{e\tau}$ (red), $a^T_{e\mu}$ (blue), $a^T_{\mu\tau}$ (green) appear in the left figure and those for $c^{TT}_{e\tau}$ (red), $c^{TT}_{e\mu}$ (blue), $c^{TT}_{\mu\tau}$ (green) are shown in the right figure. Best fit points from the six fits are also shown.

dimensional LIV operators, the present analysis focuses only on the isotropic dimension-three and dimension-four contributions,

$$H_{LV} = \pm \begin{pmatrix} 0 & a^T_{e\mu} & a^T_{e\tau} \\ (a^T_{e\mu})^* & 0 & a^T_{\mu\tau} \\ (a^T_{e\tau})^* & (a^T_{\mu\tau})^* & 0 \end{pmatrix} - E \begin{pmatrix} 0 & c^{TT}_{e\mu} & c^{TT}_{e\tau} \\ (c^{TT}_{e\mu})^* & 0 & c^{TT}_{\mu\tau} \\ (c^{TT}_{e\tau})^* & (c^{TT}_{\mu\tau})^* & 0 \end{pmatrix}.$$

The diagonal elements of H_{LV} have been neglected since they cannot be observed in neutrino oscillations. Though this matrix represents the neutrino Hamiltonian, antineutrino propagation is described by changing the sign of the first matrix and taking the complex conjugate of the a^T and c^{TT} parameters.

It should be noted that this is the first analysis to approach the problem of LIV in the SME without introducing approximations. Indeed, the usual perturbative conditions introduced to simplify analysis in this framework are invalid for the high energy Super-K atmospheric neutrino data, so the complete neutrino evolution equation has been solved when computing oscillation probabilities. After performing oscillation fits including these effects, no evidence for LIV is seen. As a result, Super-K has set limits on the isotropic parameters a^T and c^{TT} in the $e\mu$, $\mu\tau$, and $e\tau$ sectors as shown in Fig. 9. Despite the lack of a positive signal, the SK constraints on the existence of LIV phenomena in neutrino oscillations improve on existing limits [10] for a^T and c^{TT} by four and seven orders of magnitude, respectively [15].

Indirect WIMP searches

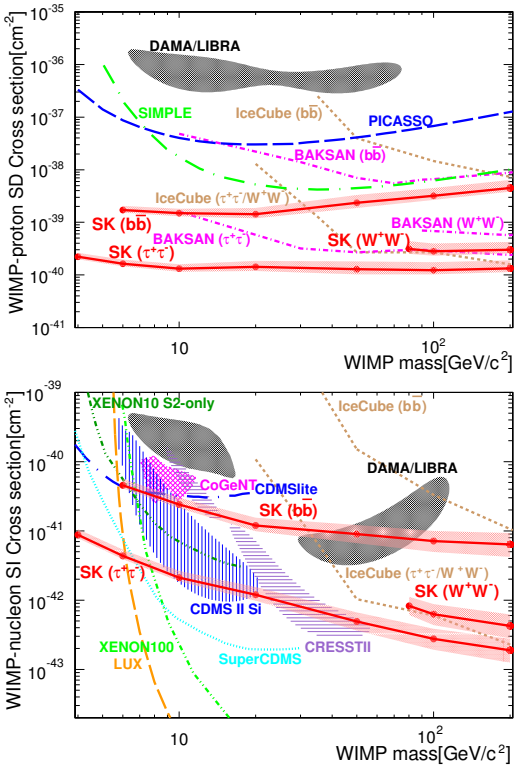

Fig. 10. The 90% C.L. upper limits on the spin-dependent (top) and spin-independent (bottom) WIMP-nucleon scattering cross section based on a search from WIMP-induced neutrinos coming from the direction of the sun are shown as a function of WIMP mass. These limits are calculated assuming WIMP annihilation into $\tau^+\tau^-$, $b\bar{b}$, and W^+W^- each with 100% branching fraction. Limits and allowed regions from other experiments are also shown.

Astronomical and cosmological observations point conclusively to the existence of dark matter and though invisible to electromagnetic probes, it is thought to represent 26% of the matter-energy content of the universe. Weakly Interacting Massive Particles (WIMPs), GeV/c^2-scale particles which have only gravitational and weak interactions, are a favored candidate to explain the existence of this as yet unknown matter. Though direct dark matter detection experiments search for the elastic scattering interactions of these proposed particles with ordinary baryonic matter, it is also possible that WIMPs decay or annihilate into Standard Model particles which can then be detected to give indirect evidence for WIMPs. If WIMPs become trapped in the gravitational potential of a massive system, such as the center of the Milky Way or the sun, their density may become sufficient for large numbers of these particles to annihilate into particles which then decay into neutrinos. In this case the neutrinos pass undeflected

through the universe and would therefore create an additional neutrino signal with a characteristic energy spectrum emerging from a common direction.

At Super-K, though the search for these particles is dominated by the atmospheric neutrino background, the expectation that they are produced at a common location in the sky is a powerful discriminant. Accordingly, the atmospheric neutrino data are binned in both lepton momentum and the reconstructed angle to either the galactic center or to the sun to search for the presence of an extra neutrino signal from those directions. Since there is no knowledge of WIMP interactions, the analysis proceeds by separately assuming annihilation into each of $\nu\bar{\nu}$, $b\bar{b}$, $t\bar{t}$, and W^+W^- with 100% branching fraction. For each assumed WIMP mass the expected neutrino energy distribution emerging from the decay chains of these particles is computed and used to define the signal spectrum at Super-K. In contrast to previous studies, the entire atmospheric neutrino data set is used and therefore gives access WIMP masses in the range of several GeV/c^2 to TeV/c^2. No evidence for a neutrino signal on top of the atmospheric neutrino background has been found in the direction of either the galactic center or the sun. Limits on the WIMP-nucleon spin-dependent and spin-independent scattering cross sections from the search for events from the sun are shown in Fig. 10 [16].

Bibliography

[1] Y. Fukuda *et al.*, "Evidence for Oscillation of Atmospheric Neutrinos", Phys. Rev. Lett. **81** 1562 (1998).

[2] Y. Fukuda *et al.* [Super-Kamiokande Collaboration], Phys. Rev. Lett. **81**, 1562 (1998) [hep-ex/9807003].

[3] P. Adamson *et al.* [MINOS Collaboration], Phys. Rev. Lett. **112**, 191801 (2014) [arXiv:1403.0867 [hep-ex]].

[4] K. Abe *et al.* [T2K Collaboration], Phys. Rev. Lett. **112**, 181801 (2014) [arXiv:1403.1532 [hep-ex]].

[5] K. Abe *et al.* [T2K Collaboration], Phys. Rev. Lett. **112**, 061802 (2014) [arXiv:1311.4750 [hep-ex]].

[6] A. Aguilar-Arevalo et al. (LSND Collaboration), Phys.Rev. **D64**, 112007 (2001), arXiv:hep-ex/0104049 [hep-ex].

[7] A. Aguilar-Arevalo et al. (MiniBooNE Collaboration), Phys.Rev.Lett. **110**, 161801 (2013).

[8] P. Huber, Phys.Rev. **C84**, 024617 (2011), arXiv:1106.0687 [hep-ph].

[9] J. Kopp, P. A. N. Machado, M. Maltoni, and T. Schwetz, JHEP **1305**, 050 (2013).

[10] V. A. Kostelecky, N. Russell and R. Tso, Phys. Lett. B **716**, 470 (2012) [arXiv:1209.0750 [hep-th]].

[11] R. Abbasi *et al.* [IceCube Collaboration], arXiv:1210.3557 [hep-ex].

[12] V. A. Kostelecky, Phys. Rev. D **69**, 105009 (2004) [hep-th/0312310].

[13] D. Cokinos and E. Melkonian, Phys. Rev. C **15**, 1636 (1977).

[14] K. Abe *et al.* [Super-Kamiokande Collaboration], Phys. Rev. D **91**, 052019 (2015) [arXiv:1410.2008 [hep-ex]].

[15] K. Abe *et al.* [Super-Kamiokande Collaboration], Phys. Rev. D **91**, no. 5, 052003 (2015) [arXiv:1410.4267 [hep-ex]].

[16] K. Choi *et al.* [Super-Kamiokande Collaboration], Phys. Rev. Lett. **114**, no. 14, 141301 (2015) [arXiv:1503.04858 [hep-ex]].

Solar Neutrinos

Solar neutrino flux measurements from Super-Kamiokande (SK) [1] and the Sudbury Neutrino Observatory(SNO) [2] have provided direct evidence for solar neutrino flavour conversion. However, there is still no clear evidence that this solar neutrino flavour conversion is indeed due to neutrino oscillations and not caused by any other mechanism. Currently there are two testable signatures unique to neutrino oscillations. The first is the observation and precision test of the MSW resonance curve [3]. Based on oscillation parameters extracted from solar neutrino and reactor anti-neutrino measurements, there is an expected characteristic energy dependence of the flavour conversion. The higher energy solar neutrinos (higher energy ^{8}B and hep neutrinos) undergo complete resonant conversion within the sun, while the flavour changes of the lower energy solar neutrinos (pp, ^{7}Be, pep, CNO and lower energy ^{8}B neutrinos) arise only from vacuum oscillations, which limits the average electron flavour survival probability to exceed 50%. The transition from the matter dominated oscillations within the sun, to the vacuum dominated oscillations, should occur near 3 MeV, making ^{8}B neutrinos the best choice when looking for a transition point within the energy spectrum. A second signature unique to oscillations arises from the effect of the terrestrial matter density on solar neutrino oscillations. This effect is tested directly by comparing solar neutrinos which pass through the Earth at nighttime to those which do not during the daytime. Those neutrinos which pass through the Earth will in general have an enhanced electron neutrino content compared to those which do not, leading to an increase in the nighttime electron elastic scattering rate (or any charged-current interaction rate), and hence a negative "day/night asymmetry". SK detects ^{8}B solar neutrinos over a wide energy range in real time, making it a prime detector to search for both solar neutrino oscillation signatures.

The start of physics data taking of SK-IV occurred on October 6th, 2008, with this report including data taken until January 31st, 2014. The total livetime is 1668.8 days. The entire data period was taken using the same low energy threshold, with about 85% triggering efficiency at 3.5-4.0 MeV kinetic energy, 99% at 4.0-4.5 MeV kinetic energy and 100% above 4.5 MeV kinetic energy. In the case of ν-e interactions of solar neutrinos in SK, the incident neutrino and recoil electron directions are highly correlated. Fig.11 shows the $\cos\theta_{\rm sun}$ distribution for events between 3.5-19.5 MeV. In order to obtain the number of solar neutrino interactions, an extended maximum likelihood fit is used. This method is also used in the

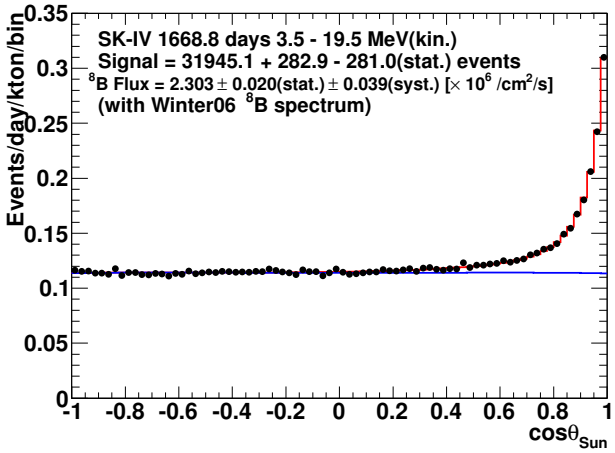

Fig. 11. Solar angle distribution for 3.5-19.5 MeV. $\theta_{\rm sun}$ is the angle between the incoming neutrino direction and the reconstructed recoil electron direction. Black points are data while the blue and red histograms are best fits to the background and signal plus background, respectively.

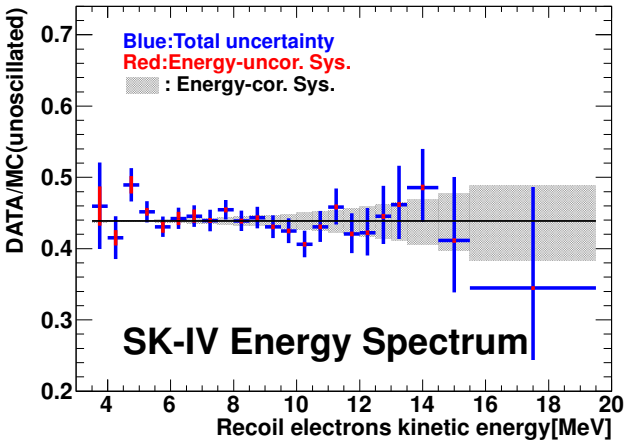

Fig. 12. SK-IV energy spectrum. The horizontal dashed line gives the SK-IV average. Error bars shown are statistical plus energy-uncorrelated systematic uncertainties. Energy-correlated systematic uncertainties are shown separately as shaded region.

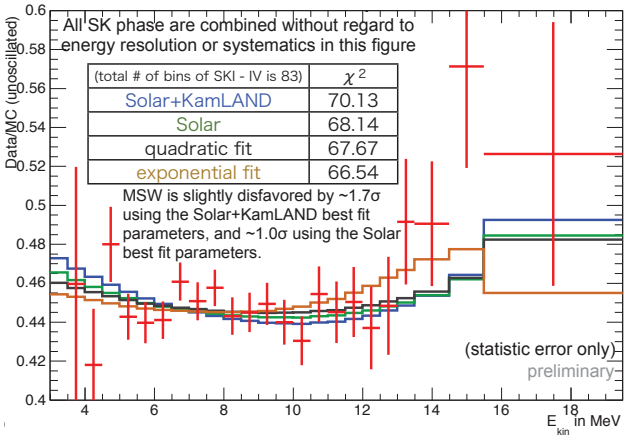

Fig. 13. All SK phase combined energy spectrum and fitted functions.

SK-I [1], II [4], and III [5] analyses. The red line of Fig.11 is the best fit to the data. The blue line shows the background component of that best fit.

The combined systematic uncertainty of the total flux in SK-IV is found to be 1.7% as the quadratic sum of all components. This is the best value seen throughout all phases of SK, much improved over 2.2% in SK-III. The main contributions to the reduction come from improvements in the uncertainties arising from the energy-correlated uncertainties (energy scale and resolution), the vertex shift, trigger efficiency and the angular resolution. SK-III data below 6.0 MeV recoil electron kinetic energy has only about half the livetime as the data above, while SK-IV's livetime is the same for all energy bins. As a consequence, the energy scale and resolution uncertainties lead to a smaller systematic uncertainty of the flux in SK-IV than in SK-III. The higher efficiency of SK-IV between 5.0 and 6.0 MeV (kinetic) of SK-IV and the addition of the 3.5 to 4.5 MeV data lessens the impact of energy scale and resolution uncertainty on the flux determination even further. The number of solar neutrino events (between 3.5 and 19.5 MeV) is $31,945^{+283}_{-281}(\text{stat.}) \pm 543(\text{syst.})$. This number corresponds to a ^{8}B solar neutrino flux of $\Phi_{^8B} = (2.303 \pm 0.020(\text{stat.}) \pm 0.039(\text{syst.})) \times 10^6/(\text{cm}^2\text{sec})$, assuming a pure ν_e flavor content.

Fig.12 shows the resulting SK-IV energy spectrum. SK-IV has $N_{\rm bin} = 23$ energy bins; 20 bins of 0.5 MeV width between 3.5-13.5 MeV, two energy bins of 1 MeV between 13.5 and 15.5 MeV, and one bin between 15.5 and 19.5 MeV.

To test the expected "upturn" below ∼6 MeV from the MSW resonance effects, the best fit oscillation parameters of solar experiments and solar + KamLAND (described later) were fitted to all the SK-I to SK-IV spectra, and it is disfavored by 1σ and 1.7σ respectively so far. Fitted results are shown in Fig.13.

As SK has observed solar neutrinos for 17 years, about 1.5 solar activity cycles to date, an analysis regarding possible correlations between the solar neutrino flux and the 11 year solar activity cycle was conducted. A constant flux was fitted and results are shown in Fig.14. ($\chi^2/\text{dof} = 13.57/17$) Super-K solar rate measurements are fully consistent with a constant solar neutrino flux emitted by the Sun.

The SK-IV livetime during the day (night) is 799.7 days (869.1 days). The solar neutrino flux between 4.5 and 19.5 MeV and assuming no oscillations is measured as $\Phi_D = (2.25 \pm 0.03(\text{stat.}) \pm 0.38(\text{sys.})) \times 10^6/(\text{cm}^2\text{sec})$ during the day and $\Phi_N = (2.36 \pm 0.03(\text{stat.}) \pm 0.40(\text{sys.})) \times 10^6/(\text{cm}^2\text{sec})$ during the night. A more sophisticated method to test the day/night effect is given in [1, 7]. For a given set of oscillation parameters, the interaction rate as a function of the solar zenith angle is predicted. Only the shape of the calculated solar zenith angle variation is used, the amplitude of it is scaled by an arbitrary parameter. The extended maximum likelihood fit to extract the solar neutrino signal is expanded to allow time-varying signals. The likelihood is then evaluated as a function of the average signal rates, the background rates and the scaling parameter which is called the "day/night amplitude". The equivalent day/night asymmetry is calculated by multiplying the fit scaling parameter with the expected day/night asymmetry. In this manner the day/night asymmetry is measured more precisely statistically. Because the amplitude fit depends

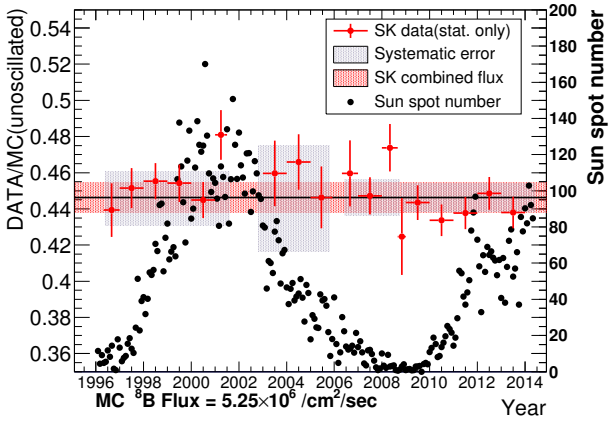

Fig. 14. Flux data from all SK phases as a function of time. Sun spot numbers [6] are also plotted

on the assumed shape of the day/night variation, it necessarily depends on the oscillation parameters, although with very little dependence expected on the mixing angles (in or near the large mixing angle solutions and for θ_{13} values consistent with reactor neutrino measurements [8]).

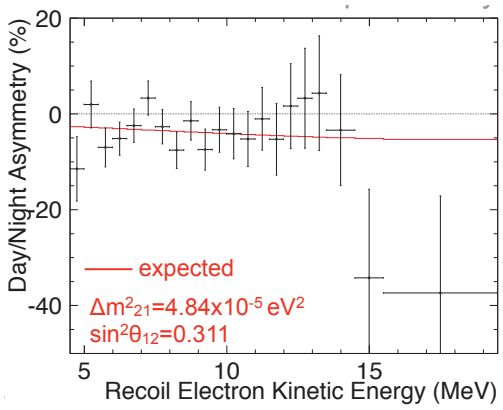

Fig. 15. SK combined energy dependence of the fitted day/night asymmetry (measured day/night amplitude times the expected asymmetry (red)) for $\Delta m^2_{21} = 4.84\times10^{-5}\mathrm{eV}^2$, $\sin^2\theta_{12} = 0.311$ and $\sin^2\theta_{13} = 0.025$. The error bars shown are statistical uncertainties only.

The day/night asymmetry coming from the SK-I to IV combined amplitude fit can be seen as a function of recoil electron kinetic energy in Fig.15, for $\Delta m^2_{21} = 4.84\times10^5\mathrm{eV}^2$, $\sin^2\theta_{12} = 0.311$ and $\sin^2\theta_{13} = 0.025$. The day/night asymmetry in this figure is found by multiplying the fitted day/night amplitude from each energy bin, to the expected day/night asymmetry (red distribution) from the corresponding bin.

Fig.16 shows the Δm^2_{21} dependence of the SK all phases combined day/night asymmetry for $\sin^2\theta_{12} = 0.311$ and $\sin^2\theta_{13} = 0.025$. Here the day/night asymmetry is also found by multiplying the fitted day/night amplitude by the expected day/night asymmetry (red curve). The point where the best fit crosses the expected curve represents the value of Δm^2_{21} where the measured day/night asymmetry is equal to the expectation. Superimposed are the allowed ranges in Δm^2_{21} from the global solar neutrino data fit (green) and from KamLAND (blue).

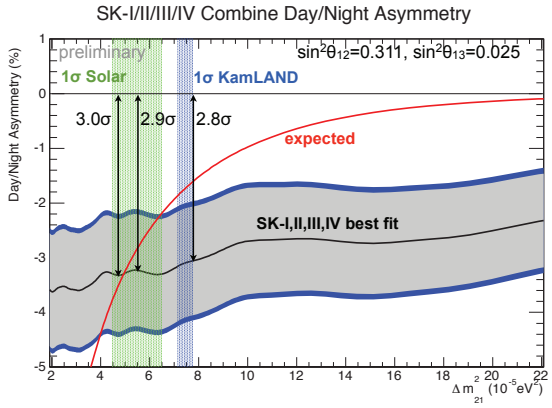

Fig. 16. Dependence of the measured day/night asymmetry (fitted day/night amplitude times the expected day/night asymmetry (red)) on Δm^2_{21} (light gray band=stat. error, dark gray band=stat.+syst. error) for $\sin^2\theta_{12} = 0.311$ and $\sin^2\theta_{13} = 0.025$. Overlaid are the allowed ranges from solar neutrino data (green band) and KamLAND (blue band).

The amplitude fit shows no dependence on the values of θ_{12} (within the LMA region of the MSW plane) or θ_{13}.

We analyzed the SK-IV elastic scattering rate, the recoil electron spectral shape and the day/night variation to constrain the solar neutrino oscillation parameters. We then combined the SK-IV constraints with those of previous SK phases, as well as other solar neutrino experiments. The allowed contours of all solar neutrino data (as well as KamLAND's constraints) are shown in Fig.17 and 18. In Fig.17 the contours from the fit to all solar neutrino data are almost identical to the ones of the SK+SNO combined fit. In the right panel some tension between the solar neutrino and reactor anti-neutrino measurements of the solar Δm^2_{21} is evident. This tension is mostly due to the SK day/night measurement. Even though the expected amplitude agrees well within 1σ with the fitted amplitude for any Δm^2_{21} in either the KamLAND or the SK range, the SK data somewhat favor the shape of the variation predicted by values of Δm^2_{21} that are smaller than KamLAND's. The best fit values are $\sin^2\theta_{12} = 0.308 \pm 0.013$, $\Delta m^2_{21} = 7.50^{+0.19}_{-0.18}\times10^{-5}\mathrm{eV}^2$, and $\sin^2\theta_{13} = 0.027^{+0.016}_{-0.014}$. The significance of non-zero θ_{13} is about 2σ.

In summary, the analysis threshold was successfully lowered to 3.5 MeV kinetic recoil electron energy in SK-IV and by adding SK-IV data, ~70,000 solar neutrino interactions has been observed in ~4,500 days (1.5 solar activity cycles), by far the largest sample of solar neutrino events in the world. It turned out Super-K solar rate measurements are fully consistent with a constant solar neutrino flux emitted by the Sun. SK spectrum results slightly disfavor the MSW resonance curves, but are consistent with MSW prediction within $1 \sim 1.7\sigma$. SK data provide the first indication (at $2.8 \sim 3.0\sigma$) of terrestrial matter effects on ^{8}B solar neutrino oscillation. This is the first observation using a single detector and identical neutrino beams that matter affects neutrino oscillations [9]. These SK measurements strongly constrain neutrino oscillation parameters: SK uniquely selects the Large Mixing Angle MSW region by $> 3\sigma$, gives world's best constraint on Δm^2_{21} using neutrinos, and significantly contributes to the measurement of θ_{12}.

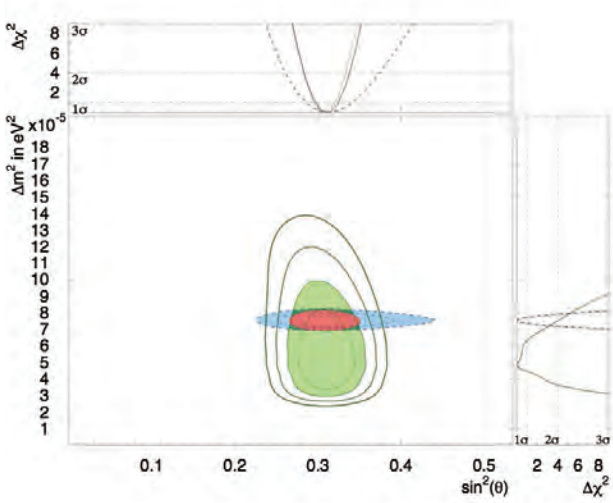

Fig. 17. Allowed contours of Δm^2_{21} vs. $\sin^2\theta_{12}$ from solar neutrino data (green) at 1, 2, 3, 4 and 5 σ and Kam-LAND data (blue) at the 1, 2 and 3 σ confidence levels. Also shown are the combined results in red. For comparison, the almost identical results of the SK+SNO combined fit are shown by the dashed dotted lines. θ_{13} is constrained by $\sin^2\theta_{13} = 0.0242 \pm 0.0026$.

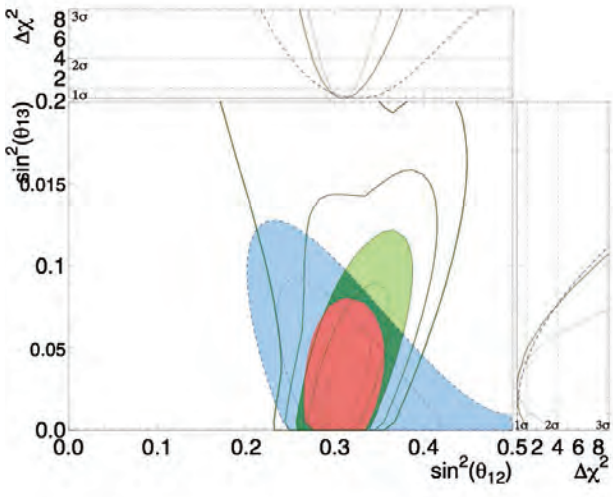

Fig. 18. Allowed contours of $\sin^2\theta_{13}$ vs. $\sin^2\theta_{12}$ from solar neutrino data (green) at 1, 2, 3, 4 and 5 σ and KamLAND measurements (blue) at the 1, 2 and 3 σ confidence levels. Also shown are the combined results in red.

Bibliography

[1] J.Hosaka et al., Phys. Rev. D73, 112001 (2006).

[2] Q.R.Ahmad et al., Phys. Rev. Lett. 87 071301 (2001).

[3] S.P.Mikheyev and A.Y.Smirnov, Sov. Jour. Nucl. Phys. 42, 913 (1985); L.Wolfenstein, Phys. Rev. D17, 2369 (1978).

[4] J.P.Cravens et al., Phys. Rev. D 78, 032002(2008).

[5] K.Abe et al., Phys. Rev. D 83 052010 (2011).

[6] `http://solarscience.msfc.nasa.gov/greenwch/spot_num.txt`

[7] M.B.Smy et al., Phys. Rev. D. 69, 011104(R) (2004).

[8] F.P.An et al., arXiv:1210.6327 (2012); J.K.Ahn et al., Phys.Rev.Lett. 108 191802 (2012); Y.Abe et al.,Phys.Rev. D86 052008 (2012).

[9] A.Renshaw et al., Phys. Rev. Lett. 112, 091805 (2014).

Supernova neutrinos

In 1987, the observation of supernova 1987a by Kamiokande and IMB etc. opened the neutrino astronomy. This observation confirmed that the energy released by neutrinos is about several$\times 10^{53}$ergs. However, the core collapse supernova mechanism is not fully understood yet. Super-Kamiokande would be able to detect several thousand neutrino events if a supernova happened near the center of our galaxy. Such an observation would enable us to investigate in detail the mechanics of the supernova explosion.

A online program called SNWATCH searches for time clustered events. The current criteria of SNWATCH are (1) more than or equal to 7 events within 0.5 sec, (2) more than or equal to 8 events within 2 sec, and (3) more than or equal to 13 events within 10 sec. When at least one of these criteria are met, SNWATCH reconstructs vertex position and energy of the events together with neighboring cosmic ray muons. In most cases, these clusters are due to spallation products whose vertex positions are aligned with their parent cosmic ray muon. Since all the SNWATCH processes are now running on online machines, if a supernova happens, we will be able to detect it within about one minute.

If SNWATCH finds an event cluster whose vertex spread is larger than a given criterion, an alarm signal is sent to experts by e-mail and an automatic call to their cellphones. Then, the experts check whether it is a real supernova signal or not by looking at various plots which are uploaded to a secured site accessible from the Internet. These alarms are usually due to the accidental coincidence of two cosmic ray induced clusters. We have a supernova drill at least once per year. So far, no real supernova neutrino burst signal has been observed at Super-Kamiokande.

In the drill, the SNWATCH conveners and the executive committee members meet via TV conference system, and discuss to make a decision for a prompt announcement to outside researchers and the press. We practice this drill as if a real supernova happened. We also have SK shift training by illuminating an LED in the SK detector a few times every month. SK shift members are notified by a dummy alarm that SNWATCH makes when the LED is illuminated. The shift members then call to the SNWATCH experts and give a report. The SK collaborators will be ready for the real supernovae through the drill and the training.

Not only the supernova burst, signals from Supernova Relic Neutrinos (SRNs) are also searched at SK. The SRN signal is

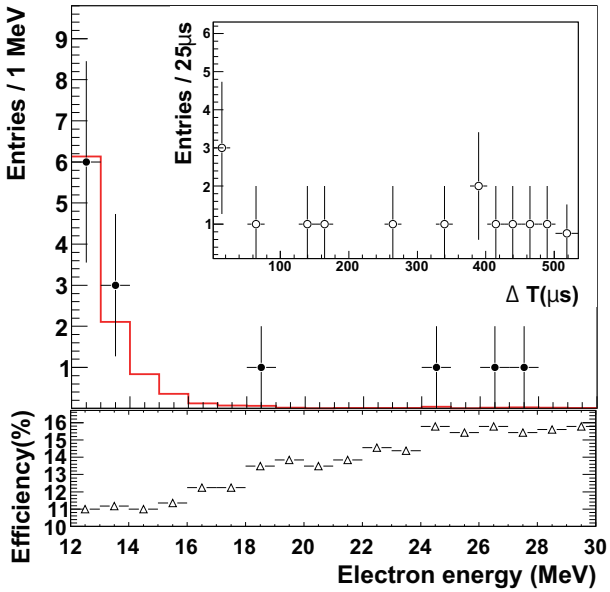

Fig. 19. Energy spectrum of prompt signals (points). The red histogram shows the expected accidental background. The plot embedded in the upper right shows the timing difference for the delayed candidates. The bottom figure shows the detection efficiency of SRN for each energy bin; the jumps at 18 MeV and 24 MeV are due to energy-dependent spallation cuts. Errors are statistical only.

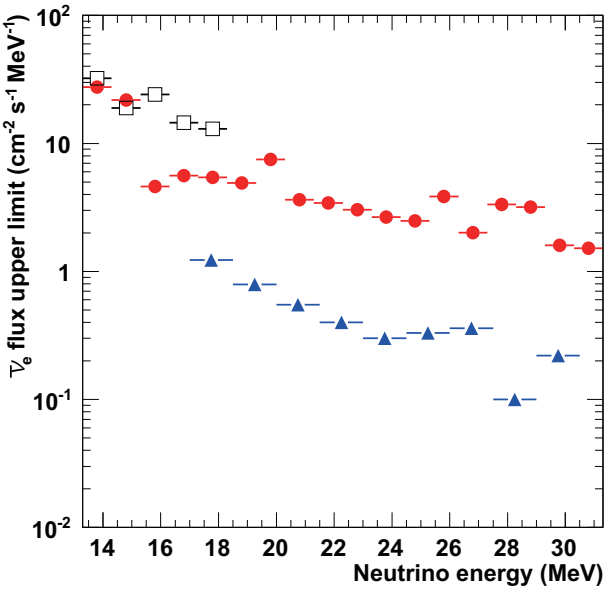

Fig. 20. Model-independent SRN 90% C.L. upper limits as a function of neutrino energy for SK-IV (solid circle). For comparison, both KamLAND result (open square) and previous SK result (solid triangle) are also shown.

Fig. 21. In the new cavern the Gd pre-mixing and pre-treatment 15 ton tank (front left), the selective filtration system (front right) and the 200 ton tank (rear of the hall) have been installed.

the diffuse supernova neutrino background from all the supernovae in the past. This signal has never been detected, but it is expected to be detectable in the 16-30 MeV energy region, which is the gap between the energy ranges of solar neutrinos and atmospheric neutrinos. Our published result [1] utilizes SK-I, II and SK-III data with analysis energy threshold 16MeV. A maximum likelihood search was performed in multiple regions of the Cherenkov angle distribution to extract the most accurate flux limit. The obtained flux limit is between 2.7 and 3.0 $\bar{\nu}cm^{-2}s^{-1}$ (positron energy $>$ 16 MeV), which actually depends on the shape of the neutrino spectrum assumed. This result currently provides the world's best limit on SRN flux. (Figure 20).

In SK-IV, a new result of the SRN search using the neutron tagging technique was also published [2]. In this analysis, neutrons from SRN reactions ($\bar{\nu}_e, p \rightarrow e^+, n$) are captured by hydrogens. After neutron captures, 2.2 MeV gammas are emitted. Thus, by detecting the prompt positron signal and the delayed 2.2 MeV gamma signal, we can reduce backgrounds, most of which are not accompanied by neutrons.

Figure 19 shows the energy spectrum of prompt signal, the time difference between a prompt signal and a delayed signal, and the detection efficiency of SRN for each energy bin. Figure 20 shows the obtained flux limit comparing with other results. Even though the detection efficiency is not good enough since 2.2 MeV is very low energy in SK (cf. the analysis threshold of solar neutrino is 3.5 MeV (kinetic)), we could obtain the world best limit in below 16 MeV. This result shows a high potential of neutron tagging techniques, which can be a strong tool for SRN detection.

Bibliography

[1] K.Bays et al., Phys. Rev. D 85, 052007 (2012)

[2] H.Zhang et al., Astropart. Phys. 60, 41 (2015)

R&D for the gadolinium project

As mentioned above, although at SK a few SRN events a year are expected, SRNs have not been detected yet because the large backgrounds constrain our search. The main goal of our research is to reduce these backgrounds and be able to detect SRNs. The observation of SRNs in general or neutrinos from distant supernovae in particular, would give us some information about the universe, for example the core collapse rate from SRNs, and about the neutrino itself too, for example its lifetime.

Currently, the SK detector can only detect the positrons efficiently but not for neutrons as shown in the previous section. In order to achieve a high detection efficiency for neutrons, it is proposed to add 0.2% of gadolinium (Gd) sulfate into SK. Since Gd has a neutron capture cross section of 49.000 barns (about 5 orders of magnitude larger than of protons) and emits a gamma cascade of 8 MeV, neutrons can be easily detected at SK (in space, vertices within tens of cm and in time, with the neutron capture delayed about 20 μsec).

EGADS (Evaluation Gadolinium's Action on Detector Systems) project was funded in 2009. The main motivation of EGADS is to show that by adding Gd, SK will be able to detect anti-neutrinos using the delayed coincidence technique, while keeping all its capabilities in the other analyses like solar and atmospheric neutrinos. Since then, a new hall near the SK detector has been excavated and a 200 ton tank with its ancillary equipment has been installed, see Fig.21, to mimic the conditions at SK. Of special importance is the selective water filtration system, that filters out water impurities while it keeps the Gd in the water.

From January 2010 to July 2011 we circulated pure water through the 200 ton tank and proved that our water system is stable and achieves a high water quality. In 2013, from February 6th to April 20th, the 200 ton tank has been stepwise loaded with Gd until the final 0.2% concentration was reached. By measuring Gd concentration at some detector positions, we confirmed that the Gd sulfate dissolves homogeneously in the 200 ton tank, and we can achieve and maintain a good water quality.

In summer 2013, we installed 240 photomultipliers and the data taking has started from September without Gd. After the water quality became good and stable, detector calibrations were performed. In April 2015, we finally achieved to make a final configuration with 0.2% $Gd_2(SO_4)_3$ concentration. Figure 22 shows the time variation of Cherenkov light left at 15m for Gd loaded water. The blue band in the figure shows the transparency range of Super-K water. As shown in the figure, it is measured that the transparency of 0.2% $Gd_2(SO_4)_3$ water is 92% of the average of Super-K water. Detailed studies, such as PMT signal stability in Gd water, Rayleigh scattering measurement in EGADS detector, and the neutron capture rate will be summarized soon, and we will start collaboration wide discussion in June 2015 based on those results. After all these evaluations finished, EGADS will become a detector with instant supernova detection capabilities.

T2K EXPERIMENT

[Spokesperson : Takashi Kobayashi]

High Energy Accelerator Research Organization (KEK)
Host institutes of the T2K experiment are KEK and ICRR

The T2K (Tokai-to-Kamioka) experiment [1] is a 295 km long-baseline neutrino oscillation experiment, employing a high intensity muon neutrino (or antineutrino) beam sent from the Japan Proton Accelerator Research Complex (J-PARC) in Tokai to the Super-Kamiokande (SK) water Cherenkov detector in Kamioka. One of the primary goals of the experiment was to observe electron neutrino appearance in the muon neutrino beam, and it was established in 2013 [2]. Now T2K experiment enters the era of measurement of θ_{13}, as well as to precisely determine the oscillation parameters, Δm^2_{32} and θ_{23}, by simultaneously observing muon neutrino disappearance. Also in 2014, we began to collect our first data of muon antineutrino beam. Neutrino oscillation effect on antineutrinos is different from that on neutrinos if the CP symmetry is violated in neutrino sector, and by comparing these two mode we can access to CP violation.

T2K is the first long-baseline experiment to adopt an off-axis beam [3]. The beam is directed 2.5° away from the direction to Super-K, which creates a narrow muon neutrino energy spectrum peaking around 0.6 GeV, the location of the first oscillation maximum for the T2K baseline.

The T2K beam is composed primarily of muon neutrinos, which are produced in the decays of charged pions and kaons created in the interactions of 30 GeV protons from the J-PARC accelerator striking a graphite target. We employ series of three magnets (called "magnetic horn") driven by pulsed electric current to generate magnetic field to forwardly focus the produced particles, and allow them to decay in the 96-m-long decay volume to generate neutrino beam. In 2014, we started collect the muon antineutrino beam by reversing the electric current of the horns.

T2K accumulated neutrino data collected during the six run periods listed in Table 2, and it corresponds to 11.04×10^{20} protons on target (POT) in total. The proton beam reached an intensity of 370 kW during this period and produced 2×10^{14} protons per pulse. Antineutrino data was obtained with 2.3×10^{20} POT. The near detector (ND) site located 280 m from the T2K target consists of two detector complexes one each on and off the beam axis. The on-axis interactive neutrino grid (INGRID [9]), composed of an array of iron scintillator sandwiches, monitors the neutrino beam intensity, direction and profile. The off-axis detector (ND280) is situated along the same direction to SK and measures the neutrino beam flux, composition and energy spectrum prior to neutrino oscillations. ND280 provides important information on the neutrino flux and interaction models, both of which are essential to T2K's oscillation measurements.

The far detector, SK [10], is a 50 kton water Cherenkov detector which uses timing information synchronized to the Global Positioning System (GPS) to records events coincident with the operation of the T2K beam. All data within $\pm500\,\mu$s of the beam arrival time at SK are recorded for use in later analysis.

The neutrino flux is calculated with a full Monte Carlo (MC) simulation considering the T2K beamline and measurements of the primary proton beam profile, the magnetic fields produced by the magnetic horns, and hadron production data from the NA61/SHINE measurements [11, 12]. Neutrino interactions are then simulated based on the flux predictions at both the ND280 and SK sites using the NEUT framework [13]. Parametric model of neutrino interaction and fluxes are con-

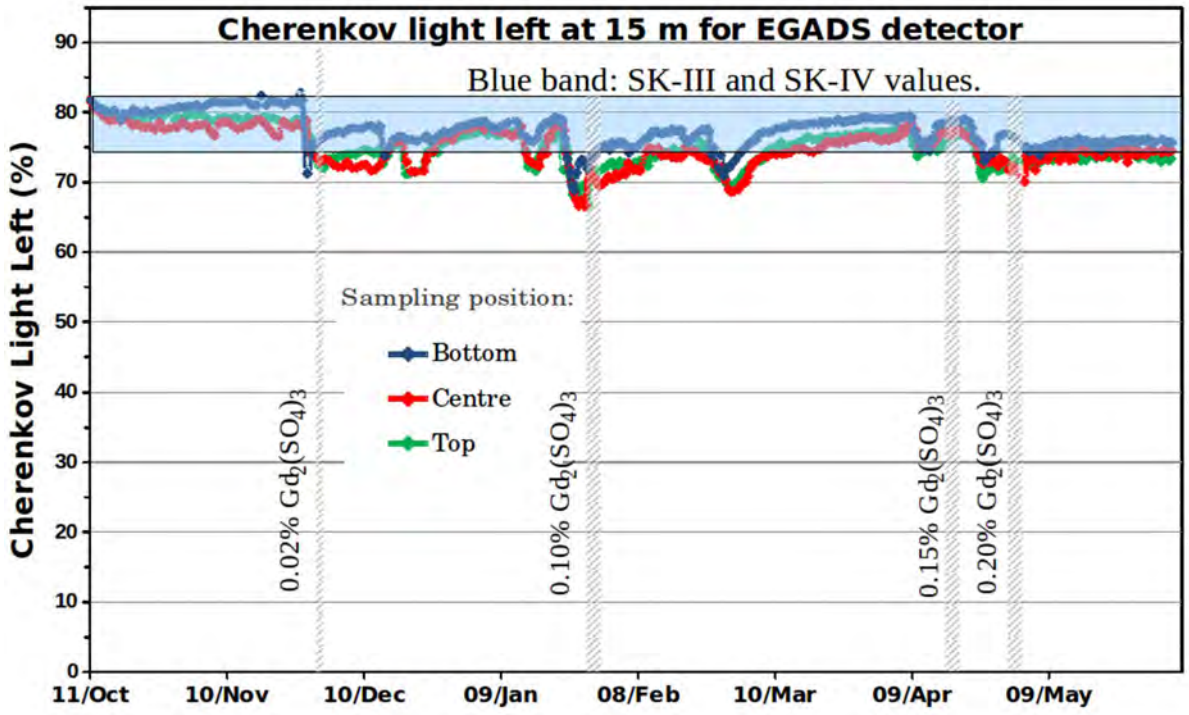

Fig. 22. Cherenkov light left at 15m for Gd loaded water. The horizontal blue band is the water transparency range of SK water. The vertical lines shows the injection date where we also indicate the concentration (% in mass) in the 200 ton tank.

Table 2. T2K data taking periods and integrated numbers of protons on target (POT) used in the neutrino oscillation analyses. References for T2K results from each data update are also listed.

Period	Dates	$\times 10^{20}$ POT	
		ν	$\overline{\nu}$
Run 1	Jan.2010 - Jun.2010	0.32	–
Run 2	Nov.2010 - Mar.2011	1.11 [4],[5]	–
Run 3	Mar.2012 - Jun.2012	1.58 [2],[6]	–
Run 4	Oct.2012 - May.2013	3.56 [7],[8]	–
Run 5	May.2014 - Jun.2014	0.24	0.51
Run 6	Oct.2014 - Mar.2015	0.10	1.81

strained with samples from ND measurements [14], and the systematic uncertainties of the model are largely reduced by this method.

In 2014, we carried out the analyses of disappearance of muon antineutrinos. In the analysis, to be able to see potential effects coming from new physics like CPT violation or non-standard interactions [15][16], we assume that mixing angle and mass differences in neutrino sector and antineutrino sector are different: we carried out an interval estimation of the parameter $(\Delta\overline{m}^2_{32}, \sin^2\overline{\theta}_{23})$ which is independent from that of neutrinos, $(\Delta m^2_{32}, \sin^2\theta_{23})$. We consider neutrino oscillation between three flavor neutrinos, and other parameters are taken from PDG [17].

An enriched sample of charged-current (CC) quasi-elastic (QE) scattering is selected for the analysis. This two body interaction ($\overline{\nu}_l + p \rightarrow l^+ + n$) is a main interaction mode of neutrino in T2K energy range, and two body scattering allows us to measure the neutrino energy. Selection is (1) All visible particles are contained inside SK (2) Interaction point is inside the nominal fiducial volume which is defined the region 2m inside from detector wall. (3) single Cherenkov ring (4) accompanied with one or zero decay electron (5) momentum is greater than 200 MeV/c. In the SK data of 2.3×10^{20} POT antineutrino beam, we observed 17 events.

Three type of the analyses had been carried out with different statistical approaches: Extended maximum likelihood method using two-dimensional distribution of muon momentum and direction, likelihood ratio using one-dimensional reconstructed neutrino energy, and simultaneous fitting of one-dimensional reconstructed neutrino energy distribution and ND-280 data. Three give consistent results with each other, and best fit value is obtained at $(\sin^2\overline{\theta}_{23}, \Delta\overline{m}^2_{32}) = (0.51, 2.32\times10^{-3}$ eV^2). Fig. 23 shows the reconstructed neutrino energy distribution with expectation with best-fitted parameters. Fig. 25 shows the overlay of the allowed region for antineutrino parameter and neutrino oscillation parameter obtained by T2K ν_μ beam analysis result [8]. This result is consistent with the assumption that $(\Delta\overline{m}^2_{32}, \sin^2\overline{\theta}_{23}) = (\Delta m^2_{32}, \sin^2\theta_{23})$. Fig. 24 shows the allowed region of the neutrino oscillation parameter by overlaying the result from MINOS [18], and two results are consistent.

Several neutrino cross section measurements with T2K beam are published in 2014. (1) The measurement of the ν_μ

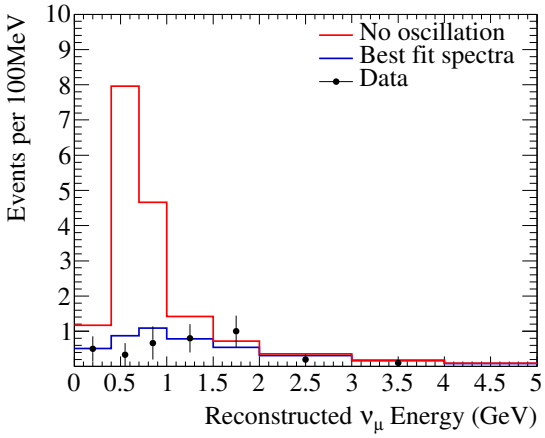

Fig. 23. The reconstructed energy spectrum of single-ring μ-like events at SK for the Run 5-6 muon antineutrino data with the best fit MC expectation (Blue). Red line shows the expectation without neutrino oscillation.

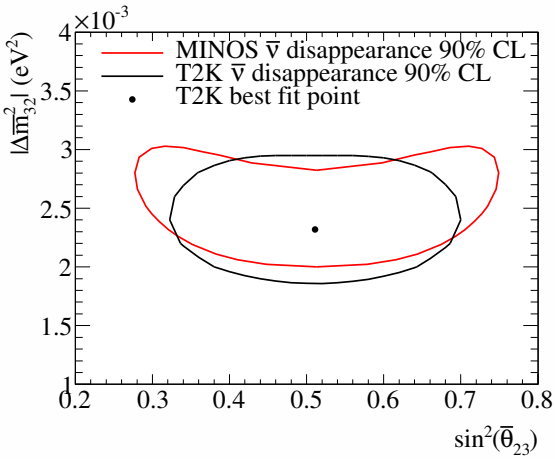

Fig. 24. The 90% confidence level allowed region of the parameter $(\sin^2\bar{\theta}_{23}, \Delta\bar{m}^2_{32})$ overlaid with MINOS result [18].

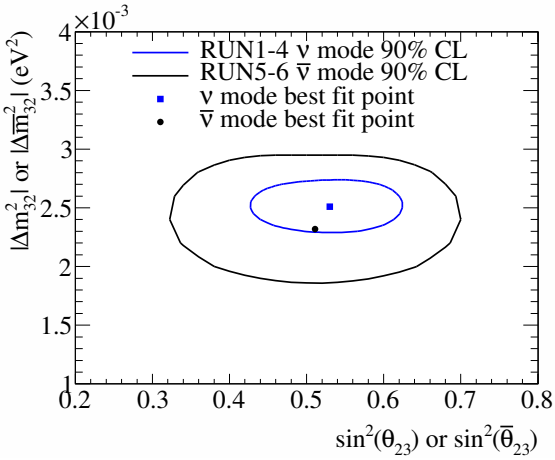

Fig. 25. The 90% confidence level allowed region of the parameter $(\sin^2\bar{\theta}_{23}, \Delta\bar{m}^2_{32})$. Allowed region of $(\Delta m^2_{32}, \sin^2\theta_{23})$ from T2K ν_μ disappearance analysis result [8] is overlaid.

inclusive CC cross sections on iron and hydrocarbon by ND detector [19]: The measured inclusive CC cross sections on iron and hydrocarbon averaged over the T2K on-axis flux with a mean neutrino energy of 1.51 GeV are 1.444±0.002(stat)+0.189-0.157(syst)$\times10^{-38}$ cm^2 / nucleon and 1.379±0.009(stat)+0.178-0.147(syst)$\times10^{-38}$ cm^2 / nucleon, respectively, (2) The first differential cross-section measurement of ν_e CC inclusive interaction at T2K beam energy [20].

Search for the electron antineutrino appearance is very interesting item, and the on-going analysis will be reported in near future. Also, several other cross section measurement done by ND will be report near future.

Bibliography

[1] K. Abe *et al.* [T2K Collaboration], Nucl. Instrum. Meth. A **659**, 106 (2011) [arXiv:1106.1238 [physics.ins-det]].

[2] K. Abe *et al.* [T2K Collaboration], Phys. Rev. D **88**, 032002 (2013) [arXiv:1304.0841 [hep-ex]].

[3] D. Beavis, A. Carroll, I. Chiang, *et al.*, Long Baseline Neutrino Oscillation Experiment at the AGS (Proposal E889), 1995. Physics Design Report, BNL 52459.

[4] K. Abe *et al.* [T2K Collaboration], Phys. Rev. Lett. **107**, 041801 (2011) [arXiv:1106.2822 [hep-ex]].

[5] K. Abe *et al.* [T2K Collaboration], Phys. Rev. D **85**, 031103 (2012) [arXiv:1201.1386 [hep-ex]].

[6] K. Abe *et al.* [T2K Collaboration], Phys. Rev. Lett. **111**, 211803 (2013) [arXiv:1308.0465 [hep-ex]].

[7] K. Abe *et al.* [T2K Collaboration], Phys. Rev. Lett. **112**, 061802 (2014) [arXiv:1311.4750 [hep-ex]].

[8] K. Abe *et al.* [T2K Collaboration], Phys. Rev. Lett. **112**, 181801 (2014) [arXiv:1403.1532 [hep-ex]].

[9] M. Otani, N. Nagai, D. Orme, A. Minamino, K. Nitta, O. Drapier, F. Moreau and M. Besnier *et al.*, Nucl. Instrum. Meth. A **623**, 368 (2010).

[10] Y. Fukuda *et al.* (Super-Kamiokande Collaboration), Nucl. Instrum. Meth. A501, 418 (2003).

[11] N. Abgrall *et al.* [NA61/SHINE Collaboration], Phys. Rev. C **84**, 034604 (2011) [arXiv:1102.0983 [hep-ex]].

[12] N. Abgrall *et al.* [NA61/SHINE Collaboration], Phys. Rev. C **85**, 035210 (2012) [arXiv:1112.0150 [hep-ex]].

[13] Y. Hayato, Nucl. Phys. (Proc. Suppl.) B112, 171 (2002).

[14] K. Abe *et al.* [T2K Collaboration], Phys. Rev. D **89**, 092003 (2014) [arXiv:1403.2552 [hep-ex]].

[15] Tommy Ohlsson Rep. Prog. Phys. **76** 044201, (2013)

[16] I. Girardi *et al.* Nucl. Phys. B **886** 31-42 (2014)

[17] K. Olive *et al.* [Particle Data Group], Review of Particle Physics, Chin. Phys. C **38**, 090001 (2014).

[18] Phys. Rev. Lett. **108**, 191801 (2012)

[19] K. Abe *et al.* [T2K Collaboration], Phys. Rev. D **90**, 052010 (2014)

[20] K. Abe *et al.* [T2K Collaboration], Phys. Rev. Lett. **113**, 241803 (2014)

XMASS EXPERIMENT

[Spokesperson : Yoichiro Suzuki]
Kavli IPMU, the University of Tokyo

Overview

The XMASS project is designed to detect dark matter, neutrinoless double beta decay, and ^{7}Be/pp solar neutrinos using highly-purified liquid xenon scintillator in an ultra-low radioactivity environment [1]. The advantages of using liquid xenon are a large amount of scintillation light yield, scalability of the size of the detector mass, an easy purification to reduce internal radioactive backgrounds, and a high atomic number ($Z = 54$) to shield radiations from outside of the detector. As the first stage of the XMASS project (XMASS-I), the detector with 835 kg of liquid xenon was constructed. Its construction started in April 2007 and completed in September 2010. After completion of the detector, commissioning data was taken from December 2010 to May 2012. We have published results from a search for light weekly interacting massive particle (WIMP) dark matter [2] and a search for solar axions [3], both using 6.7 live days of data collected with the full 835 kg liquid xenon volume and with the lowest energy threshold of 0.3 keV$_{ee}$, where the subscript *ee* stands for the electron equivalent energy deposition. During the commissioning data-taking, we found that a majority of events at low energy originated from radioactive contamination in the aluminum seal of the photomultiplier tube (PMT) window. In order to reduce the backgrounds, detector refurbishment was conducted. The contaminated parts of PMTs were covered by copper rings and plates in order to stop scintillation lights and radiations caused by its contamination. PMTs were cleaned by acid and copper parts were electropolished in order to remove possible surface contamination. After a year of detector refurbishment, data-taking resumed in November 2013 and is continuing for more than a year till now.

In this report, we present recent results from the full 165.9 live days of commissioning data, status of annual modulation analysis from data taken after refurbishment, and next steps of the project.

XMASS-I detector

XMASS-I is a single phase liquid xenon scintillator detector located underground (2700 m water equivalent) at the Kamioka Observatory. Fig. 26 shows a schematic drawing of the XMASS-I detector. It contains 835 kg of liquid xenon in an active region. The volume is viewed by 630 hexagonal and 12 cylindrical Hamamatsu R10789 PMTs arranged on an 80 cm diameter pentakis-dodecahedron support structure. A total photocathode coverage of more than 62% is achieved. The spherical arrays of PMTs are arranged in a double wall vessel made of oxygen free high conductivity (OFHC) copper. The detector is calibrated regularly with a ^{57}Co source inserted along the central vertical axis of the detector. By the data taken with the ^{57}Co source at the center of the detector volume, the photoelectron yield was determined to be $\sim$14 photoelectrons/keV$_{ee}$. In order to shield the liquid xenon detector from external gammas, neutrons, and muon-induced backgrounds, the copper vessel was placed at the center of a ϕ10 m$\times$ 10.5 m cylindrical tank filled with pure water. The water tank is equipped with 72 Hamamatsu R3600 20-inch PMTs to provide both an active muon veto and passive shielding against these backgrounds. XMASS-I is the first direct detection dark matter experiment equipped with such an active water Cherenkov shield. The liquid xenon and water Cherenkov detectors are hence called an Inner Detector (ID) and an Outer Detector (OD), respectively. More details are described in Ref. [4].

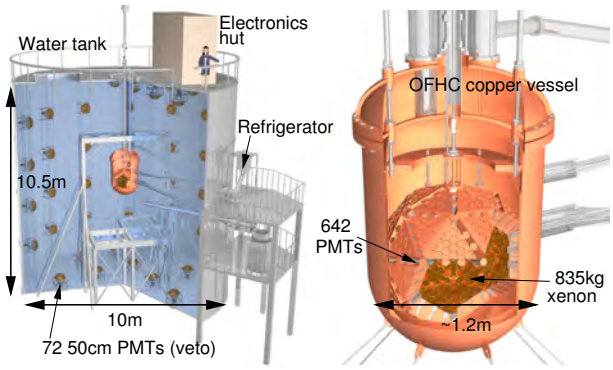

Fig. 26. Schematic drawing of the XMASS-I detector.

Recent results from commissioning data

In our recent analyses, we have achieved an unprecedented low-background level of $\sim 10^{-4}$ day^{-1}kg^{-1}keV$_{ee}^{-1}$ in the energy range around a few tens of keV$_{ee}$. This background level is an order of magnitude lower than XENON100 and LUX before their e/γ rejection. Three physics results were obtained from our 165.9 live days of the commissioning data with a restricted target mass of 41 kg at the central region of the detector.

Search for inelastic WIMP-nucleus scattering on ^{129}Xe [5]

Inelastic scattering that excites low-lying nuclear states in suitable target nuclei provides another avenue to probe WIMP dark matter. Its advantage is that nuclear excited states and their de-excitation mechanisms are typically well known, and thus the expected energy deposit in the detector is calculated, resulting in the readily identifiable signature of a line in the energy spectrum. ^{129}Xe has the lowest-lying excited nuclear state at 39.58 keV and almost the highest natural abundance of 26.4% among the xenon isotopes. A high-energy tail of the peak at 39.58 keV is expected since the scintillation lights

from the recoil of ^{129}Xe nucleus and from the nuclear de-excitation γ-ray cannot be separated since lifetime of the excited state is much shorter than the decay time constant of scintillation light. We searched for such an inelastic scattering of WIMPs on ^{129}Xe. No significant excess of the events was observed, and hence the 90% confidence level (C.L.) upper limits on the cross section for inelastic scattering on ^{129}Xe was derived as shown in Fig. 27 (left). We also obtained the 90% upper limit for spin dependent WIMP-neutron cross section for e.g. a 50 GeV/c^2 WIMP at 1.1×10^{-37} cm^2 and 4.2×10^{-38} cm^2, respectively, using the different model of form factors of ^{129}Xe nuclei as shown in Fig.27 (right). These limits are the first derived exclusively from data on inelastic scattering.

Search for bosonic superweakly interacting massive dark matter particles [6]

Although a WIMP dark matter is a well-motivated model and fits the cold dark matter paradigm, simulations based on this cold dark matter scenario expect a richer structure on galactic scales than those observed. Furthermore, there is so far no evidence of supersymmetric particles at the LHC, and therefore, it is important to investigate various types of dark matter candidates. These facts strengthen an interest to consider lighter and more weakly interacting particles such as super-WIMPs, a warm dark matter candidate. Bosonic super-WIMPs are experimentally interesting since their absorption in a target material would deposit an energy essentially equivalent to the super-WIMP's rest mass. We conducted a search for vector and pseudoscalar super-WIMPs in the mass range between 40 and 120 keV. Fig. 28 (left) shows the energy spectra of the observed events and simulated events. No significant excess above background was observed, and hence the 90% C.L. upper limits on coupling constants for pseudoscalar bosons and vector bosons were obtained as shown in Fig. 28 (right). This is the first direct detection experiment exploring the vector super-WIMPs and the obtained limit for the vector super-WIMPs excludes the possibility that such particles constitute all of the dark matter. The absence of the signal also provides the most stringent direct constraint on the coupling constant of pseudoscalar dark matter to electrons. This result was published in Physical Review Letters, selected as Editors' Suggestion.

Search for two-neutrino double electron capture on ^{124}Xe

Neutrinoless double beta decay and its inverse, neutrinoless double electron capture, are lepton number violating processes, and their existence is an evidence that neutrino is a Majorana particle. On the other hand, two-neutrino modes of double beta decay and double electron capture are allowed within the standard model of particle physics. Although two-neutrino double beta decay has been observed in more than ten isotopes, there exists only a few positive experimental results for two-neutrino double electron capture so far: a geochemical measurement for ^{130}Ba and a direct measurement for ^{78}Kr. Any measurement of two-neutrino double electron capture will provide a new reference for the calculation of nuclear matrix elements. Natural xenon contains the double electron capture nuclei ^{124}Xe (0.095%). In the case that two K-shell electron in the ^{124}Xe atom are captured simultaneously, the daughter atom of ^{124}Te is formed with two vacancies in the K-shell and de-excites by by emitting atomic X-rays and/or Auger electrons. The total energy deposition in the detector is 63.6 keV, which is twice of the binding energy of a K-shell electron in a tellurium atom. We performed a search for two-neutrino double electron capture on ^{124}Xe. Fig. 29 shows energy spectra of the observed events and simulated events after each reduction step. After all cuts, 5 events remain in the signal region while the expected background is 5.3 ± 0.5 events originating from the ^{222}Rn daughter ^{214}Pb in the detector. No significant peak above background was observed and hence we set the 90% C.L. lower limit on the half-life of 4.9×10^{21} years after subtracting background, which provides the most stringent limit for ^{124}Xe.

Annual modulation analysis from data after refurbishment

The count rate of dark matter signal experiences an annual modulation due to the relative motion of the Earth around the Sun. The dark matter flux at the detector becomes maximal in June and minimal in December. The annual modulation is a strong signature for dark matter since most of backgrounds are not expected to show this kind of time dependence. We are conducting the annual modulation analysis from data taken after refurbishment using full-volume of the XMASS-I detector without particle identification. Fig. 30 (left) shows the history of the accumulated livetime after data quality cut. As of the end of March 2015, we have collected 359.2 live days of data since November 2013. Fig. 30 (right) shows the observed count rate after cuts as a function of time in the 0.5-1.0 keV$_{ee}$ energy interval. The energy region corresponds to 4.8-8.0 keV nuclear recoil energies. Our data is overlaid with the expected annual modulation assuming 8 GeV/c^2 WIMP with the WIMP-nucleon cross section of 3×10^{-40} cm^2. XMASS has a high sensitivity to the annual modulation claimed by the DAMA/LIBRA group. The results from our one-year data will come soon.

XMASS-1.5 and beyond

We are planning to build the next stage detector, XMASS-1.5, with total 5 tons of liquid xenon. Increasing the fiducial mass is indispensable to examine cross sections smaller than current constraints for standard WIMPs. The basic design of the detector is same as the one for the XMASS-I detector but with an essential improvement of the discrimination between the surface background and the inner events. For this purpose, we have developed a new type of PMT which has a dome-shaped photocathode as shown in Fig. 31 (left). Fig. 31 (right) illustrates a comparison of response to surface events of PMT with a flat photocathode and a dome-shaped photocathode. The dome-shaped PMTs are more efficient for detecting scintillation photons originated at the inner surface of the detector than the flat-shaped PMTs used for the XMASS-I detector. Fig. 32 shows the expected sensitivity to WIMP-nucleon cross section with the XMASS-1.5 detector.

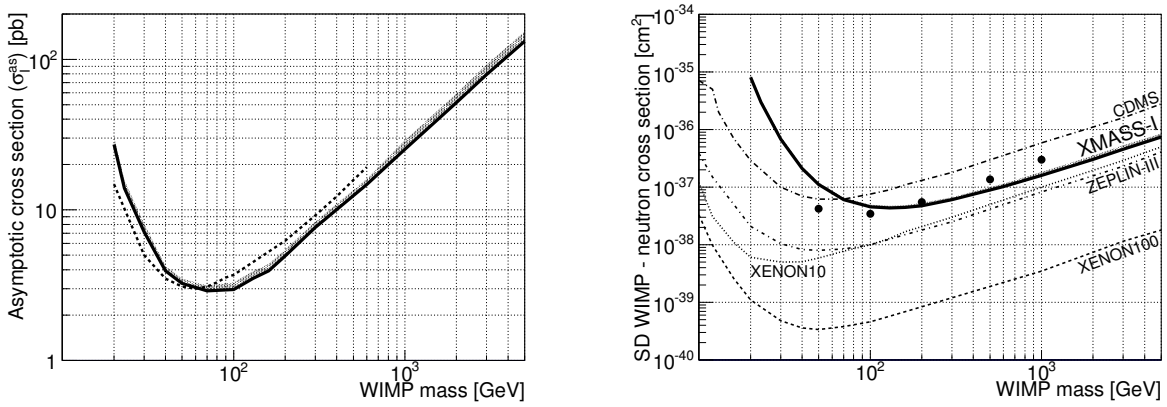

Fig. 27. (Left) The solid line is our 90% C.L. upper limit on the asymptotic cross section for inelastic scattering on ^{129}Xe using the same form factors as DAMA. The gray band covers its variation with our systematic uncertainty. The dashed line is the limit obtained by the DAMA group. (Right) The solid line and dots represent our 90% C.L. upper limit on the spin-dependent cross section of WIMPs on neutron using two different recent calculations of form factors. The dashed, dotted, dash-dotted, and long dash-dotted lines represent experimental constraints on spin-dependent WIMP nucleon cross sections extracted from elastic scattering data. Our own limit is the first derived exclusively from data on inelastic scattering.

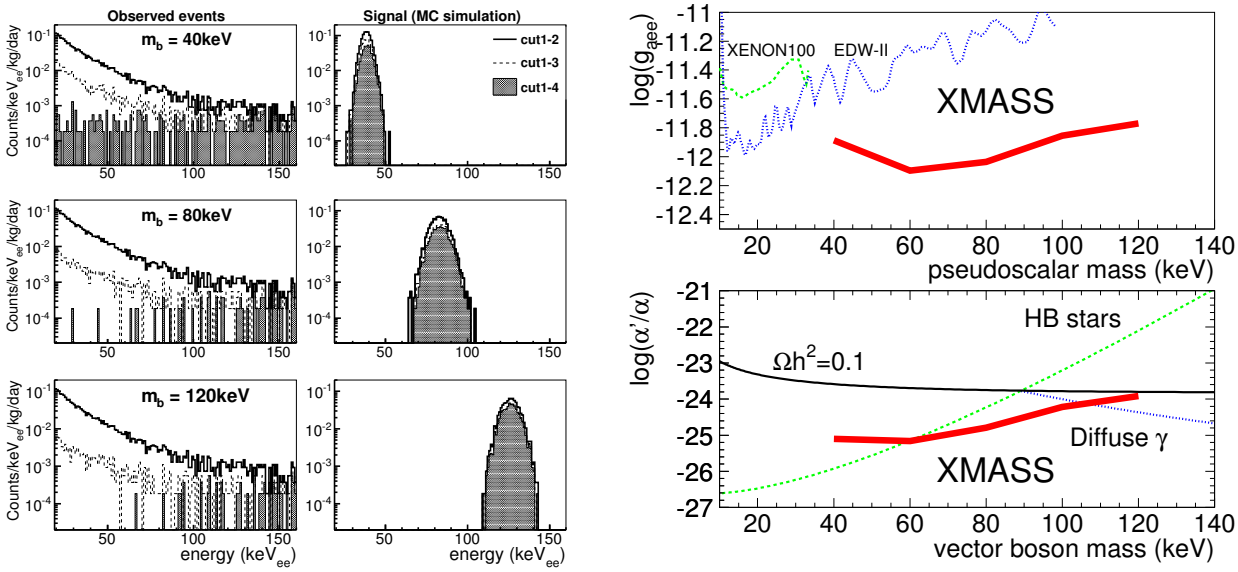

Fig. 28. (Left) Energy spectra of the observed events and simulated events after each reduction step for each vector super-WIMP mass. Hatched histograms show remaining events after applying radius cut, timing cut and hit pattern cut. (Right) Obtained 90% C.L. upper limits on coupling constants for electrons and pseudoscalar super-WIMPs (top) and for electrons and vector super-WIMPs (bottom).

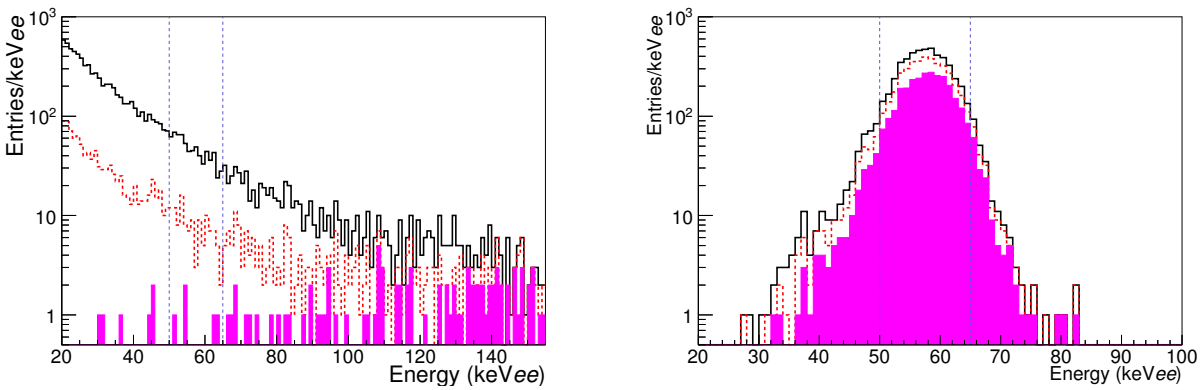

Fig. 29. Energy spectra of the observed events (left) and simulated events (right) after each reduction step for two-neutrino double electron capture on ^{124}Xe. Filled histograms show remaining events after applying radius cut, timing cut and hit pattern cut. Vertical dashed lines indicate the energy window for signal.

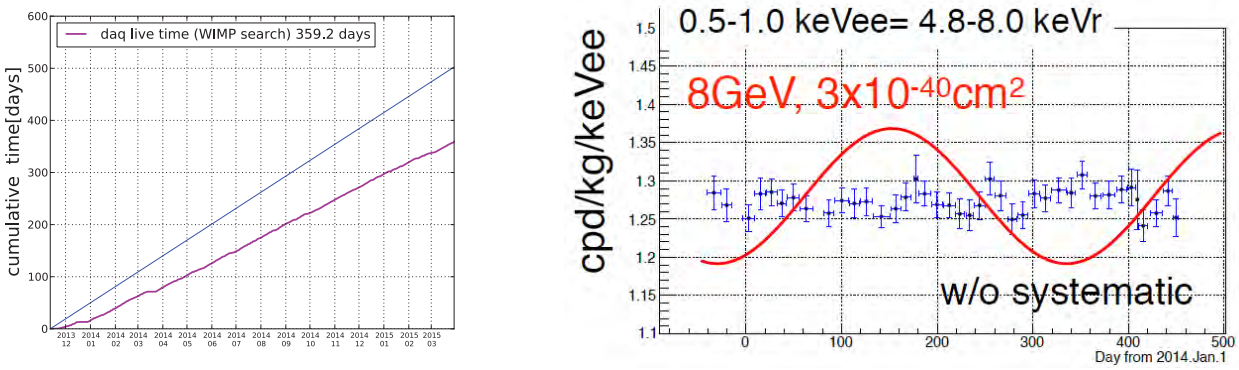

Fig. 30. (Left) History of the accumulated livetime after data quality cuts for annual modulation analysis. The blue straight line indicates realtime. (Right) Observed count rate as a function of time in the 0.5-1.0 keV$_{ee}$ energy interval which corresponds to 4.8-8.0 keV nuclear recoil energies. The red curve is the expected annual modulation assuming 8 GeV/c^2 WIMP with the WIMP-nucleon cross section of 3×10^{-40} cm^2.

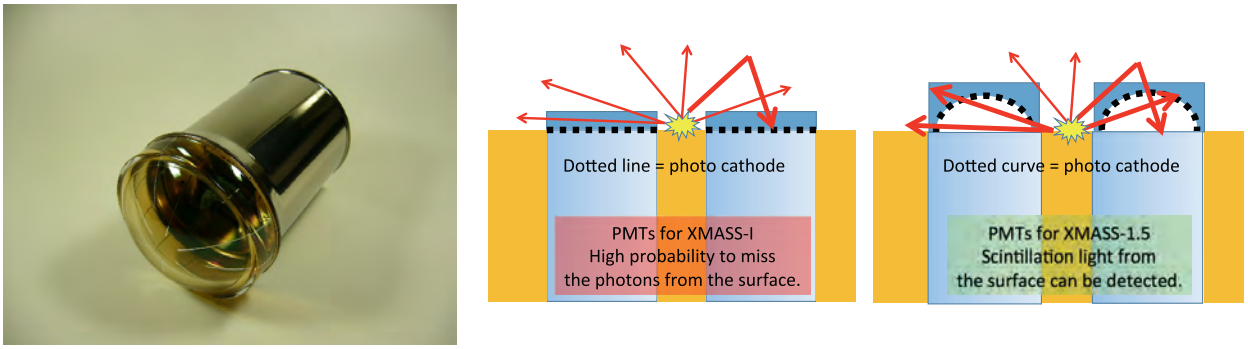

Fig. 31. (Left) Picture of a newly-developed 3-inch PMT for the next generation XMASS detector. (Right) Comparison of response to surface events of PMT with a flat photocathode and a dome-shaped photocathode. Since the dome-shaped photocathode has a large acceptance for scintillation light from the inner surface of the detector, identification of surface events is much more efficient with the dome-shaped PMTs.

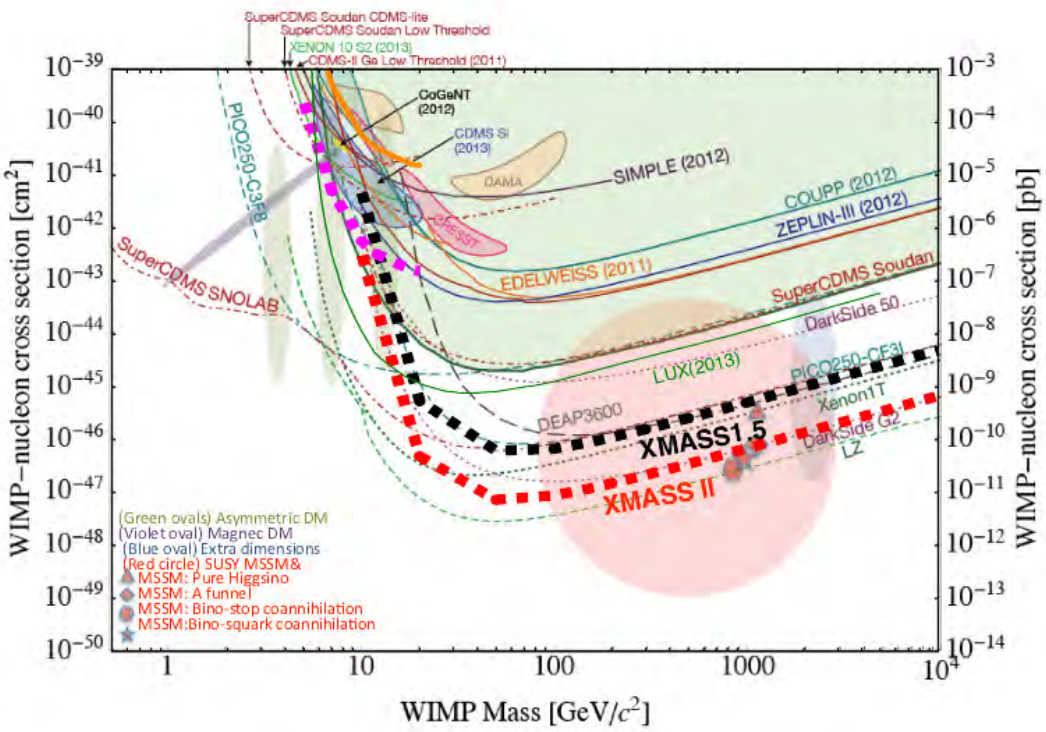

Fig. 32. Expected sensitivity with XMASS-1.5 (XMASS-II) assuming fiducial mass of 1 ton (10 tons) and 1-year (5-year) running, respectively.

With newly-developed PMTs, we can search for heavy WIMPs with cross sections less than 10^{-46} cm^2 even for the same background level of the XMASS-I. Beyond XMASS-1.5, XMASS-II with total 24 tons of liquid xenon is planned. The expected sensitivity to WIMP-nucleon cross section with the XMASS-II detector is also shown in Fig. 32. It is noteworthy that XMASS has an unique feature that it has a very low energy threshold as well as high sensitivity for other types of dark matter. The low energy threshold is essentially important for a low mass WIMP search and achieved by the high light yield as confirmed with the XMASS-I detector. The detector is sensitive to axion-like particles as well as bosonic super-WIMPs as discussed above because the detector is designed to realize low background even without e/γ rejection. These unique features are particularly important to have a detector sensitive to broad range of dark matter candidates.

Bibliography

[1] Y. Suzuki *et al.*, hep-ph/0008296.

[2] K. Abe *et al.* (XMASS Collaboration), Phys. Lett. B **719** (2013) 78.

[3] K. Abe *et al.* (XMASS Collaboration), Phys. Lett. B **724** (2013) 46.

[4] K. Abe *et al.* (XMASS Collaboration), Nucl. Instrum. Meth. A **716** (2013) 78.

[5] H. Uchida *et al.* (XMASS Collaboration), Prog. Theor. Exp. Phys. **2014** (2014) 063C01.

[6] K. Abe *et al.* (XMASS Collaboration), Phys. Rev. Lett. **113** (2014) 121301.

HYPER-KAMIOKANDE PROJECT

[Project Leader: Masato Shiozawa]

Kamioka Observatory, ICRR, The University of Tokyo

The Hyper-Kamiokande is the third generation nucleon decay and neutrino detector at Kamioka, that aims to explore unification of elementary particles and full picture of neutrino masses and mixings [1, 2]. The schematic view of the Hyper-K detector is illustrated in Fig. 33.

A letter of intent [3] (LoI) of the Hyper-Kamiokande project has been released, in which the baseline design of the detector and physics potential of Hyper-K are described. The water Cherenkov detector with the mass of 1 million tones has capability to search for the nucleon decays with sensitivity of 10 times longer than the lifetime limits given by the Super-Kamiokande. For example, the sensitivity for the decay mode $p \to e^+\pi^0$ is expected to be beyond 1×10^{35} years [3]. The detector also aims to study neutrino properties, such as Dirac *CP* phase δ_{CP}, mass hierarchy, octant of θ_{23}, by using a high

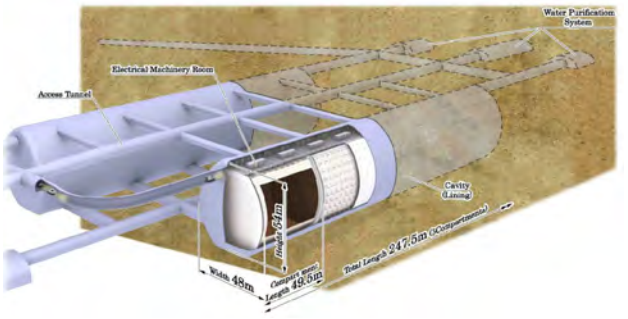

Fig. 33. Schematic view of the Hyper-Kamiokande. The detector consists of two cylindrical tanks holding ~ 500 kton ultrapure water (~ 1 Mton in total). The each tank is divided by segmentation walls every 50 m.

power accelerator based neutrino beam and atmospheric neutrinos.

The neutrino oscillation physics sensitivities of Hyper-K with J-PARC neutrino beam and atmospheric neutrinos have been updated from LoI using the framework and systematic uncertainties derived from the T2K experiment [4]. The updated Hyper-K sensitivity studies have been published in a journal [5]. Figure 34 shows the expected size of allowed re-

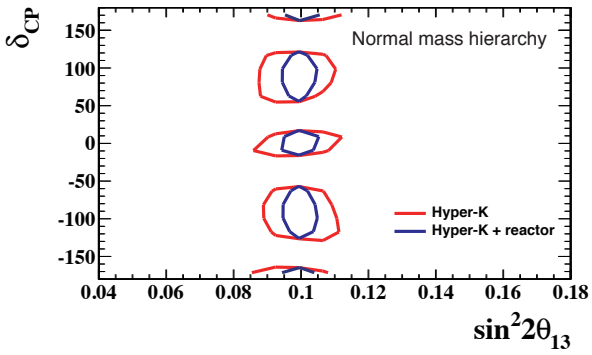

Fig. 34. Expected sensitivity for $\sin^2 2\theta_{13}$ and *CP* phase δ_{CP} (normal mass hierarchy case). Red (blue) lines show the result with Hyper-K only (with $\sin^2 2\theta_{13}$ constraint from reactor experiments). The figure is quoted from the published paper [5].

gions for the parameter space of θ_{13} and δ_{CP} by using upgraded J-PARC neutrino beam with the power of 0.75 MW $\times 10$ years and the Hyper-Kamiokande detector with the fiducial volume of 0.56 Megaton. Hyper-K has a good sensitivity in the whole relevant θ_{13} and δ_{CP} parameter space. The high statistics data sample of atmospheric neutrinos obtained by Hyper-K will also allow us to extract information on the mass hierarchy and the octant of θ_{23} (Fig. 35). With a full 10 year period of data taking, the significance for the mass hierarchy determination is expected to reach 3σ or greater as is shown in left panel of Fig. 35.

Hyper-Kamiokande international proto-collaboration has been formed in January 2015 [7]. The proto-collaboration consists of about 240 people in 67 institutes from 13 countries. Figure 36 shows a group photo of the Hyper-Kamiokande proto-collaboration at 'The Inaugural Symposium of the Hyper-K Proto-Collaboration' held on January 31st, 2015 [7]. In order to promote the proto-collaboration to further advance the Hyper-Kamiokande project, the Institute for Cosmic Ray

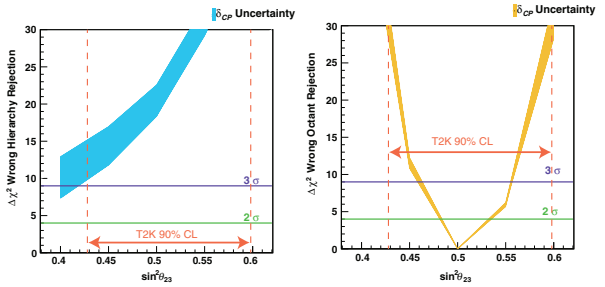

Fig. 35. Atmospheric neutrino sensitivities for a ten year exposure of Hyper-K assuming the mass hierarchy is normal. Left: the $\Delta\chi^2$ discrimination of the wrong hierarchy hypothesis as a function of the assumed true value of $\sin^2\theta_{23}$. Right: the discrimination between the wrong octant for each value of $\sin^2\theta_{23}$. The uncertainty from δ_{CP} is represented by the thickness of the band. Vertical dashed lines indicate 90% confidence intervals of $\sin^2\theta_{23}$ from the T2K measurement in 2014 [6]. The figures are quoted from the publication [5].

Fig. 36. Group photo of Hyper-Kamiokande proto-collaboration at 'The Inaugural Symposium of the Hyper-K Proto-Collaboration.' The photo is quoted from [7].

Research (ICRR) of the University of Tokyo and the Institute of Particle and Nuclear Studies of the High Energy Accelerator Research Organization (KEK) signed a memorandum of understanding (MoU) for cooperation on the Hyper-Kamiokande project. Figure 37 shows Prof. Masanori YAMAUCHI, KEK (left) and Prof. Takaaki KAJITA, ICRR (right) signed the MoU.

Fig. 37. Photo of Prof. Masanori YAMAUCHI, KEK (left) and Prof. Takaaki KAJITA, University of Tokyo (right) signed a memorandum of understanding for cooperation on the Hyper-Kamiokande project.

The proto-collaboration intensively develop various aspects of Hyper-K project such as geological surveys at the detector candidate sites, design of cavern and tank, water purification and circulation system design, new photon-sensor and DAQ system, detector calibration system, analysis software, and physics sensitivities.

Although the detector baseline design and the physics sensitivities studies of Hyper-K [3, 5] assume to use Super-K style 20-inch Photomultiplier Tubes (PMTs), two new photo-sensors, called 'Box and Line' PMT and 'Hybrid Photo-Detector' (HPD), have been intensively developed for Hyper-K, which are potentially lower-cost and higher-sensitivity than Super-K style PMT. The new photo-sensors employ an improved technologies for the photo-detection; Box and Line PMT has an improved dynode structure and HPD employs semiconductor for signal amplification. Figure 38 shows photograph of new photo-sensors. The Box and Line PMT has an higher quantum efficiency and collection efficiency of the photo-electrons than SK style PMT. Figure 39 shows photon detection rate (count rate) for the Box and Line PMT (R12860) and Super-K style PMT (R3600). As shown in the figure, the Box and Line PMTs show about twice better photo-detection efficiency (quantum efficiency times collection efficiency) than Super-K style PMTs. In addition to the improvement of photo-detection efficiency, the timing resolution for 1 photo-electron level of light is improved to 1.1 nsec from 2.1 nsec of SK style PMT. Another new photo-sensor, HPD, has also been developed. Prototypes of 20-inch HPD became available in 2014 and confirmed HPD has a better timing and charge resolutions than Super-K style PMT. Further detailed performance evaluation and development of new photo-sensors are in progress.

Fig. 38. Photographs of two new photo-sensors. The top left image shows a Hybrid Photo-Detector and the top right picture shows a Box and Line PMT. The electrodes for signal amplification of each sensor are in the bottom panel.

The first Hyper-Kamiokande proto-collaboration meeting will hold in June 2015 to discuss the progresses of studies and various aspects of the project face to face.

Bibliography

[1] M. Shiozawa, "The Hyper-Kamiokande project," Nucl. Phys. B (Proc. Suppl.) **237-238**, 289-294 (2013).

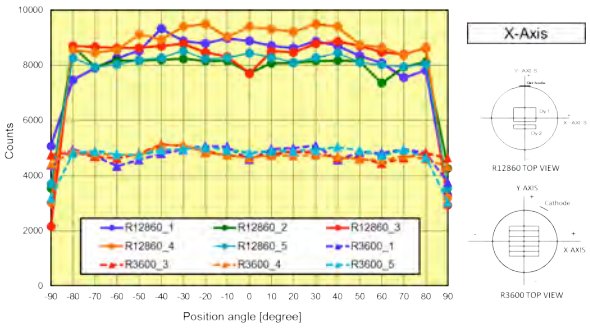

Fig. 39. Photon count rate as a function of photon incident position (angle) on the photocathode. The photon incident position is defined in the right-hand side figure. Dashed-lines (triangle) are for R3600 which are used in Super-Kamiokande and solid-lines (circle) are Box and Line PMT. Figure courtesy of Hamamatsu Photonics K.K.

[2] M. Diwan, R. Edgecock, T. Hasegawa, T. Patzak, M. Shiozawa and J. Strait, "Future long-baseline neutrino facilities and detectors," Adv. High Energy Phys. **2013**, 460123 (2013).

[3] K. Abe, T. Abe, H. Aihara, Y. Fukuda, Y. Hayato, K. Huang, A. K. Ichikawa and M. Ikeda *et al.*, "Letter of Intent: The Hyper-Kamiokande Experiment — Detector Design and Physics Potential —," arXiv:1109.3262 [hep-ex].

[4] K. Abe *et al.* [T2K Collaboration], "Neutrino oscillation physics potential of the T2K experiment," PTEP **2015**, no. 4, 043C01 (2015) [arXiv:1409.7469 [hep-ex]].

[5] K. Abe *et al.* [Hyper-Kamiokande Proto-Collaboration], "Physics potential of a long-baseline neutrino oscillation experiment using a J-PARC neutrino beam and Hyper-Kamiokande," PTEP **2015**, no. 5, 053C02 (2015) [arXiv:1502.05199 [hep-ex]].

[6] K. Abe *et al.* [T2K Collaboration], "Precise Measurement of the Neutrino Mixing Parameter θ_{23} from Muon Neutrino Disappearance in an Off-Axis Beam," Phys. Rev. Lett. **112**, no. 18, 181801 (2014) [arXiv:1403.1532 [hep-ex]].

[7] ICRR Press Release: "ICRR signs a MOU with KEK on the Hyper-Kamiokande proto-collaboration" http://www.icrr.u-tokyo.ac.jp/2015/01/31150000.html, http://www.hyper-k.org/en/news/news-20150205-1.html

HIGH ENERGY COSMIC RAY DIVISION

Overview

There are three major experimental research activities in the High Energy Cosmic Ray Division, the study of high energy gamma rays and the development of the next generation gamma-ray telescopes by the Cherenkov Cosmic Gamma Ray group, the study of extremely high energy cosmic rays by the Telescope Array (TA) group, and the study of very high energy cosmic rays and gamma rays by the Tibet ASγ group.

Other activities, such as experiments utilizing the Akeno observatory, the Norikura observatory, the Mt. Chacaltaya observatory (jointly operated with Bolivia) are closely related to inter-university joint research programs. Also an all-sky high resolution air-shower detector (Ashra) is in partial operation on the Hawaii island. The High Energy Astrophysics group created in the fiscal year 2009 aims to explore various high energy astrophysical phenomena, through theoretical and observational approaches.

The CANGAROO telescopes had been in operation in South Australia since 1992, with a 3.8 m small telescope and then with four 10 m telescopes. The major scientific objective was the study of Very High Energy (VHE) gamma-ray sources in our galaxy in the southern hemisphere. The mission of these telescopes was completed and the CANGAROO observation site was closed in 2011.

For further development of VHE gamma-ray astronomy, the Cherenkov Cosmic Gamma Ray group is working on the design study and development of the next generation international ground-based gamma-ray observatory CTA which will offer an order of magnitude better sensitivity than currently running Cherenkov telescopes, three times better angular resolution, and wider energy coverage from 20 GeV to 100 TeV or higher.

At the Akeno observatory, a series of air shower arrays of increasing geometrical sizes were constructed and operated to observe extremely high energy cosmic rays (EHECRs). The Akeno Giant Air Shower Array (AGASA) was operated from 1991 to January 2004 and covered the ground area of 100 km^2 as the world largest air shower array. In 13 years of operation, AGASA observed a handful of cosmic rays exceeding the theoretical energy end of the extra-galactic cosmic rays (GZK cutoff) at 10^{20} eV.

The Telescope Array (TA), a large plastic scintillator array with air fluorescence telescopes, has been constructed in Utah, USA, which succeeds AGASA and measures the EHECRs with an order of magnitude larger aperture than that of AGASA for the further study of EHECRs. The full-scale TA is accumulating data as the largest array viewing the northern sky and observed the energy spectrum with high statistics, which is in good agreement with the GZK suppression.

An air shower experiment aiming to search for celestial gamma-ray point sources started in 1990 with Chinese physicists at Yangbajing (Tibet, 4,300 m a.s.l.). This international collaboration is called the Tibet ASγ Collaboration. An extension of the air shower array was completed in 1995 and an emulsion chamber has been combined with this air shower array since 1996 to study the primary cosmic rays around the knee energy region. After successive extensions carried out in 1999, 2002 and 2003, the total area of the air shower array amounts to 37,000 m^2. The sun's shadow in cosmic rays affected by the solar magnetic field was observed for the first time in 1992, utilizing its good angular resolution at multi-TeV energy region.

The High Energy Astrophysics group is conducting theoretical researches on fundamental processes responsible for non-thermal particle acceleration in various astrophysical environments, including first-order diffusive shock acceleration, second-order stochastic acceleration in shock downstream regions, modification of shock structure by pick-up interstellar neutrals, as well as injection processes of suprathermal particles. In addition to these theoretical works, R/D studies for radio observations of pulsars and cosmic ray air showers are also being made.

Cherenkov Cosmic Gamma-Ray Group

CTA Project (Cherenkov Telescope Array)

CTA-Japan Consortium
[Spokespersons : M.Teshima and H.Kubo]

Collaboration list:
Institute for Cosmic Ray Research, The University of Tokyo, Chiba, Japan; Department of Physics, Aoyama Gakuin University, Tokyo, Japan; Department of Physics, Hiroshima University, Hiroshima, Japan; Hiroshima Astrophysical Science Center, Hiroshima University, Hiroshima, Japan; Faculty of Science, Ibaraki University, Ibaraki, Japan; Institute of Particle and Nuclear Studies, High Energy Accelerator Research Organization (KEK), Ibaraki, Japan; Department of Physics, Konan University, Hyogo, Japan; Faculty of Medical Engineering and Technology, Kitasato University, Kanagawa, Japan; Graduate School of Science and Technology, Kumamoto University, Kumamoto, Japan; Department of Physics, Kyoto University, Kyoto, Japan; Department of Applied Physics, University of Miyazaki, Miyazaki, Japan; Department of Physics, Nagoya University, Aichi, Japan; Solar-Terrestrial Environment Laboratory, Nagoya University, Aichi, Japan; Kobayashi-Maskawa Institute, Nagoya University, Aichi, Japan; Department of Earth and Space Science, Osaka University, Japan; Department of Physics, Kinki University, Osaka, Japan; Astrophysical Big Bang laboratory, RIKEN, Wako, Japan; Department of Physics, Rikkyo University, Tokyo, Japan; Department of Physics, Saitama University, Saitama, Japan; Institute of Space and Astronautical Science, JAXA, Kanagawa,

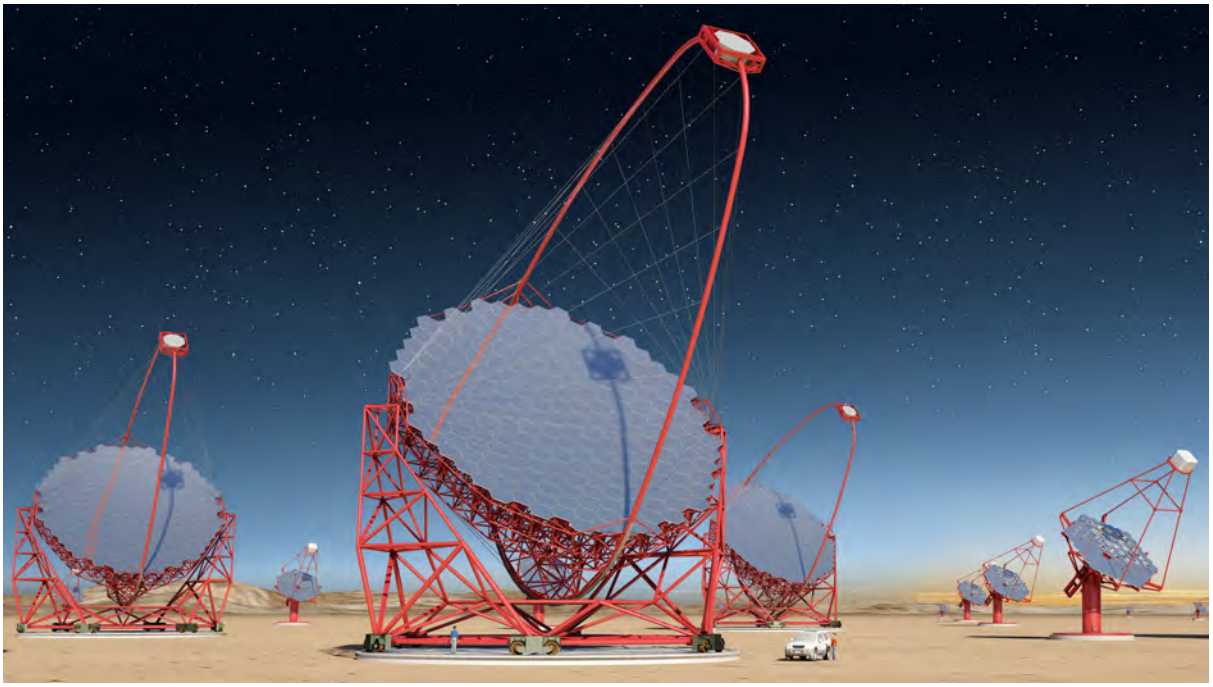

Fig. 1. Artist view of the CTA observatory. CTA consists of three types of telescopes, Large Size Telescopes (23m diameter), Mid Size Telescopes (12m) and Small Size Telescopes (4m), and covers the broad energy band from 20GeV to 100TeV.

Japan; Department of Physics, Tokai University, Kanagawa, Japan; Faculty of Integrated Arts and Sciences, The University of Tokushima; Department of Astronomy, The University of Tokyo, Tokyo, Japan; Department of Physics, The University of Tokyo, Tokyo, Japan; Faculty of Science and Engineering, Waseda University, Tokyo, Japan; Department of Physics, Yamagata University, Yamagata, Japan; Faculty of Management Information, Yamanashi Gakuin University, Yamanashi, Japan; Center for Cosmology and AstroParticle Physics, Ohio State University, Ohio, USA; Max-Planck-Institute for Physics, Munich, Germany [1].

CTA Project

During the past several years, Very High Energy (VHE) gamma-ray astronomy has made spectacular progress and has established itself as a vital branch of astrophysics. To advance this field even further, we propose the Cherenkov Telescope Array (CTA) [5], the next generation VHE gamma ray observatory, in the framework of a worldwide, international collaboration. CTA is the ultimate VHE gamma ray observatory, whose sensitivity and broad energy coverage will attain an order of magnitude improvement above those of current Imaging Atmospheric Cherenkov Telescopes (IACTs). By observing the highest energy photons known, CTA will clarify many aspects of the extreme Universe, including the origin of the highest energy cosmic rays in our Galaxy and beyond, the physics of energetic particle generation in neutron stars and black holes, as well as the star formation history of the Universe. CTA will also address critical issues in fundamental physics, such as the identity of dark matter particles and the nature of quantum gravity.

VHE gamma rays from 100GeV to 10TeV can be observed with ground-based IACTs. The history of VHE gamma ray astronomy began with the discovery of VHE gamma rays from the Crab Nebula by the Whipple Observatory in 1989. To date, the current generation IACTs featuring new technologies, such as H.E.S.S., MAGIC, VERITAS, and CANGAROO, have discovered more than 100 Galactic and extragalactic sources of various types.

CTA is designed to achieve superior sensitivity and performance, utilizing established technologies and experience gained from the current IACTs. The project is presently in its preparatory phase, with international efforts from Japan, the US and EU. It will consist of several 10s of IACTs of three different sizes (Large Size Telescopes, Mid Size Telescopes, and Small Size Telescopes). With a factor of 10 increase in sensitivity (1m Crab $\sim 10^{-14} erg\ s^{-1}\ cm^{-2}$), together with a much broader energy coverage from 20GeV up to 100TeV, CTA will bring forth further dramatic advances for VHE gamma ray astronomy. The discovery of more than 1000 Galactic and extragalactic sources is anticipated with CTA.

CTA will allow us to explore numerous diverse topics in physics and astrophysics. The century-old question of the origin of cosmic rays is expected to be finally settled through detailed observations of supernova remnants and other Galactic objects along with the diffuse Galactic gamma ray emission, which will also shed light on the physics of the interstellar medium. Observing pulsars and associated pulsar wind nebulae will clarify physical processes in the vicinity of neutron stars and extreme magnetic fields. The physics of accretion onto supermassive black holes, the long-standing puzzle of the origin of ultrarelativistic jets emanating from them, as well as their cosmological evolution, will be addressed by extensive studies of active galactic nuclei (AGN). Through dedicated observing strategies, CTA will also elucidate many aspects of the mysterious nature of gamma ray bursts (GRBs), the most

energetic explosions in the Universe. Detailed studies of both AGNs and GRBs can also reveal the origin of the highest energy cosmic rays in the Universe, probe the cosmic history of star formation including the very first stars, as well as provide high precision tests of theories of quantum gravity. Finally, CTA will search for signatures from elementary particles constituting dark matter with the highest sensitivity yet. Realization of the rich scientific potential of CTA is very much feasible, thanks to the positive experience gained from the current IACTs.

The CTA-Japan consortium [1] is aiming at contributing in particularly to the construction of the Large Size Telescopes (LSTs) and is involved in their development. The LST covers the low energy domain from 20GeV to 1000GeV and is especially important for studies of high redshift AGNs and GRBs. The diameter and area of the mirror are 23m and 400m^2, respectively, in order to achieve the lowest possible energy threshold of 20GeV. All optical elements/detectors require high specifications, for example, high reflectivity, high collection efficiency, high quantum efficiency and ultra fast digitization of signal, etc. For this purpose, CTA-Japan is developing high quantum efficiency photomultipliers, ultrafast readout electronics and high precision segmented mirrors. On the strength of their experience gained from construction of the MAGIC telescope, the Max-Planck-Institute for Physics in Munich is responsible for the design of the 23m diameter telescope structure, based on a carbon fiber tube space frame. The LSTs require very fast rotation (180 degrees/20seconds) for promptly observing GRBs. The first LST will be built in the CTA North, La Palma, Spain in 2016 and three more LSTs will be built during 2017 and 2020 in parallel with the construction of four more LSTs in the CTA South, ESO site in Paranal, Chile. The location of the LST array in the CTA North will overlap with MAGIC telescopes, which will allow us to operate CTA-LSTs and MAGIC telescopes together in the first phase of the construction.

The Cherenkov Cosmic Gamma Ray group is also operating the MAGIC Telescopes [9] on La Palma, Canary Islands. This facility is used not only for scientific observations but also for technological development toward the future observatory CTA.

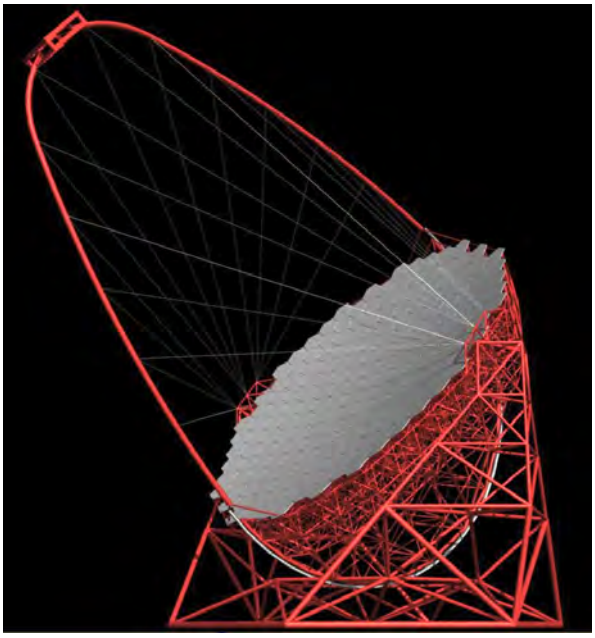

Fig. 2. Large Size Telescope (23m diameter) designed by Max–Planck-Institute for Physics. CTA Japan is contributing to the design and prototyping of the imaging camera at the focal plane, ultrafast readout electronics, and high precision segmented mirrors.

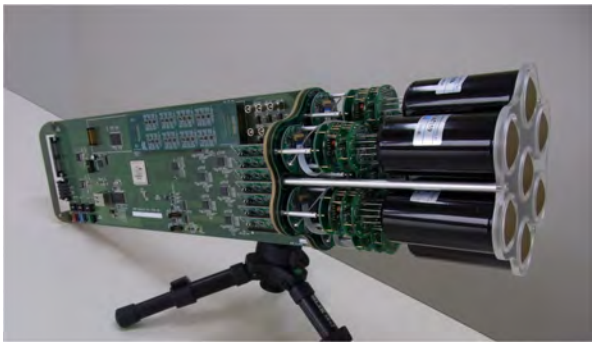

Fig. 3. Camera cluster for the Large Size Telescope (LST) developed by CTA-Japan. This cluster consists of seven high quantum efficiency photomultipliers (R11920-100), CW High Voltages, pre-amplifier, Slow Control Board, DRS4 Ultra fast waveform recording system and Trigger. The LST camera can be assembled with 265 of these clusters, cooling plates and camera housing.

Fig. 4. The high precision segmented mirrors for the Large Size Telescope (LST) developed by CTA-Japan in cooperation with Sanko Co.LTD. The mirror is made of a 60mm thick aluminum honeycomb sandwiched by 3mm thin glass on both sides. A surface protection coat consisting of the materials SiO2 and HfO2 is applied to enhance the reflectivity and to elongate the lifetime.

Bibliography

[1] CTA Consortium website: `http://www.cta-observatory.jp/` and `http://www.cta-observatory.org/`.

[2] The Cherenkov Telescope Array potential for the study of young supernova remnants, Astropart. Phys. 62 (2015) 152-164.

[3] Introducing the CTA concept, The CTA Consortium, Astropart. Phys. 43 (2013) 3-18.

[4] Gamma-ray burst science in the era of the Cherenkov Telescope Array, S. Inoue et al., Astropart. Phys. 43 (2013) 252-275.

[5] Design Concepts for The Cherenkov Telescope Array,

Fig. 5. MAGIC Stereo System with two Cherenkov telescopes of 17m diameters, so far achieved the threshold energy of 25GeV. It locates near the mountain top of the Roque de los Muchachos on the Canary Island of La Palma. Two telescopes are located with the distance of 85 meters.

Fig. 6. R & D system of 32 pixel imaging camera and electronics installed to the Akeno atmospheric Cherenkov telescope.

The CTA Consortium, Exper. Astron. 32 (2011) 193-316.

[6] Status of Very High Energy Gamma Ray Astronomy and Future Prospects, M. Teshima, The Astronomical Herald, 104 (2011) 333-342.

[7] Design Study of a CTA Large Size Telescope, Proc. of ICRC2012 at Beijing China, M. Teshima, arXiv:1111.2183.

[8] Introducing the CTA Concept, B. Acharya et al., Astroparticle Physics, 34 (2013) 3.

[9] MAGIC Collaboration website: `http://magic.mppmu.mpg.de/`.

MAGIC

The MAGIC Collaboration has built in 2002 / 2003 a first large atmospheric imaging Cherenkov telescope, MAGIC-I, with a mirror surface of 236 sq.m. and equipped with photomultiplier tubes of optimal efficiency. In 2009, a second telescope of essentially the same characteristics was added; MAGIC-II was installed at a distance of 85m from MAGIC-I. With the accent of these instruments on large mirror surface and best light collection, cosmic gamma-rays at an energy threshold lower than any existing or planned terrestrial gamma-ray telescope have become accessible. So far achieved has been a threshold of 25 GeV. The Japanese group has joined the MAGIC collaboration since 2010, and contributed to the operation, observations and data analysis. The MAGIC telescopes are upgraded with new cameras, electronics and partially new mirrors in 2012, and are now operated with an unprecedented sensitivity by an international collaboration of 17 institutes from 8 countries.

The recent highlights from MAGIC are, 1) the successful observation of pulsed gamma ray signal from the Crab pulsar up to TeV regime [1], 2) the discoveries of the most distant blazers 3S 0218 + 35 with the redshift of 0.944 [2] and PKS 1441 + 25 with the redshift of 0.939 [3], 3) the observation of the very fast flare of 1min time scale from the blazar inside Perseus cluster, IC310 [4]. These results brought new questions on the pulsar emission mechanism, the EBL energy density, and gamma ray emission mechanism from the supermassive blackholes or vicinity of them.

Bibliography

[1] Phase-resolved energy spectra of the Crab pulsar in the range of 50-400 GeV measured with the MAGIC telescopes, the MAGIC Collaboration, Aleksić et al. A&A 540 (2012) A69.

[2] ATEL 6349.

[3] ATEL 7416.

[4] Black hole lightning due to particle acceleration at subhorizon scales, the MAGIC collaboration, Science 346 (2014) 1080-1084.

Other Activities

As a test bench for domestic R & D activities of future ground-based gamma-ray observatory projects, a used atmospheric Cherenkov telescope of a 3 m diameter was obtained and placed at the Akeno Observatory in November 2010. This is currently the only atmospheric Cherenkov telescope located in Japan. In the fiscal year 2014, performance of the telescope optics realigned as a Davies-Cotton reflector in 2013 was measured using several bright stars. The size of the optical point spread function is 0.°06–0.°07 in standard deviation, which is sufficiently smaller than the pixel size of an R & D imaging camera system originally prepared for the Ten-Ten project[1, 2, 3], and installed to the telescope in March 2014 (Figure 6). We could successfully record 32 waveform data (1 GHz sampling) of the same LED flash with 32 pixels (PMTs) of the system, but still have some noise problem in the triggering system. Test observations of air-shower events are going to be carried out with the system after fixing the problem. The telescope will also be used for various field tests including test observations with some prototype imaging cameras for CTA.

Bibliography

[1] G. P. Rowell et al., Nucl. Instrum. Meth. A, **588**, 48–51 (2008).

[2] T. Yoshikoshi et al., Proc. of 32nd Internat. Cosmic Ray Conf. (Beijing), **9**, 226–229 (2011).

[3] M. Ohishi et al., Proc. of 33rd Internat. Cosmic Ray Conf. (Rio de Janeiro), 587 (2013).

TA: Telescope Array Experiment

[Spokespersons: H. Sagawa[1], G. B.Thomson[2]]

1 : ICRR, The Univ. of Tokyo, Kashiawa, Chiba 277-8582
2 : Dept. of Physics, University of Utah

Collaborating Institutions:

Chiba Univ., Chiba, Japan; Chubu Univ., Kasugai, Japan; Earthquake Research Institute, Univ. of Tokyo, Tokyo, Japan; Ehime Univ., Matsuyama, Japan; Ewha W. Univ., Seoul, Korea; Hiroshima City Univ., Hiroshima, Japan; Hanyang Univ., Seoul, Korea; ICRR, Univ. of Tokyo, Kashiwa, Japan; INR, Moscow, Russia; IPMU, Univ. of Tokyo, Kashiwa, Japan; Kanagawa Univ., Yokohama, Japan; KEK/ IPNS, Tsukuba, Japan; Kinki Univ., Higashi-Osaka, Japan; Kochi Univ., Kochi, Japan; Kyushu Univ., Fukuoka, Japan; Nat. Inst. of Rad. Sci., Chiba, Japan; Osaka City Univ., Osaka, Japan; RIKEN, Wako, Japan; Ritsumeikan Univ., Kusatsu, Japan; Rutgers Univ., Piscataway, NJ, USA; Saitama Univ., Saitama, Japan; Shinshu Univ., Nagano, Japan; Tokyo City Univ., Tokyo, Japan; Tokyo Inst. of Tech., Tokyo, Japan; Tokyo Univ. of Science, Noda, Japan; ULB, Brussels, Belgium; UNIST, Ulsan, Korea; Univ. of Utah, Salt Lake City, USA; Univ. of Yamanashi, Kofu, Japan; Waseda Univ., Tokyo, Japan; Yonsei Univ., Seoul, Korea

Overview and Status of TA and TALE

TA

The Telescope Array (TA) is the largest Ultra-High-Energy Cosmic-Ray (UHECR) observatory in the Northern Hemisphere, located in the West Desert in Utah, USA (latitude 39.3° N, longitude 112.9° W, altitude ∼1400 m) [1]. TA is designed to observe extensive air showers (EAS) induced by UHECRs with energies from about 10^{18} to $10^{20.5}$ eV, and measures the energy spectrum, mass composition, and arrival direction distribution of UHECRs, and searches for ultra-high-energy photon and neutrino primaries. The aim of these measurements is to explore the origin, propagation and interaction of UHECRs. The TA detector consists of an air shower surface detector (SD) array of plastic scintillation counters to measure the lateral distribution of secondary particles on the ground, and fluorescence detectors (FDs) to measure the longitudinal development of the EAS in the atmosphere. The SD array consists of 507 counters each with an area of 3 m^2, which were deployed on a square grid with 1.2-km spacing between each, covering an area of approximately 700 km^2. Three FD stations are located at the periphery, looking inward over the SD array. The Middle Drum (MD) FD site is located to the north of the SD array, and is instrumented with 14 refurbished telescopes that were used at the High-Resolution Fly's Eye (HiRes) [2]. The Black Rock Mesa (BRM) and Long Ridge (LR) FD sites are located to the southeast and southwest of the SD array, respectively. They are each instrumented with 12 new telescopes. The TA detector is operated by an international collaboration of researchers from Japan, the USA, Korea, Russia, and Belgium. Hybrid observations using both SDs and FDs commenced in March 2008.

TALE

The TA Low Energy Extension (TALE) enables detailed studies of the energy spectrum and composition from about 10^{16} eV upwards. Previous experiments reported the second knee in the cosmic-ray spectrum around the 10^{17}-eV decade. The energy scales of these detectors differed by about a factor of two, so the energy at which this spectral break occurred was quite uncertain. There is a possibility that the transition from galactic cosmic rays to extragalactic cosmic rays occurs in this energy region. Thus we expect to observe the transition from heavy to light composition. A 14-TeV center-of-mass collision at the LHC corresponds to a proton of about 10^{17} eV colliding with another proton at rest. The cosmic-ray data observed by the TALE could be compared with the air shower Monte Carlo (MC) simulation tuned by the results of the LHC experiments.

The TALE detector is located north of the TA site. Ten additional TALE FDs view 31°–59° in elevation angle, and have been operational using refurbished HiRes-II telescopes. The TALE infill SD array consists of approximately 100 plastic scintillation counters, which are identical to those of the TA SD array. These counters have graded spacings, ranging from 400 m near the FD to 600 m further away, which merge into the TA SD array with 1200-m spacing at its northwestern corner. The TALE FD operation was commenced in the spring of 2013. The 35 TALE surface detectors were deployed at that time, and 16 surface detectors are running.

Energy Spectrum

The energy spectrum for four years of the TA SD data with zenith angles less than 45 degrees has been published [3]. Here, we update the energy spectrum using the SD data for six years of observations from May 2008 to May 2014 with an exposure of ∼5400 km^2 sr yr. The MC data were generated by a CORSIKA air shower simulation with the QGSJET-II-03 model. A GEANT4 simulation was used for the detector simulation. We use the correlation of S_{800}, which is the charge density at a distance of 800 m from the shower core, and zenith angle with primary energy from the MC study for the first estimation of the cosmic-ray energy.

The energy scale uncertainty in the SD MC simulation can be large, mainly due to the modeling of hadronic interactions. The energy scale uncertainty is experimentally controlled by the FD, because the energy measurement is calorimetric. We correct our energy scale to the TA FD using events detected by both the FD and SD. The observed differences between the FD and SD events are well described by a simple proportionality relationship, where the SD energy must be reduced by 27% to agree with the FD energy.

The resulting cosmic-ray flux multiplied by E^3 is shown together with a broken power-law fit in Figure 7. We found the two breaks at $10^{18.70\pm0.02}$ eV and $10^{19.74\pm0.04}$ eV. These are consistent with the ankle and the GZK suppression [4, 5], respectively. We observed 32 events above the suppression, whereas a linear extrapolation of the power law below the

break predicts 85.9 events above the break. This result provides evidence for the flux suppression with a statistical significance of 6.59σ. The Auger spectrum after energy-scale shift by +10% agrees with the TA spectrum below $10^{19.4}$ eV, whereas the suppression points differ between the two spectra.

We check the compatibility of the measured TA energy spectrum with E $>10^{18.2}$ eV using a publicly available numerical code [6] to simulate the propagation and attenuation of protons by setting the injection spectral index (p for E^p), the source evolution (m for $(1+z)^m$) and energy scale as free parameters, where z is the red shift. We obtain the preliminary best fit $\chi^2/d.o.f.$ = 15.5/17 with $p = 2.16$, $m = 7.0$, and $\Delta\log E = -0.04$ for the isotropic model [7].

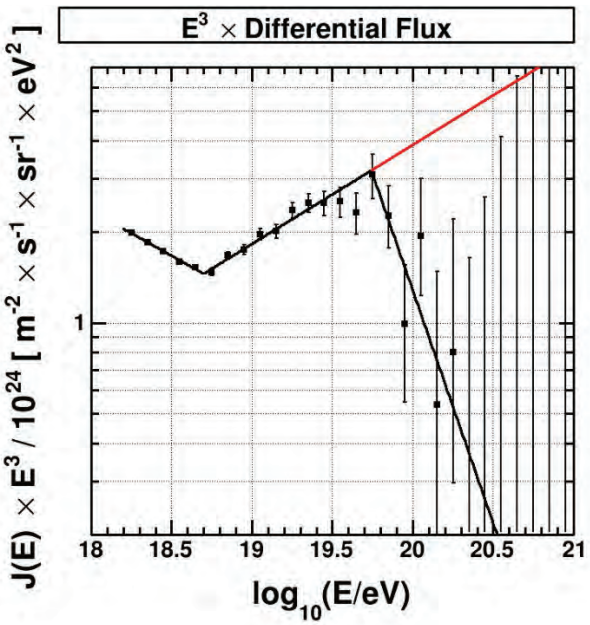

Fig. 7. The preliminary cosmic-ray flux multiplied by E^3 using six years of the TA surface-detector data. The solid line shows the fit of the TA data to a broken power law.

Figure 8 shows the energy spectrum using the TALE FD data and TA SD data. In the fluorescence detection observation, Cherenkov light produced in the air shower was considered to be a contamination to the fluorescence signal and events that had high fractions of Cherenkov light in the signals were discarded. The spectrum of events with energies above $10^{16.5}$ eV that are selected to dominate by scintillation light is shown by red filled circles. For the lower energies, the TALE FD is also sensitive to Cherenkov light. Low energy cosmic rays in the PeV energy range are detectable by the TALE as Cherenkov events. Using these events, we measured the energy spectrum of cosmic rays with energies from $10^{15.6}$ eV to $10^{17.2}$ eV as shown by red open squares. We see two clear breaks at around $10^{16.3}$ eV and $10^{17.3}$ eV.

Mass Composition

The dependence of shower maximum depth, $X_{\rm max}$, on the primary energy is used to determine the mass composition. The HiRes result is consistent with proton-dominated composition for E $> 10^{18}$ eV [8], whereas the Auger result is compatible with mixed composition [9].

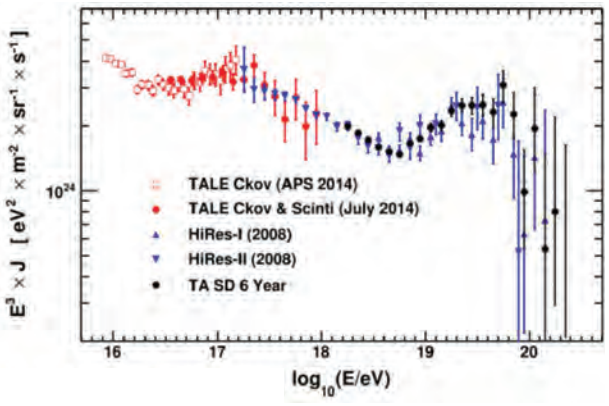

Fig. 8. The preliminary energy spectra using the TALE telescope data together with the HiRes (blue triangles) and TA SD (black circles) energy spectra. The TALE spectra using Cherenkov-light dominant analysis and fluorescence-light dominant analysis are denoted by red open squares and red closed circles, respectively.

The $X_{\rm max}$ result using the events observed with the MD FD and SDs (hybrid events) from May 2008 through May 2013 is presented [10]. The distribution of reconstructed $X_{\rm max}$ for the TA data is in agreement with the distribution of the QGSJET II-03 proton model in each energy range as shown in Figure 9. Here the $X_{\rm max}$ values include reconstruction and acceptance bias both for the TA data and MC simulation. The evolution of the average $X_{\rm max}$ with energy for the TA hybrid data is shown with the MC simulation in the energy range of $10^{18.2}$ to $10^{19.8}$ eV in Figure 10. The TA hybrid $X_{\rm max}$ result is in agreement with light, largely protonic, composition.

Anisotropy in Arrival Directions of UHECRs

We have published an analysis of UHECRs for correlations with Active Galactic Nuclei (AGNs), as well as for autocorrelations and correlations with the Large-Scale Structure (LSS) for a 40-month TA data set [11]. Here, we update the anisotropy results using the full six years of the TA data with zenith angles below 55° and a more relaxed border cut than the cut used for the measurement of the energy spectrum. The data set contains 2560 events with E $> 10^{19}$ eV, 164 events with E $> 4\times10^{19}$ eV, and 66 events with E $> 5.7\times10^{19}$ eV for the LSS correlations. There are 53 events with E $> 5.7\times10^{19}$ eV for zenith angles below 45° for AGN correlations [12].

Hotspot for highest-energy cosmic rays

We searched for intermediate-scale anisotropy of cosmic-ray events with energy greater than 5.7×10^{19} eV using five years of the TA SD data [13]. Here we use the event selection somewhat looser than the above analyses in order to increase the number of events with maintaining reasonable energy and angular resolution. By the looser cuts, of which major change is abolishing the cut of the SD array edge, we obtain 87 cosmic-ray events. Figure 11 (a) shows a sky map in equatorial coordinates of these events. A cluster of events that we call a "hotspot" appears in this map centered near right ascension $\sim$150° and declination $\sim$40°, with a diameter of $\sim$30° to 40°. In order to estimate the significance of this hotspot, we use oversampling with circles 20° in radius. Figure 11 (b) shows a pretrial significance map of the cosmic-ray

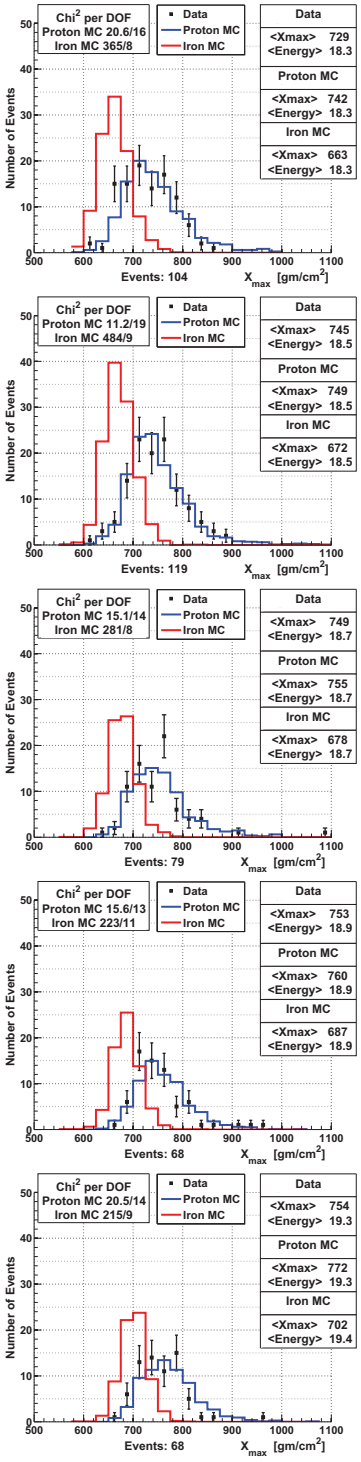

Fig. 9. The reconstructed $X_{\max}$ distributions for the TA hybrid data (points) with QGSJET II-03 MC simulation for five energy regions, of which powers are 18.2−18.4, 18.4−18.6, 18.6−18.8, 18.8−19.0, and > 19.0 from top to bottom panels. The blue and red histograms are the proton and iron predictions, respectively.

events with energies greater than 5.7×10^{19} eV using six years of the TA SD data. The maximum excess in our Field-of-View (FoV) appears as a hotspot centered at right ascension of 148.4° and declination of 44.5° with a statistical significance of 5.55σ (the number of observed events = 23, and the number of events expected in an isotropic cosmic-ray sky = 5.49). The probability of such a hotspot appearing by chance

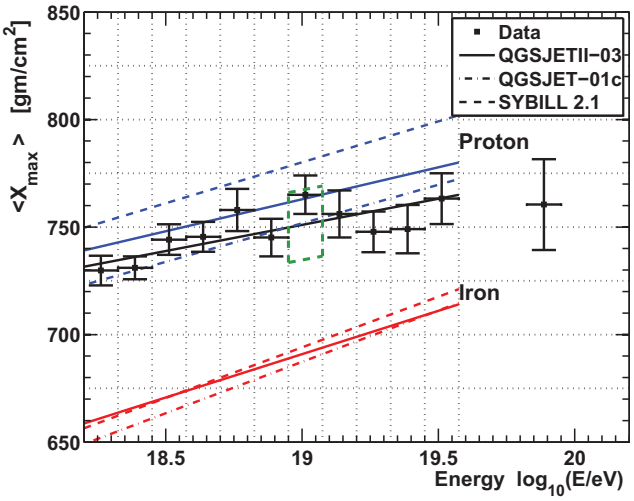

Fig. 10. The average reconstructed $X_{\max}$ (black points) as a function of energy for the TA hybrid data. The blue lines are the pure proton predictions with three interaction models: QGSJET-01c (dot-dash line), QGSJET II-03 (solid line), and SYBILL (dashed line). The red lines show the iron predictions. The green line shows the size of the systematic error of the average Xmax.

in an isotropic cosmic-ray sky is estimated to be 3.1×10^{-5} (4.0σ).

Correlations with AGNs

The Auger Collaboration reported correlations between the arrival directions of UHECRs with E > 5.7×10^{19} eV and the positions of nearby AGNs from the Véron 2006 catalog with $0< z \leq 0.018$ in 2007 [14]. The number of correlating events for angular separations of less than 3.1° was 8 out of 13, whereas 2.7 events were expected to correlate by chance for an isotropic distribution. The probability that the correlation occurred by chance was 1.7×10^{-3}. The Auger analysis has been updated, and it was found that the number of correlating events was 41 out of 146 above 5.3×10^{19} eV, which corresponds to about 28.1% of events, which was 2 standard deviation above an isotropic expectation [15].

We searched for AGN correlations using the same requirements as Auger, and found 21 correlating events (40%) out of 53 total events with E > 5.7×10^{19} eV . The number of random coincidences expected for this total number of events is 12.5. Using a binomial distribution with a single-event correlation probability of $p_{iso} = 0.24$, the probability of this excess occurring by chance is 0.7% (2.7σ), assuming an isotropic distribution.

Correlations with LSS

We use galaxies at distances of 5 to 250 Mpc and with Ks magnitudes of less than 12.5 in the 2MASS Galaxy Redshift Catalog (XSCz) [16]. This catalog provides the most accurate information about the three-dimensional distribution of galaxies. We assume that UHECRs are protons, and that the effects of galactic and extragalactic magnetic fields on each arrival direction can be approximated by a Gaussian probability density function with an angular resolution (called a smearing angle) of θ, which is treated as a free parameter. The data with E

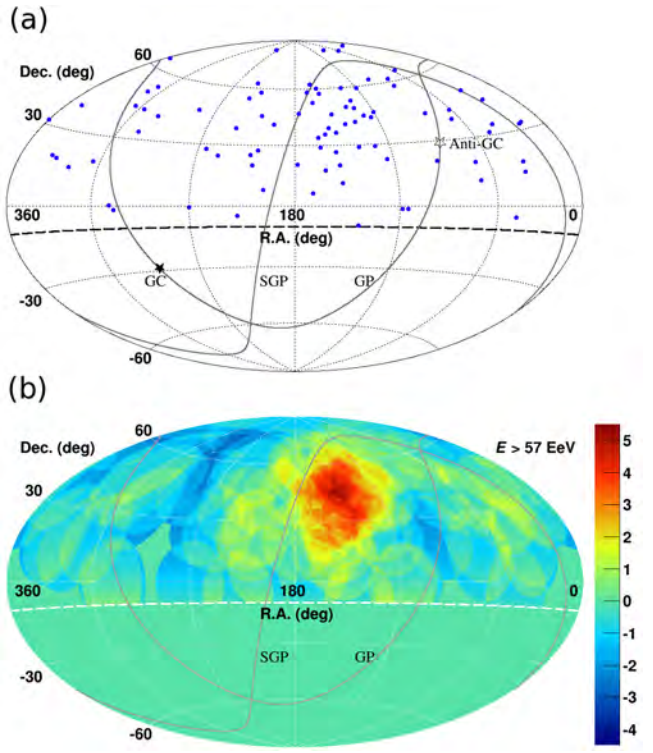

Fig. 11. Aitoff projection of the UHECR maps in the equatorial coordinates. The solid curves indicate the galactic plane (GP) and supergalactic plane (SGP). Our FoV is defined as the region above the dashed curve at declination of -10°. (a) The points show the directions of the UHECRs with $E > 5.7\times10^{19}$ eV observed by the TA SD array, and the closed and open stars indicate the Galactic center (GC) and the anti-Galactic center (Anti-GC), respectively. The line labelled SGP is the super-galactic plane, and the line labelled GP is the galactic plane. (b) Significance map using oversampling with circles 20° in radius. Color scale denotes significance value.

$> 5.7\times10^{19}$ eV is compatible with the LSS model, of which p-value is about 10%, and is incompatible with the isotropy model, of which p-value is about 0.1% at a smearing angle of 6°.

Search for point-like sources at around EeV

We search for steady point-like sources of neutral particles around EeV energy observed by the TA SD data between 2008 May and 2013 May [17]. The air-shower reconstruction and data selection are optimized for the EeV air showers. The number of air-shower events with E $>$ 0.5 EeV is increased by $\sim$10 times, which corresponds to 180,644 events, after the optimization. In order to search for the point-like sources, the Equi-Zenith Angle method was applied to these cosmic-ray air showers. As a result, we find no significant excess with E $>$ 0.5 EeV in the northern sky. Subsequently, we also searched for coincidence with the Fermi bright Galactic sources, and no significant coincidence was found within the statistical error. Hence, we set upper limits at 95% C.L. on the neutron flux, which is an averaged flux 0.07 km^{-2}yr^{-1} above 1 EeV in the northern sky. The upper limit at the 95% confidence level on the neutron flux from Cygnus X-3 is also set to 0.2 km^{2}yr^{-1} above 0.5 EeV. This is the most stringent flux upper limit in the northern sky survey assuming the point-like sources.

Prospects

We present preliminary results from the ELS, and outline the status of joint studies by the TA and Auger collaborations. We also describe the TA extension plans and R&D of future detectors.

The Electron Light Source (ELS): Measurement of Fluorescence Yield

The basic idea of the end-to-end calibration of the FD with the ELS, which is an electron linear accelerator in the TA site, is to compare measured ADC values with those from a MC simulation, and then correct the MC simulation for the difference from the data, which affects the energy scale. The beam energy is measured with an accuracy of less than 1% using a bending magnet. We worked for the precise measurement of the beam charge using a Faraday cup, and checked the relevant geometry with GEANT4 simulation. The first step of calibrating the TA FD using the ELS involves measuring the air fluorescence yield. This requires all of the FD calibration parameters. For this purpose, we select the following two air fluorescence models described.

The first model uses a fluorescence spectrum measured by the FLASH experiment [18] for 300–420 nm. The fluorescence yield integrated over 300–400 nm in the above-mentioned fluorescence spectrum is normalized to the yield measured by Kakimoto *et al.* [19]. This model is used in the analysis of air showers by the TA. The second is a combined model for air fluorescence yield [20] proposed by the dedicated working group of the UHECR2012 symposium [21]. This model adopts the fluorescence spectrum measured by AIRFLY. This spectrum is normalized for the air fluorescence yield at 337 nm measured by AIRFLY [22].

The air fluorescence yield was measured by comparing the ELS data with the MC simulation. The preliminary average fluorescence yield ratios of the data to the MC simulation for the first and second models were 1.257 and 1.003 with the total systematic uncertainty of 6.6% [23].

In addition, the ELS has been used by groups outside the TA collaboration from around the world to calibrate new detectors under development, and to search for radio signals from cosmic ray showers. Several groups are searching for molecular bremsstrahlung signals [24, 25] and radar echoes.

TA and Auger Joint Studies

The TA and Auger collaborations began a program of joint studies in order to understand the differences of the TA and Auger results for the energy spectra, $X_{\rm max}$, and arrival directions. The following progress reports were presented at UHECRC2014 [26]:

- High energy spectrum working group between the TA and Auger groups
  - After energy shift, the spectral slopes and the ankle energy are in a good agreement, but there is a flux difference at the highest energies.
- The TA and Auger anisotropy working group and the IceCube-TA-Auger anisotropy working group

  - A large-scale anisotropy result with full sky coverage using the TA and Auger data above 1×10^{19} eV was published by developing a method to combine the two data sets [27].

- High energy composition working group
  - The $X_{\rm max}$ analysis of ad hoc data that is compatible with the Auger composition model via TA reconstruction is being studied in order to know how well the TA detector distinguishes between the Auger mixed composition and protonic composition.

- TA muon project and Auger surface detector at the TA site
  - The number of muons observed in the Auger data is 1.8 times that of QGSJET II-03 simulation assuming proton primaries at 10^{19} eV. In order to make direct comparisons between the SD detection techniques used by Auger and TA, we deployed a water Cherenkov tank of the Auger North design at the TA Central Laser Facility, where the TA muon detector project consisting of scintillators with concrete blocks and the detector with a lead sheet sandwiched between two scintillator plates is also ongoing. We took data of one muon signals from Auger SD for calibration purpose and observed signals from Auger SD that coincided with the air-shower events observed by the TA surface detectors.

- FAST (the Fluorescence detector Array of Single-pixel Telescopes)
  - A Fluorescence detector Array of Single-pixel Telescopes (FAST) was proposed for large area and low-cost detection of ultra-high energy cosmic rays for the next generation of UHECR experiments [28]. The test of the FAST prototype was performed, and laser shots at distances of several kilometers as well as several UHECR shower candidates were detected.

TA Low Energy Extension

We saw two clear breaks at around $10^{16.3}$ eV and $10^{17.3}$ eV in the energy spectrum measured with the TALE FD as shown in Figure 8. It is of importance to measure $X_{\rm max}$ precisely adding timing information of surface detectors near the shower core on the ground. Therefore we proposed to complete the TALE surface detectors by adding remaining surface detectors.

We are also proposing the observation of cosmic rays with energies further down to 10^{15} eV, which we call the Non-Imaging CHErenkov (NICHE) array [29]. The plan is to install an array of simple Cherenkov counters of PMTs each three inches in diameter on the ground looking upwards, deployed with 100-, 200-, and 400-meter spacings within the TALE infill array We use counter timing to reconstruct the shower geometry, counter pulse heights to reconstruct the shower energy, and counter signal widths to reconstruct $X_{\rm max}$. The part of the NICHE with 15 PMTs that we call jNICHE was approved in Japan in 2014. It is being constructed. The full NICHE will be proposed to the NSF in the USA.

TA$\times$4 proposal

The TA confirmed the flux suppression consistent with the GZK cutoff at $10^{19.74}$ eV in the energy spectrum. The fit curve using extragalactic proton propagation corresponds well with the TA energy spectrum of cosmic rays with energies greater than $10^{18.2}$ eV. The TA found evidence for intermediate-scale anisotropy of the highest-energy cosmic rays ($E > 5.7\times10^{19}$ eV). The TA $X_{\rm max}$ result is consistent with light, largely protonic composition above $10^{18.2}$ eV although we need more statistics above $10^{19.5}$ eV. If the proton GZK exists, the sources of the highest-energy cosmic rays are expected to be restricted to nearby objects. If their sources are related to nearby matter distribution that is very anisotropic, we expect to observe anisotropy of the arrival directions of the highest-energy cosmic rays assuming their rectilinear propagation in the galactic and extragalactic magnetic field. Based on this picture, we propose the TA$\times$4, which will quadruple the TA aperture. We plan to install additional 500 counters of the current TA SD design, which will be deployed on a square grid with wider, 2.08-km spacing between each [30]. Including the existing TA SD array, we will extend the aperture of the surface detector array in total to approximately 3000 km^2. The new array would need two FDs overlooking it to increase the number of hybrid events for the confirmation of the energy scale and the measurement of $X_{\rm max}$. These FDs will be formed using additional refurbished HiRes telescopes. The layout of TA$\times$4 is shown in Figure 12. Assuming two-year construction and three-year observation for the additional SD array and FD and five-year observation by the current TA, we expect to have obtained in total the equivalent of 21 and 19 years of TA SD and hybrid exposures, respectively, by adding seven years of the TA data that have already been recorded. After five years, the recorded data will clarify anisotropy of arrival directions of highest-energy cosmic rays, which can be originated from the matter structure or extreme phenomena in the nearby universe, with a significance greater than 5σ if the correlation continues at the current level.

R&D for future detectors with larger aperture

To collect much better statistics at the highest energies, significantly larger detectors are needed to identify sources via anisotropy studies. Because of the prohibitive cost, it may be difficult to build a sufficiently large detector using existing technologies. Hence, it is important to explore new detection techniques.

It is advantageous that the FD on the ground detects air showers at a distance, but the FD has only a 10% duty cycle. Radio echoes from EASs have not been proven to be a successful technology. The TA RAdar Experiment (TARA) provides a controlled test of the bistatic radar technique, and is now operating a 40-kW transmitter at 54.1 MHz in the TA site, with receivers located 40 km away, west of the SD [31]. This project aims to look for coincidences between radar signals and either the SD or FD of TA.

The JEM-EUSO is a new type of observatory that will utilize very large volumes of the earth's atmosphere as a detector of the highest-energy cosmic rays in the Universe. It will be mounted to the International Space Station (ISS) at an al-

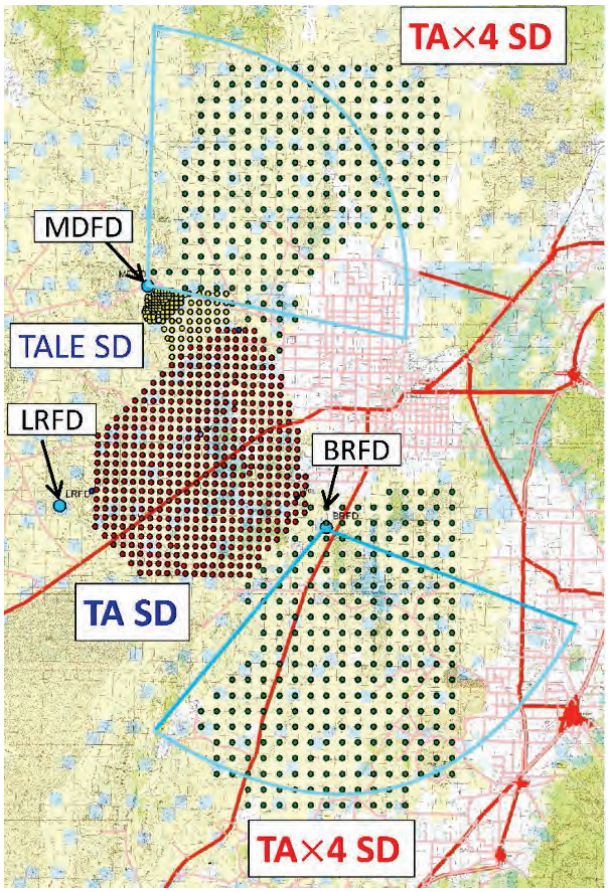

Fig. 12. The layout of the proposed TA×4. The array of 507 SDs (red filled circles on the left) is the current TA SD array. There are three TA FD stations (MD to the north, LR to the west, and BRM to the east of the TA array). The array of surface detectors to the north of the TA SD array is the TALE SD array. Additional two sub-arrays of 500 surface detectors in total (green filled circles) for TA×4 are located to the northeast and southeast of the TA SD array. Additional two FD stations with refurbished HiRes telescopes for the TA×4 are located at the MD and BRM FD sites and view to the northeast and southeast as denoted by the fans in light blue.

titude of approximately 400 km. The light sensor is a very wide-field, very fast, and large telescope, and observes brief UV flashes in the earth's atmosphere caused by the highest-energy cosmic rays. In ICRR, we set up the calibration system of Multi-Anode PMTs (MAPMT) which will be used at the focal surface detector of JEM-EUSO [32]. We calibrated MAPMTs for the EUSO prototype test at the TA site (EUSO-TA), which was resumed in February, 2015.

Summary

The TA confirmed the flux suppression above $10^{19.74}$ eV, which is consistent with the GZK suppression expected for protons, with a statistical significance of 6.59σ and the ankle at $10^{18.70}$ eV. The preliminary $X_{\rm max}$ measurement above $10^{18.2}$ eV is consistent with light, largely protonic composition although we need more statistics above $10^{19.5}$ eV. We found an indication of a cluster of cosmic rays with energy greater than 5.7×10^{19} eV by oversampling using 20°-radius circles. Its significance appearing in an isotropic cosmic-ray sky is 3.1×10^{-5} (4.0σ). Analyses of these highest-energy cosmic-ray arrival directions for correlations with AGNs, and correlations with the LSS proton model show a hint of anisotropy at a level of 2σ to 3σ.

The TA results suggest that anisotropy of arrival directions of highest-energy cosmic rays could be related to the matter distribution or extreme phenomena in the nearby universe. Therefore we propose the TA×4, which will quadruple the TA SD aperture and will add two FD stations. After five years, the TA×4 is expected to have obtained in total the equivalent to 21 years of TA SD data and 19 years of TA hybrid data by adding seven years of the TA data taken before the TA×4. The signal at a level of 3σ in the current anisotropy studies is expected to result in an observation at more than 5σ. And we will have more events for the measurement of energy spectrum and $X_{\rm max}$ at around or above the cutoff.

The TA, TALE, and the proposed TA×4 and NICHE will provide important measurements of the spectrum, composition, and anisotropy from the knee region up to the highest-energy region of over five to six decades in energy, with a single energy scale calibrated with the ELS.

For the future detectors with larger aperture, the R&D of a new technology investigating the detection of radio echoes from EASs (TARA), and the prototype test of the JEM-EUSO that will be the observation of extreme-energy cosmic rays in the space are been performed in the TA site. The calibration test of JEM-EUSO MAPMTs for the EUSO-TA was performed in ICRR, and the test at the TA site was resumed in February, 2015.

Bibliography

[1] K. Kawai *et al.*, J. Phys. Soc. Jpn. Suppl. A 78 (2009) 108.

[2] G. Thomson *et al.*, Nucl. Phys. B 36 (2004) 28.

[3] T. Abu-Zayyad *et al.*, Astrophys. J. Lett. 768 (2013) L1 (5pp).

[4] K. Greisen, Phys. Rev. Lett. 16 (1966) 748-750.

[5] G.T. Zatsepin and V.A. Kuz'min, JETP Lett. 4 (1966) 78-80.

[6] O.E. Kalashev and E. Kido, J. of Exp. and Theo. Phys. 120 (2015) 790-797.

[7] E Kido, Proc. of UHECR2014 (2014).

[8] R.U. Abbasi *et al.*, Phys. Rev. Lett. 104 (2010) 161101.

[9] A. Aab *et al.*, Astrophys. J. 794 (2014) 172 (15pp).

[10] R.U Abbasi *et al.*, Astropart. Phys. 64 (2015) 49-62.

[11] T. Abu-Zayyad *et al.*, Astrophys. J. 757 (2012) 26 (11pp).

[12] P. Tinyakov *et al.*, UHECR2014.

[13] R.U. Abbasi *et al.*, Astrophys. J. Lett. 790 (2014) 21.

[14] J. Abraham *et al.*, Science 318 (2007) 939; J. Abraham *et al.*, Astropart. Phys. 29 (2008) 188-204.

[15] A. Aab *et al.*, Astrophys. J. 804 (2015) 15.

[16] T. Jarrett, arXiv:astro-ph/0405069.

[17] R.U. Abbasi *et al.*, Astrophys. J. 804 (2015) 133.

[18] R. Abbasi *et al.*, Astrophys. J. 29 (2008) 77.

[19] F. Kakimoto *et al.*, Nucl. Instrum. and Meth. Phys. Res. A 372 (1996) 527.

[20] B. Keihauer *et al.*, arXiv:1210.1319.

[21] http://www.epj-conferences.org/index.php?option=com_toc&url/articles/epjconf/abs/2013/14/contents/contents.html

[22] M. Ave *et al.*, Astropart. Phys. 42 (2013) 90.

[23] B.K. Shin *et al.*, JPS 70th Annual Meeting (2015).

[24] R. Engel *et al.*, ICRC 2013, #1200.

[25] T. Yamamoto *et al.*, ICRC 2013, #1003.

[26] http://uhecr14.telescopearray.org/index.html

[27] A. Aab *et al.*, Astrophys. J. 794 (2014) 172.

[28] T. Fujii *et al.*, Proc. of UHECR 2014.

[29] D. Bergman *et al.*, Proc. of UHECR 2014.

[30] H. Sagawa *et al.*, Proc. of UHECR 2014.

[31] J. Belz *et al.*, Proc. of UHECR 2014.

[32] M. Casolino *et al.* Proc. of UHECR 2014.

Tibet ASγ Project

[Spokespersons : M. Takita]

ICRR, The Univ. of Tokyo, Kashiawa, Chiba 277-8582

Experiment

The Tibet air shower experiment has been successfully operated at Yangbajing (90°31' E, 30°06' N; 4300 m above sea level) in Tibet, China since 1990. It has continuously made a wide field-of-view (approximately 2 steradian) observation of cosmic rays and gamma rays in the northern sky.

The Tibet I array was constructed in 1990 and it was gradually upgraded to the Tibet II by 1994 which consisted of 185 fast-timing (FT) scintillation counters placed on a 15 m square grid covering 36,900 m^2, and 36 density (D) counters around the FT-counter array. Each counter has a plastic scintillator plate of 0.5 m^2 in area and 3 cm in thickness. All the FT counters are equipped with a fast-timing 2-inch-in-diameter photomultiplier tube (FT-PMT), and 52 out of 185 FT counters are also equipped with a wide dynamic range 1.5-inch-in-diameter PMT (D-PMT) by which we measure up to 500 particles which saturates FT-PMT output, and all the D-counters have a D-PMT. A 0.5 cm thick lead plate is put on the top of each counter in order to increase the counter sensitivity by converting gamma rays into electron-positron pairs in an electromagnetic shower. The mode energy of the triggered events in Tibet II is 10 TeV.

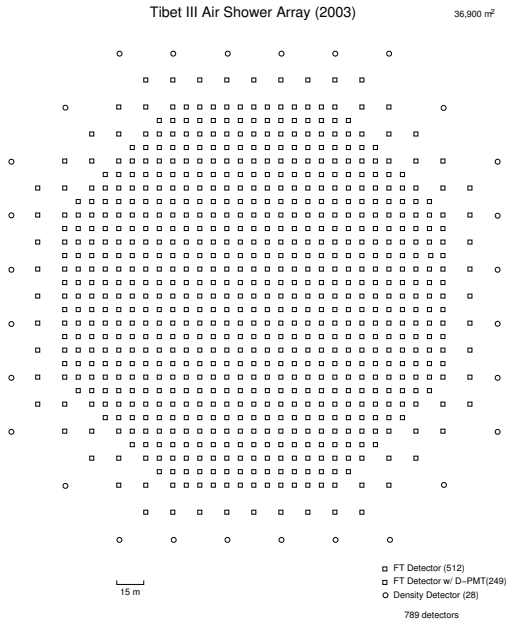

Fig. 13. Schematic view of Tibet III.

In 1996, we added 77 FT counters with a 7.5 m lattice interval to a 5,200 m^2 area inside the northern part of the Tibet II array. We called this high-density array Tibet HD. The mode energy of the triggered events in Tibet HD is a few TeV.

In the late fall of 1999, the array was further upgraded by adding 235 FT-counters so as to enlarge the high-density area from 5,200 m^2 to 22,050 m^2, and we call this array and further upgraded one Tibet III. In 2002, all of the 36,900 m^2 area was covered by the high-density array by adding 200 FT-counters more. Finally we set up 56 FT-counters around the 36,900 m^2 high density array and equipped 8 D-counters with FT-PMT in 2003. At present, the Tibet air shower array consists of 761 FT-counters (249 of which have a D-PMT) and 28 D-counters as in Fig. 13.

The performance of the Tibet air shower array has been well examined by observing the Moon's shadow (approximately 0.5 degrees in diameter) in cosmic rays. The deficit map of cosmic rays around the Moon demonstrates the angular resolution to be around 0.9° at a few TeV for the Tibet III array. The pointing error is estimated to be better than $\sim$0.01°, as shown in Fig. 14, by displacement of the shadow center from the apparent center in the north-south direction, as the east-west component of the geomagnetic field is very small at the experimental site. On the other hand, the shadow center displacement in the east-west direction due to the geomagnetic field enables us to spectroscopically estimate the energy

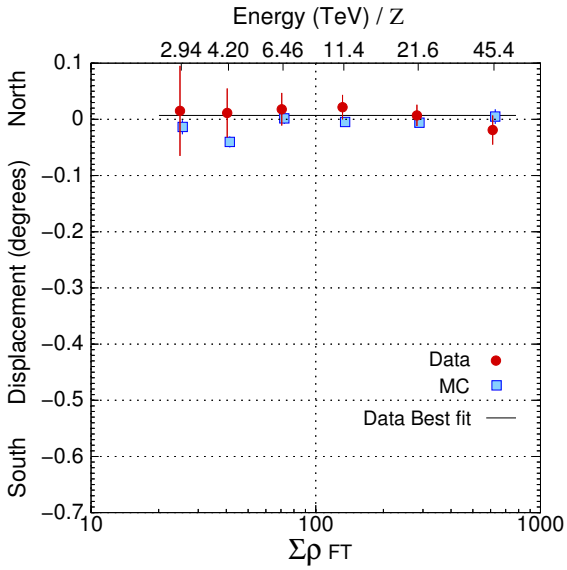

Fig. 14. From [1]. The Moon's shadow center displacement from the apparent position in the north-south direction as a function of energy, observed by Tibet III.

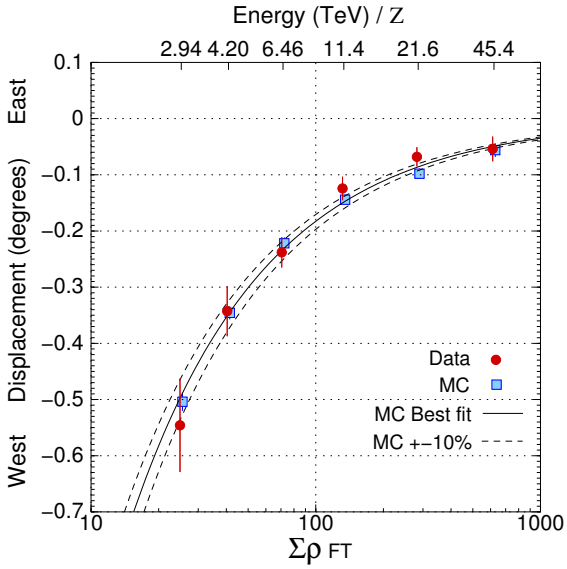

Fig. 15. From [1]. The Moon's shadow center displacement from the apparent position in the east-west direction as a function of energy, observed by Tibet III.

scale uncertainty at ±12 % level, as shown in Fig. 15. Thus, the Tibet air shower experiment introduces a new method for energy scale calibration other than the conventional estimation by the difference between the measured cosmic-ray flux by an air shower experiment and the higher-energy extrapolation of cosmic-ray flux measured by direct measurements by balloon-borne or satellite experiments.

Physics Results

Our current research theme is classified into 4 categories:

(1) TeV celestial gamma-ray point/diffuse sources,

(2) Chemical composition and energy spectrum of primary cosmic rays in the knee energy region,

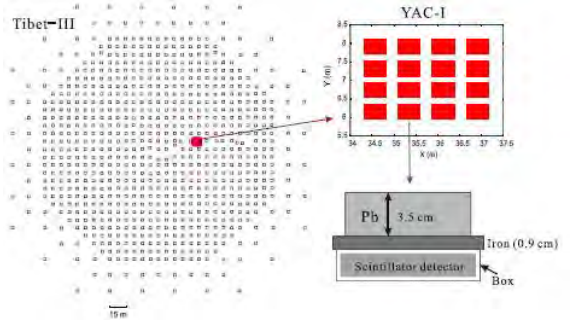

Fig. 16. From Ref. [2]. Schematic view of YAC-I.

(3) Cosmic-ray anisotropy in the multi-TeV region with high precision,

(4) Global 3-dimensional structure of the solar and interplanetary magnetic fields by observing the Sun's shadow in cosmic rays.

We will introduce a part of the results obtained in this fiscal year.

We have a plan to set up an air shower core detectors (Yangbajing Airshower Core detector array) around the center of the Tibet air shower array (TIbet-AS) to measure the energy spectra and chemical component of primary cosmic rays around the knee energy region. As the first step, we set up its prototype experiment (YAC-I) composed of 16 detectors in May 2009 as shown in Fig. 16, aiming at measuring the light elements.

The Tibet-AS and YAC-I has been jointly operated. We have made a detailed Monte Carlo simulation to estimate the sensitivity of the hybrid experiment Tibet-AS+YAC-I to the light elements of cosmic rays around the knee energy region. Various experimental conditions of Tibet-AS + YAC-I are taken into considerations in the Monte Carlo simulation. We extract light components from all-particle energy spectrum, by means of artificial neural network (ANN) method. Our Monte Carlo simulation demonstrates that the energy spectrum of the light component reconstructed by our method reproduces the input energy spectra within 10 % uncertainty as shown in Fig. 17 and that there is approximately 30 % systematic uncertainty arising from primary cosmic-ray energy spectrum models and hadronic interaction models in the Monte Carlo simulation. We find that the Tibet AS + YAC will be an important experiment in order to study the primary cosmic-ray composition, especially, to measure the energy spectra of light component (proton and helium) around the knee energy region.

Other Activities

The emulsion-pouring facilities can meet the demands for making any kind of nuclear emulsion plates which are used for cosmic ray or accelerator experiments. The thermostatic emulsion-processing facilities are operated in order to develop nuclear emulsion plates or X-ray films. Using these facilities, it is also possible to make and develop emulsion pellicles in 600-micron thickness each. In this way, these facilities have been open to all the qualified scientists who want to carry

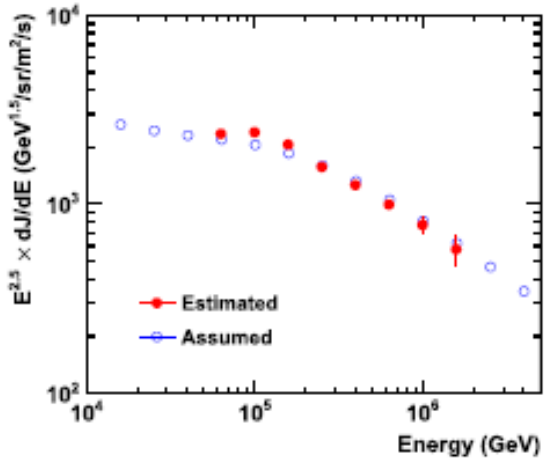

Fig. 17. From Ref. [2]. An example of reconstruction of energy spectrum of primary cosmic-ray proton + helium component by Tibet AS + YAC-I Monte Carlo simulation.

Fig. 18. YAC2 set up at Yangbajing.

out joint research programs successfully. Of recent, however, the shrinking demand for the facilities let us decide that we should suspend calls for joint research programs to utilize the emulsion-pouring facilities, starting from 2012.

Future Plans

(1)Chemical composition of primary cosmic rays making the knee in the all-particle energy spectrum

We have measured the energy spectra of primary cosmic-ray protons, helium, all particles around the knee energy region. The main component responsible for making the knee structure in the all particle energy spectrum is heavier nuclei than helium. The next step is to identify the chemical component making the knee in the all particle energy spectrum. We have a plan to install an Yangbajing Air shower Core detector array (YAC) around the center of Tibet III to distinguish the chemical component making the knee. We completed construction of YAC2 ($\sim$100 detectors over $\sim$160m^2 in area), as is shown in Fig. 18, and started data-taking in March 2013. YAC2 aims at mainly studying the energy spectra of proton and helium components in the knee energy region.

Currently, we are planning to set up YAC3 ($\sim$400 detectors over $\sim$5000m^2 in area) to measure the iron flux in the knee energy region.

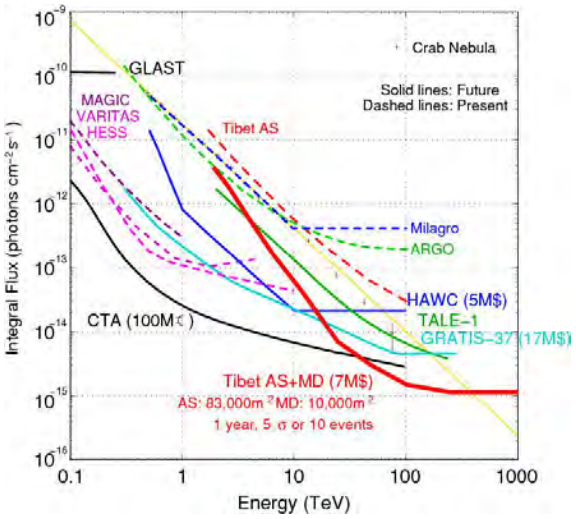

Fig. 19. Tibet AS + MD (red curve) integral flux sensitivity (5σ or 10 events/1yr) for a point source.

(2) Gamma-ray astronomy in the 100 TeV region

We have a plan[3] to construct a large ($\sim 10,000$ m$^2 \times$1.5m deep) underground ($\sim$ 2.5 m soil+concrete overburden) water Cherenkov muon detector array (Tibet MD) around an extended version (Tibet AS, $\sim$83,000 m^2) of Tibet III. By Tibet AS + MD, we aim at background-free detection of celestial point-source gamma rays in the 100 TeV region (10 TeV – 1000 TeV) with world-best sensitivity and at locating the origins of cosmic rays accelerated up to the knee energy region in the northern sky. The measurement of cut off energies in the energy spectra of such gamma rays in the 100 TeV region may contribute significantly to understanding of the cosmic-ray acceleration limit at SNRs. Search for extremely diffuse gamma-ray sources by Tibet AS + MD, for example, from the galactic plane or from the Cygnus region may be very intriguing as well. Above 100 TeV, the angular resolution of Tibet AS with 2-steradian wide field of view is 0.2° and the hadron rejection power of Tibet MD is 1/10000. The proposed Tibet AS + MD, demonstrated in Fig. 19, has the world-best sensitivity in the 100 TeV region, superior to HESS above 10-20 TeV and to CTA above 30-40 TeV.

In addition to unknown point-like sources, we expect to detect established sources in the 100 TeV region: TeV J2032 + 4130, HESS J1837-069, Crab, MGRO J2019+37, MGRO J1908+06, Milagro candidate sources, Mrk421, Mrk501 are sufficiently detectable and Cas A, HESS J1834-087,LS I+63 303, IC443 and M87 are marginal.

Furthermore, our integral flux sensitivity to diffuse gamma rays will be the world-best as well. The diffuse gamma rays from the Cygnus region reported by the Milagro group and also diffuse gamma-rays from the galactic plane will be clearly detected. Diffuse gamma-rays of extragalacitic origin may be an interesting target as well.

In fall, 2007, a prototype underground muon detector, com-

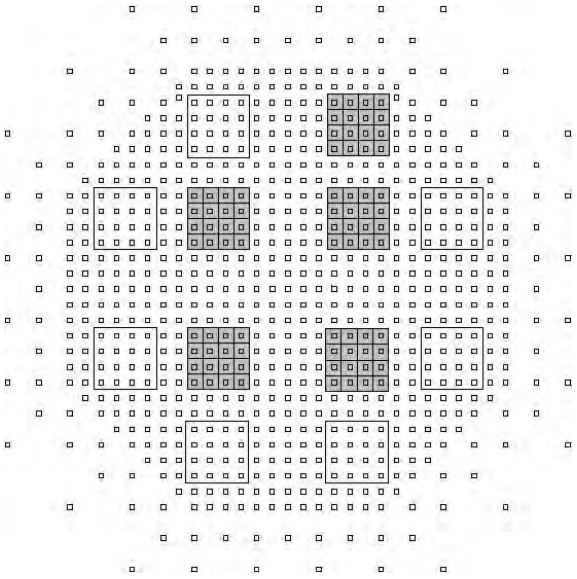

Fig. 20. The 5 shaded squares represent the constructed 5 MD pools.

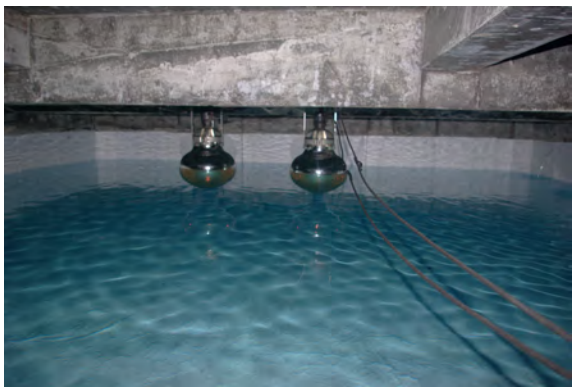

Fig. 21. PMTs mounted in a MD cell filled with water.

posed of two 52m^2 water pools, was successfully constructed in Tibet to demonstrate the technical feasibility, cost estimate, validity of our Monte Carlo simulation. Data analyses demonstrate that our MC simulation reproduces real data quite reasonably.

In March 2013, construction of 5/12 of the full-scale MD, as is shown in Fig. 20, was successfully completed and data-taking started. We have accumulated approximately one-year data. One of the detector cell filled with water is demonstrated in Fig. 21.

Development of Monte Carlo simulation is under way for comparison with real data. Various analysis tools are also extensively being developed. According to the simulation, the sensitivity of the current configuration (Tibe AS + 1/3 scale MD) is demonstrated in Fig. 22.

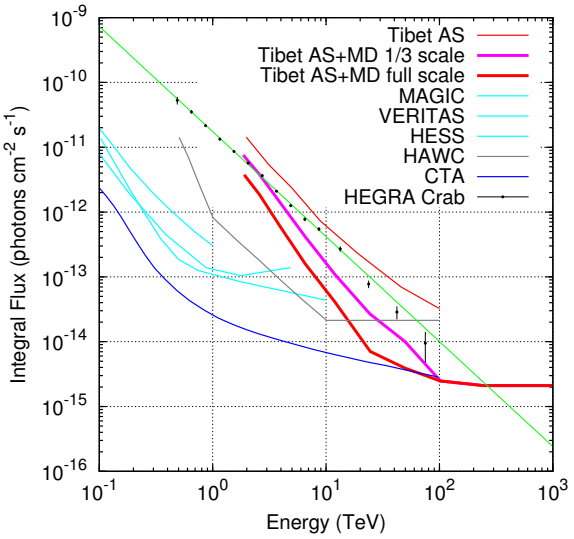

Fig. 22. Sensitivity to point-like gamma-ray sources with the current configuration (Tibet AS + 1/3 scale MD) by pink curve.

Bibliography

Papers in refereed journals

[1] "Multi-TeV Gamma-Ray Observation from the Crab Nebula Using the Tibet-III Air Shower Array Finely Tuned by the Cosmic-Ray Moon's Shadow", M. Amenomori *et al.*, Astrophysical Journal, **692** , 61-72 (2009).

[2] "Sensitivity of YAC to measure the light-component spectrum of primary cosmic rays at the 'knee' energies", L.M.. Zhai*et al.*, J. Phys. G. Nucl. Part. Phys., **42** , 045201 (1-14pp) (2015).

[3] "Exploration of a 100 TeV gamma-ray northern sky using the Tibet air-shower array combined with an underground water-Cherenkov muon-detector array", T.K. Sako *et al.*, Astroparticle Physics, **32** , 177-184 (2009).

The Tibet ASγ Collaboration

M. Amenomori,[1] X. J. Bi,[2] D. Chen,[3] T. L. Chen,[4] W. Y. Chen,[2] S. W. Cui,[5] Danzengluobu,[4] L. K. Ding,[2] C. F. Feng,[6] Zhaoyang Feng,[2] Z. Y. Feng,[7] Q. B. Gou,[2] Y. Q. Guo,[2] H. H. He,[2] Z. T. He,[5] K. Hibino,[8] N. Hotta,[9] Haibing Hu,[4] H. B. Hu,[2] J. Huang,[2] H. Y. Jia,[7] L. Jiang,[2] F. Kajino,[10] K. Kasahara,[11] Y. Katayose,[12] C. Kato,[13] K. Kawata,[14] M. Kozai,[13] Labaciren,[4] G. M. Le,[15] A. F. Li,[16,6,2] H. J. Li,[4] W. J. Li,[2,7] C. Liu,[2] J. S. Liu,[2] M. Y. Liu,[4] H. Lu,[2] X. R. Meng,[4] T. Miyazaki,[13] K. Mizutani,[11,17] K. Munakata,[13] T. Nakajima,[13] Y. Nakamura,[13] H. Nanjo,[1] M. Nishizawa,[18] T. Niwa,[13] M. Ohnishi,[14] I. Ohta,[19] S. Ozawa,[11] X. L. Qian,[6,2] X. B. Qu,[2] T. Saito,[20] T. Y. Saito,[21] M. Sakata,[10] T. K. Sako,[14] J. Shao,[2,6] M. Shibata,[12] A. Shiomi,[22] T. Shirai,[8] H. Sugimoto,[23] M. Takita,[14] Y. H. Tan,[2] N. Tateyama,[8] S. Torii,[11] H. Tsuchiya,[24] S. Udo,[8] H. Wang,[2] H. R. Wu,[2] L. Xue,[6] Y. Yamamoto,[10] K. Yamauchi,[12] Z. Yang,[2] S. Yasue,[25] A. F. Yuan,[4] T. Yuda,[14] L. M. Zhai,[2] H. M. Zhang,[2] J. L. Zhang,[2] X. Y. Zhang,[6] Y. Zhang,[2] Yi Zhang,[2] Ying Zhang,[2] Zhaxisangzhu,[4] X. X. Zhou[7]

[1]*Department of Physics, Hirosaki University, Hirosaki 036-8561, Japan*
[2]*Key Laboratory of Particle Astrophysics, Institute of High Energy Physics, Chinese Academy of Sciences, Beijing 100049, China*

[3]*National Astronomical Observatories, Chinese Academy of Sciences, Beijing 100012, China*
[4]*Department of Mathematics and Physics, Tibet University, Lhasa 850000, China*
[5]*Department of Physics, Hebei Normal University, Shijiazhuang 050016, China*
[6]*Department of Physics, Shandong University, Jinan 250100, China*
[7]*Institute of Modern Physics, SouthWest Jiaotong University, Chengdu 610031, China*
[8]*Faculty of Engineering, Kanagawa University, Yokohama 221-8686, Japan*
[9]*Faculty of Education, Utsunomiya University, Utsunomiya 321-8505, Japan*
[10]*Department of Physics, Konan University, Kobe 658-8501, Japan*
[11]*Research Institute for Science and Engineering, Waseda University, Tokyo 169-8555, Japan*
[12]*Faculty of Engineering, Yokohama National University, Yokohama 240-8501, Japan*
[13]*Department of Physics, Shinshu University, Matsumoto 390-8621, Japan*
[14]*Institute for Cosmic Ray Research, University of Tokyo, Kashiwa 277-8582, Japan*
[15]*National Center for Space Weather, China Meteorological Administration, Beijing 100081, China*
[16]*School of Information Science and Engineering, Shandong Agriculture University, Taian 271018, China*
[17]*Saitama University, Saitama 338-8570, Japan*
[18]*National Institute of Informatics, Tokyo 101-8430, Japan*
[19]*Sakushin Gakuin University, Utsunomiya 321-3295, Japan*
[20]*Tokyo Metropolitan College of Industrial Technology, Tokyo 116-8523, Japan*
[21]*Max-Planck-Institut für Physik, München D-80805, Deutschland*
[22]*College of Industrial Technology, Nihon University, Narashino 275-8576, Japan*
[23]*Shonan Institute of Technology, Fujisawa 251-8511, Japan*
[24]*Japan Atomic Energy Agency, Tokai-mura 319-1195, Japan*
[25]*School of General Education, Shinshu University, Matsumoto 390-8621, Japan*

High Energy Astrophysics Group

[Spokesperson: T. Terasawa]
ICRR, Univ. of Tokyo, Kashiwa, Chiba 277-8582

Overview

Since its creation in December 2009, the high energy astrophysics group has been making theoretical and observational studies of violent astrophysical phenomena in which nonthermal cosmic ray particles are being accelerated. In April 2013, new members, a research associate and a JPSP fellow, joined the group, who have been contributing to extend the group activity significantly. Targets of the group's study include high energy astrophysical objects such as supernova remnants/pulsar magnetospheres, giant flares and repeating bursts of magnetars, a giant galactic explosion called 'Fermi bubble', neutron star merger events, fast radio bursts (FRBs), jets from active galactic nuclei (AGN), as well as mysterious gamma ray bursts (GRBs). Research works on the origin of ultra high energy cosmic rays (UHECRs) are also within the coverage of the group.

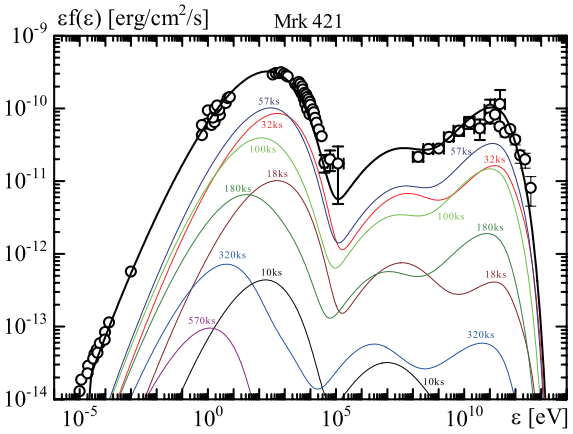

Fig. 23. Our model spectrum (thick black line) with the stochastic acceleration for the steady emission from blazar Mrk 421. The data points are taken from the data of the 4.5 month campaign (Abdo et al. 2011). Thin lines show the evolution of the photon spectrum emitted from one shell, neglecting the emission from the other shells. The steady spectrum can be interpreted as a superposition of those spectra. The time (ks) labeling each thin line is for observers at Earth.

Research topics: 1. Stochastic Acceleration in AGNs

The wide-band photon spectra of AGN jets are usually explained by synchrotron radiation (from radio to X-ray) and inverse Compton scattering (gamma-ray) by non-thermal electrons. Such high-energy electrons have been supposed to be accelerated via shocks in jets. To reproduce complex feature of photon spectra by such models, however, we need to assume broken power-law spectra for electrons at injection into the emission region. The break energies and power-law indices of the electron spectra seem to be determined ad hoc. There is no convictive model to explain such breaks in the electron spectra. Furtheremore, the maximum energy of electrons is far below the most optimistic prediction of the shock acceleration theory, which successfully agrees with observed electron spectra in young supernova remnants.

Alternatively, we consider a stochastic acceleration model, which is so called the 2nd order Fermi acceleration. In this process, electrons are scattered with turbulences, and and gain energy stochastically. This acceleration mechanism can produce harder electron spectra than the spectra the shock acceleration yields. We carry out time-dependent numerical simulations of the electron acceleration and photon emission in relativistic jets from AGNs. As shown in Figure 23, we succeed to reproduce the curved photon spectra of BL Lac object Mrk 421 by taking into account the temporal evolutions of the acceleration and injection.

We further consider the other possibility; the electron spectrum in the jet is in a steady state, in which the electron injec-

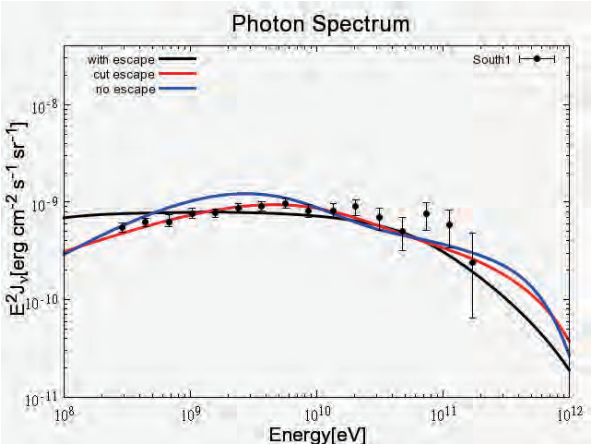

Fig. 24. Gamma-ray model spectra for the Fermi bubble with the data points. Electrons are stochastically accelerated by a turbulence, and emit gamma-rays via inverse Compton scattering with photons from CMB, dusts and stars. The evolution of the momentum diffusion coefficient is assumed to be the same as that in Mertsch and Sarkar (2011). The blue line shows the model without the escape effect. The other lines are the models with the escape effect, but in the red one emission from the escaped electrons is neglected. The emission from the escaped electrons significantly softens the low-energy spectrum (see black one).

tion, stochastic acceleration, escape and cooling are balancing each other. The results show very different acceleration and escape efficiencies from previous studies. The stochastic acceleration models for blazars may have wide variety. Now, we develop this model to adopt FSRQs, gamma-ray bursts, the Fermi bubble (see the next section), and pulsar wind nebulae.

Research topics: 2. Time and Space Dependent Stochastic Acceleration Model for the Fermi Bubbles

Fermi-LAT reveals two huge gamma-ray bubbles existing in the Galactic Center, called 'Fermi Bubbles'. The existence of two microwave bubbles at the same region are also reported by the observation by WMAP, dubbed 'WMAP haze'. In order to explain these components, It has been argued that the gamma-rays arise from Inverse-Compton scattering of relativistic electrons accelerated by plasma turbulence, and the microwaves are radiated by synchrotron radiation. But no previous research reproduces both the Fermi Bubbles and WMAP haze under typical magnetic fields in the galaxy.

We assume that shocks present in the bubbles and the efficiency of the acceleration by plasma turbulence, 'stochastic acceleration', changes with the distance from the shock front. The distance from the shock front increases with time, accordingly the efficiency of the acceleration changes with time. We also consider the time development of the electrons escape from the turbulence by diffusive loss. Our model succeeds to reproduce both the observed characteristics of the Fermi Bubbles and WMAP haze under typical magnetic fields (Figure 24).

Research topics: 3. Electromagnetic counterparts of neutron star merger events

The compact binary merger (CBM) is the most promising target for gravitational wave (GW) detectors. KAGRA, aLIGO and aVirgo, which will start observation until 2017, are expected to detect a few or a few tens CBM signals per year. However, several problems such as low S/N, uncertaintity in theoretical template of wave form, and low accuracy of source direction, are inherent in GW observation so that GW detection alone is not sufficient to identify the source. We therefore need follow-up observations of electromagnetic wave counterparts. One of counterparts is afterglow, whose theoretical details are important issues. The afterglow model has been refered from the theories of supernova remnant and gamma-ray burst. A fraction of binary mass is explosively ejected, and collide with the interstellar matter forming shock wave, where a magnetic field is amplified, and electrons are accelerated. Such non-thermal electrons emit electromagnetic waves from radio to gamma-ray via synchrotron and inverse Compton scattering. In the previous studies, theoretical formulations were based on non-relativistic approximation, and the temporal evolution of the electron energy distribution was not solved. Based on one-zone shell approximation, we solve the evolution of the blast wave from relativistic to non-relativistic periods with the energy conservation. We accurately compute the evolution of the electron energy distribution and emissions in the blast wave. Our results show frequency-dependent behaviour of the afterglow lightcurves, which are more complex than the previous predictions. Especially, the peak time of the radio afterglow (about 1-10yr) strongly depends on frequency and initial ejecta velocity. Those results will be tested future follow-up observations with SKA, Subaru, Chandra and so on.

Research topics: 4. pulsar wind properties

Pulsar winds are considered as relativistically moving electron-positron plasmas and are one of promising objects for the origin of cosmic ray positrons. Actually, high energy emissions from pulsars and their nebulae are unambiguous evidences that the pulsars are the generators of high energy electron-positron plasmas. However, because of extreme physical conditions of the pulsar magnetosphere, we have not fully understood the particle acceleration and creation processes around them. Induced Compton scattering off radio pulses of the pulsar by the pulsar wind plasmas has been considered to constrain the physical conditions of the pulsar wind. Because induced Compton scattering is a nonlinear interaction between intense electro-magnetic radiations and plasmas, it is known that there is a difficulty to treat the nonlinear regime of this process.

We propose a new approach to treat evolution of photon spectra affected by induced Compton scattering. Starting from the higher-order Kompaneets equation, we find a new equation that resolves the unphysical behavior of photon spectra. Figure 25 is simulated photon spectra with the use of our new approach. We find that photons rapidly lose their energy by induced Compton scattering with continuously forming solitary structures in frequency-space. The solitary structures have the logarithmically same width characterized by an electron temperature. Detections of these spectra in radio wavelength from pulsars would give us unique constraints on pulsar wind properties.

Research topics: 5. Observational study of the Crab pul-

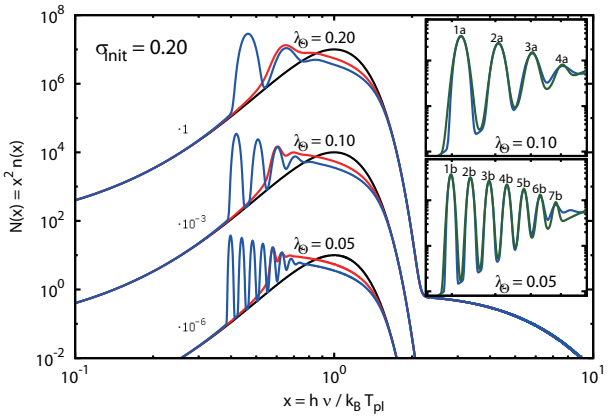

Fig. 25. Numerical calculations of photon spectra affected by induced Compton scattering. Horizontal axis is normalized photon frequency and vertical axis is normalized photon number. Three calculations whose electron temperatures are different from each other are plotted. Initial spectra that are not affected by induced Compton scattering are black lines and the spectra evolve from red to blue lines. Induced Compton scattering creats solitary structures of a logarithmic width on the spectra and the width is large for the scattering by hot electrons, i.e., the uppermost lines labeled as $\lambda_\Theta = 0.20$ have the largest electron temperature. Insets are zoom of solitary structures.

Table 1. Multi-frequency observation of the Crab pulsar.

ID†	UHF 325 MHz	L 1.6 GHz	S 2.2 GHz	C 6.7 GHz	X 8.4 GHz
Itt	◯				
Kas		◯			
Usd			◯		◯
Miz				◯	
Tkg				◯	
Ymg					◯

† Observatory IDs, Itt: Iitate, Kas: Kashima, Usd: Usuda, Miz: Mizusawa, Tkg: Takahagi, Ymg: Yamaguchi.

sar

Crab pulsar, the remnant of the supernova explosion in 1054 A.D., is one of the most studied neutron stars. While its physical properties have been investigated for more than 40 years since its discovery, there remains an enigma about the origin of giant radio pulses (GRPs). Considering their importance, we have been conducting observational studies of Crab's GRP since 2009 in close collaboration with radio astronomers in Japan. In 2014, we made a campaign of multi-frequency observations of the Crab pulsar from UHF (325MHz) to X (8GHz), providing one of the widest frequency coverage as simultaneous Crab pulsar observations ever done (Table 1).

From these observations, we found that the majority of GRPs have frequency spectra not inconsistent with a single power-law, an finding important for the future theoretical consideration of the GRP origin. Figure26 shows an example of a wide band spectrum of a Crab GRP, simultaneously detected at Iitate (325Hz), Kashima (1.6 GHz), Usuda (2.2 GHz, 8.4 GHz) and Takahagi (6.7 GHz) during 01:32:49-51 UTC on 7 September 2014[1].

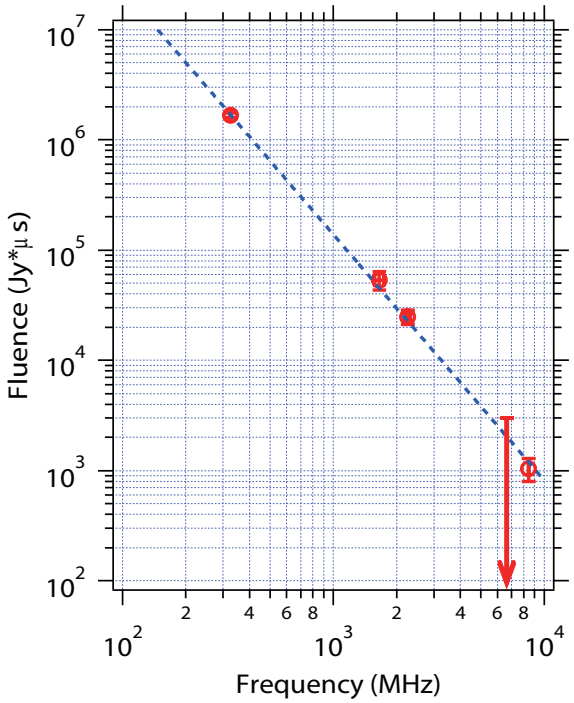

Fig. 26. Wide frequency spectrum of a Crab GRP on 7 September 2014. Time-integrated flux density (fluence) spectrum of the GRP is shown. Blue dotted line is best-fit line for the data points, $\propto \nu^{-2.23}$. Calculated χ^2/(degree of freedom) is ~ 0.48, not inconsistent with a single power-law at a confidence level of 95%.

Research topics: 6. CALET project — a R/D study

CALET, CALorimetric Electron Telescope (Figure 27), is a new mission for the Japanese Experiment Module-Exposed Facility (JEM-EF) on the International Space Station. The CALET mission aims at revealing unsolved problems in high energy phenomena of the Universe by carrying out accurate measurements of high energy spectra of electrons, gamma-rays and nuclei. The instrument will be flown in JFY 2015, and is scheduled to be operated for five years. Major scientific objectives are to search nearby cosmic ray sources and dark matter signatures by carrying out accurate measurements of cosmic ray electrons in 1 GeV - 20 TeV and gamma-rays in 4 GeV - 10 TeV. Since proton background is very large, high proton rejection power is mandatory for high energy electron and gamma-ray measurements. CALET has an imaging and deep calorimeter with 30 X_0 for electromagnetic particles, which provides high proton rejection and excellent energy resolution. We have been carrying out Monte Carlo simulations to study the detector performance and acceleration beam tests at CERN-SPS to assess the validity of our simulations. We have presented measured performance of particle identification such as electron/proton separation and electron/gamma-ray separation compared to the simulation results, and expected spectra of electron and gamma-ray observed by CALET.

*[1] The interstellar group delay caused ~ 2 sec difference in pulse arrival times between the highest (Usuda, 8.4GHz, earliest) and lowest (Iitate, latest) frequencies.

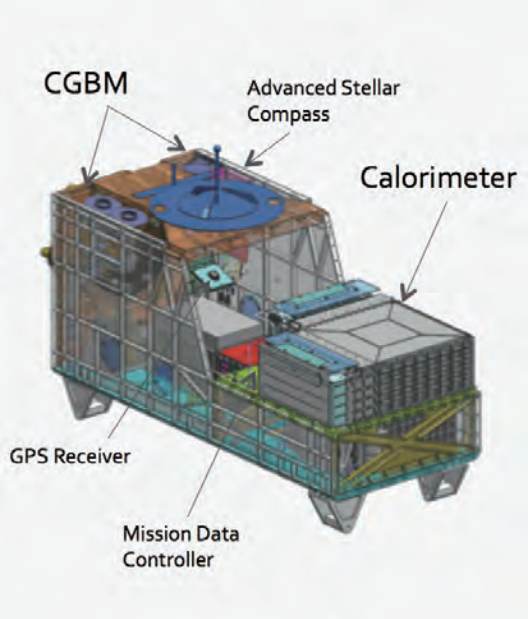

Fig. 27. The outlook of the CALET, CALorimetric Electron Telescope, to be installed on the International Space Station in JFY 2015.

Bibliography

Papers in refereed journals

1. Asano, K., P. Meszaros, "Neutrino and Cosmic-Ray Release from Gamma-Ray Bursts: Time-Dependent Simulations", Astrophys. J., 785, 54.1-5 (2014).

2. Kakuwa, J., K. Toma, K. Asano, M. Kusunose, and F. Takahara, "Synchrotron Self-Compton Emission by Relativistic Electrons under Stochastic Acceleration: Application to Mrk 421 and Mrk 501", Mon. Not. R. Astron. Soc., 449, 551-558 (2015).

3. Kisaka, S., and S. J. Tanaka, "Synchrotron X-ray emission from old pulsars", Mon. Not. R. Astron. Soc. 443, 2063-2076 (2014).

4. Niita, T., S. Torii, K. Kasahara, H. Murakami, S. Ozawa, Y. Ueyama, Y. Akaike, T. Tamura, K. Yoshida, Y. Katayose, Y. Shimizu, and H. Fuke, "A balloon experiment using CALET prototype (bCALET-2)", Adv. Space Res., 55, 753-760 (2015).

5. Takamoto, M., S. Kisaka, T. Suzuki, and T. Terasawa, "The Evolution of High Temperature Plasma in Magnetar Magnetospheres and its Implications for Giant Flares", Astrophys. J. 787, 84.1-13, (2014).

Thesis

6. Sasaki, K., "Stochastic particle acceleration and emission from the Fermi bubbles", Master thesis (in Japanese), Department of Physics, University of Tokyo, March 2015.

7. To, S., "Non-thermal emission from coalescence of compact binary stars", Master thesis (in Japanese), Department of Physics, University of Tokyo, March 2015.

Conference papers

8. Akaike, Y., and CALET collaboration, "Performance of particle identification with the CALET calorimeter expected by CERN-SPS beam tests", 40th COSPAR Scientific Assembly, 2-10 August 2014, Moscow, Russia, Abstract E1.6-88-14.

9. Asano, K., F. Takahara, K. Toma, M. Kusunose, J. Kakuwa, "Second-Order Fermi Acceleration and Emission in Blazar Jets", 40th COSPAR Scientific Assembly, 2-10 August 2014, Moscow, Russia Abstract E1.5-13-14.

10. Takamoto, M., T. Terasawa, S. Kisaka, T. Suzuki, "Evolution of Hot Plasma in Magnetar Magnetospheres and its Implications for Initial Spikes of Giant Flares", 40th COSPAR Scientific Assembly. Held 2-10 August 2014, Moscow, Russia, Abstract E1.12-13-14.

11. Tanaka, S. J., "Spectral Model of Wind Nebulae Powered by a Magnetar", 40th COSPAR Scientific Assembly, 2-10 August 2014, Moscow, Russia, Abstract E1.16-38-14.

12. Sasaki, K., K. Asano, T. Terasawa, "Time and Space Dependent Stochastic Acceleration Model for the Fermi Bubbles", 2014 Fermi Symposium, 20-24 October 2014, Nagoya, Japan, eConf C14102.1.

Other Activities

Ashra NTA

[Spokesperson: Makoto Sasaki]

ICRR, Univ. of Tokyo, Kashiwa, Chiba 277-8582

Astronomy to ν&γ-Astronomy:

IceCube announced three PeV scale astrophysical neutrino events [1]. What if one had better *sensitivity* and accurate *pointing* information? Astronomical high-energy νs should be produced at the accelerators through charged pion production in collisions with radiation fields or the ambient matter, in reactions such as: $p+\gamma \rightarrow \Delta^{+} \rightarrow \pi^{0}+p,\ \pi^{+}+n; p+$ nucleus $\rightarrow \pi^{\pm,0}+X$. The discovery of the proton accelerators in the Universe is just revealing the above particle reaction processes around the acceleration sites. The secondary PeV-EeV νs are the direct evidence of the acceleration and must point to the accelerators. The secondary γ rays produced from the π^0 could also indicate the evidence and give direction, but we must distinguish them from γ rays generated through the inverse-Compton process. The detection of both particles would be fascinating, as it would explore the accelerators in the Universe in the context of "multi-particle" approach [2], which can be performed by Ashra NTA with the same one detector system. For many astronomical objects, ambient photons are expected to be in the UV region. The kinetic threshold for photopion production through delta resonance corresponds to several PeV.

Earth-skimming ν_τ Method:

The Earth-skimming tau ν technique enjoys a large target mass by detecting extensive air-showers produced by tau lepton decays in the atmosphere. The tau leptons, produced by VHE tau νs that interact with the Earth matter they traverse, emerge out of a mountain or the ground facing the detector. This method has detection sensitivity in the PeV-EeV region, and can be used to search for νs originating from hadron acceleration in astronomical objects. Additional advantages are perfect shielding of cosmic ray secondaries, precise arrival direction determination, and negligible background from atmospheric νs [3].

Ashra-1 and 1st Search for GRB ν_τ:

Ashra [4] Phase I, or Ashra-1 was developed with the aim of "multi-particle" astronomy [2], i.e. optimized for the detection of VHE particles.

Starting from an optical system with 42° field-of-view (FOV), the Ashra-1 Light Collector (LC) has total resolution of ~ 3 arcmin., and can cover Mauna Kea surface at 35 km distance from Mauna Loa. Combined with a high resolution imaging system with trigger, very cost-effective pixels compared with conventional PMT arrays are achieved. With each of its 12 Detector Units (DU) consisting of several aligned LCs, Ashra-1 can observe the entire sky with arcminute resolution.

The key technical feature is the use of electrostatic rather than optical lenses to generate convergent beams (the 20 inch Photoelectric Lens Image, or PLI tube [5], the world's largest image intensifier), demagnifying to 1 inch at focal surface, enabling high resolution over a wide FOV. The electron optics of photoelectric lens imaging links wide angle precision optics [6], with improved quantum efficiency and precision, to the image pipeline [7]. The Photoelectric Image Pipeline (PIP) splits the focal image into trigger/image capture devices after amplification, sending the same fine image to multiple triggers. This allows the simultaneous measurement of three phenomena on different time scales, i.e. Cherenkov emission (ns), fluorescence (μs), and starlight (s), without sacrificing the S/N ratio.

The demonstration phase has been running since 2008 at the Mauna Loa Observation Site (ML-OS) at 3300 m above sea level on Hawaii Big Island, with 77% mono and 27% stereo. With alert for GRB081203A given by SWIFT satellite, Ashra-1 succeeded in the first search for PeV-EeV ν_τs originating from a GRB [8] with the Earth-skimming ν_τ technique using one LC, setting stringent limits. Moreover, Ashra-1 has achieved the best-yet instantaneous sensitivity in the 100 PeV energy region subsequent to a January 2012 trigger upgrade.

Neutrino Telescope Array (NTA):

Based on Ashra-1 performance, we aim at forming a new collaboration, NTA an air shower imaging $\nu\&\gamma$ detector for the aim/scientific goal [9]: Clear Discovery and Identification of Nonthermal Hadronic Processes in the Universe, be it Galactic, Extragalatic, or Cosmogenic. As stated in Prologue, stimulation has come from the IceCube experiment, which has recently reported [1] the "first indication of an astrophysical ν flux". They observe three fully contained ν-induced particle showers with deposited energy $\sim$ 1–2 PeV, which provides great motivation for exploring the PeV-EeV region. *"What if one had better Sensitivity and accurate Pointing?"* With much better than 0.2° pointing accuracy, NTA would be able to discern the origins of such events.

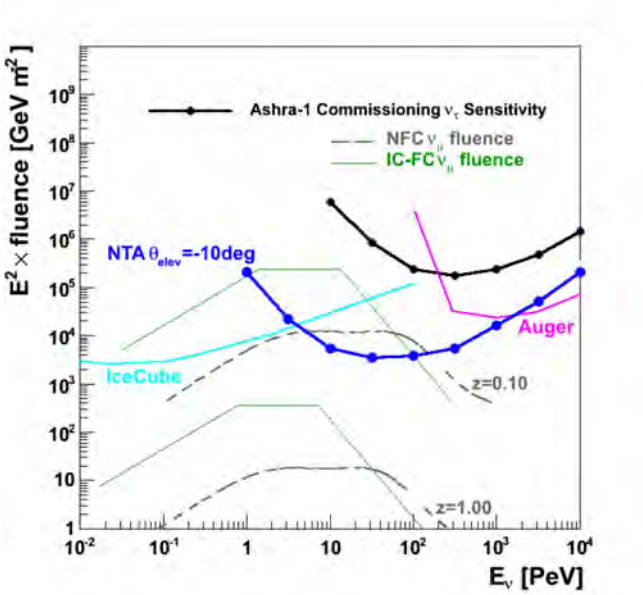

Fig. 28. Differential sensitivities calculated as Feldman-Cousins 90% CL limit for various LC designs and $\theta_{\rm elev} = -10°$, in comparison with (earlier) ones of IceCube and Auger, together with theoretical models (dashed lines for Ref. [11]).

From the detailed studies with three stages for the simulation: (1) $\nu_\tau \to \tau$ conversion in the earth; (2) τ shower development; (3) detector performance, we evaluate the arrival direction of PeV-scale ν_τs to be within 0.1° of the original direction of the generated air-shower [9, 10]. This means NTA can point ν_τ sources with much better accuracy than 0.2° even if taking into account systematics. The accurate reconstruction of arrival direction by means of fine imaging will be a very powerful technique in the determination of point sources of PeV ν_τs. We show on right side of Fig. 28 the differential sensitivity for NTA, compared side by side with IceCube and Auger capabilities (for illustration only). The solid theoretical fluence curve is ruled out by IceCube, but subsequent models for GRB ν flux, e.g. Ref. [11], can be probed by NTA. Given the PeV neuntrino events observed by IceCube, this search is now mandatory. The power of NTA is to survey ν_τ point source objects with the best-yet sensitivity in the detection solid angle for ν_τ defined as $-30° < \theta_{\rm elev} < 0°$ and $0° < \phi_{\rm azi} < 360°$, and for 10 PeV $< E_{\nu_\tau} <$ 1 EeV. Fig. 28 (right) shows that the NTA survey depth can reach $z < 0.15$, of order 600 Mpc. The location of NTA on Hawaii Big Island allows us to survey the Galactic Center (GC) for more than several hundred hours each year, assuming the standard 10–20% duty cycle. We refer further on angular resolution and background simulation to the LOI [9].

Epilogue:

There is an ongoing list of experiments aiming for this "grail": ANITA, ARA, etc. There were worries in "CR Composition" raised by Auger [12], suggesting the CR composition moves away from protons towards iron, starting $\sim 10^{18.6}$ eV. This would deplete the expected GZK flux.

With the GZK ν in backdrop, we assert that the scientific

goal of: "*Clear Discovery and Identification of Nonthermal Hadronic Processes in the Universe, be it Galactic, Extragalatic, or Cosmogenic*." is reachable, and in view of the IceCube PeV astro-ν events, it has become mandatory. A Collaboration, the NTA, is needed to achieve this. Once we succeed in pinning down the PeV ν sources, we will start a full-fledged "multi-particle" approach [2], both with PeV-EeV νs and TeV-PeV γs by using the advantage of Ashra NTA, which could reveal violations of fundamental physics lows, e.g. Super-cutoff γ-rays, Lorentz Invariance, and so on. In that case, the extremely high energy (EHE; PeV or above) Universe will become a new testing laboratory for the EHE particle physics and astronomy.

Bibliography

[1] M. Aartsen *et al.*, PRL **113**, 101101 (2014).

[2] M. Sasaki, ICRR2000 Sat. Sympo., 109 (2000).

[3] M. Sasaki, *et al.*, Astropart. Phys. **19**, 37 (2003).

[4] M. Sasaki, Prog. Theoret. Phys. Suppl. **151**, 192 (2003).

[5] Y. Asaoka and M. Sasaki, NIMA **647**,34 (2011).

[6] M. Sasaki, *et al.*, NIMA **492**, 49 (2002).

[7] M. Sasaki *et al.*, NIMA **501**, 359 (2003).

[8] Y. Aita *et al.*, ApJ Lett. **736**, L12 (2011).

[9] M. Sasaki and G. Hou, arXiv:1408.6244 (2014).

[10] Y. Asaoka and M. Sasaki, Astropart. Phys. **41**, 7 (2013).

[11] S. Hümmer, *et al.*, PRL **108**, 231101 (2012).

[12] J. Abraham *et al.*, PRL **104**, 091101 (2010).

γI ***Project***

γI Consortium
[Spokesperson : R.Enomoto]

Collaboration list:
Institute for Cosmic Ray Research, The University of Tokyo, Chiba, Japan; Faculty of Science, Ibaraki University, Ibaraki, Japan; Faculty of Medical Engineering and Technology, Kitasato University, Kanagawa, Japan;

γI Project

We have developed a novel low-cost gamma-ray imaging Compton camera [1] γI that has a high detection efficiency [2]. Our motivation for the development of this detector was to measure the arrival directions of gamma rays produced by radioactive nuclides that were released by the Fukushima Daiichi nuclear power plant accident in 2011. The detector comprises two arrays of inorganic scintillation detectors as shown in Fig.29, which act as a scatterer and an absorber as shown in Fig.30. Each array has eight scintillation detectors, each comprising a large CsI (Tl) scintillator cube of side 3.5 cm,

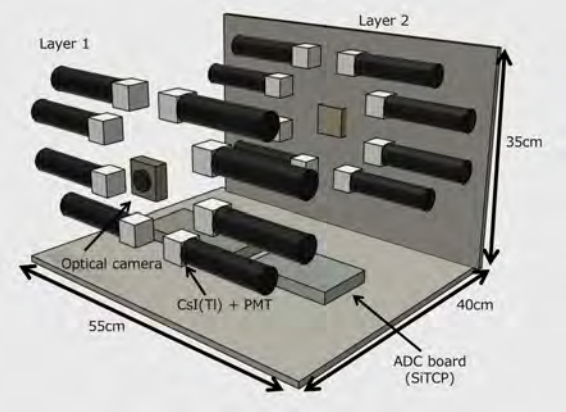

Fig. 29. A schematic view of γI.

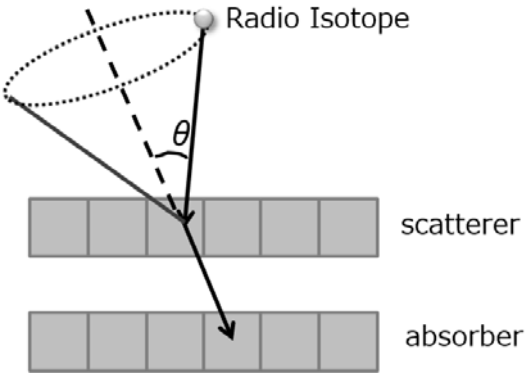

Fig. 30. Conceptual design of the Compton camera conprizing a scatterer and an absorber.

which is inexpensive and has a good energy resolution. Energies deposited by the Compton scattered electrons and subsequent photoelectric absorption, measured by each scintillation counter, are used for image reconstruction. Compton kinematics allows us to calculate the scattering angle of the incoming gamma ray as follows:

$$\cos\theta = 1 - m_e c^2 \left(\frac{1}{E_2} - \frac{1}{E_1 + E_2} \right), \qquad (1)$$

where E_1, E_2, θ, m_e, and c denote the energy of the recoil electron in the first layer, the energy of the scattered gamma-ray photon in the second layers, the scattering angle, the electron mass, and the speed of light, respectively. The probability distribution of the location of a radiation source is estimated by back-projection as a smeared ring shape due to the angular resolution of the detector. The position of a radiation source can be reconstructed by accumulating at least three reconstructed rings in the case of a single source. The angular resolution was found to be 3.5° after using an image-sharpening technique [3] (see Fig.31). With this angular resolution, we can resolve a 1 m^2 radiation hot spot that is located at a distance of 10 m from the detector with a wide field of view of 1 sr. The angular dependence of the acceptance is within ±15% in a 50° field of view. The cost is less than $100,000. Moreover, the detection efficiency 0.68 cps/MBq at 1 m for 662 keV (7.6 cps/μSv/h) is sufficient for measuring low-level contamination (i.e., less than 1 μSv/h) corresponding to typ-

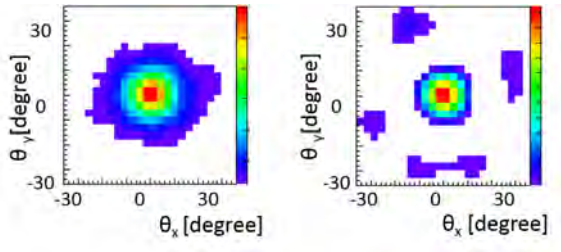

Fig. 31. Images of reconstructed gamma rays without the image-sharpening technique (left) and with the image-sharpening technique (right).

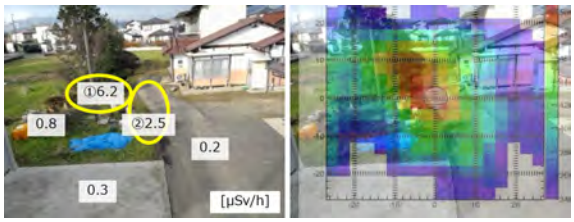

Fig. 32. The figure on the left-hand side shows the dose rates measured by a survey meter in a yard. We used a scintillation-type (Na (Tl)) survey meter and all the measurements were conducted at a height of 1 cm from the ground. The maximum dose rate was 6.2 μSv/h at the bottom of the trees. The yellow circles show the hot spots. The figure on the right-hand side shows the gamma-ray distribution. The exposure time was 90 min, and the distance of the detector from the trees at the top-left of the figure was 15 m. The region with maximum intensity is shown in red, the level just above the average within the field of view is shown in blue, and the level below the average in the field of view is transparent.

ical values in large areas of eastern Japan. In addition to the laboratory tests, the imaging capability of our detector was verified in various regions with dose rates less than 1 μSv/h (e.g., Fukushima city).

We performed field trials in Fukushima city. In these cases, we selected events with energies of 605 keV and 796 keV from ^{134}Cs, and 662 keV from ^{137}Cs, which were released by the Fukushima Daiichi nuclear power plant accident. Fig. 32 shows the distribution of the gamma rays. We set the detector on a lift at a height of 4 m in order to cover a wide area of approximately 15 m $\times$ 15 m. The position of the maximum dose rate was located at the bottom of the trees shown. Another highly contaminated spot was the area between the trees and the road made of concrete. The distribution of the gamma rays detected by the γI was consistent with the measurements of the dose rate by a survey meter.

Then, we performed a comparison between the distributions of the gamma rays before and after decontamination. Fig. 33 shows the result of measurements. From the image before decontamination (left of Fig. 33), we found a hot spot on the left-hand side. The dose rate of the hot spot was around 1 μSv/h. After the decontamination, we measured the same area from the same angle. The image on the right-hand side of Fig. 33 is shown in blue and green, which means that the dose rate after the decontamination decreased to $\sim$0.4 μSv/h at the hot spot where the average dose rate is considered to be $\sim$0.23 μSv/h. Hence, we confirmed that our detector can measure low-level gamma rays of less than 1 μSv/h, which is expected after decontamination.

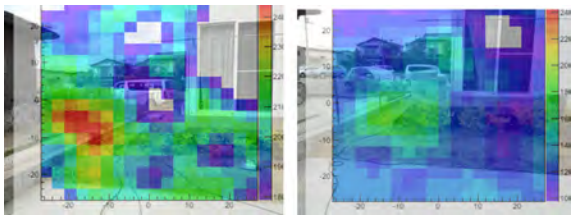

Fig. 33. Images of the gamma rays before (left) and after (right) the decontamination.

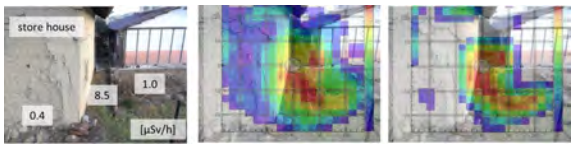

Fig. 34. A photo of the measurement area showing the dose rates measured by a survey meter (left), and a gamma-ray image without the image-sharpening technique (middle) and one with the image-sharpening technique (right). The exposure time was 60 min.

Furthermore, we measured the distribution of gamma rays beside a storehouse made of mortar, as shown in Fig. 34. We found a small hot spot where rainwater flows off from the roof, which is long and narrow. Fig. 34 (right) shows the resulting image obtained by applying the image-sharpening technique. We confirmed that a sharper image can be obtained by this technique.

With the help of the field works conducted in Fukushima city, we demonstrated the capability of our detector in the measurement of the arrival direction of gamma rays in environments with even the dose rate of about 1 μSv/h and less ($\sim 0,23\mu$Sv/h).

Mass production of the cameras based on the design in this paper is being done. Moreover, we plan to develop various types of scintillation Compton cameras based on the technology in this paper. One of the cameras is a lower-cost Compton panorama camera that comprises fewer scintillation detectors. This camera will be developed to measure the rough distribution of gamma rays for decontamination operations. This camera can also be used for measuring pollution by radioactive medicine at a nuclear medical facility. Another type of camera has a high angular resolution. This can be used as a nuclear medicine diagnostic device. Moreover, by applying these techniques, we plan to design a detector for the measurement of gamma ray lines for astrophysics, such as a positron annihilation peak of 511 keV.

Bibliography

[1] T.Kamae, R.Enomoto, and N.Hanada, NIM-A 260(1987)254.

[2] M.Kagaya et al., to be published in NIM-A.

[3] H.Muraishi et al., J. Japan Academy of Health Sci. 17(2014)159.

ASTROPHYSICS AND GRAVITY DIVISION

Overview

Astrophysics and Gravity Division consists of Gravitational Wave Group, The Observational Cosmology Group, Primary Cosmic Ray Group and Theory Group. The Gravitational Wave Group conducts experimental research of gravitational wave with researchers of gravitational wave experiment and theory in Japan. The main items are the construction of the large scale cryogenic interferometer(KAGRA) at Kamioka underground and the operation of CLIO.

The Observational Cosmology Group studies the cosmic history based on deep multi-wavelength observations in collaboration with worldwide researchers. This group has started a new optical deep survey project with the wide-field imager of Hyper Suprime-Cam mounted on the Subaru telescope.

Theory Group conducts both theoretical study of the Universe and astroparticle physics.

Gravitational Wave Group

Gravitational Wave Project Office (GWPO)

[Spokesperson : Masatake OHASHI]
ICRR, The Univ. of Tokyo, Hida, Gifu 506-1205

Overview

Gravitational Wave Project Office (GWPO) was established at the beginning of the fiscal year of 2011 to assist the construction of KAGRA gravitational wave telescope. Main office was built at Kamioka, Hida-city Gifu in 2014. It is an intramural office belonging to Astrophysics and Gravity Division of ICRR

KAGRA project is hosted by ICRR, which means the funding comes through the University of Tokyo and all procurements are made through ICRR. However, the number of researchers working for KAGRA construction belonging to other organizations is larger than the staffs belonging to ICRR. Therefore, three collaboration members of KEK are recruited as guest researchers of ICRR.

The role of this office is to support execution of KAGRA project by ICRR staffs together with these collaboration members. Main works are

- finance planning
- management of collaboration
- support for the execution of KAGRA budget
- coordination of collaboration meetings
- technical supports for the KAGRA construction
- support for education of graduate students
- bridging collaboration members and ICRR administration office
- others

Activity in FY 2014

We supported the collaboration meetings held in University of Toyama and in Department of physics, the University of Tokyo. They were two face-to-face international collaboration meetings [2] and four KAGRA collaboration remote meetings (two international and two domestic) [3]. We supported the External Peer Review of KAGRA in April, 2014, the KAGRA council meeting on 17th, September, Program Advisory Board meeting on 31st, October and 1st, November, and The 3rd ELiTES General meeting was held the 9th-10th of February 2015, in Tokyo. The first day hosted by the European Delegation in Japan and the second day by the University of Tokyo, in the SEIHOKU gallery in Yayoi Auditorium Annex

We took care of travel supports for the following events:
- The 6th Korea-Japan workshop on KAGRA at the National Astronomical Observatory of Japan on June 20th-21st, 2014.
- The 7th Korea-Japan workshop on KAGRA at University of Toyama on Dec. 19 and 20, 2014.

We supported the execution of research programs adopted as ICRR collaborative researches in processing invoices for experimental goods and domestic travels.

KAGRA Project Status

[Spokesperson : Seiji KAWAMURA]
ICRR, The Univ. of Tokyo, Hida, Gifu 506-1205

Overview

KAGRA, Large-scale Cryogenic Gravitational wave Telescope, aims at detecting gravitational waves for the first time and establishing a new astronomy, gravitational wave astronomy, by a 3 km L-shaped laser interferometer with a cryogenic mirror system placed underground at Kamioka. The KAGRA development is divided into two stages: the initial KAGRA (iKAGRA) and baseline KAGRA (bKAGRA). The iKAGRA detector will be a simple Michelson interferometer with a 2-Watt laser, room-temperature mirrors, and a simple seismic isolation system. We plan to complete the iKAGRA detector with a one-month observation run by the end of 2015. Then we will proceed to bKAGRA. The bKAGRA detector will employ a Resonant Sideband Extraction (RSE) interferometer with 180-Watt laser, cryogenic test mass mirrors, and an advanced Seismic Attenuation System (SAS). The bKAGRA

*2 http://gwwiki.icrr.u-tokyo.ac.jp/JGWwiki/KAGRA/Meeting/F2F
*3 http://gwwiki.icrr.u-tokyo.ac.jp/JGWwiki/KAGRA/Meeting/Collaboration

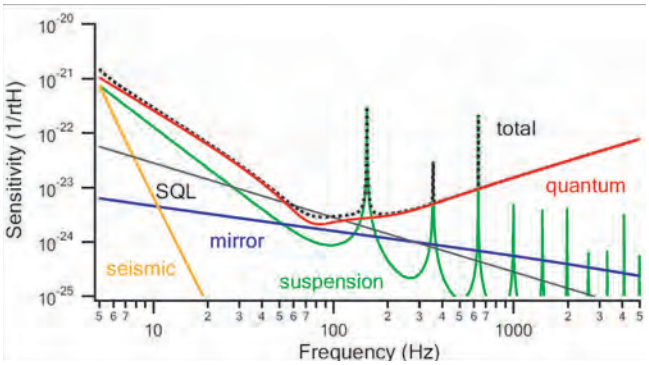

Fig. 1. Ultimate sensitivity limit of KAGRA.

detector should attain the sensitivity high enough for the detection of gravitational waves with the help of the high power laser and RSE interferometer to reduce the quantum noise, the cryogenic mirrors to reduce the thermal noise, and the SAS to reduce the seismic noise. We plan to start operating the bKAGRA detector by the end of 2017, then repeat short-time observation runs and noise hunting to improve the sensitivity until it reaches the target sensitivity of KAGRA.

Figure 1 shows the estimated ultimate sensitivity limits of KAGRA, where incoherent sum of the fundamental noise sources is assumed. The observation range for an inspiral and merger of neutron-star binary with the ultimate sensitivity limit of KAGRA is about 173Mpc with the same definition of the observation range as LIGO and Virgo.

Major milestones and and important progress we accomplished between April 2013 and March 2014 are the following: The photos of KAGRA taken in March 2014 are also shown (Fig. 2 - Fig. 10).

- Many facility items of KAGRA were completed. They include an electrical equipment, a water supply and drainage system, an air ventilation and circulation, an optical fiber network, an anti-dust painting, an automatic control of water pumping system, a PHS phone system, a fire warning system, a cottage for fans and staffs, separating walls and doors between laboratories, countermeasure for water dropping from ceilings and water flooding in floors, forced draining ducts, a clean room for the laser system, clean rooms for vacuum chambers and a shelter.

- All the beam tubes (500 x 12 meter in length and 800 mm in diameter) were installed. The leak test was performed for the beam tubes and no leak was found. All four cryostats were installed. The leak test was performed for the cryostats at the end stations and no leak was found. Other Eighteen vacuum chambers were also installed.

- We designed the cryogenic suspension system. We measured the quality factor of the connecting part of the Sapphire suspension and found that the design suffices the requirement of KAGRA.

- The prototype of the payload including the bottom filter was assembled at NAOJ. The transfer function of the isolation system was measured using the OSEM sensor/actuator, and the result agreed well with the model.

- All the mirrors for iKAGRA (the test masses, mode cleaner mirrors, beam splitter, and folding mirrors for power recycling) were manufactured and it was verified that the very challenging requirements were satisfied. A Sapphire mirror for bKAGRA with very low optical loss was test-coated for real coating.

- The solid laser amplifier was successfully operated in addition to the coherent addition of the fiber laser. The laser output power reached 210 W, although the quality of the beam was still to be improved.

- The design and fabrication of the electronic circuits necessary for the control of the main interferometer was in progress. The optimal configuration of the output optics of bKAGRA was discussed.

- The pre-stabilized laser for iKAGRA was assembled and tested at Kashiwa. Especially it was demonstrated that the frequency stabilization system using the fiber ring cavity as a reference worked well. After that the pre-stabilized laser was installed in the clean booth at the KAGRA site. The pre-mode cleaner was locked and operated successfully.

- Some environmental measurements were performed and the analysis tool was developed to understand the environmental noise of the underground facility. For example the transmission of the magnetic field due to Schuman resonance in the tunnel was investigated. The long-term measurement system at the X-end station was also prepared to understand the noise due to melting water in spring.

- Two hundred fifty baffles were installed inside two 3-km beam tubes.

- A control system using real time computers was developed and installed into a frontal room at the KAGRA site. It was connected to outside through a network and remotely controlled from the outside control room. Some electronic circuits were developed and tested to connect between subsystems and the control system.

- The Virtual Private Network (VPN) connection was extended from the Kamioka system to Osaka/Osaka City university. It made it possible to search gravitational waves in a low-latency pipeline.

- The development of KAGALI, the data analysis software for KAGRA, was initiated. The basic part of KAGALI, such as the error handling function and Fourier transformation routine using FFTW was developed. Also the compile environment using KAGALI's autotools was introduced and the text function of a code using doxygen was developed.

Fig. 2. Entrance of the KAGRA tunnel.

Fig. 3. Access tunnel to the central area

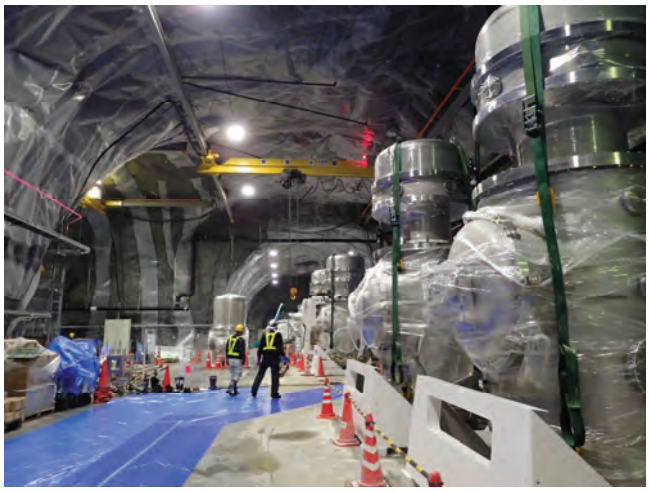

Fig. 4. Vacuum chambers in the central area.

Fig. 5. Cryostat for the cryogenic mirror and the shaft for the vibration isolation system.

Fig. 6. Slope to the 2nd floor.

- Vacuum chambers for the geophysics interferometer were installed on the rock, and beam tubes with a total length of 1,500 meter were installed and connected.

We also enhanced the international collaborations with the Einstein Telescope (ET) project, LIGO, Virgo, Korean and other Asian groups mainly based on the JSPS core-to-core program.

LIGO finished the installation phase and proceeded to the commissioning phase. Since there are many common technologies on the laser, interferometer, control system, and data analysis between LIGO and KAGRA, we performed collaboration researches mainly by mutual visits.

ET and KAGRA have two advanced technologies in common: the underground site and cryogenic mirrors. Therefore, we had a close collaboration on these items. Especially the cryogenic suspension system was developed by many ET researchers visiting Japan and working with the KAGRA researchers as well as many KAGRA researchers visiting Europe and working with the ET researchers.

We also had a close collaboration with the Korean gravi-

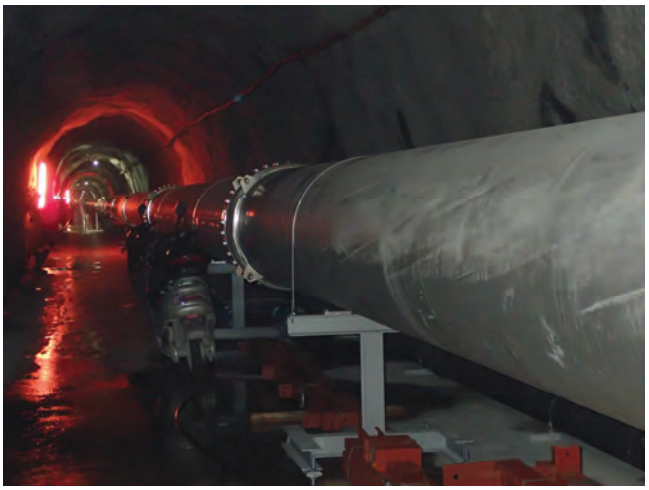

Fig. 7. 3-km beam tube in the Y-arm tunnel.

Fig. 8. Clean room for the pre-stabilized laser.

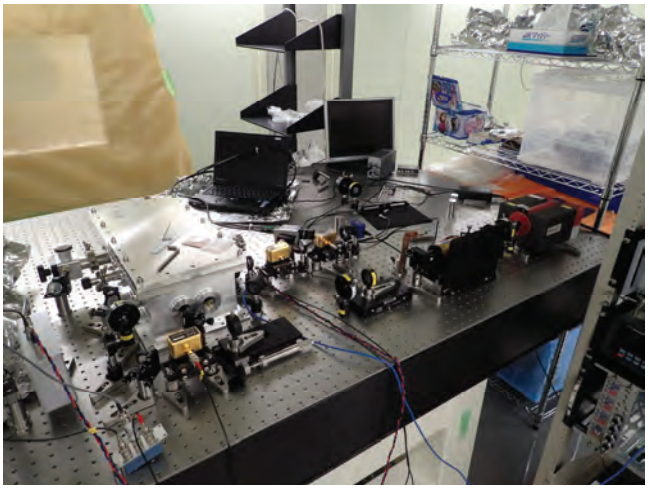

Fig. 9. Pre-stabilized laser for iKAGRA.

Fig. 10. Chamber and beam tube for the input mode cleaner.

tational wave group on the interferometer, detector characterization, and data analysis . We had two Korea-Japan workshops on KAGRA in this fiscal year, and discussed various aspects of collaboration vigorously. Two ICRR visiting professors from Korea spent almost two months to work on the fiber ring cavity and tilt sensor, respectively. We also had collaboration research with the Chinese, Indian, and Australian group, and started discussing possible collaboration with Taiwan and Vietnam.

The rapidly progressing status of KAGAR were presented in many international conferences. Many papers about the progress of KAGRA were also published [1], [2], [3], [4], [5], [6], [7], [8]. We also presented activities on our web-page.[9]

Bibliography

[1] "Mechanical loss of a multilayer tantala/silica coating on a sapphire disk at cryogenic temperatures: Toward the KAGRA gravitational wave detector", Eiichi Hirose, Kieran Craig, Hideki Ishitsuka, Iain W. Martin, Norikatsu Mio, Shigenori Moriwaki, Peter G. Murray, Masatake Ohashi, Sheila Rowan, Yusuke Sakakibara, Toshikazu Suzuki, Kouichi Waseda, Kyohei Watanabe, and Kazuhiro Yamamoto, Phys. Rev. D **90**, 6 (2014)

[2] "A Study of Cooling Time Reduction of Interferometric Cryogenic Gravitational Wave Detectors Using a High-Emissivity Coating", Y. Sakakibara, N. Kimura, T. Suzuki, K. Yamamoto, D. Chen, S. Koike, C. Tokoku, T. Uchiyama, M. Ohashi, K. Kuroda, Adv. Cryog. Eng. **59**, 1176-1183 (2014)

[3] "Progress on the Cryogenic System for the KAGRA Cryogenic Interferometric Gravitational Wave Telescope", Yusuke Sakakibara, Tomotada Akutsu, Dan Chen, Aleksandr Khalaidovski, Nobuhiro Kimura, Shigeaki Koike, Tatsuya Kume, Kazuaki Kuroda, Toshikazu Suzuki, Chihiro Tokoku and Kazuhiro Yamamoto, Class. Quantum Grav. **31**, 224003 (2014)

[4] "Excavation of an underground site for a km-scale

laser interferometric gravitational-wave detector", T Uchiyama, K Furuta, M Ohashi, S Miyoki, O Miyakawa and Y Saito, Class. Quantum Grav. **31**, 224005 (2014)

[5] "Sapphire screws and strength test on them at liquid nitrogen temperature", Eiichi Hirose, Yusuke Sakakibara, Yukihiko Igarashi and Takashi Ishii, Rev. Sci. Instrum. **85**, 104503 (2014)

[6] "Vibration measurement in the KAGRA cryostat", D Chen, L Naticchioni, A Khalaidovski, K Yamamoto, E Majorana, Y Sakakibara, C Tokoku, T Suzuki, N Kimura, S Koike, T Uchiyama and S Kawamura, Class. Quantum Grav. **31**, 224001 (2014)

[7] "Update on development of cryogenic sapphire mirrors and their seismic attenuation system for KAGRA", E Hirose,T Sekiguchi, R Kumar, R Takahashi, Class. Quantum Grav. **31**, 224004 (2014)

[8] "Evaluation of heat extraction through sapphire fibers for the GW observatory KAGRA", A Khalaidovski, G Hofmann, D Chen, J Komma, C Schwarz, C Tokoku, N Kimura, T Suzuki, AO Scheie, E Majorana, R Nawrodt, K Yamamoto, Class. Quantum Grav. **31**, 105004 (2014)

[9] http://gwcenter.icrr.u-tokyo.ac.jp/en/

Tunnel and vacuum system for KAGRA

[Spokesperson : Takashi UCHIYAMA]
ICRR, The Univ. of Tokyo, Hida, Gifu 506-1205

KAGRA is a laser interferometric gravitational-wave detector with a 3 km arm length. It is to be constructed in tunnels of Kamioka mine (Hida, Gifu, Japan). The use of an underground site for small seismic motion is a key feature of KAGRA. Kajima corporation (Kajima) in Japan carried out KAGRA tunnel excavation work from 22th May, 2012 to the end of March, 2014. The total length and the total volume of the tunnels are 7,697 m and 156,301 m^3, respectively. Kajima used the New Austrian Tunneling Method.

Figure 11 shows a location map of the KAGRA tunnels. The tunnels have been excavated in Mt. Ikenoyama of Kamioka mine, whose top is at about 1,300 m. There are two 3,000 m arm tunnels connected perpendicularly. One arm tunnel in north-east direction is called Xarm; the other arm tunnel is called Yarm. The Center area, Xend area, and Yend area, where some experiment rooms exist are located at the connecting corner of the arm tunnels and at the end of both arm tunnels, respectively. All of the areas are inside at more than 200 m from the surface of the mountain, in order to obtain a quiet seismic motion environment as we expected at the underground site. Both arm tunnels are tilted by 1/300 for natural water drainage. The Xend area is at the highest altitude of about 382 m, and the Yend area is at the lowest altitude of about 362 m.The altitude of the Center area is 372 m. The KAGRA tunnels have two entrances: New Atotsu entrance and Mozumi entrance. The New Atotsu entrance was newly constructed for the KAGRA tunnels, whose dimensions are a width of 4 m and a height of 4 m. The cross section of the New Atotsu entrance is the same of standard cross section of the arm tunnels.

After the completion of the KAGRA tunnel excavation works, construction of facilities and infrastructures, and installation works in the KAGRA tunnel have been done in the fiscal year of 2014. The constructed facilities are floor concretes, walls separating experiment rooms, anti dust paintings to surfaces of experiment rooms, 10 cranes, 6 clean booths including a Class-1 clean booth housed in an anti-sound room for laser sources of the KAGRA interferometer, a house for digital control systems, a ventilation fan house in front of the KAGRA tunnel entrance, and so on. The constructed infrastructures are water supply and drainage systems, a ventilation system for the experiment rooms, electric power lines, optical fiber networks for internet connection to the outside, a PHS system, an oxygen monitor, a fire alarm system, and so on. The installed items were vacuum systems and granite stones for basements of vacuum chambers and optical tables for geophysical interferometers. Those construction works and installation works have been conducted by companies such as Kajima corporation, MESCO, Inc., and S. P. Engineering Co., Ltd., and so on.

Figure 12 shows a schematic view of vacuum systems of the KAGRA interferometer and the geophysical interferometers, and clean booths for the KAGRA interferometer. The vacuum systems consists of vacuum chambers for housing optics, vacuum ducts for traveling laser beams in the arm tunnels, baffles to reduce scattering light in the vacuum ducts, gate valves, vacuum pumping units, gaskets to connect each parts, and so on.

We have manufactured 500 vacuum ducts which have the diameter of 800 mm and the length of 12 m for the KAGRA interferometer. Using those vacuum ducts, we have constructed 2 sets of a straight 3 km vacuum duct. We have also manufactured 250 vacuum ducts which have the diameter of 400 mm and the length of 12 m for the geophysical interferometer. Using those vacuum ducts, we have constructed 2 sets of a 1.5 km straight vacuum duct. All of the vacuum ducts are made of stainless steel (SUS304). Surfaces passivation by electro-polish followed by baking has done inside the vacuum ducts in order to realize vacuum pressure of $2 \times 10^{-}7[\mathrm{Pa}]$. All the vacuum ducts were once stored in an existed tunnel near the KAGRA site. MESCO transported typically 8 vacuum ducts per day from the storage tunnel into the KAGRA tunnel. Transporting a vacuum duct in arm tunnels in the KAGRA tunnel was done by special transporters. After transporting a vacuum duct to the designed location, the vacuum duct was put on duct supports and was adjusted its position and height. 125 baffles were inserted in the KAGRA vacuum ducts. Finally, all the vacuum ducts were connected by metal O-rings which are made of silvering stainless steel (SUS321) and evacuated by turbo-molecular pump units. As for the KAGRA vacuum ducts, vacuum pressure of the order of 10^{-5} [Pa] has been achieved by only a week evacuation. After the evacuation, leak checks have been done. The results of leak checks were satisfied with our requirements that is leaks are less than $1 \times 10^{-10}\,[\mathrm{Pa\,m^3/s}]$.

We also manufactured 27 vacuum chambers which are

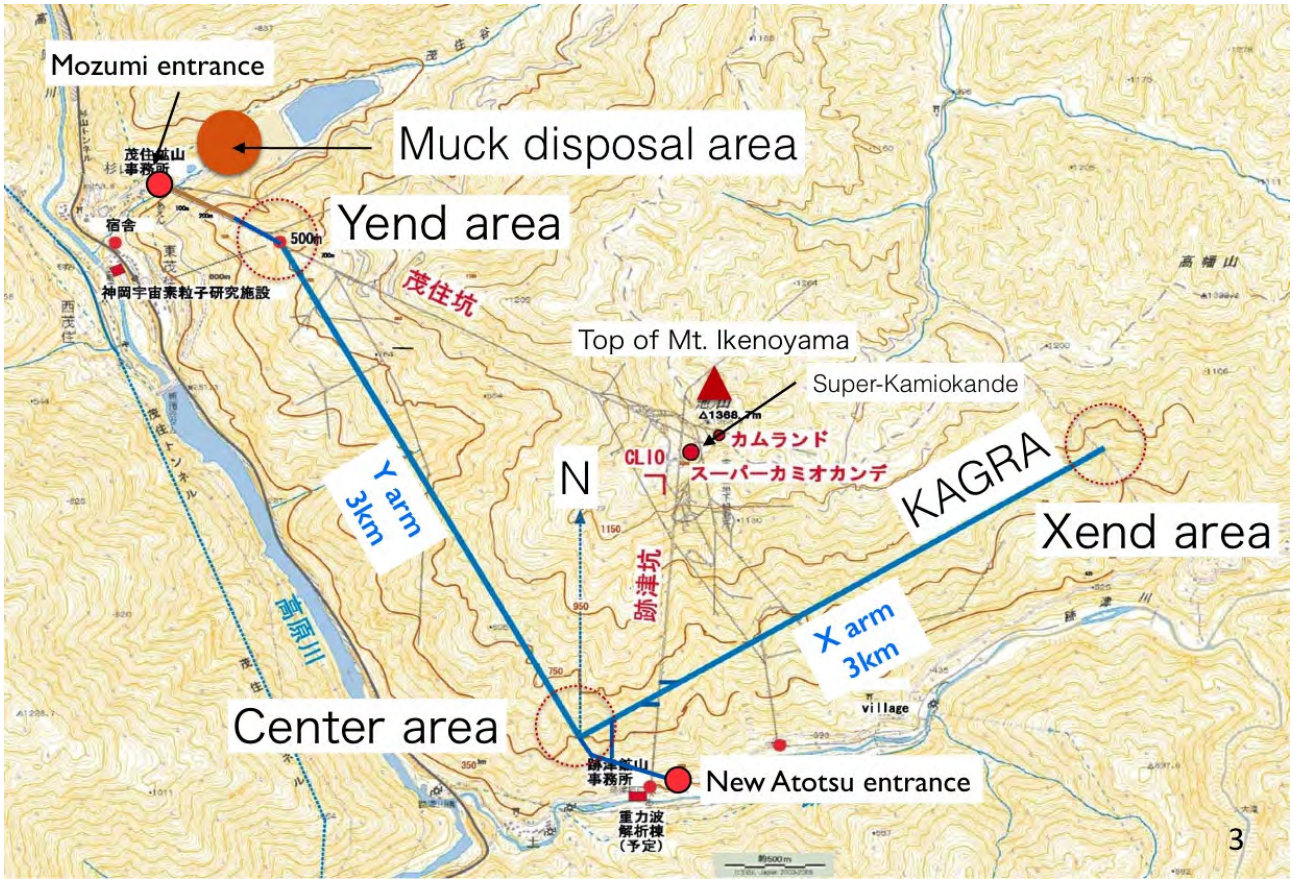

Fig. 11. Location map of the KAGRA tunnels. The tunnels are in Mt. Ikenoyama of Kamioka mine, whose top is at about 1,300 m. There are two 3,000 m arm tunnels connected perpendicularly. One arm tunnel in the north east direction is called Xarm; the other arm tunnel is called Yarm. The Center area, Xend area, and Yend area, contain some experiment rooms, which are located at the connecting corner of the arm tunnels and at the end of both arm tunnels, respectively. All of the areas are inside at more than 200 m from the surface of the mountain in order to obtain the quiet seismic motion environment that we expected to be achieved at the underground site. Both arm tunnels are tilted by 1/300 for natural water drainage. The Xend area is at the highest altitude of about 382 m, and the Yend area is at the lowest altitude of about 362 m.The altitude of the Center area is 372 m.

made of stainless steel (SUS304). Table 1 shows dimensions of the vacuum chambers. 4 vacuum chambers, IXC, IYC, EXC, EYC are cryostats for the KAGRA test masses to be cooled in cryogenic temperature. 4 vacuum chambers, IXG, IYG, EXG, EYG are used for the geophysical interferometers. The rest of 19 vacuum chambers will house optics not to be cooled for the KAGRA interferometer. All the vacuum chambers for the KAGRA interferometer have been placed on surfaces made of shrinkage-compensating mortar on floor to make exact height as we designed and fixed by anchor bolts. Precision of the fixed positions are within a circle that has the diameter of 2 mm. The vacuum chambers for the geophysical interferometer have been fixed on the granite stones put on mountain rock directly.

Table 1. Dimensions of vacuum chambers

Chamber name Chamber name	Diameter [mm]	Height [mm]	Weight [kg]
MCE, MCF	1500	2232	1705
IFI, IMM	1200	2232	1200
PRM, PR2, PR3	1500	3338	2772
IXA, IYA, EXA, EYA	1500	3400	2860
BS	1500	4515	3981
SRM, SR2, SR3	1500	4585	4870
IXV, IYV, EXV, EYV	1500	1615	1449
IXC, IYC, EXC, EYC	2700	3200	12000
IXG, IYG, EXG, EYG	1100	1270	1240

Input and Output Optics

[Spokesperson : Seiji KAWAMURA]
ICRR, The Univ. of Tokyo, Hida, Gifu 506-1205

The input and output optics of KAGRA consists of the pre-stabilization system of laser, input mode cleaner, input Faraday isolator, input optics chain, output mode cleaner, output optics chain, and photo detectors. The pre-stabilization system contains the frequency stabilization system, intensity stabilization system, and pre-mode cleaner. Some components of the input and output system will be used both for iKAGRA and bKAGRA, while some other components that are used for iKAGRA will be replaced later for bKAGRA, since bKAGRA requires more stringent performances of the system. For example bKAGRA uses high power laser (180 W), thus all the optics in the pre-stabilization system should use optical com-

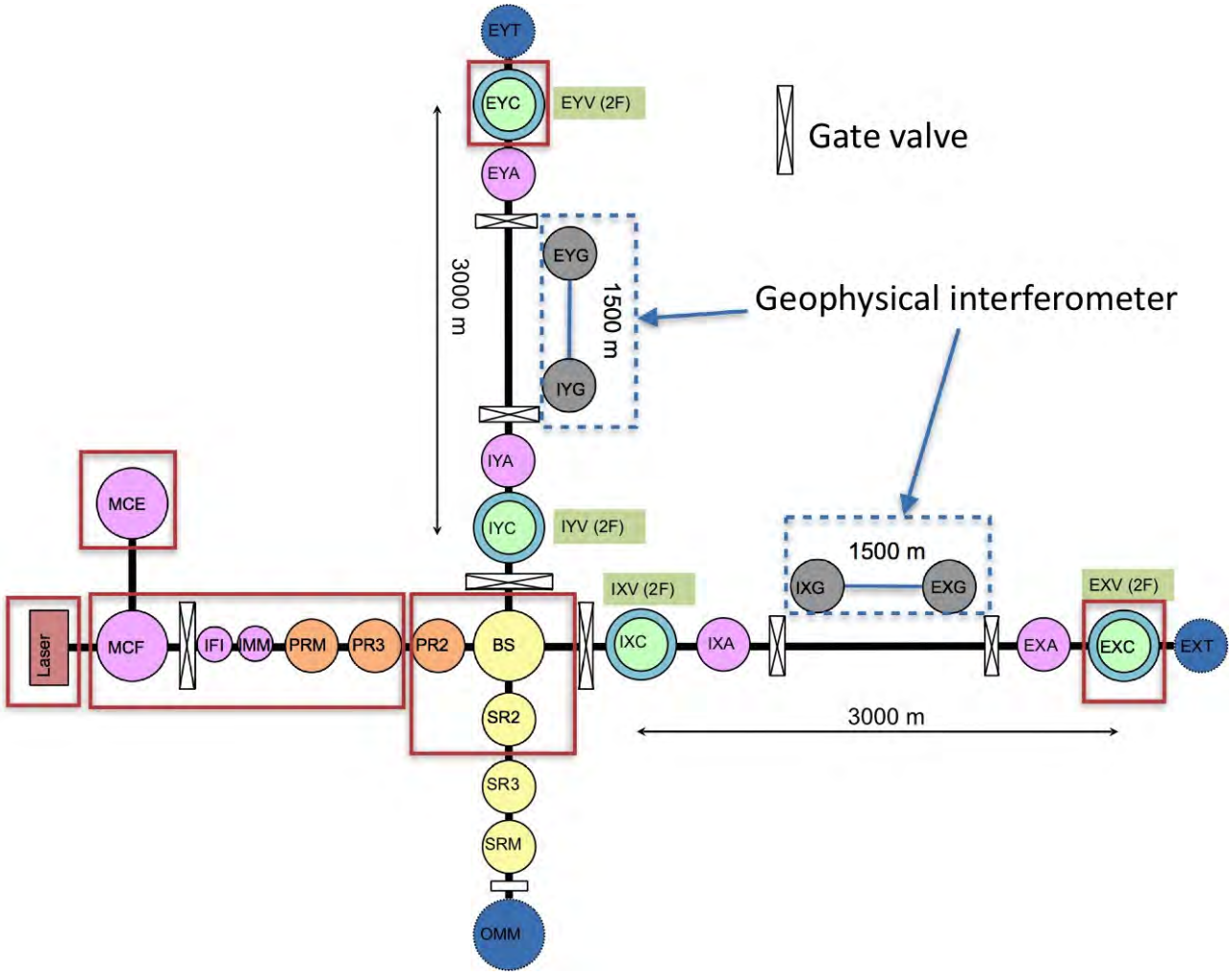

Fig. 12. A schematic view of vacuum systems of the KAGRA interferometer and the geophysical interferometers, and clean booths for the KAGRA interferometer. 30 circles indicate vacuum chambers, 7 square symbols with cross lines indicate $\phi 1000$ or $\phi 800$ gate valves for the KAGRA interferometer, and solid lines indicated vacuum ducts. 3 vacuum chambers named OMM, EXT, and EYT are planning. 6 squares indicate clean booths. The square surrounding "Laser" indicates the clean booth for laser sources for the KAGRA interferometer.

ponents that can handle such high power laser beam. Another example is that in order to attain the target sensitivity of bKAGRA, the output mode cleaner is necessary, but it is not necessary for iKAGRA. The input mode cleaner and input Faraday isolator will be used for both iKAGRA and bKAGRA, since otherwise it will be time-consuming to replace these systems inside the chambers for bKAGRA.

In the fiscal year of 2014, the performance test and installation of the pre-stabilization system for iKAGRA, the preparation of the input mode cleaner suspension system, and the assembly and adjustment of the input Faraday isolator were mainly performed. The spring water problem was identified and the adequate remedy was proposed.

The pre-stabilization system for iKAGRA consists of 2 W NPRO laser, pre-mode cleaner, and fiber ring cavity (See Fig. 13). The intensity stabilization system will not be implemented for iKAGRA. The pre-mode cleaner is a triangular optical cavity, consisting of three mirrors. It has a finesse of about 200 and a free spectral range of 750 MHz. Its purpose is to clean the transverse mode of the laser beam and passively reduce the intensity noise of the laser light at radio frequencies (RF). The length of the pre-mode cleaner cavity is controlled to resonate the light in the cavity using the piezoelectric transducer attached to one of the mirrors, and the light transmitting the pre-mode cleaner is cleaned both in transverse mode and RF intensity. This light is picked off and injected to the fiber ring cavity. The fiber ring cavity consists of a fiber with a coupler and it is contained in the sound-proof box with a simple vibration isolation system. The length of the fiber is 5.8 m, and the free spectral range of the fiber ring cavity is 35.4 MHz. The purpose of the fiber ring cavity is to stabilize the frequency of the light using the fiber ring cavity as frequency reference.

The pre-stabilized laser was assembled and tested at Kashiwa. The pre-mode cleaner was successfully locked and operated stably. The throughput of the pre-mode cleaner was about 0.4 and the unity gain frequency of the control system was measured to be about 4 kHz. The fiber ring cavity was also successfully locked and operated stably. Figure 14 shows the frequency stability of the light measured with the pre-mode cleaner as a reference with and without the frequency stabilization system using the fiber ring cavity. This indicates that

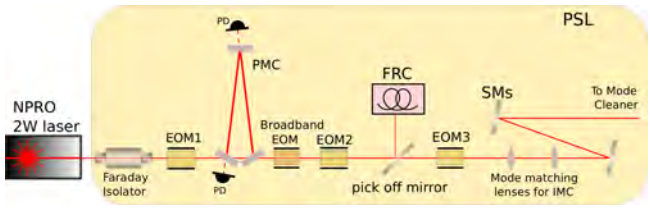

Fig. 13. Schematic diagram of the pre-stabilized laser for iKAGRA.

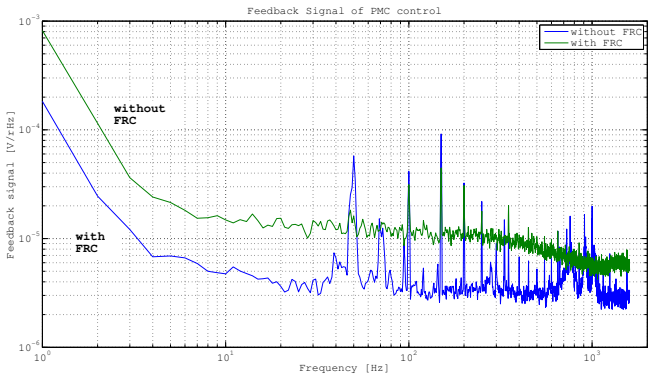

Fig. 14. Frequency stability of the light measured with the pre-mode cleaner as a reference with and without the frequency stabilization using the fiber ring cavity.

the laser frequency is successfully stabilized by the frequency stabilization system using the fiber ring cavity.

The pre-stabilization system was then transfered to the KAGRA site, and it was installed in the laser clean room (See Fig. 15). The pre-mode cleaner was locked and operated stably. The fiber ring cavity was aligned and to be locked and operated soon.

The high-power Faraday isolator is required to be installed after the input mode cleaner to prevent the light reflected from the main interferometer from being injected into the input mode cleaner. It should be compatible with the high vacuum and high laser power, and also a high extinction ratio is required. It should also provide the light for the symmetric port of the Michelson interferometer. The Faraday isolator was successfully assembled in the laser clean room at the site with the help of researchers from the University of Florida. The throughput of the Faraday isolator was measured to be 0.94, and an extinction ratio of 44 dB was obtained.

As for the input mode cleaner suspension system, we used the suspension system for TAMA300. It had to be modified to make it compatible with the optical configuration for the input mode cleaner of KAGRA. After the new parts were fabricated, the new suspension system was assembled at NAOJ. The transfer function from torque applied to the dummy mirror to angular motion of the dummy mirror was measured using the coil magnet actuator and the optical lever. The measured transfer function agreed well with the simulation.

Fabrication of cryostat and R&D for cryogenic items

[Spokesperson : Kazuhiro YAMAMOTO]
ICRR, The Univ. of Tokyo, Kashiwa, Chiba 277-8582

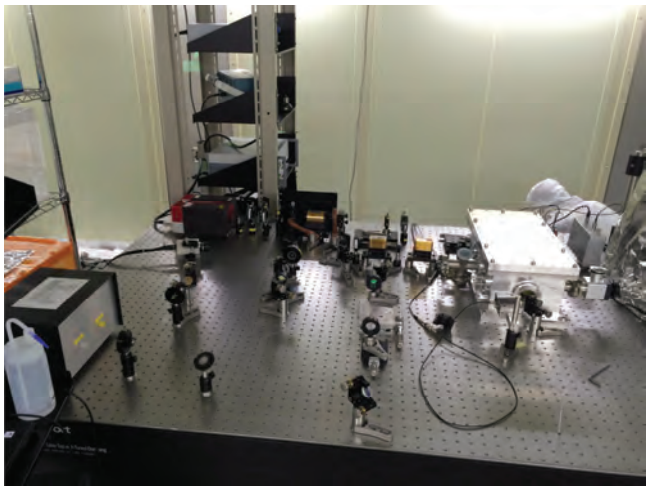

Fig. 15. Pre-stabilized laser installed in the laser clean room at the KAGRA site.

Outlines A key feature of KAGRA is the operation of the interferometer mirrors made from sapphire at cryogenic temperature. This mirror is suspended by sapphire fibers (sapphire suspension). This suspension is a part of the cryogenic payload and this payload is cooled in the cryostat.

Our activity for the cryogenic system in 2014 is as follows. All four KAGRA cryostats were put at KAGRA site. We investigated cryo ducts to terminate the invasion of 300K radiation into the cryostats. The fabrication of these ducts is in progress and the four ducts were connected with the two cryostats in the center room of KAGRA site. We are also proceeding with design of a cryogenic payload and prepared some parts of a prototype. We checked almost all components of the sapphire suspension (strength, thermal resistance, mechanical dissipation). Some parts of a prototype of this sapphire suspension were delivered. In the following, the details of these items and an international collaboration (ELiTES) are explained.

Here, it must be noted that the KAGRA cryogenic system review paper was published in 2014 (Y. Sakakibara *et al.*, Classical and Quantum Gravity **31**(2014)224003).

Installation of cryostats at KAGRA site By November of 2014, all four KAGRA cryostats were carried into KAGRA site. Two cryostats were transported along 3km arms to end sites of KAGRA. It took about a half of a day for each cryostat. The other two of them were put in the center room. All of them were fixed on the ground by February 2015. Although we faced a lot of small troubles, there were no serious or fatal accidents.

In the center room, the cryo coolers and cryo ducts (details are explained later) were connected with both two cryostats.

At the both end sites, we checked whether there are leaks around the top flanges of the cryostats. A helium leak detector found no leaks which are larger than 10^{-12}Pa m^3/sec (the leaks should be smaller than 10^{-10}Pa m^3/sec for KAGRA).

We also proceed with the survey of the cryostats themselves (position and alignment) and around cryostats. The

seismic motion at both end sites was measured and these values are comparable with those at center of Kamioka mine (two orders of magnitude smaller than those near Tokyo) as we expected.

Cryogenic duct The radiation shields should have two large holes for the laser beam which are comparable in size with the diameter of the cooled mirror (220 mm). Through these holes, 300 K radiation will invade the radiation shield. Cryogenic ducts with baffles are necessary to prevent the propagation of 300 K radiation. In order to enhance emissivity, black coating (Solblack) is deposited on the inner surface of cryo ducts and baffles.

By 2014, we investigated and designed the cryo ducts. We measured the heat transfer by the cryogenic ducts and found that it is enough small for KAGRA as our calculation result (using ZEMAX). Since the vibration of cryo ducts can contaminate the output of the KAGRA interferometer via the scattered light by ducts themselves, we measured vibration of cryo duct and calculated the scattered light noise (again, using ZEMAX) based on the measured vibration. It is (at least, 100 times) smaller than the KAGRA goal.

We started fabrication of the cryo ducts. Each cryostat has two cryo ducts. In total, eight cryo ducts are necessary for KAGRA. Six of them were manufactured by March 2015. Four cryo ducts were connected with the cryostats in the center room.

Cryogenic payload The cooled sapphire mirror is at the bottom of the cryogenic payload. This payload is in the radiation shield for cooling and suspended from the Type A vibration isolation system in vacuum but at room temperature. The cryocoolers and payload are connected by heat links made from pure aluminum for cooling. The payload is necessary to control the position and angle of the mirror (otherwise, the interference of the light can never be realized), and for the vibration isolation (especially, the vibration via heat links) and so on.

The design of the cryo payload is in progress. Some parts of the prototype have already been delivered. The next step is the test of a prototype. In this prototype, a sapphire mirror and fibers are replaced by dummy ones made from metal. We will conduct assembly, cooling and control tests and so on. The cryostat for this prototype test is in KEK.

Mirror angle adjustment systems and sensors to observe positions and angles of components of the cryogenic payload must work at cryogenic temperature. We are testing candidates of the angle adjustment systems and sensors.

In 2013, we investigated vibration via heat links. This result appeared in refereed journal (F. Frasconi *et al*., Meas. Sci. Technol. **25** (2014) 015103, D. Chen *et al.*, Classical and Quantum Gravity **31**(2014) 224001).

Sapphire lop-eared suspension The cooled mirror is suspended by four sapphire fibers. We call this system sapphire lop-eared suspension. This sapphire suspension consists of a mirror, fibers with nail heads, ears for connection between fibers and a mirror, blade springs to compensate the length differences between four fibers. All of them are made from sapphire. Two joint techniques are adopted. Between the ears and mirror, Hydroxide Catalysis Bonding is applied. This technique is also adopted in Advanced LIGO and Advanced Virgo. On the nail heads of the fibers, indium is applied for joint with the ear or blade spring. When fibers are broken, heat is applied to melt indium (melting point is 157 degree Celsius) and the broken fibers are removed.

By 2014, we investigated almost all components and joint techniques; we measured strength, thermal resistance to check whether they can support a 23kg sapphire mirror, and transmit 1W heat absorbed in the mirror, respectively. Some results were published in refereed journals; A. Khalaidovski *et al.*, Classical and Quantum Gravity **31**(2014)105004 (thermal conductivity of sapphire fiber), K Haughian *et al.*, Classical and Quantum Gravity **32**(2015)075013 (strength of Hydroxide Catalysis Bonding). Moreover, mechanical loss of fibers and joint techniques at cryogenic temperature was measured. According to Fluctuation- Dissipation Theorem, the mechanical dissipation generates thermal noise. We derived the thermal noise by the fibers and joint techniques from measured mechanical loss, Fluctuation-Dissipation Theorem, and Finite Element Method. We found the largest contribution stems from the fibers and it is smaller than KAGRA sensitivity.

Our next important step is the prototype test of the sapphire suspension. Based on above investigation, we designed the sapphire parts and ordered to manufacture. Some of them were sent to us. Although our measured loss of a fiber was quite small, it is loss of a short test piece. We are continuing experiments for the mechanical loss measurement of sapphire fibers whose length is same as that for KAGRA.

ELiTES ELiTES (ET-LCGT interferometric Telescope Exchange of Scientists) is a European grant (European 7th Framework Programme Marie Curie action between Mar. 2012 and Feb. 2016) for the collaboration between KAGRA and Einstein Telescope (European future project). This grant supports people in Europe to visit Japan for KAGRA. In 2014, 26 visitors (from Germany, Netherland, U.K., Italy, and France) came. A part of them helped and supported cryogenic experiments for sapphire, reflective coating and so on (The result of the reflective coating was published as E. Hirose *et al.*, Physical Review D **90**(2014) 102004). Accroding to the ELiTES web site (http://www.et-gw.eu/elites-related-publications), 9 papers (or proceedings) related with ELiTES were published in 2014.

Moreover, ELiTES stimulated Japanese graduate student to visit Europe. One graduate student in Ph.D. course of our project office stayed at Friedrich-Schiller-Universitaet Jena and University of Rome La Sapienza, in total, about four months in 2014.

Integrated DAQ/control system using real time computers and analog electronics

[Spokesperson : Osamu MIYAKAWA]
ICRR, The Univ. of Tokyo, Hida, Gifu 506-1205

KAGRA produces many signals from all of subsystems in the interferometer, not only for main gravitational wave sig-

Fig. 16. KAGRA cryostat at center room of KAGRA site. The cryocoolers and cryo duct are connected to the cryostat.

Fig. 17. A remote control room in the outside building at Kamioka.

nals but also many additional signals for length and alignment controls, physical environmental monitor signals and so on. The total number of signals will be more than 2000 channels at the final stage of bKAGRA. These signals are collected into a data acquisition (DAQ) system and some of the signals are used to control the interferometer and some of the signals are sent to a storage to be analyzed. By the end of last fiscal year, we constructed and tested a full scale DAQ/contols system for KAGRA in the outside building at Kamioka. This test system was also designed and developed as a system which can be moved as it is and can be used as an actual DAQ and control system in the mine. One of the milestones of this fiscal year was the installation of these DAQ/control system into the kAGRA mine.

We have constructed a frontal room in the mine to operate ~ 40 computer servers above and $\sim$60 high current DC power supplies. Humidity in the laboratory area in the mine is about 90% and it is too high for such computers/electronics. The frontal room with some air conditionings protects computers and some electronics from the damage by water and humidity. After the completion of the frontal room, we moved the test DAQ/control system into the room in the KAGRA mine as an actual system. To connect between the real time computers for control and subsystems, or to make a subsystem itself work, many analog circuits will be used in KAGRA. The total number of circuit will be more than 800 boxes. We are continuously designing, developing and providing circuits to other KAGRA's subgroups to test their subsystems or to connect the subsystems to the real time controllers. Circuits can be damaged by water drop or humidity if they are placed in the laboratory area in the mine. We prepared a plastic film case to cover a 19 inch rack. Some circuits inside the rack with the rack cover with can heat the rack inside if the power to the circuits was enabled. Relative humidity inside the rack can be lower because of the heating, and we had a result of 40% of humidity with this cover.

Network in the mine and network between mine and the outside building have been connected by fiber-optic cables. Control system is a kind of independent network only existing in the mine. All the control loop is closed between the interferometer and the real time computers. Specially for the fast length control loops with 3km long distance, time delay is critical, so that we have prepared very low latency networks using so-called the reflective memory technology for the fast control loop in the mine. People can access signals only by reading the streaming data for the fast loops. On the other hand, to extract data from the mine is very important for the DAQ side. We have prepared a 10Gb network with some low latency protocol to transport GW data from the mine to outside building. A remote control room has been partially prepared at the outside building at Kamioka. Fig.17 shows the current control room. This room will be a main control/analysis room for KAGRA during observations. This room is continuously being prepared with many monitors and desks specially for commissioning tasks from now on.

Combined system with analog and digital will provide us not only to control the interferometer but also to establish a total monitoring/diagnostic system for the observation of gravitational waves in the future.

Observational Cosmology Group

[Spokesperson : Yoshiaki Ono]

ICRR, The Univ. of Tokyo, Kashiwa, Chiba 277-8582

Hubble Frontier Fields First Complete Cluster Data: Faint Galaxies at $z \sim 5-10$ for UV Luminosity Functions and Cosmic Reionization [1]

In collaboration with the members of The University of Tokyo and Kavli Institute for the Physics and Mathematics of the Universe.

We present comprehensive analyses of faint dropout galaxies up to $z \sim 10$ with the first full-depth data set of the Abell 2744 lensing cluster and parallel fields observed by the Hubble Frontier Fields (HFF) program. We identify 54 dropouts at $z \sim 5-10$ in the HFF fields and enlarge the size of $z \sim$

9 galaxy sample obtained to date. Although the number of highly magnified ($\mu \sim 10$) galaxies is small because of the tiny survey volume of strong lensing, our study reaches the galaxies' intrinsic luminosities comparable to the deepest-field HUDF studies. We derive UV luminosity functions with these faint dropouts, carefully evaluating by intensive simulations the combination of observational incompleteness and lensing effects in the image plane, including magnification, distortion, and multiplication of images, with the evaluation of mass model dependencies. Our results confirm that the faint-end slope, α, is as steep as -2 at $z \sim 6-8$ and strengthen the evidence for the rapid decrease of UV luminosity densities, $\rho_{\rm UV}$, at $z > 8$ from the large $z \sim 9$ sample. We examine whether the rapid $\rho_{\rm UV}$ decrease trend can be reconciled with the large Thomson scattering optical depth, $\tau_{\rm e}$, measured by cosmic microwave background experiments, allowing a large space of free parameters, such as an average ionizing photon escape fraction and a stellar-population-dependent conversion factor. No parameter set can reproduce both the rapid $\rho_{\rm UV}$ decrease and the large $\tau_{\rm e}$. It is possible that the $\rho_{\rm UV}$ decrease moderates at $z \gtrsim 11$, that the free parameters significantly evolve towards high z, or that there exist additional sources of reionization such as X-ray binaries and faint active galactic nuclei.

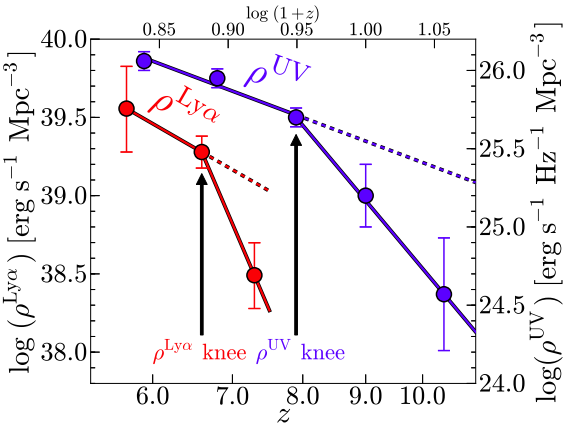

Fig. 19. Evolution of Lyα and UV luminosity densities. The red circles are the Lyα luminosity densities obtained by this study for $z = 7.3$ and by previous studies for $z = 6.6$ and 5.7. The blue circles are the UV luminosity densities obtained in the literature. The left ordinate axis refers to the Lyα luminosity densities, and the right ordinate axis is for the UV luminosity densities. The Lyα luminosity density starts evolving faster at $z \sim 7$, while the UV luminosity density rapidly decreases at $z \sim 8$ and beyond. The $\rho^{\rm Ly\alpha}$ and $\rho^{\rm UV}$ knees are indicated with the arrows. This figure is reproduced by permission of the AAS.

Bibliography

[1] Ishigaki, M., Kawamata, R., Ouchi, M., Oguri, M., Shimasaku, K., & Ono, Y. 2015, Astrophys. J., 799, 12

Accelerated Evolution of the Lyα Luminosity Function at $z \gtrsim 7$ Revealed by the Subaru Ultra-deep Survey for Lyα Emitters at $z = 7.3$ [2]

In collaboration with the members of The University of Tokyo, University of Tsukuba and National Astronomical Observatory of Japan.

We present the ultra-deep Subaru narrowband imaging survey for Lyα emitters (LAEs) at $z = 7.3$ in the Subaru/*XMM-Newton* Deep Survey (SXDS) and Cosmic Evolution Survey (COSMOS) fields (~ 0.5 deg^2) with a total integration time of 106 hr. Exploiting our new sharp bandwidth filter, *NB101*, installed on the Suprime-Cam, we have reached $L({\rm Ly}\alpha) = 2.4 \times 10^{42}$ erg s^{-1} (5σ) for $z = 7.3$ LAEs, about four times deeper than previous Subaru $z \gtrsim 7$ studies, which allows us to reliably investigate the evolution of the Lyα luminosity function (LF) for the first time down to the luminosity limit same as those of Subaru $z = 3.1-6.6$ LAE samples. Surprisingly, we only find three and four LAEs in the SXDS and COSMOS fields, respectively, while one expects a total of ~ 65 LAEs by our survey in the case of no Lyα LF evolution from $z = 6.6$ to 7.3. We identify a decrease of the Lyα LF from $z = 6.6$ to 7.3 at the $> 90\%$ confidence level from our $z = 7.3$ Lyα LF with the best-fit Schechter parameters of $L^*_{\rm Ly\alpha} = 2.7^{+8.0}_{-1.2} \times 10^{42}$ erg s^{-1} and $\phi^* = 3.7^{+17.6}_{-3.3} \times 10^{-4}$ Mpc^{-3} for a fixed $\alpha = -1.5$. Moreover, the evolution of the Lyα LF is clearly accelerated at $z > 6.6$ beyond the measurement uncertainties including cosmic variance. Because no such accelerated evolution of the UV-continuum LF or the cosmic star-formation rate (SFR) is found at $z \sim 7$, but suggested only at $z > 8$, this accelerated Lyα LF evolution is explained by physical mechanisms different from a pure SFR decrease but related to the Lyα production and escape in the process of cosmic reionization. Because a simple accelerating increase of intergalactic medium neutral hydrogen absorbing Lyα cannot be reconciled with Thomson scattering optical depth measurements from *WMAP* and *Planck*, our findings may support new physical pictures suggested by recent theoretical studies, such as the existence of HI clumpy clouds within cosmic ionized bubbles that are selectively absorbing Lyα and the large ionizing photon escape fraction of galaxies causing weak Lyα emission.

Bibliography

[2] Konno, A., Ouchi, M., Ono, Y., Shimasaku, K., Shibuya, T., Furusawa, H., Nakajima, K., Naito, Y., Momose, R., Yuma, S., & Iye, M. 2014, Astrophys. J., 797, 16

Faint Submillimeter Galaxies Revealed by Multifield Deep ALMA Observations: Number Counts, Spatial Clustering, and a Dark Submillimeter Line Emitter [3]

In collaboration with the member of Joint ALMA Observatory.

We present the statistics of faint submillimeter/millimeter galaxies (SMGs) and serendipitous detections of a submillimeter/millimeter line emitter (SLE) with no multi-wavelength continuum counterpart revealed by the deep ALMA observations. We identify faint SMGs with flux densities of $0.1-1.0$ mJy in the deep Band-6 and Band-7 maps of 10 independent fields that reduce cosmic variance effects. The differential number counts at 1.2 mm are found to increase with decreasing flux density down to 0.1 mJy. Our number counts indicate that the faint ($0.1-1.0$ mJy, or ${\rm SFR_{IR}} \sim 30-300 M_\odot$

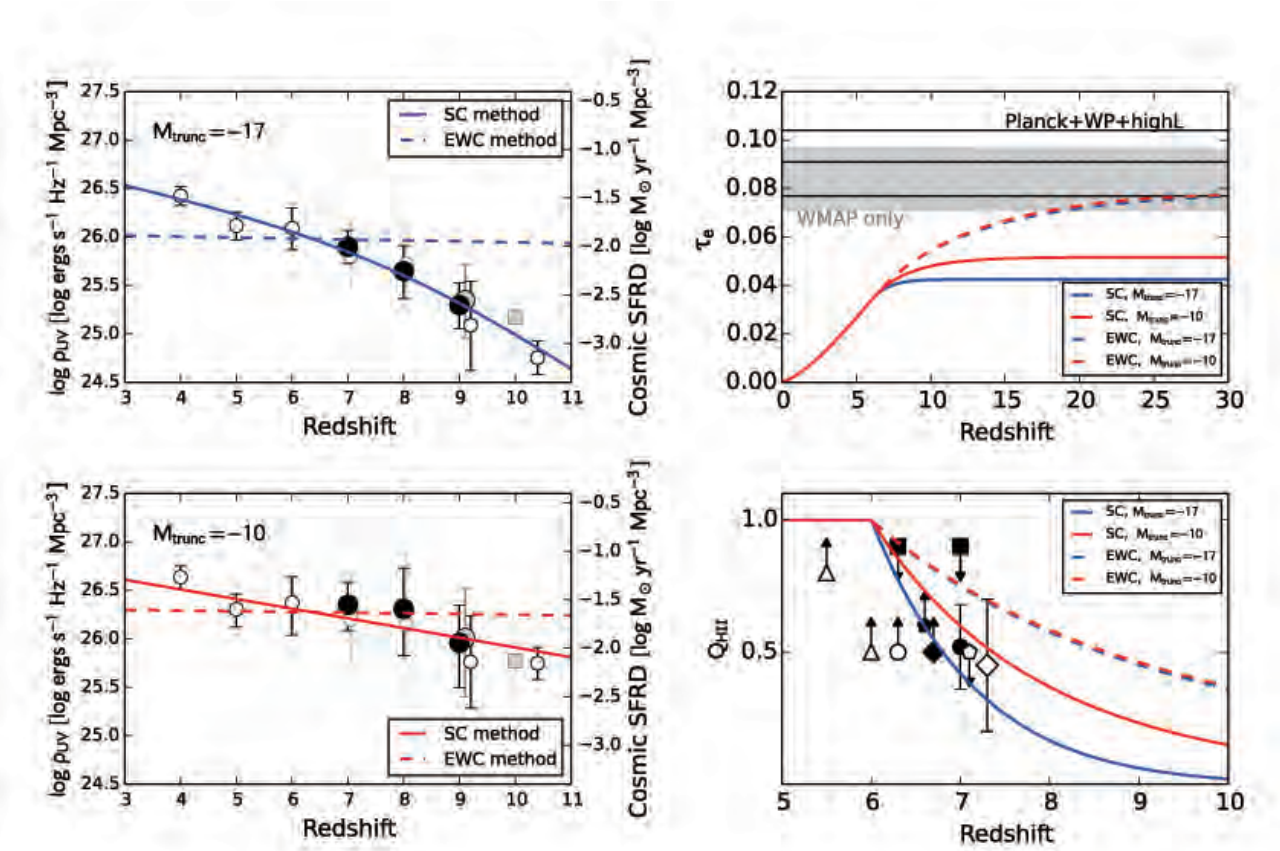

Fig. 18. Upper left panel: the UV luminosity densities calculated with a truncation magnitude of $M_{\rm trunc} = -17$. The filled and open circles represent the UV luminosity densities from this work and from the literature, respectively. The gray circles and squares denote the UV luminosity densities from the HFF data only in this work and in previous studies, respectively. The solid and dashed lines present our best-fit functions of $\rho_{\rm UV}$ with the simple χ^2 (SC) method and the equally weighted χ^2 (EWC) method, respectively. The right axes show cosmic SFR densities at a given UV luminosity density. Bottom left panel: same as the top left panel, but for $M_{\rm trunc} = -10$. Upper right panel: electron scattering optical depth integrating from $z \sim 0$ to a redshift, z, for our best-fit parameters by the SC method with $M_{\rm trunc} = -17$ (blue solid line), the EWC method with $M_{\rm trunc} = -10$ (red solid line), the EWC method with $M_{\rm trunc} = -17$ (blue dashed line), and the EWC method with $M_{\rm trunc} = -10$ (red dashed line), respectively. The hatched and gray regions indicate the 1σ range of τ_e obtained by *WMAP+Planck+highL* and the nine-year *WMAP*, respectively. Bottom right panel: the evolution of ionized hydrogen fraction $Q_{\rm H_II}$ of IGM for our best-fit parameters with four lines, whose notations are the same as the right upper panel. Each symbol represents the observational limit obtained in the literature. This figure is reproduced by permission of the AAS.

yr^{-1}) SMGs contribute nearly a half of the extragalactic background light (EBL), while the remaining half of the EBL is mostly contributed by very faint sources with flux densities of < 0.1 mJy (SFR$_{\rm IR} \lesssim 30 M_\odot$ yr^{-1}). We conduct counts-in-cells analysis with multifield ALMA data for the faint SMGs, and obtain a coarse estimate of galaxy bias, $b_{\rm g} < 4$. The galaxy bias suggests that the dark halo masses of the faint SMGs are $\lesssim 7 \times 10^{12} M_\odot$, which is smaller than those of bright (> 1 mJy) SMGs, but consistent with abundant high-z star-forming populations, such as sBzKs, LBGs, and LAEs. Finally, we report the serendipitous detection of SLE–1, which has no continuum counterparts in our 1.2 mm-band or multi-wavelength images, including ultra deep *HST*/WFC3 and *Spitzer* data. The SLE has a significant line at 249.9 GHz with a signal-to-noise ratio of 7.1. If the SLE is not a spurious source made by the unknown systematic noise of ALMA, the strong upper limits of our multi-wavelength data suggest that the SLE would be a faint galaxy at $z \gtrsim 6$.

Bibliography

[3] Ono, Y., Ouchi, M., Kurono, Y., & Momose, R. 2014, Astrophys. J., 795, 5

Diffuse Lyα Haloes around Galaxies at $z = 2.2 - 6.6$: Implications for Galaxy Formation and Cosmic Reionization [4]

In collaboration with the members of Kavli Institute for the Physics and Mathematics of the Universe, The University of Tokyo, and University of Tsukuba.

We present diffuse Lyα halos (LAHs) identified in the composite Subaru narrowband images of $100-3600$ Lyα emitters (LAEs) at $z = 2.2$, 3.1, 3.7, 5.7, and 6.6. First, we carefully examine potential artifacts mimicking LAHs that include a large-scale point-spread function made by instrumental and atmospheric effects. Based on our critical test with composite images of non-LAE samples whose narrowband-magnitude

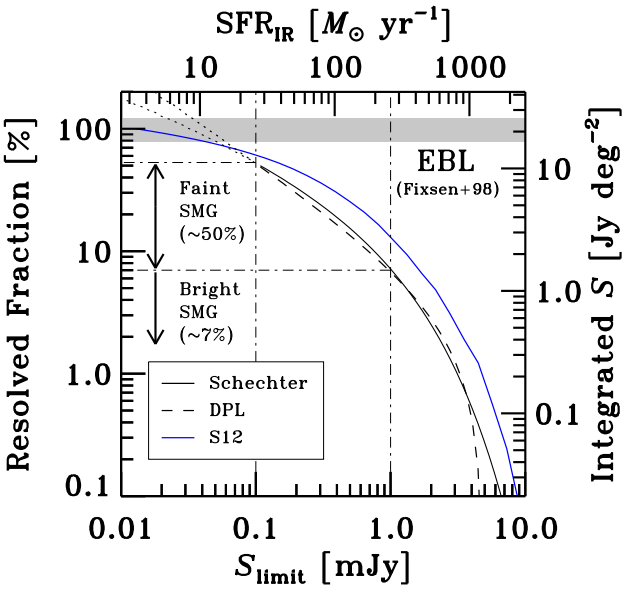

Fig. 20. Fraction of resolved background light as a function of flux density limit at 1.2 mm, $S_{\rm limit}$ with corresponding SFR$_{\rm IR}$ on the upper axis. The right axis shows the absolute value of the integrated flux density, $\int_{S_{\rm limit}}^{\infty} S\phi(S)dS$. The black solid curve and the dashed curve correspond to the cases of our best-fit Schechter function and double power-law (DPL) function, respectively. The dotted curves represent simple extrapolations of the best-fit functions down to fainter $S_{\rm limit}$ than our survey limit. The blue curve is calculated from the number counts predicted in previous work. The gray-hatched region is the extragalactic background light measured by the *COBE* satellite. This figure is reproduced by permission of the AAS.

and source-size distributions are the same as our LAE samples, we confirm that no artifacts can produce a diffuse extended feature similar to our LAHs. After this test, we measure the scale lengths of exponential profile for the LAHs estimated from our $z = 2.2-6.6$ LAE samples of $L_{{\rm Ly}\alpha} \gtrsim 2\times10^{42}$ erg s^{-1}. We obtain the scale lengths of $\simeq 5-10$ kpc at $z = 2.2-5.7$, and find no evolution of scale lengths in this redshift range beyond our measurement uncertainties. Combining this result and the previously known UV-continuum size evolution, we infer that the ratio of LAH to UV-continuum sizes is nearly constant at $z = 2.2-5.7$. The scale length of our $z = 6.6$ LAH is larger than $5-10$ kpc just beyond the error bar, which is a hint that the scale lengths of LAHs would increase from $z = 5.7$ to 6.6. If this increase is confirmed by future large surveys with significant improvements of statistical and systematical errors, this scale length change at $z \gtrsim 6$ would be a signature of increasing fraction of neutral hydrogen scattering Lyα photons, due to cosmic reionization.

Bibliography

[4] Momose, R., Ouchi, M., Nakajima, K., Ono, Y., Shibuya, T., Shimasaku, K., Yuma, S., Mori, M., & Umemura, M. 2014, Monthly Notices Roy. Astron. Soc., 442, 110–120

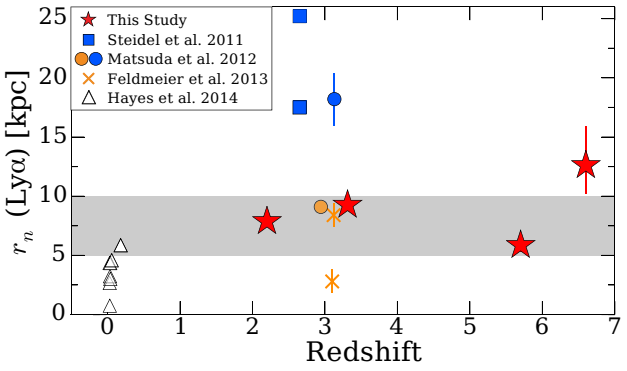

Fig. 21. Scale length as a function of redshift. The red stars represent the scale lengths estimated by the mean-combined method in this study. The gray shade indicates the range of $5-10$ kpc in which our reliable scale length estimates at $z = 2.2-5.7$ fall. The blue squares and circle denote scale lengths of LAHs found around LBGs in the literature. The orange circle represents the lowest density region LAEs, which are slightly shifted along the abscissa for clarity. The orange crosses are the scale lengths of LAHs around LAEs obtained in previous work. For reference, we plot Lyα Petrosian radii of local LAEs with the open triangles in the literature. Here, we regard galaxies with a Lyα equivalent width of ≥ 20Å as local LAEs, and plot Petrosian radii of their samples that meet this equivalent-width criterion. This figure is reproduced by permission of the RAS.

What is the Physical Origin of Strong Lyα Emission? II. Gas Kinematics and Distribution of Lyα Emitters

[5]

In collaboration with the members of University of Tsukuba, The University of Tokyo, Kavli Institute for the Physics and Mathematics of the Universe, Carnegie Observatories, and California Institute of Technology.

We present a statistical study of velocities of Lyα, interstellar (IS) absorption, and nebular lines and gas covering fraction for Lyα emitters (LAEs) at $z \simeq 2$. We make a sample of 22 LAEs with a large Lyα equivalent width (EW) of $\gtrsim 50$ Å based on our deep Keck/LRIS observations, in conjunction with spectroscopic data from the Subaru/FMOS program and the literature. We estimate the average velocity offset of Lyα from a systemic redshift determined with nebular lines to be $\Delta v_{{\rm Ly}\alpha} = 234\pm9$ km s^{-1}. Using a Kolmogorv-Smirnov test, we confirm the previous claim of Hashimoto et al. that the average $\Delta v_{{\rm Ly}\alpha}$ of LAEs is smaller than that of LBGs. Our LRIS data successfully identify blueshifted multiple IS absorption lines in the UV continua of four LAEs on an individual basis. The average velocity offset of IS absorption lines from a systemic redshift is $\Delta v_{\rm IS} = 204\pm27$ km s^{-1}, indicating LAEs' gas outflow with a velocity comparable to typical LBGs. Thus, the ratio, $R_{\rm IS}^{{\rm Ly}\alpha} \equiv \Delta v_{{\rm Ly}\alpha}/\Delta v_{\rm IS}$ of LAEs is around unity, suggestive of low impacts on Lyα transmission by resonant scattering of neutral hydrogen in the IS medium. We find an anti-correlation between Lyα EW and the covering fraction, f_c, estimated from the depth of absorption lines, where f_c is an indicator of average neutral hydrogen column density, $N_{\rm HI}$. The results of our study support the idea that $N_{\rm HI}$ is a key quantity determining Lyα emissivity.

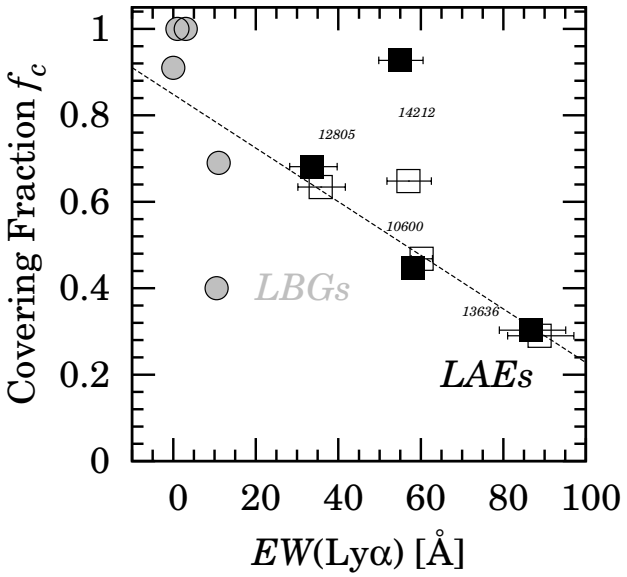

Fig. 22. Covering fraction of H I gas, f_c, as a function of Lyα EW. The f_c values of the four LAEs are estimated from the depth of the average values in the individual profile-fitting (open squares) and average LIS absorption line profiles (filled squares). The gray circles indicate LBGs at $z = 2-3$ in the literature. The dashed line denotes a linear fit to the data. This figure is reproduced by permission of the AAS.

Bibliography

[5] Shibuya, T., Ouchi, M., Nakajima, K., Hashimoto, T., Ono, Y., Rauch, M., Gauthier, J., Shimasaku, K., Goto, R., Mori, M., & Umemura, M. 2014, Astrophys. J., 788, 74

MOSFIRE and LDSS3 Spectroscopy for an [OII] Blob at $z = 1.18$: Gas Outflow and Energy Source [6]

In collaboration with the members of The University of Tokyo, Carnegie Observatories, and National Astronomical Observatory of Japan.

We report our Keck/MOSFIRE and Magellan/LDSS3 spectroscopy for an [OII] Blob, OIIB 10, that is a high-z galaxy with spatially extended [OII]$\lambda\lambda$3726,3729 emission over 30 kpc recently identified by a Subaru large-area narrowband survey. The systemic redshift of OIIB 10 is $z = 1.18$ securely determined with [OIII]$\lambda\lambda$4959,5007 and Hβ emission lines. We identify FeIIλ2587 and MgII$\lambda\lambda$2796,2804 absorption lines blueshifted from the systemic redshift by 80 ± 50 and 260 ± 40 km s^{-1}, respectively, which indicates gas outflow from OIIB 10 with the velocity of $\sim 80-260$ km s^{-1}. This outflow velocity is comparable with the escape velocity, 250 ± 140 km s^{-1}, estimated under the assumption of a singular isothermal halo potential profile. Some fraction of the outflowing gas could escape from the halo of OIIB 10, suppressing OIIB 10's star-formation activity. We estimate a mass loading factor, η, that is a ratio of mass outflow rate to star-formation rate, and obtain $\eta > 0.8\pm0.1$ which is relatively high compared with low-z starbursts including U/LIRGs and AGNs. The major energy source of the outflow is unclear with the available data. Although no signature of AGN is found in the X-ray data, OIIB 10 falls in the AGN/star-forming composite region in the line diagnostic diagrams. It is possible that the outflow is powered by star formation and a type-2 AGN with narrow FWHM emission line widths of $70-130$ km s^{-1}. This is the first detailed spectroscopic study of oxygen-line blobs, which includes the analyses of the escape velocity, the mass loading factor, and the presence of an AGN, and a significant step to understanding the nature of oxygen-line blobs and the relation with gas outflow and star-formation quenching at high redshift.

Bibliography

[6] Harikane, Y., Ouchi, M., Yuma, S., Rauch, M., Nakajima, K., & Ono, Y. 2014, Astrophys. J., 794, 129

NIR spectroscopic observation of massive galaxies in the protocluster at $z = 3.09$ [7]

In collaboration with the members of Tohoku University, Ehime University, and National Astronomical Observatory of Japan.

We present the results of near-infrared spectroscopic observations of the K-band-selected candidate galaxies in the protocluster at $z = 3.09$ in the SSA22 field. We observed 67 candidates with $K_{\rm AB} < 24$ and confirmed redshifts of the 39 galaxies at $2.0 < z_{\rm spec} < 3.4$. Of the 67 candidates, 24 are certainly protocluster members with $3.04 \leq z_{\rm spec} \leq 3.12$, which are massive red galaxies that have been unidentified in previous optical observations of the SSA22 protocluster. Many distant red galaxies (DRGs; $J-K_{\rm AB} > 1.4$), hyper extremely red objects (HEROs; $J-K_{\rm AB} > 2.1$), *Spitzer* MIPS 24 μm sources, active galactic nuclei (AGNs) as well as the counterparts of Lyα blobs and the AzTEC/ASTE 1.1 mm sources in the SSA22 field are also found to be protocluster members. The mass of the SSA22 protocluster is estimated to be $\sim 2-5\times10^{14}\ M_\odot$ and this system is plausibly a progenitor of the most massive clusters of galaxies in the current universe. The reddest ($J-K_{\rm AB} \geq 2.4$) protocluster galaxies are massive galaxies with $M_{\rm star} \sim 10^{11}\ M_\odot$ showing quiescent star formation activities and plausibly dominated by old stellar populations. Most of these massive quiescent galaxies host moderately luminous AGNs detected by X-ray. There are no significant differences in the [OIII] λ5007/Hβ emission line ratios, and [OIII] λ5007 line widths and spatial extents of the protocluster galaxies from those of massive galaxies at $z \sim 2-3$ in the general field.

Bibliography

[7] Kubo, M., Yamada, T., Ichikawa, T., Kajisawa, M., Matsuda, Y., & Tanaka, I. 2015, Astrophys. J., 799, 38

Theory Group

Overview

We have theoretically studied particle physics (mainly particle physics phenomenology) and astroparticle physics (mainly particle cosmology).

In early 2014, BICEP2 experiment had given us a significant impact by reporting the observation of B-mode polarization of the cosmic microwave background (CMB). If the signal originates from gravitational waves generated by inflation, the result might be a fingerprint of the inflationary Universe. In order to explain the result, a lot of inflationary models which predict such a large primordial B-mode signature are proposed and investigated by theoretical physist in the world. However, in early 2015, the 2015 Planck results are released and it implied that the large primordial B-mode polarization reported by BICEP2 might be a contamination by galactic foregrounds and not be a inflationary signal. Although the result by Planck is negative about such a large primordial B-mode, it make us confirm the standard model of Big bang Universe and particle physics, and also give us many implications for extensitions of the standard scenarios.

The supersymmetric (SUSY) extension of the standard model (SM) in the particle physics is considered to be one of the most promising models beyond the standard model. It solves the naturalness problem for the Higgs boson mass term in the standard model, and it is also compatible with the grand unified theories (GUTs). Our group has been studying phenomenological and cosmological aspects of the SUSY models.

Recent cosmological observations including the Planck data determine precisely the mean densities of matter and baryon in the Universe, and existence of non-baryonic dark matter is established. Weakly interacting massive particles (WIMPs) are considered to be good candidates of the dark matter. They act as the cold dark matter in the structure formation of the universe. Our group has been studying model building for dark matter and detectability in direct and indirect search experiments.

For understanding of the early universe, a role of the elementary particle physics is crucial. Recent progress in the particle physics such as grand unification theories and supersymmetry leads us to a more deeper insight into the fundamental aspects of the early universe. In the inflationary universe, the quantum fluctuations of the scalar field which drives the inflation become the density fluctuations and lead to formation of the structure observed in the present universe. On the other hand cosmology and astrophysics are used to test new theories in particle physics. Such particle cosmology is one of main subjects of our group.

Big Bang Nucleosynthesis (BBN) is one of the most important subjects in modern cosmology. Predicted abundances of the light elements are very sensitive to the cosmological scenario. On the other hand, physics beyond the standard model predicts the new particles which would have existed at the BBN epoch. Such particles may spoil the success of BBN, which leads to constraints on the new particles and the particle physics models.

The grand unified theories (GUT) predict that our universe undergoes several vacuum phase transitions. In the course of phase transitions topological defects (monopoles, cosmic strings and domain walls) are generally produced depending on symmetries of the vacua. Our group has studied evolution of various topological defects.

Particle Phenomenology

[Spokesperson : M. Ibe]
ICRR, The Univ. of Tokyo, Kashiwa, Chiba 277-8582

Dark Matter, Inflation

• *Simple realization of inflaton potential on a Riemann surface*

In collaboration with the members of ICRR and Kavli IPMU

The observation of the B-mode in the cosmic microwave background radiation combined with the so-called Lyth bound suggests the trans-Planckian variation of the inflaton field during inflation. Such a large variation generates concerns over inflation models in terms of the effective field theory below the Planck scale. If the inflaton resides in a Riemann surface and the inflaton potential is a multivalued function of the inflaton field when it is viewed as a function on a complex plane, the Lyth bound can be satisfied while keeping field values in the effective field theory within the Planck scale. We show that a multivalued inflaton potential can be realized starting from a single-valued Lagrangian of the effective field theory below the Planck scale [1].

• *Vanishing Higgs potential at the Planck scale in a singlet extension of the standard model*

In collaboration with the members of ICRR and Shimane University

We discuss the realization of a vanishing Higgs potential at the Planck scale, which is required by the multiple point criticality principle (MPCP), in the standard model with singlet scalar dark matter and a right-handed neutrino. We find the scalar dark matter and the right-handed neutrino play crucial roles for realization of the MPCP, where a neutrino Yukawa becomes effective above Majorana mass of the right-handed neutrino. Once the top mass is fixed, the MPCP at the (reduced) Planck scale and the suitable dark matter relic abundance determine the dark matter mass, m_S, and Majorana mass of the right-handed neutrino, M_R, as $8.5\ (8.0) \times 10^2$ GeV $\leq m_S \leq 1.4\ (1.2) \times 10^3$ GeV and $6.3\ (5.5) \times 10^{13}$ GeV $\leq M_R \leq 1.6\ (1.2) \times 10^{14}$ GeV within current experimental values of the Higgs and top masses. This scenario is consistent with current dark matter direct search experiments and will be checked by future experiments such as LUX with further exposure and/or the XENON1T [2].

•*Wino Dark Matter and Future dSph Observations*

In collaboration with the members of ICRR and Kavli IPMU

We discuss the indirect detection of the wino dark matter utilizing gamma-ray observations of dwarf spheroidal galaxies (dSphs). After carefully reviewing current limits with particular attention to astrophysical uncertainties, we show prospects of the wino mass limit in future gamma-ray observation by the Fermi-LAT and the GAMMA-400 telescopes. We find that the improvement of the so-called J-factor of both the classical and the ultra-faint dSphs will play a crucial role to cover whole mass range of the wino dark matter. For example, with $\delta(\log 10J) = 0.1$ for both the classical and the ultra-faint dSphs, whole wino dark matter mass range can be covered by 15 years and 10 years data at the Fermi-LAT and GAMMA-400 telescopes, respectively [3].

• *Dynamical fractional chaotic inflation*

In collaboration with the members of ICRR and Kavli IPMU

Chaotic inflation based on a simple monomial scalar potential, $V(\phi) \propto \phi^p$, is an attractive large-field model of inflation capable of generating a sizable tensor-to-scalar ratio r. Therefore, assuming that future cosmic microwave background observations will confirm the large r value reported by BICEP2, it is important to determine what kind of dynamical mechanism could possibly endow the inflaton field with such a simple effective potential. In this paper, we answer this question in the context of field theory, i.e. in the framework of dynamical chaotic inflation, where strongly interacting supersymmetric gauge dynamics around the scale of grand unification dynamically generate a fractional power-law potential via the quantum effect of dimensional transmutation. In constructing explicit models, we significantly extend our previous work, as we now consider a large variety of possible underlying gauge dynamics and relax our conditions on the field content of the model. This allows us to realize almost arbitrary rational values for the power p in the inflaton potential. The present paper may hence be regarded as a first step toward a more complete theory of dynamical chaotic inflation [4].

• *Phase Locked Inflation – Effectively Trans-Planckian Natural Inflation*

In collaboration with the members of ICRR and Kavli IPMU

A model of natural inflation with an effectively trans- Planckian decay constant can be easily achieved by the phase locking mechanism while keeping field values in the effective field theory within the Planck scale. We give detailed description of phase locked inflation based on this mechanism. We also construct supersymmetric natural inflation based on this mechanism and show that the model is consistent with low scale supersymmetry. We also investigate couplings of the inflaton with the minimal supersymmetric standard model to achieve an appropriate reheating process. Interestingly, in a certain class of models, we find that the inflation scale is related to the mass of the right-handed neutrino in a consistent way with the seesaw mechanism [5].

• *R-symmetric Axion/Natural Inflation in Supergravity via Deformed Moduli Dynamics*

In collaboration with the members of ICRR and Kavli IPMU

We construct a natural inflation model in supergravity where the inflaton is identified with a modulus field possessing a shift symmetry. The superpotential for the inflaton is generated by meson condensation due to strong dynamics with deformed moduli constraints. In contrast to models based on gaugino condensation, the inflaton potential is generated without R - symmetry breaking and hence does not depend on the gravitino mass. Thus, our model is compatible with low scale supersymmetry [6].

• *Mass of Decaying Wino from AMS-02 2014*

In collaboration with the members of ICRR and Kavli IPMU

We revisit the decaying wino dark matter scenario in the light of the updated positron fraction, electron and positron fluxes in cosmic ray recently reported by the AMS-02 collaboration. We show the AMS-02 results favor the mass of the wino dark matter at around a few TeV, which is consistent with the prediction on the wino mass in the pure gravity mediation model [7].

• *Coupling Unification and Dark Matter in a Standard Model Extension with Adjoint Majorana Fermions*

In collaboration with the members of ICRR

We revisit an extension of the Standard Model with Majorana fermions in the adjoint representations. There, a precise coupling unification and the good candidate for dark matter (the $SU(2)_L$ triplet fermion) are achieved simultaneously. In particular, we show that the $SU(3)_c$ octet fermion which is required for successful unification can be a good non-thermal source of the triplet fermion dark matter. We also show that the scenario predicts a rather short lifetime of the proton compared with the supersymmetric Standard Model, and the most parameter space can be explored by the future experiments such as the Hyper-Kamiokande experiment[8].

Bibliography

[1] K. Harigaya and M. Ibe, Phys. Lett. B **738**, 301 (2014) [arXiv:1404.3511 [hep-ph]].

[2] N. Haba, H. Ishida, K. Kaneta and R. Takahashi, Phys. Rev. D **90**, 036006 (2014) [arXiv:1406.0158 [hep-ph]].

[3] B. Bhattacherjee, M. Ibe, K. Ichikawa, S. Matsumoto and K. Nishiyama, JHEP **1407** (2014) 080 [arXiv:1405.4914 [hep-ph]].

[4] K. Harigaya, M. Ibe, K. Schmitz and T. T. Yanagida, Phys. Rev. D **90** (2014) 12, 123524 [arXiv:1407.3084 [hep-ph]].

[5] K. Harigaya and M. Ibe, JHEP **1411** (2014) 147 [arXiv:1407.4893 [hep-ph]].

[6] K. Harigaya, M. Ibe and T. T. Yanagida, Phys. Lett. B **739** (2014) 352 [arXiv:1409.0330 [hep-ph]].

[7] M. Ibe, S. Matsumoto, S. Shirai and T. T. Yanagida, Phys. Lett. B **741**, 134 (2015) [arXiv:1409.6920 [hep-ph]].

[8] T. Aizawa, M. Ibe and K. Kaneta, Phys. Rev. D **91**, no. 7, 075012 (2015) [arXiv:1411.6044 [hep-ph]].

Extensions of the Standard Model

• *Gaugino coannihilations*

In collaboration with the members of ICRR and Kavli IPMU.

The high-scale supersymmetry (SUSY) breaking scenario is now attracting many attentions, because it is consistent with almost all experiments of particle physics, astrophysics, and cosmology performed so far: e.g. it is possible to explain the Higgs mass of about 126 GeV and contains WIMP dark matter candidates. In the scenario, gauginos are predicted to be around the TeV scale, and thus within a kinematically accessible range of near future experiments. Calculation of the thermal relic abundance for gaugino (bino or wino) dark matter is then of particular importance in order to clarify its mass consistent with cosmology and to determine future directions for exploring the high-scale SUSY breaking scenario. In this article, we calculate the abundance of the gaugino dark matter, with especially focusing on various coannihilations between gauginos, which has not been extensively studied so far. Our calculation involves the Sommerfeld effect on wino and gluino annihilations, which is known to give significant contributions to their cross sections. Based on obtained results, we discuss some implications to gaugino searches at collider and indirect detection experiments of dark matter [1]. See Fig. 23.

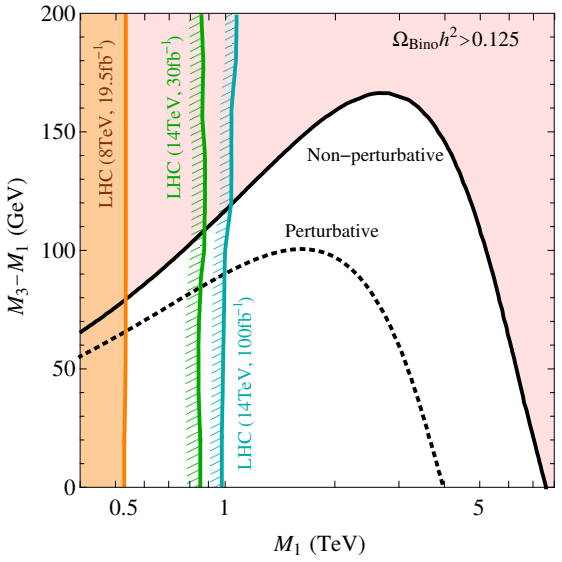

Fig. 23. Coannihilation region between bino and gluino. The bino dark matter is over-produced in the region above the black line. For comparison, the result without the Sommerfeld effect is shown as the black dotted line. Current and future- expected limits on the region from the LHC experiment are also shown.

• *CνB absorption line in the neutrino spectrum at IceCube*

In collaboration with the members of ICRR

The IceCube experiment has recently reported high energy neutrino spectrum between TeV−PeV scale. The observed neutrino flux can be as a whole well fitted by a simple power-law of the neutrino energy E_ν, $E_\nu^{-\gamma_\nu}$ ($\gamma_\nu \simeq 2$). As a notable feature of the spectrum, however, it has a gap between 500 TeV and 1 PeV. Although the existence of the gap in the neutrino spectrum is not statistically significant at this point, it is very enticing to ask whether it might hint some physics beyond the Standard Model. In this paper, we investigate a possibility that the gap can be interpreted as an absorption line in the power-law spectrum by the cosmic neutrino background through a new resonance in the MeV range. We also show that the absorption line has rich information about not only the MeV scale new particle but also the neutrino masses as well as the distances to the astrophysical sources of the high energy neutrinos. Viable models to achieve this possibility are also discussed [2].

• Gravitational effects on vanishing Higgs potential at the Planck scale

In collaboration with the members of ICRR, Shimane University and Hokkaido University

We investigate gravitational effects on the so-called multiple point criticality principle (MPCP) at the Planck scale. The MPCP requires two degenerate vacua, whose necessary conditions are expressed by vanishing Higgs quartic coupling $\lambda(M_{\rm Pl}) = 0$ and vanishing its β function $\beta_\lambda(M_{\rm Pl}) = 0$. We discuss a case that a specific form of gravitational corrections are assumed to contribute to β functions of coupling constants although it is accepted that gravitational corrections do not alter the running of the standard model (SM) couplings. To satisfy the above two boundary conditions at the Planck scale, we find that the top pole mass and the Higgs mass should be $170.8\,{\rm GeV} \lesssim M_t \lesssim 171.7\,{\rm GeV}$ and $M_h = 125.7 \pm 0.4\,{\rm GeV}$, respectively, as well as include suitable magnitude of gravitational effects (a coefficient of gravitational contribution as $|a_\lambda| > 2$). In this case, however, since the Higgs quartic coupling λ becomes negative below the Planck scale, two vacua are not degenerate. We find that $M_h \gtrsim 131.5\,{\rm GeV}$ with $M_t \gtrsim 174\,{\rm GeV}$ is required by the realization of the MPCP. Therefore, the MPCP at the Planck scale cannot be realized in the SM and also the SM with gravity since $M_h \gtrsim 131.5\,{\rm GeV}$ is experimentally ruled out [3].

• *Anomaly Mediated Gaugino Mass and Path-Integral Measure*

In collaboration with the members of ICRR and Kavli IPMU

In recent years, there has been controversy concerning the anomaly-mediated gaugino mass in the superspace formal-

ism of supergravity. In this paper, we reexamine the gaugino mass term in this formalism by paying particular attention to the symmetry that controls gaugino masses in supergravity. We first discuss super-diffeomorphism invariance of path-integral measures of charged superfields. As we will show, the super-diffeomorphism-invariant measure is not invariant under a super-Weyl transformation, which is the origin of the anomaly-mediated gaugino mass. We show how the anomaly-mediated gaugino mass is expressed as a local operator in a Wilsonian effective action in a super-diffeomorphism-covariant way. We also obtain a gaugino mass term independent of the gauge choice of the fictitious super-Weyl symmetry in the super-Weyl compensator formalism, which reproduces the widely accepted result. We also discuss how to reconcile the gaugino mass term in the local Wilsonian effective action and the gaugino mass term appearing in a nonlocal one-particle irreducible quantum effective action [4].

• *Light Higgsinos in Pure Gravity Mediation*

In collaboration with the members of ICRR, Kavli IPMU and Minnesota University

Pure gravity mediation, with two free parameters, is a minimalistic approach to supergravity models, yet it is capable of incorporating radiative electroweak symmetry breaking, a Higgs mass in agreement with the experimental measurement, without violating any phenomenological constraints. The model may also contain a viable dark matter candidate in the form of a wino. Here, we extend the minimal model by allowing the term to be a free parameter equivalent to allowing the two Higgs soft masses, m1 and m2, to differ from other scalar masses, which are set by the gravitino mass. In particular, we examine the region of parameter space where łm3/2, in which case the Higgsino becomes the lightest supersymmetric particle and a dark matter candidate. We also consider a generalization of pure gravity mediation that incorporates a Peccei-Quinn symmetry which determines the term dynamically. In this case we show that the dark matter may either be in the form of an axion and/or a neutralino and that the lightest supersymmetric particle may be either a wino, bino, or Higgsino [5].

Bibliography

[1] K. Harigaya, K. Kaneta and S. Matsumoto, Phys. Rev. D **89**, no. 11, 115021 (2014) [arXiv:1403.0715 [hep-ph]].

[2] M. Ibe and K. Kaneta, Phys. Rev. D **90**, no. 5, 053011 (2014) [arXiv:1407.2848 [hep-ph]].

[3] N. Haba, K. Kaneta, R. Takahashi and Y. Yamaguchi, Phys. Rev. D **91**, no. 1, 016004 (2015) [arXiv:1408.5548 [hep-ph]].

[4] K. Harigaya and M. Ibe, Phys. Rev. D **90**, no. 8, 085028 (2014) [arXiv:1409.5029 [hep-th]].

[5] J. L. Evans, M. Ibe, K. A. Olive and T. T. Yanagida, Phys. Rev. D **91**, no. 5, 055008 (2015) [arXiv:1412.3403 [hep-ph]].

Particle Cosmology

[Spokesperson : M. Kawasaki]
ICRR, The Univ. of Tokyo, Kashiwa, Chiba 277-8582

Inflation and Thermal History in the early Universe

• *Physics in the early Universe in light of Planck and BICEP2*

In collaboration with the members of ICRR, Kavli IPMU, University of Helsinki, Saga University and Tokyo University of Science

In March 2014, BICEP2 experiment has reported a large tensor-to-scalar ratio, $r \approx 0.2$ from the cosmic microwave background (CMB) B-mode polarization data. On the other hand, Planck satellite has given a tight constraint on the tensor-to-scalar -ratio as $r \lesssim 0.1$ from the CMB observations.

In such a situation, first we show that a simple curvaton model can realize a compensation for large tensor modes with iso-curvature perturbations in the CMB temperature anisotropies [1]. We also investigate the degeneracy of the isocurvature perturbations and the primordial gravitational waves, by using recent CMB observations reported by Planck and BICEP2 collaborations. We show that the tension in the bound on the tensor-to-scalar ratio r between Planck and BICEP2 can be resolved by introducing the anti-correlated isocurvature perturbations. Quantitatively, we find that with the anti-correlated isocurvature perturbations the constraints on r from Planck alone and BICEP2 results can be consistent at 68 % C.L. [2].

We also comprehensively explore the quadratic curvaton models in the chaotic inflation. In the light of the BICEP2 result $r \approx 0.2$, all model parameters and relevant observables are computed. It is found the curvaton field value is constrained into a narrow range, $\sigma_* = O(10^{-2} - 10^{-1})$ and the running of the spectral index is $n_s' \gtrsim -10^{-3}$. We show that if the curvaton is added, the models are heavily degenerated on the n_s - r plane. However, introducing a new plane, the degeneracy can be resolved. To distinguish the curvaton models, precise measurements of not only r but also n_s and the tensor tilt n_T are required [3].

BICEP2 result also motivates the study of blue-tilted primordial gravitational waves. We investigate constraints on the spectral index of primordial gravitational waves (GWs), paying particular attention to a blue-tilted spectrum. Such constraints can be used to test a certain class of models of the early Universe. We investigate observational bounds from LIGO+Virgo, pulsar timing and big bang nucleosynthesis, taking into account the suppression of the amplitude at high frequencies due to reheating after inflation and also late-time entropy production. Constraints on the spectral index are presented by changing values of parameters such as reheating temperatures and the amount of entropy produced at late time. We also consider constraints under the general modelling approach which can approximately describe various scenarios of the early Universe. We show that the constraints on the blue spectral tilt strongly depend on the underlying assumption and, in some cases, a highly blue-tilted spectrum can still be allowed [4]. See Fig. 24.

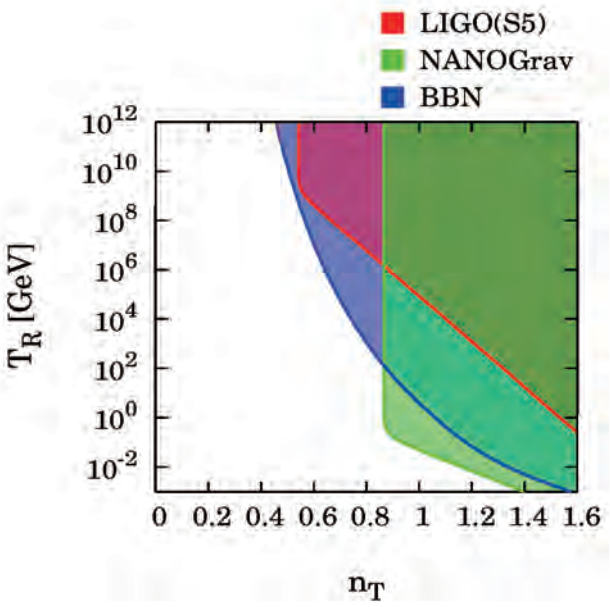

Fig. 24. 2σ excluded region (colored) in the $n_T - T_R$ plane for the case of the standard reheating scenario. The tensor-to-scalar ratio is assumed to be $r = 0.2$.

• *Lower bound of the tensor-to-scalar ratio $r \gtrsim 0.1$ in a nearly quadratic chaotic inflation model in supergravity*

In collaboration with the members of ICRR and Kavli IPMU

We consider an initial condition problem in a nearly quadratic chaotic inflation model in su- pergravity. We introduce shift symmetry breaking not only in the superpotential but also in the Kahler potential. In this model the inflaton potential is nearly quadratic for inflaton field values around the Planck scale, but deviates from the quadratic one for larger field values. As a result, the prediction on the tensor-to-scalar ratio can be smaller than that of a purely quadratic model. Due to the shift symmetry breaking in the Kahler potential, the inflaton potential becomes steep for large inflaton field values, which may prevent inflation from naturally taking place in a closed universe. We estimate an upper bound on the magnitude of the shift symmetry breaking so that inflation takes place before a closed universe with a Planck length size collapses, which yields a lower bound on the tensor-to-scalar ratio, $r \gtrsim 0.1$ [5].

• *Inflatonic baryogenesis with large tensor mode*

In collaboration with the members of ICRR

We consider the complex inflaton field with a CP asymmetric term for its potential. This CP asymmetric term produces the global charge of the inflaton after inflation. With the assignment of the baryon number to the inflaton, the baryon asymmetry of the universe is produced by inflaton's decay. In addition to this, the $U(1)$ breaking term modulates the curvature of the inflaton radial direction depending on its phase, which affects the tensor to scalar ratio. In this paper, we have studied the relation between the baryon asymmetry and the tensor to scalar ratio, then verified that the future CMB observation could test this baryogenesis scenario with large tensor mode [6].

• *No quasi-stable scalaron lump forms after R^2 inflation*

In collaboration with the members of ICRR and RESCEU

In the Einstein frame picture of Starobinky's R^2 inflation model, cosmic inflation is driven by a slowly rolling inflaton field, called scalaron, and followed by a coherently oscillating scalaron phase. Since the scalaron oscillates excessively many times in its potential, which has a quadratic minimum and is a little shallower than quadratic on the positive side, it may fragment into long-living localized objects, called oscillons or I-balls, due to nonlinear growth of fluctuations before reheating of the universe. We show that while parametric self-resonances amplify scalaron fluctuations in the Minkowski background, the growth cannot overcome the decay due to expansion in the Friedmann background after R^2 inflation. By taking into account back-reaction from the metric of space-time, modes that are larger than a critical scale are indeed amplified and become non-decaying. However, those non-decaying modes are not growing enough to form spatially localized lumps of the scalaron. Thus, reheating processes are unaltered by oscillons/I-balls and they proceed through perturbative decay of the scalaron as studied in the original work [7].

• *Thermal Effects and Sudden Decay Approximation in the Curvaton Scenario*

In collaboration with the members of ICRR, Tohoku University, APC-Paris and Saga University

We study the impact of a temperature-dependent curvaton decay rate on the primordial curvature perturbation generated in the curvaton scenario. Using the familiar sudden decay approximation, we obtain an analytical expression for the curvature perturbation after the decay of the curvaton. We then investigate numerically the evolution of the background and of the perturbations during the decay. We first show that the instantaneous transfer coefficient, related to the curvaton energy fraction at the decay, can be extended into a more general parameter, which depends on the net transfer of the curvaton energy into radiation energy or, equivalently, on the total entropy ratio after the complete curvaton decay. We then compute the curvature perturbation and compare this result with the sudden decay approximation prediction [8].

• *CDM/baryon isocurvature perturbations in a sneutrino curvaton model*

In collaboration with the members of ICRR, Kavli IPMU and Rikkyo University

Matter isocurvature perturbations are strictly constrained from cosmic microwave background observations. We study a sneutrino curvaton model where both cold dark matter (CDM)/baryon isocurvature perturbations are generated. In our model, total matter isocurvature perturbations are reduced since the

CDM/baryon isocur- vature perturbations compensate for each other. We show that this model can not only avoid the stringent observational constraints but also suppress temperature anisotropies on large scales, which leads to improved agreement with observations [9].

• *Consistent generation of magnetic fields in axion inflation models*

In collaboration with the members of ICRR, Kavli IPMU and Nagoya Univsersity

There has been a growing evidence for the existence of magnetic fields in the extra-galactic regions, while the attempt to associate their origin with the inflationary epoch alone has been found extremely challenging. We therefore take into account the consistent post-inflationary evolution of the magnetic fields that are originated from vacuum fluctuations during inflation. In the model of our interest, the electromagnetic (EM) field is coupled to a pseudo-scalar inflaton ϕ through the characteristic term $\phi F\tilde{F}$, breaking the conformal invariance. This interaction dynamically breaks the parity and enables a continuous production of only one of the polarization states of the EM field through tachyonic instability. The produced magnetic fields are thus helical. We find that the dominant contribution to the observed magnetic fields in this model comes from the modes that leave the horizon near the end of inflation, further enhanced by the tachyonic instability right after the end of inflation. The EM field is subsequently amplified by parametric resonance during the period of inflaton oscillation. Once the thermal plasma is formed (reheating), the produced helical magnetic fields undergo a turbulent process called inverse cascade, which shifts their peak correlation scales from smaller to larger scales. We consistently take all these effects into account within the regime where the perturbation of ϕ is negligible and obtain $B_{\rm eff} \sim 10^{-19}$G, indicating the necessity of additional mechanisms to accommodate the observations [10].

Bibliography

[1] M. Kawasaki and S. Yokoyama, JCAP **1405**, 046 (2014) [arXiv:1403.5823 [astro-ph.CO]].

[2] M. Kawasaki, T. Sekiguchi, T. Takahashi and S. Yokoyama, JCAP **1408**, 043 (2014) [arXiv:1404.2175 [astro-ph.CO]].

[3] T. Fujita, M. Kawasaki and S. Yokoyama, JCAP **1409**, 015 (2014) [arXiv:1404.0951 [astro-ph.CO]].

[4] S. Kuroyanagi, T. Takahashi and S. Yokoyama, JCAP **1502**, 003 (2015) [arXiv:1407.4785 [astro-ph.CO]].

[5] K. Harigaya, M. Kawasaki and T. T. Yanagida, Phys. Lett. B **741**, 267 (2015) [arXiv:1410.7163 [hep-ph]].

[6] N. Takeda, Phys. Lett. B **746**, 368 (2015) [arXiv:1405.1959 [astro-ph.CO]].

[7] N. Takeda and Y. Watanabe, Phys. Rev. D **90**, no. 2, 023519 (2014) [arXiv:1405.3830 [astro-ph.CO]].

[8] N. Kitajima, D. Langlois, T. Takahashi, T. Takesako and S. Yokoyama, JCAP **1410**, no. 10, 032 (2014) [arXiv:1407.5148 [astro-ph.CO]].

[9] K. Harigaya, T. Hayakawa, M. Kawasaki and S. Yokoyama, JCAP **1410**, no. 10, 068 (2014) [arXiv:1409.1669 [hep-ph]].

[10] T. Fujita, R. Namba, Y. Tada, N. Takeda and H. Tashiro, JCAP **1505**, no. 05, 054 (2015) [arXiv:1503.05802 [astro-ph.CO]].

Dark Matter, Baryogenesis, Big-Bang nucleosynthesis

• *Affleck-Dine Baryogenesis and Dark Matter Production after High-scale Inflation*

In collaboration with the members of ICRR, Kavli IPMU, and The University of Tokyo

The discovery of the primordial B-mode polarization by the BICEP2 experiment indicates inflation with a relatively high energy scale. Taking this indication into account, we propose consistent scenarios to account for the observed baryon and dark matter densities in gravity and gauge mediated supersymmetry breaking models. The baryon asymmetry is explained by the Affick-Dine mechanism, which requires relatively low reheating temperature to avoid a sizable baryonic isocurvature perturbation. The low reheating temperature then requires non-thermal production of dark matter to account for the correct relic density of dark matter. Our scenarios can account for the observations of baryon and dark matter density in gravity and gauge mediation and predict some parameters, including the mass of dark matter [1].

• *A solution to the baryon-DM coincidence problem in the CMSSM with a 126-GeV Higgs boson*

In collaboration with the members of ICRR and Kavli IPMU

We show that the baryon-dark matter coincidence problem is solved in the CMSSM. The baryons and dark matter are generated simultaneously through the late-time decay of non-topological solitons, Q-balls, which are formed after the Affleck-Dine baryogenesis. A certain relation between the universal scalar mass, m_0, and the universal gaugino mass, $M_{1/2}$, is required to solve the coincidence problem, marginally depending on the other CMSSM parameters, and the result is consistent with the observation of the 126-GeV Higgs boson [2]. See Fig25.

• *Affleck-Dine baryogenesis after D-term inflation and solutions to the baryon-DM coincidence problem*

In collaboration with the members of ICRR and Kavli IPMU

We investigate the Affleck-Dine baryogenesis after D-term inflation with a positive Hubble-induced mass term for a $B-L$ flat direction. It stays at a large field value during D-term inflation, and just after inflation ends it starts to oscillate around

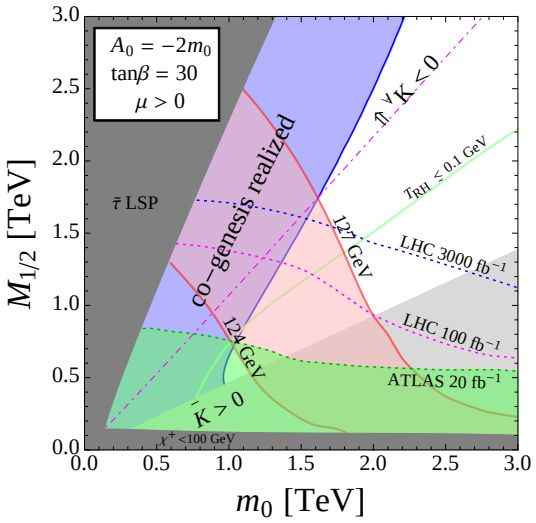

Fig. 25. . Allowed contours consistent with observations in $(m_0, M_{1/2})$ planes of the CMSSM, with $\tan\beta = 30$ and $A_0 = -2m_0$ with $\mathrm{sign}[\mu] = +1$.

the origin of the potential due to the positive Hubble-induced mass term. The phase direction is kicked by higher-dimensional Kahler potentials to generate the $B-L$ asymmetry. The scenario predicts nonzero baryonic isocurvature perturbations, which would be detected by future observations of CMB fluctuations. We also provide a D-term inflation model which naturally explain the coincidence of the energy density of baryon and dark matter [3].

• *Q-ball dark matter in gauge mediated SUSY breaking models*

In collaboration with the members of Kanagawa University, ICRR and Kavli IPMU

We investigate the scenario that one flat direction creates baryon asymmetry of the universe, while Q balls from another direction can be the dark matter in the gauge-mediated supersymmetry breaking for high-scale inflation. Isocurvature fluctuations are suppressed by the fact that the Affleck-Dine field stays at around the Planck scale during inflation. We find that the dark matter Q balls can be detected in IceCube-like experiments in the future [4, 5].

• *Axion dark matter from topological defects*

In collaboration with the members of Tokyo Institute of Technology, University of Helsinki, Kavli IPMU and ICRR

The cosmological scenario where the Peccei-Quinn symmetry is broken after inflation is investi- gated. In this scenario, topological defects such as strings and domain walls produce a large number of axions, which contribute to the cold dark matter of the universe. The previous estimations of the cold dark matter abundance are updated and refined based on the field-theoretic simulations with improved grid sizes. The possible uncertainties originated in the numerical calculations are also discussed. It is found that axions can be responsible for the cold dark matter in the mass range $m_a = (0.9-1.4)\times 10^{-4}$ eV for the models with the domain wall number $N_{\rm DW} = 1$, and $m_a \simeq O(10^{-4}-10^{-2})$ eV with a mild tuning of parameters for the models with $N_{\rm DW} > 1$. Such higher mass ranges can be probed in future experimental studies [6].

• *Relaxing Isocurvature Bounds on String Axion Dark Matter*

In collaboration with the members of Tohoku University, Kavli IPMU and ICRR

If inflation scale is high, light scalars acquire large quantum fluctuations during inflation. If sufficiently long-lived, they will give rise to CDM isocurvature perturbations, which are highly constrained by the Planck data. Focusing on string axions as such light scalars, we show that thermal inflation can provide a sufficiently large entropy production to dilute the CDM isocur- vature perturbations. Importantly, efficient dilution is possible for the string axions, because effectively no secondary coherent oscillations are induced at the end of thermal inflation, in contrast to the moduli fields. We also study the viability of the axion dark matter with mass of about 7keV as the origin of the 3.5keV X-ray line excess, in the presence of large entropy production. [7]

• *Chemical separation of primordial Li^+ during structure formation caused by nanogauss magnetic field*

In collaboration with the members of Kavli IPMU and ICRR

During the structure formation, charged and neutral chemical species may have separated from each other at the gravitational contraction in primordial magnetic field (PMF). It is shown that the charged fluid, i.e., proton, electron and $^7Li^+$, can significantly decouple from the neutral fluid depending on the field amplitude. This type of chemical separation can reduce the abundance ratio of Li/H in early structures because of inefficient contraction of $^7Li^+$ ion. Therefore, it may explain Li abundances of Galactic metal-poor stars which are smaller than the prediction in standard big bang nucleosynthesis model [8].

Bibliography

[1] K. Harigaya, A. Kamada, M. Kawasaki, K. Mukaida and M. Yamada, Phys. Rev. D **90**, no. 4, 043510 (2014) [arXiv:1404.3138 [hep-ph]].

[2] A. Kamada, M. Kawasaki and M. Yamada, Phys. Rev. D **91**, no. 8, 081301 (2015) [arXiv:1405.6577 [hep-ph]].

[3] M. Kawasaki and M. Yamada, Phys. Rev. D **91**, no. 8, 083512 (2015) [arXiv:1502.03550 [hep-ph]].

[4] S. Kasuya and M. Kawasaki, Phys. Lett. B **739**, 174 (2014) [arXiv:1408.1176 [hep-ph]].

[5] S. Kasuya, M. Kawasaki and T. T. Yanagida, PTEP **2015**, no. 5, 053B02 (2015) [arXiv:1502.00715 [hep-ph]].

[6] M. Kawasaki, K. Saikawa and T. Sekiguchi, Phys. Rev. D **91**, no. 6, 065014 (2015) [arXiv:1412.0789 [hep-ph]].

[7] M. Kawasaki, N. Kitajima and F. Takahashi, Phys. Lett. B **737**, 178 (2014) [arXiv:1406.0660 [hep-ph]].

[8] M. Kusakabe and M. Kawasaki, Mon. Not. Roy. Astron. Soc. **446**, 1597 (2015) [arXiv:1404.3485 [astro-ph.CO]].

Gravitational waves

• *Gravitational waves as a probe of SUSY scale*

In collaboration with the members of ICRR and IPMU

We investigate the sources of the Hubble-induced mass for a flat direction in supersymmetric theories and show that the sign of the Hubble-induced mass generally changes just after the end of inflation. This implies that global cosmic strings generally form after the end of inflation in a wide class of supersymmetric models, including the Minimal Supersymmetric Standard Model. The cosmic strings emit gravitational waves whose frequency corresponds to the Hubble scale, until they disappear when the Hubble parameter decreases down to the soft mass of the flat direction. As a result, the peak frequency of gravitational waves is related to the supersymmetric scale. The observation of this gravitational wave signal, in conjunction with results from collider experiments and dark matter searches, can yield information of supersymmetry-breaking parameters [1].

• *Gravitational waves from domain walls in the next-to-minimal supersymmetric standard model*

In collaboration with the members of Institute for Basic Science, Tokyo Institute of Technology, ICRR and IPMU

The next-to-minimal supersymmetric standard model predicts the formation of domain walls due to the spontaneous breaking of the discrete Z3-symmetry at the electroweak phase transition, and they collapse before the epoch of big bang nucleosynthesis if there exists a small bias term in the potential which explicitly breaks the discrete symmetry. Signatures of gravitational waves produced from these unstable domain walls are estimated and their parameter dependence is investigated. It is shown that the amplitude of gravitational waves becomes generically large in the decoupling limit, and that their frequency is low enough to be probed in future pulsar timing observations [2].

Bibliography

[1] A. Kamada and M. Yamada, Phys. Rev. D **91**, 063529 (2015) [arXiv:1407.2882 [hep-ph]].

[2] K. Kadota, M. Kawasaki and K. Saikawa, arXiv:1503.06998 [hep-ph].

OBSERVATORIES and A RESEARCH CENTER

Location of the Institute and the Observatories in Japan

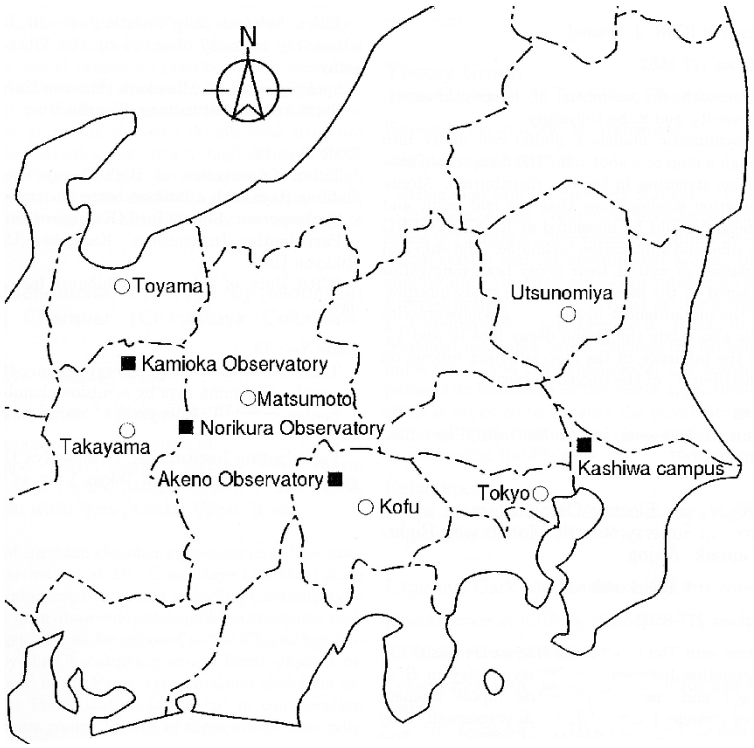

Norikura Observatory

Location:	Norikuradake, Nyukawa-cho, Takayama-shi, Gifu Prefecture 506-2100 N 36°06′, E 137°33′, 2770 m a.s.l.
Telephone (Fax):	050-3730-3809
Telephone (satellite):	090-7721-5674
Telephone (car):	090-7408-6224

Akeno Observatory

Location:	5259 Asao, Akeno-machi, Hokuto-shi, Yamanashi Prefecture 408-0201 N 35°47′, E 138°30′, 900 m a.s.l.
Telephone / Fax:	+551-25-2301 / +551-25-2303

Kamioka Observatory

Location:	456 Higashi-mozumi, Kamioka-cho, Hida-shi, Gifu Prefecture 506-1205 N 36°25′26″, E 137°19′11″, 357.5 m a.s.l.
Telephone / Fax:	+578-85-2116 / +578-85-2121

Research Center for Cosmic Neutrinos

Location:	5-1-5 Kashiwanoha, Kashiwa, Chiba Prefecture 277-8582
Telephone / Fax:	+4-7136-3138 / +4-7136-3115

NORIKURA OBSERVATORY

Introduction

Norikura Observatory (36.10°N and 137.55°E) was founded in 1953 and attached to ICRR in 1976. It is located at 2770 m above sea level, and is the highest altitude manned laboratory in Japan. Experimental facilities of the laboratory are made available to all the qualified scientists in the field of cosmic ray research and associated subjects. The AC electric power is generated by the dynamo and supplied throughout the observatory. In 1996, two dynamos of 70 KVA each were replaced with the new ones. The observatory can be accessed easily by car and public bus in summer (July-September). The 50th anniversary of Norikura Observatory was celebrated in 2003.

Fig. 1. Norikura Observatory.

The feasibility of the automatic operation of Norikura Observatory during winter period has been tested since winter 2004 in order to study the possibilities to reduce maintenance and labor costs without seriously damaging to the use of researches. A long-distance (∼40km) wireless LAN system (11M bps) was set up in 2003. Two new easy-to-handle and easy-to-maintain dynamos of 115 KVA each were installed in 2004 as well. The unmanned operation of Norikura Observatory has been mostly successful in winter, during which the battery backed-up solar panels and/or wind power generators kept supplying the electricity to the wireless LAN and on-going cosmic-ray experiments. The 60th anniversary of Norikura Observatory was celebrated in 2013.

Present major scientific interests of the laboratory is focused on the modulation of high energy cosmic rays in the interplanetary space associated with the solar activity and the generation of energetic particles by the solar flares, both of which require long-term monitoring. This research has been carried out by the group of universities, where ICRR provides them with laboratory facility. A part of the facility has been open for the environmental study at high altitude such as

Fig. 2. A dynamo of 115KV.

aerosol-related mechanism in the atmosphere, observation of total ozone and UV solar radiation, for botanical study in the high-altitude environment, etc.

Cosmic Ray Physics

A neutron monitor has been continuously operated to study the correlation of solar activities and cosmic ray flux for a long time. It is the only active one in Japan now. The neutron monitor data are open to researchers worldwide as a world observation network point (WDC). In addition, space weather observation is actively made by a 25 m^2 muon hodoscope at Norikura Observatory[1], [2], [3], [4], [5], [6], [7], [8], [9].

The anisotropy observed with the global muon detector network (GMDN) provides us with a unique information of the spatial gradient of the GCR density which reflects the large-scale magnetic structure in the heliosphere. The solar cycle variation of the gradient gives an important information on the GCR transport in the heliosphere, while the short-term variation of the gradient enables us to deduce the large-scale geometry of the magnetic flux rope and the interplanetary coronal mass ejection (ICME). Real-time monitoring of the precursory anisotropy which has often been observed at the Earth preceding the arrival of the ICME accompanied by a strong shock may provide us with useful tools for forecasting the space weather with a long lead time. By using a self-supporting power system utilizing the solar panels and batteries, we keep a 25 m^2 muon hodoscope running at the Mt. Norikura Cosmic Ray Observatory as an important component detector of the GMDN. The total power consumption of this detector has been suppressed as low as 36 Watt by replacing all amplifier boards with those using CMOS ICs and by introducing a new recording system using the FPGA. This new system, in which the observation has been automatically carried out by a PC connected with the internet, also enabled us

to monitor the data on the real-time basis for the space weather study.

The Sun is the nearest site to the Earth capable of accelerating particles up to high energies. When the Sun becomes active, flares are frequently observed on its surface. The flare accelerates the proton and ion to high energy and they are detected on the Earth soon after the flare. Among the particles generated by the flare, high energy neutrons provide the most direct information about the acceleration mechanism as they come straight from the flare position to the Earth without deflected by the magnetic field.

Observation of solar neutron has been conducted at the Norikura Observatory since 1990. Neutron is used to clarify the acceleration mechanism of high energy particles in association with solar flares, because the neutron is not reflected by the interplanetary magnetic field. The 64m^2 solar neutron telescope was constructed in 1996, which is one of 7 solar neutron telescopes deployed at different longitudes to make up a network of 24 hour observation of solar neutrons. The Norikura 64m^2 solar neutron telescope has been operated by solar batteries and windmills since 2004.

This collaborative work has started since fiscal 2007 succeeding to the previous project titled 'Observation of solar neutrons by using a new method.' Although solar cycle 24 has started since 2008, the solar activity has continued to be inactive, and no new solar neutron event has been detected by the network since 2006. The last solar neutron event was on September 7, 2005. This event is unique because it indicates ions were accelerated or trapped at the acceleration region longer than electrons. The summary of 11 solar neutron events detected until 2005 shows that it may not be probable that a very efficient acceleration such as the shock acceleration works for ions at solar flares. This is given by deriving the energy spectrum of neutrons at the solar surface for each solar neutron event with a power law. Power law indices obtained span from 3 to 7. The energy spectrum of the original ions is softer than that of neutron. Therefore an efficient acceleration has not been detected by the observation of solar neutrons so far.This work continues in solar cycle 24 to accumulate more events to obtain definite results related with particle acceleration at the solar surface.

Another effort aiming at observation of highest-energy solar cosmic rays started at the Norikura Observatory. The Sun is an accelerator of protons and electrons in the universe. In association with large solar flares, protons and electrons are accelerated into high energies. It is known that protons are accelerated over 50 GeV in the largest solar flares[24]. These high energy particles produce the Ground Level Enhancement (GLE).

In order to understand the acceleration mechanism of protons, we have prepared several solar neutron telescopes at the high altitude laboratories in the world. They are located at Gornergrat (3,135m), Mt. Aragats in Armenia (3,200m), Tibet (4,200m), Mauna-Kea in Hawaii (4,200m), Mt. Chacaltaya in Bolivia (5,250m), and at Mt. Sierra Negra in Mexico (4,900m). We have constructed a solar neutron telescopes at Mt. Norikura Cosmic Ray Observatory (2,770m) in 1990 and operated it until 2004[21]. However due to the lack of power supply during the winter time since 2005, the first solar neutron telescope (36 m^2) has not been operated.

From 2008 to 2009, we have decided to make a new solar neutron telescope to utilize the large amount of the plastic scintillator (0.5m^3), as shown in Fig. 3, left at the observatory.

Fig. 3. 0.5-m^2 plastic scintillation counter for a new neutron telescope.

The new solar neutron telescope with use of the recycled plastic scintillator consists of main target where neutrons are converted into protons and of the anti-counters surrounding the target. The signals of neutrons converted into protons are observed by using one photomultiplier from bottom side to reduce the electric power. Furthermore a lead plate with the thickness of 1cm is located over the target and the lead plate is sandwiched by two layers of the plastic scintillator to identify gamma-rays from neutrons.

The new solar neutron telescope has a function to reject charged particles with an efficiency of 90%. Therefore the new solar neutron telescope has capability of 1/3 of the 64m^2 large solar neutron telescope located at the same place. We are waiting large solar flares over our detectors.

In addition to the long-term cosmic-ray observations mentioned above, various kinds of short-dated experiments are carried out every year taking an advantage of the high altitude of the observatory.

High-energy radiations from thunderstorms have been observed by flight measurement, high-mountain observations and

ground-based measurement. There are two types of those radiations associated with thunderstorms. One is short-duration radiations with duration of 1 ms or less. The other is long-duration emissions lasting for a few seconds to a few minutes, or a few tens of minutes on rare occasions. It is believed that both emissions originate from electrons accelerated in strong electric fields formed in lightning and thunderclouds. However, compared with the former, the latter has remained less understood due to lack of a large sample of observations.

To investigate production mechanism of long-duration emissions and the relevant electron acceleration, we installed at Norikura Cosmic-ray Observatory a radiation detection system and environmental sensors to measure light and electric fields during 2008−2010. The radiation system consists of a spherical NaI scintillator and a thin plastic scintillator that is placed just above the NaI counter. During the period, the system detected one long-duration bursts as well as five short-duration events.

Fig. 4 (top) shows the long-duration event observed during thunderstorms on 2008 September 20th [25]. The event lasted for 90 sec. Fig. 4 (bottom) represents an observed photon spectrum extending from 10 keV to 10 MeV. This indicates that electrons can be accelerated to at least 10 MeV in a quasi-stable thundercloud electric field. In addition, we compared the observed spectrum with model ones, and concluded that a gamma-ray source is located 60 m−130 m (at 90% confidence level) apart from our detector. Given these results, the observed emission was found to consist of not only gamma rays but also electrons. This was the first simultaneous observation of gamma rays and electrons in long-duration bursts

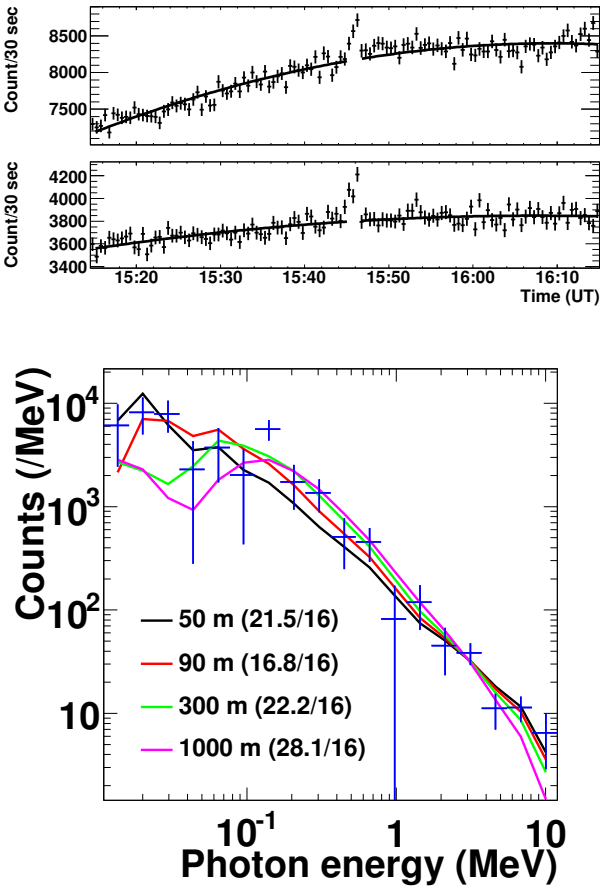

Fig. 4. (Top) Count rates per 30 sec observed by the >10 keV NaI scintillator (upper) and > 100 keV plastic one (lower). (Bottom) The photon spectrum observed by the NaI scintillator.

Observation of night sky background is carried out at Mt. Norikura for basic study of ultra high energy cosmic-ray physics.

The JEM-EUSO mission is going on in order to study ultra high energy cosmic rays (UHECRs), especially above 10^{20}eV. A 2.5m telescope with 60° FoV will be attached to the International Space Station in 2017 and detect fluorescence in near UV band from extensive air showers induced by UHECRs. Observation of UHECRs from a satellite orbit has not been done yet, so that the knowledge of background light intensity is important to realize the observation. We have measured it from a balloon altitude, but the opportunity is limited. We started the background measurement at Mt. Norikura.

Two 1 inch multi-anode photomultipliers (MAPMTs) developed for EUSO was used with UV filters. The center wavelengths of the filters were 337, 350, 358, 370, 380, 391, 400nm with 10nm band width. In addition BG3 filter was used to detect light in wider range from 330nm to 430nm. The MAPMTs were collimated to 7° FoV. The data was taken with the photon counting method.

We have observed several nights for three years. The intensity at zenith was almost constant at 600-800 photons/ns∼sr m^2 for BG3 filter. The spectral intensity was about 1.5-2 times larger than those measured at La Palma and Namibia. The estimated portion of star light and zodiacal light was ∼30% and artificial light and nightglow at upper atmosphere may be the main components at Mt.Norikura.

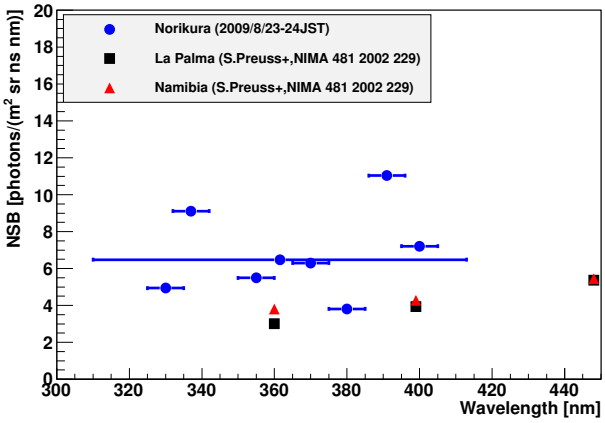

Fig. 5. Spectrum of night sky background measured at Mt.Norikura compared with those at La Palma and Namibia.

Environmental Study

One of the interesting topics is atmospheric environment especially relating with atmospheric aerosol particles and water soluble gases. The cosmic ray observatory at Mt. Norikura provides us very unique opportunity for the observations of atmosphere at free-tropospheric conditions with its high altitude, AC power supply at the site, accommodation facility,

and easy accessibility. From year 2000 to 2007, we conducted continuous monitoring (mostly mid-May to mid-October) of meteorological parameters, number-size distribution of aerosols, aerosol chemical composition, ozone and radon concentrations, and column amount of aerosols from sky radiometer and ceilometers. We also collected rain, fog, water-condensed aerosol samples. These samples combined with other observed parameters were used in publications in the following subjects [26, 27, 28]:

(1) Polluted air pumping effects over central Japanese Alps in summer
(2) Seasonal variation of aerosol chemistry in free troposphere
(3) Vertical profiles of aerosols and clouds near the top of the atmospheric boundary layer.

Ceilometer (lidar with small output energy) was installed in summer 2002, and was operated in 6 summer seasons. The aerosol and cloud profiles near the top of the atmospheric boundary layer have been observed. Some events of Asian dust were detected.

Observations of total ozone and UV solar radiation with Brewer spectrophotometer on the Norikura mountains are also made[29, 30, 31].

Aerological Observatory started " Observations of total ozone and UV solar radiation with Brewer spectrophotometer at Norikura mountains " as a joint project with Institute for Cosmic Ray Research (ICRR), University of Tokyo at the Norikura Observatory of ICRR (Brewer site: 36.11 N, 137.56 E, 2,772 m a.s.l.), locating at the Northern Japanese Alps in every summer seasons from 2009 (Ito *et al.*: 2011). Purpose of this study is based on the concept of developing Regional Brewer Calibration Centre in Asia and study of total ozone, total sulfur oxide and global/diffuse UV included solar radiation on the high mountains. Observation results by using Brewer spectrophotometers and other instruments for the observation period of three summer seasons of recent three years between 2009 to 2011 are summarized as follows;

(1) Daily means of ds O_3 (total ozone) at Norikura for the observation periods were approx. 280 to 290 m atm-cm and were running on the lower values of approx. -3 to -6% compared to the value at Tsukuba (36.06 N, 140.13 E, 39 m a.s.l.) at almost same latitude. Day-to-day variations at Norikura were also small against Tsukuba. On the other hand, daily mean of ds SO_2 (total sulfur oxide) values were not recognized at Norikura.

(2) Absolute calibration of Brewers for ds O_3 and ds SO_2 observations could be carried out within the range of air mass from 7.928 (maximum) to 1.028 (minimum) at Norikura in the clear day. O_3 and SO_2 Extra-Terrestrial Coefficients (=ETC) of Brewers could be produced as about 10 samples satisfying the condition of "$R^2 > 0.9997$" by the calibrations. As an example of the calibration in 2011, the average of O_3 ETC of Brewers was identical within 1% to the currently used coefficient.

(3) In comparison to the data acquired at Tsukuba, the average of daily total GL_{UV} (global UV, e.g. CIE) for the observation periods indicated the intensities of approx. +23 % in 2009 to -6 % in 2011. The low intensity in 2011 was due to the bad weather on the Norikura Mountain. In the case of clear days, the GL_{UV} at Norikura indicated high intensities of approx. +35 to +52 % against the values at Tsukuba. On the other hand, the GL_{UV} increased in the short wavelength range at Norikura against the average at Tsukuba. The altitudinal increasing rate of GL_{UV} in the clear day indicated the calculated amounts of approx. +13 to +18 % per 1,000 m.

This joint project had been clarifying the low total O_3, high UV in clear day, low turbidity and etc. at Norikura against the value at Tsukuba. Those environmental conditions are useful for the intercomparison and the absolute calibrations with Brewers. The continuous observations with Brewers and other instrument are very important for the clarification of the seasonal variation and the coefficient trends.

Botanical Study

Effects of snow cover on pine shrub Pinus pumila in the alpine region of Mt. Norikura

High mountainous habit is one of the most severe habits for plant life and sometimes dwarf shrubs cannot survive. In the alpine regions of Japan, the dwarf shrub Pinus pumila (Japanese name : Haimatsu) forms communities together with small alpine plants, whereas dwarf shrubs occur only in the transition zone between the alpine region and the subalpine forest in Europe and North America. This characteristic of alpine vegetation is considered to be owing to winter heavy snow in the alpine regions of Japan. The purpose of this study is to elucidate how snow cover protects Haimatsu from winter environmental stresses in the alpine region of Mt. Norikura.

Study site

Tree height of Haimatsu and snow depth differ greatly as a result of slight difference in topography. Two site of the study area were selected. (i) site P (wind-protected) and (ii) site E (wind-exposed). At site P, mean tree height was 1.1 m. There was a lot of snow accumulation and Haimatsu was almost entirely covered with snow during the winter. Needle browning and death occurred rarely. At site E, mean tree height was 0.4 m. Snow accumulation was minimal, and Haimatsu was not entirely covered with snow. Needle browning and death was observed frequently.

Winter needle death in Haimatsu[32]

At site E, the browning and death of needles of Haimatsu occurred mainly in early spring at the point where the shoot protrudes from the snowpack. They are thought to be caused by excessive water loss due to mechanical damage to the cuticle and/or to a thinner cuticle. However, needle browning and death in Haimatsu were not related to mechanical damage of the cuticle but might be due to changes in the quality and structure of the cuticle wax and resultant increase in water loss from needle cells.

Photosynthetic capacity in Haimatsu[33]

At site E, needles of Haimatsu had lower biomass, nitrogen, Rubisco (enzyme) and cell wall per unit area, and had higher photosynthetic capacity and shorter needle life-span than Haimatsu at site P. These results suggest that Haimatsu at wind-exposed site produces needles at low cost with high productivity to compensate for a short leaf life-span which may be imposed by wind stress when needles appear above the snow surface in winter.

Bibliography

[1] K. Munakata, S. Yasue, C. Kato, J. Kota, M. Tokumaru, M. Kojima, A. A. Darwish, T. Kuwabara and J. W. Bieber, "On the cross-field diffusion of galactic cosmic rays into the magnetic flux rope of a CME", *Advances in Geosciences*, 2, 115-124, eds. W. H. Ip and M. Duldig (World Scientific Publishing Co., USA), (2006).

[2] T. Kuwabara, J. W. Bieber, J. Clem, P. Evenson, R. Pyle, K. Munakata, S. Yasue, C. Kato, S. Akahane, M. Koyama, Z. Fujii, M. L. Duldig, J. E. Humble, M. R. Silva, N. B. Trivedi, W. D. Gonzalez and N. J. Schuch, "Real-time cosmic ray monitoring system for space weather", *Space Weather*, 4, S08001-1 10, (2006).

[3] M. R. Da Silva, A. Dal Lago, E. Echer, A. de Lucas, W. D. Gonzalez, N. J. Schuch, K. Munakata, L. E. A. Vieira, and F. L. Guarnieri, "Muon and neutron observations in connection with the corotating interaction regions", *Adv. Space Res.*, 40, pp348-352, (2007).

[4] Y. Okazaki, A. Fushishita, T. Narumi, C. Kato, S. Yasue, T. Kuwabara, J. W. Bieber, P. Evenson, M. R. Da Silva, A. Dal Lago, N. J. Schuch, Z. Fujii, M. L. Duldig, J. E. Humble, I. Sabbah, J. Kóta and K. Munakata, "Drift effects and the cosmic ray density gradient in a solar rotation period: First observation with the Global Muon Detector Network (GMDN)", *Astrophys. J.*, 681, 693-707, (2008).

[5] T. Kuwabara, J. W. Bieber, P. Evenson, K. Munakata, S. Yasue, C. Kato, A. Fushishita, M. Tokumaru, M. L. Duldig, J. E. Humble, M. R. Silva, A. Dal Lago, and N. J. Schuch, "Determination of ICME Geometry and Orientation from Ground Based Observations of Galactic Cosmic Rays", *J. Geophys. Res., 114*, A05109-1 10, doi:10.1029/2008JA013717, (2009).

[6] A. Fushishita, T. Kuwabara, C. Kato, S. Yasue, J. W. Bieber, P. Evenson, M. R. Da Silva, A. Dal Lago, N. J. Schuch, M. Tokumaru, M. L. Duldig, J. E. Humble, I. Sabbah, H. K. Al Jassar, M. M. Sharma, and K. Munakata, "Precursors of the Forbush Decrease on 2006 December 14 observed with the Global Muon Detector Network (GMDN)", *Astrophys. J.*, 715, 1239-1247, (2010).

[7] A. Fushishita, Y. Okazaki, T. Narumi, C. Kato, S. Yasue, T. Kuwabara, J. W. Bieber, P. Evenson, M. R. Da Silva, A. Dal Lago, N. J. Schuch, M. Tokumaru, M. L. Duldig, J. E. Humble, I. Sabbah, J. Kóta, and K. Munakata, "Drift effects and the average features of cosmic ray density gradient in CIRs during successive two solar minimum periods", *Advances in Geosciences*, eds. W. H. Ip and M. Duldig (World Scientific Publishing Co., USA), 21, 199-210, (2010).

[8] M. Tokumaru, M. Kojima, K. Fujiki, K. Munakata, T. Kuwabara and K. Marubashi, "Relation between loop-shaped interplanetary disturbances and the magnetic flux rope", *Advances in Geosciences*, eds. W. H. Ip and M. Duldig (World Scientific Publishing Co., USA), 21, 21-32, (2010).

[9] M. Rockenbach, A. Dal Lago, W. D. Gonzalez, K. Munakata, C. Kato, T. Kuwabara, J. W. Bieber, N. J. Schuch, M. L. Duldig, J. E. Humble, H. K. Al Jassar, M. M. Sharma, and I. Sabbah, "Geomagnetic Storms Precursors Observed from 2001 to 2007 with the Global Muon Detector Network GMDN", *Geophys. Res. Lett.*, 38, L16108-1 4, doi:10.1029/2011GL048556, (2011).

[10] "Solar neutron events of October—November 2003", Watanabe, K. *et al.*, Astrophys. J., **636**, 1135–1144, 2006.

[11] "Solar neutron events in association with large solar flares in November 2003", Watanabe, K. *et al.*, Adv. Space Res., **38**, 425–430, 2006.

[12] "Long-lived solar neutron emission in comparison with electron-produced radiation in the 2005 September 7 solar flare", Sako, T. *et al.*, Astrophys. J., **651**, L69–L72, 2006.

[13] "Highly significant detection of solar neutrons on 2005 September 7", Watanabe, K. *et al.*, Adv. Space Res., **39**, 1462–1466, 2007.

[14] "A solar neutron telescope in Tibet and its capability examined by the 1998 November 28th event", Muraki, Y. *et al.*, Astroparticle Phys., **28**, 119–131, 2007.

[15] "Simultaneous detection of high-energy solar neutrons and protons at Chacaltaya observatory on April 15, 2001", Muraki, Y. *et al.*, in Proc. 30th Int. Cosmic Ray Conf, Merida, **1**, 25–28, 2007.

[16] "Search for solar neutrons associated with series of X-class flares during the declining period of solar cycle 23", Matsubara, Y. *et al.*, in Proc. 30th Int. Cosmic Ray Conf, Merida, **1**, 29–32, 2007.

[17] "Ion acceleration and neutral emission mechanisms for 2005 September 7 flare", Watanabe, K. *et al.*, in Proc. 30th Int. Cosmic Ray Conf, Merida, **1**, 45–48, 2007.

[18] "Emission profile of solar neutrons obtained from the ground-based observations for the 7 September 2005 event", Sako, T. *et al.*, in Proc. 30th Int. Cosmic Ray Conf, Merida, **1**, 53–56, 2007.

[19] "Energy spectrum for the solar neutron event of September 7 2005, derived from the SNT at Sierra Negra", Gonzalez, L. X. *et al.*, in Proc. 30th Int. Cosmic Ray Conf, Merida, **1**, 57–60, 2007.

[20] “Status of the world-wide network of solar neutron telescopes in solar cycle 24”, Matsubara, Y. *et al.*, in Proc. 31st Int. Cosmic Ray Conf, Lodz, **1**, On Conference homepage, 2009.

[21] “Detection of high-energy solar neutrons and protons by ground level detectors on April 15, 2001”, Muraki, Y. *et al.*, Astropart. Phys., **29**, 229–242, 2008.

[22] “Solar neutron events as a tool to study particle acceleration at the Sun”, Valdes-Galicia, J. F. *et al.*, Adv. Space Res., **43**, 565–572, 2009.

[23] “Physics of ion acceleration in the solar flare on 2005 September 7 determines γ-ray and neutron production”, Watanabe, K. *et al.*, Adv. Space Res., **44**, 789–793, 2009.

[24] “Observation of solar neutrons associated with the large flare on 1991 June 4”, Muraki, Y. *et al.*, ApJ, **400**, L75-L78 , 1992.

[25] “Observation of an energetic radiation burst from mountain-top thunderclouds”, H. Tsuchiya *et al.*, Phys. Rev. Lett. **102**, 255003 (2009), Citation Index:13.

[26] Nishita, C., K. Osada, K. Matsunaga, Y. Iwasaka, e, J. Geophys. Res., **113**, D06202, doi:10.1029/2007JD009302, 2008.

“Nucleation mode particles in up-slope valley winds at Mt. Norikura, Japan: implications for the vertical extent of new particle formation events in the lower tropospher”, Nishita, C., K. Osada, K. Matsunaga, Y. Iwasaka, J. Geophys. Res., **113**, D06202, doi:10.1029/2007JD009302, 2008.

[27] “Temporal variation of water-soluble ions of free tropospheric aerosol particles over central Japan”, Osada, K., Kido, M., Nishita, C., Matsunaga, K., Iwasaka, Y., Nagatani, M., Nakada, H., Tellus, **59B**, 742-754, 2007.

[28] “Number-size distributions of free tropospheric aerosol particles at Mt. Norikura, Japan: effects of precipitation and air-mass transportation pathways”, Nishita, C., K. Osada, K. Matsunaga, Y. Iwasaka, J. Geophys. Res., 112, doi:10.1029/2006JD007969, 2007.

[29] “Observations of total ozone and UV solar radiation with Brewer spectrophotometers on the Norikura mountains in 2009.”, Ito, M., M. Takano, H. Oguri, M. Takita, H. Shimodaira and H. Ishitsuka, Jour. of the Aerological Observatory, **69**, 41-54 2011.

[30] “Observations of total ozone and UV solar radiation with Brewer spectrophotometers on the Norikura mountains, Northern Japanese Alps, from 2009.”, Ito, M., S. Shimizu, Y. Noto, T. Shimamura, M. Takano, M. Takita, H. Shimodaira and H. Ishitsuka, The 13th WMO Biennial Brewer Workshop, Beijing, China in 2011, 2011.

[31] “Total ozone and UV solar radiation with Brewer spectrophotometers at Norikura of Northern Japanese Alps, in recent three years.”, Ito, M., S. Shimizu, Y. Noto, T. Shimamura, M. Takita, H. Shimodaira and H. Ishitsuka, Jour. of the Aerological Observatory, **70**, in contribution.

[32] “Needle browning and death in Pinus pumila in the alpine region of central Japan were not related to mechanical damage of cuticle and cuticle thickness.”, Nakamoto A., Ikeda T., Maruta E., Can. J. For. Res. 42, 167-178 (2012).

[33] “Needle traits of an evergreen, coniferous shrub growing at wind-exposed and protected sites in a mountain region: does Pinus pumila produce needles with greater mass per area under wind-stress conditions?”, Nagano S., Nakano T., Hikosaka K and Maruta E., Plant Biology 11(Suppl.1), 94-100, (2009).

AKENO OBSERVATORY

Introduction

The Akeno Observatory is situated in Akeno of Hokuto-city, 20 km northwest of Kofu and 130 km west of metropolitan Tokyo. The location is at the longitude of 138.5°E and the latitude of 35.8°N. The altitude is ∼900 m above sea level. It was established in 1977 as a research center for air shower studies in the very high energy region, and it has been administered by the ICRR as a facility of joint-university-use.

Akeno Air Shower Experiments

The Akeno Air Shower Experiment started in 1979 with an array covering 1 km^2 area (the 1 km^2 array, see Fig.1). The array was enlarged to 20 km^2 in 1984 and was gradually expanded to Akeno Giant Air Shower Array (AGASA) of approximately 100 km^2 area by 1990. The AGASA was built

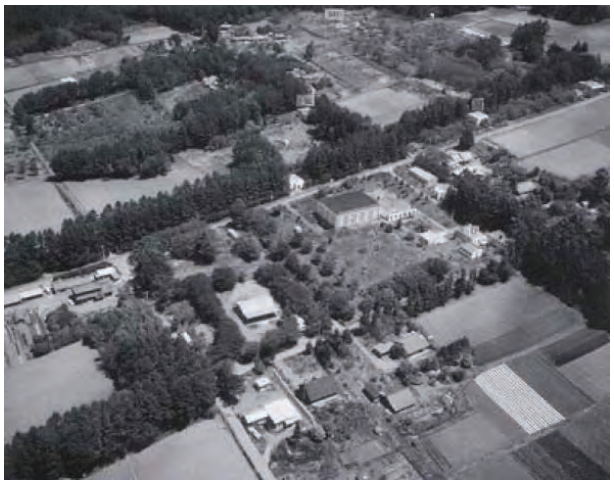

Fig. 1. Aerial View of Akeno Observatory and 1 km^2 Array Area

to detect Ultra-High Energy Cosmic Rays (UHECRs) in the energy range of 10^{20} eV.

One of the distinctive features of Akeno experiments is that the measurements were made over five decades of energies well covering 10^{15} eV - 10^{20} eV by using both the surface detector for electromagnetic component, and the shielded detector for muon component (Fig.2). The wide energy coverage was accomplished by the arrays of scintillation detectors of various inter-detector spacings from 3 m to 1 km and with different triggering conditions. This feature of Akeno air shower measurement is well demonstrated in Fig.3, in which the spectra from Akeno 1 km^2 array for $10^{14.5}$ eV - $10^{18.8}$ eV [4] and AGASA for $10^{18.5}$ eV - $10^{20.3}$ eV [5] are plotted.

*4 M. Nagano et al., J. Phys. **G10**, 1295 (1984); M. Nagano et al., J. Phys. **G18**, 423 (1992).
*5 M. Takeda et al., Astropart. Phys. **19**, 447 (2003).

Fig. 2. One of the muon detector housings with concrete shielding.

AGASA

The AGASA was composed of 111 surface detectors, each with plastic scintillator of 2.2 m^2 area and 5 cm thickness. The counters were deployed with ∼1 km spacing covering the ground area of about 100 km^2 in the suburban area of Akeno, outside of the observatory campus. All counters were connected with optical fibers for the timing measurement and digital data transfer to the observatory. The AGASA served as the largest air shower array in the world since its commissioning in 1990 until it stopped data taking in January 2004, when the construction of the succeeding experiment, Telescope Array (TA), started in Utah. It was dismantled in 2007 together with other Akeno air shower arrays.

An exposure of 5.8 $\times$ 10^{16} m^2 s sr above 10^{19} eV was accumulated by AGASA in 13 years of operation. Extensive air showers with zenith angles smaller than 45° and with core locations inside the array area were used for the analysis. The AGASA reported an extension of the energy spectrum beyond the predicted Greisen-Zatsepin-Kuzmin (GZK) cutoff in 1998 [6] and a total of eleven UHECR events were observed above 10^{20} eV by 2003.

Measurement of UHECRs

Since the AGASA measurement in 1998, High Resolution Fly's Eye (HiRes) [7], Pierre Auger Observatory (PAO) [8], and Telescope Array (TA) [9] measured the energy spectra of UHECRs with higher statistics.

The HiRes observed the UHECR using the fluorescence telescope. The PAO and TA measure the spectrum using the surface array consisting of either water tanks (PAO) or plastic

*6 M. Takeda et al., Phys. Rev. Lett. **81**, 1163 (1998).
*7 R.U. Abbasi et al., Phys. Rev. Lett. **100**, 101101 (2008).
*8 J. Abraham et al., Phys. Lett. **B685**, 239 (2010).
*9 T. Abu-Zayyad et al., arXiv:1205.5067v1 (2012).

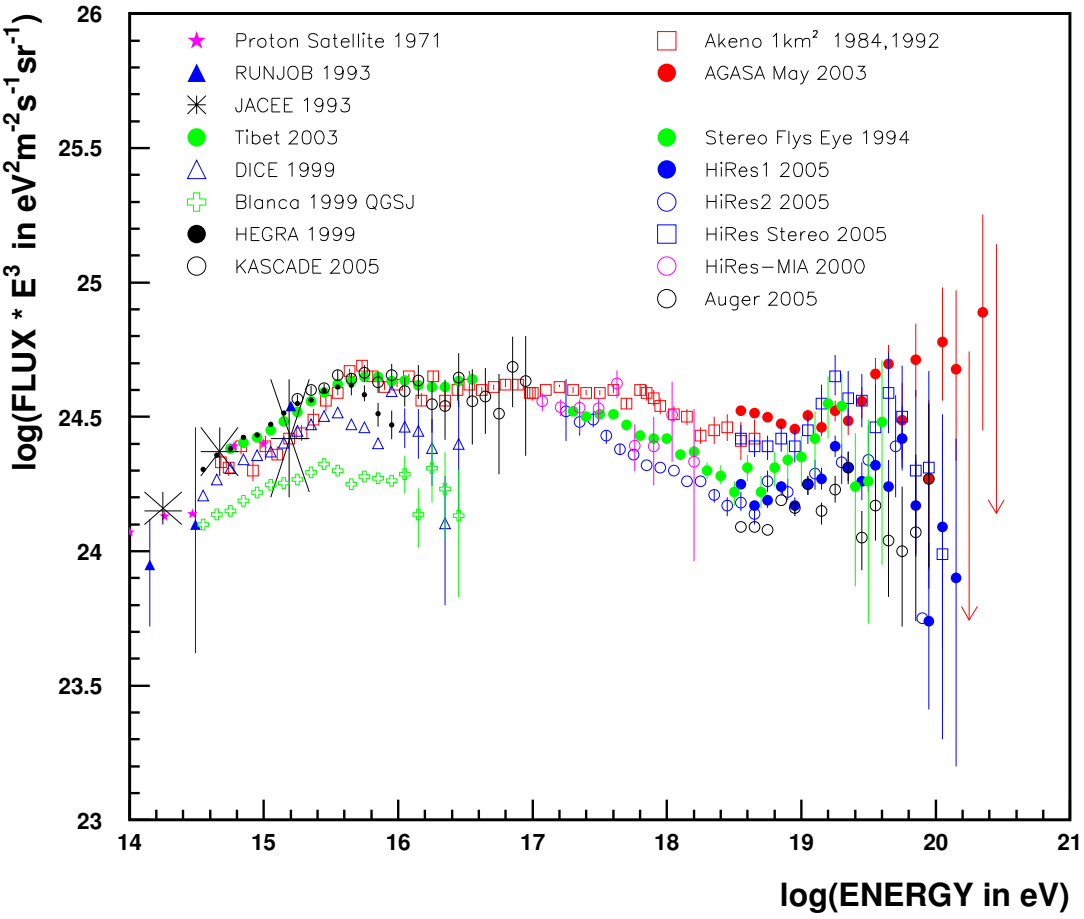

Fig. 3. Akeno energy spectrum measurements for 10^{15} eV - 10^{20} eV.

scintillators (TA), but the energy scale of the array is determined by the fluorescence telescope using a subset of events observed by the fluorescence telescope and surface array at the same time. The adoption of the energy scale by the fluorescence telescopes is based on its small dependence on the air shower simulation.

The energy spectra above 10^{18} eV by AGASA and other experiments are compiled and compared by the working group represented by UHECR experiments in the UHECR-2012 symposium held at CERN for Feb. 13th - 16th, 2012 [10]. The result is plotted in Fig.4 with the energy scale of each experiment adjusted to a reference energy, which is set halfway between the PAO and TA/HiRes.

Following factors were applied for the energy scale; $\times 1.10$ for PAO, $\times 0.91$ for TA and HiRes, $\times 0.65$ for AGASA and $\times 0.56$ for Yakutsk.

As seen in Fig.4, the overall agreement between experiments is good, and a "dip" structure was seen around $10^{18.7}$ eV by all experiments. The HiRes, PAO and TA confirmed a strong flux suppression above approximately $10^{19.7}$ eV. Although the AGASA spectrum does not demonstrate the cutoff structure, the number of events above 10^{20} eV became only two after the energy rescaling, making the claim of the extended spectrum statistically insignificant. The estimate of systematic uncertainty of the energy measurement is approximately 20% for all the experiments, and rescalings for the TA/HiRes and PAO are within this limit. Rescaling of the surface array energy, $\times 0.65$ for AGASA and $\times 0.56$ for Yaktsuk, indicates that there exist larger systematic uncertainties than originally estimated by running the air shower simulation. This difference of energy scale obtained by the surface array and by the fluorescence telescope remains as a basic question in the understanding of the air shower phenomena.

Recent Research Activities

The study of UHECRs by AGASA in Akeno was succeeded by the Telescope Array (TA) experiment in Utah, USA since 2008. After the cessation of AGASA, the Akeno observatory has been used for small scale cosmic ray experiments, astrophysical observations and as a test and maintenance facility of TA by the ICRR and university researchers.

*[10] http://indico.cern.ch/conferenceDisplay.py?confId=152124

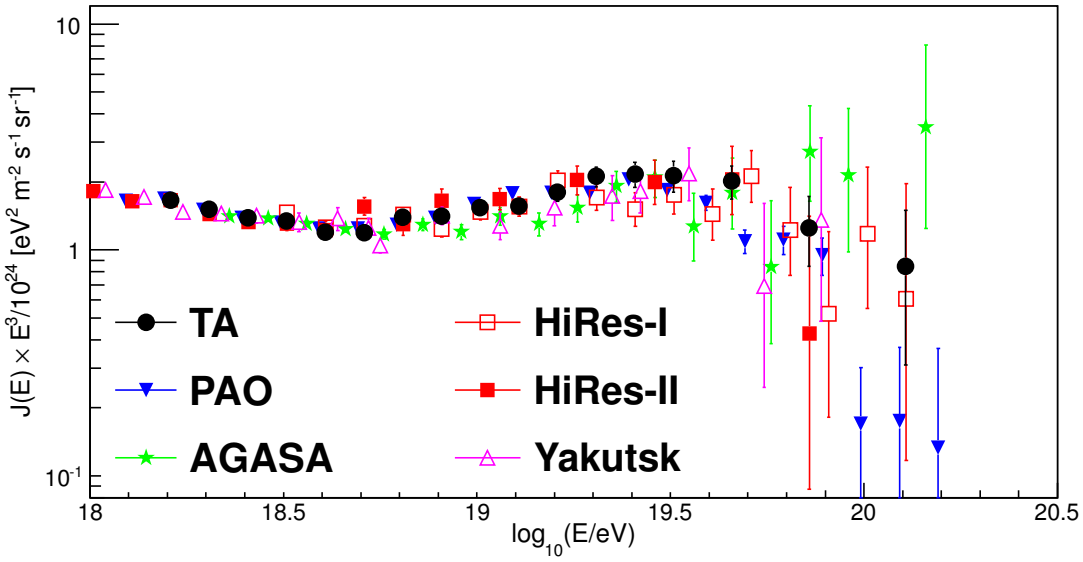

Fig. 4. Recent compilation of UHECR energy spectra. The energy scale of each experiment is adjusted as described in the text.

Research and development for the Telescope Array observation in Utah by the TA collaboration

All the fluorescence imaging cameras and a part of the surface detectors of TA were assembled in the Akeno observatory by the TA collaboration team. The detectors were tested in Akeno and shipped to the Utah observation site for the installation. All the unit mirrors of the TA fluorescence telescope were tested in Akeno and the atmospheric monitoring lidar of TA using YAG laser was developed in Akeno. In JFY 2013, a certain number of scintillator counters were assembled for TA muon detectors and were sent to Utah.

Research activities in JFY 2014 (April 2014 - March 2015) are described in the following.

Observation by the multi-color imager for transients, survey and monstrous explosions (MITSuME) by N. Kawai (Tokyo Institute of Technology) et al.

One of the three MITSuME robotic telescopes was installed in the Akeno observatory in 2003. The telescope has an aperture of 50 cm, an FOV of 28' $\times$ 28' and is equipped with a tricolor CCD camera capable of $g'R_CI_C$-bands photometry. It is operated remotely from the Tokyo Tech using dedicated ADSL connections. Upon receiving a GRB alert from Swift or Fermi satellite, it quickly directs the telescope (9°/s maneuverability) toward the GRB direction, and makes a prompt observation of the GRB and its afterglow. In JFY 2014, 36 GRBs were observed, and 5 were identified as visible objects. The monitor observation of AGNs has been performed since 2008 during the periods when GRBs did not appear. The analysis of the data began this fiscal year.

Observation of galactic cosmic rays by large area muon telescope by S. Shibata (Chubu University) et al.

Four layers of proportional counter telescopes, each with 25 m^2 area, were installed in three muon houses in Akeno (Fig.2) and have been continuously measuring the cosmic ray muons since 2003. The mode energy of the primary cosmic rays is approximately 2.5 GeV corresponding to 2m thick concrete ceiling of the muon house and the latitude of Akeno observatory. The measurement in Akeno is combined with a simultaneous measurement in Ooty, India, and the modulation effects of galactic cosmic rays by the solar activity such as the Forbush decrease and its precursor have been continuously monitored [11]. In JFY 2014, one of three muon detectors has been operating and being monitored via network relatively for long time after the improvement of network and power supply since the year before last.

Research and development for a small atmospheric Cherenkov telescope in Akeno observatory by T. Yoshikoshi (ICRR) et al.

A small alt-azimuth telescope is being setup in Akeno for prototype tests with atmospheric Cherenkov observations of gamma rays [12]. The focusing performance of the telescope optics was checked, and it was confirmed that the size of its point spread function is smaller enough than the pixel size.

A part of the experimental hall was used for the research on ultra-low frequency anti-vibration system and temporary storage of the KAGRA, Large-scale Cryogenic Gravitational Wave Telescope Project.

Other tests using facilities or detectors in the Akeno observatory were also performed.

*[11] T. Nonaka.et al, Proc. of the 29th ICRC, **1**, 363-366 (2005).
*[12] M. Ohishi et al., 33rd ICRC, (Rio deJaneiro), **9**, in press (2013).

KAMIOKA OBSERVATORY

Kamioka observatory is located at 1000 m underground (2700 m water equivalent) in the Kamioka Mine, Gifu prefecture, about 200 km west of Tokyo. The observatory was established in 1995 in order to operate Super-Kamiokande experiment (SK). The underground laboratories are located under Mt.Ikeno-yama and accessible to the experimental site through a 1.7 km horizontal tunnel. The observatory also has surface research buildings and a dormitory located at the distance of 15 minutes drive from the entrance of the underground laboratories.

The Super-Kamiokande experiment had discovered neutrino oscillations through the observations of atmospheric and solar neutrinos (see the section for Neutrino and Astroparticle Division). The atmospheric neutrino oscillation was confirmed by the long baseline neutrino oscillation experiment, K2K, using accelerator neutrino beam, which was conducted between 1999 and 2004. A new long baseline neutrino oscillation experiment (the T2K experiment) using a high intensity beam, 50 times of the K2K neutrino beam, by the J-PARC proton accelerator has started in 2009. In 2011, the experiment has observed 6 ν_e appearance events indicating non-zero θ_{13} which was as yet determined the last neutrino oscillation parameter. In 2012 and 2013, the collaboration accumulated more electron neutrino appearance events and strengthen the discovery of non-zero θ_{13}. Since 2014, anti-neutrino beam data also has been taken in order to search for CP violation.

The low cosmic ray flux and low seismic noise environment in the underground site enables us to conduct various researches. There is a 100 m long laser interferometer, which is a proto-type of the 3 km gravitational wave antenna (see section of Astrophysics Gravity Division) under construction. Using the low radioactive background environment in the Kamioka Mine, a dark matter experiment, called XMASS is operated in Lab-C. The XMASS group constructed a 800kg liquid xenon detector and started commissioning run in late 2010. The detector was improved to remove backgrounds on the inner surface of the PMT plane in 2013, and stable data has been taken since 2014. The R&D study of a tracking type detector for dark matter detection lead by the Kobe University group (the NEWAGE experiment) has also been performed in Lab-B. The commissioning run of the CANDLE experiment in Lab-D (Osaka Univ.), a double beta decay experiment is now conducted. The study to improve the neutrino detection sensitivity by adding gadolinium to Super-Kamiokande is on going. A 200 ton test tank dedicated for the R&D study of the gadolinium project was constructed in Lab-E and a feasibility study has been performed. In order to support those experiments and also related R&D works, the Observatory is equipped with low background Germanium detector in Lab-1 and Lab-A, ICP-MS and so on to measure extremely low radioactive backgrounds.

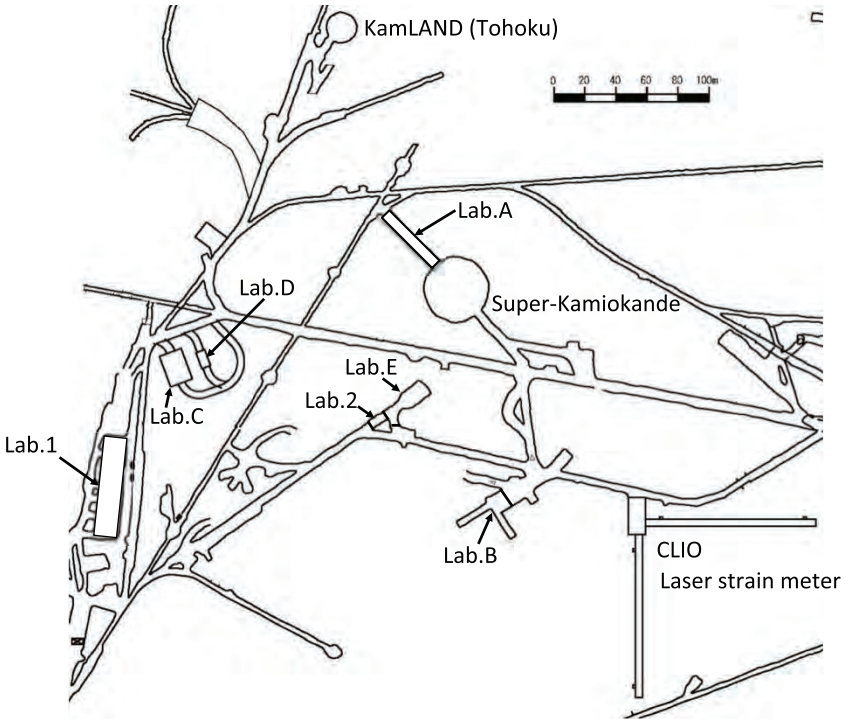

Fig. 1. Kamioka Underground Observatory.

RESEARCH CENTER FOR COSMIC NEUTRINOS

The main objective of Research Center for Cosmic Neutrinos (RCCN) is to study neutrinos based on data from various observations and experiments. In order to promote studies of neutrino physics, it is important to provide the occasion to discuss theoretical ideas and experimental results on neutrino physics. Therefore, one of the most important practical jobs of this center is to organize neutrino-related meetings. On February 21, 2015, we hosted one domestic neutrino workshop on "Neutrinos and its non-standard framework–sterile neutrinos and non-standard interactions–". 33 physicists participated in this meeting.

Members of this center have been involved in the Super-Kamiokande and T2K experiments, carrying out researches in neutrino physics. Also we have been involved in the future project, Hyper-Kamiokande. (Please see the relevant pages for the scientific results.) Atmospheric neutrino data from Super-Kamiokande give one of the most precise pieces of information on neutrino oscillations. With increased data, it is more important to have better predictions of the neutrino flux. Therefore, in addition to data analysis of the above experiments, we work on the calculation of the atmospheric neutrino flux.

It is important to share our scientific achievements with the general public. For this reason, we hold public lectures every year. Since JFY2009, ICRR and the Kavli Institute for the Physics and Mathematics of the Universe (Kavli-IPMU) have co-sponsored two public lectures each year. The public lecture held in Spring is co-organized by RCCN and the Public Relation Office of ICRR. The Spring public lecture in FY2014 was held on April 12, 2014. Two scientists lectured on the Universe seen by mathematics and the shock waves in the Universe.

RCCN, together with the computer committee of ICRR, is in charge of operating the central computer system in ICRR. In FY 2014, the computer system has been operated without any serious problems. RCCN also supports the users of the computer system, including physicists in the cosmic ray community in Japan.

Since 2004, RCCN has been acting as a body for accepting the ICRR inter-university programs related to the low-background underground facility in the Kashiwa campus. The facility is currently equipped with 4 Ge detectors mainly for the measurements of cosmic radioactive isotopes. The scientific activities related to this facility is described elsewhere.

APPENDICES

A. ICRR Workshops and Ceremonies

6th Korea-Japan workshop on KAGRA

Date: June 20-21, 2014
Place: National Astronomical Observatory of Japan, Japan

Outline: This workshop was the 6th Korea-Japan workshop on KAGRA, and was held at National Astronomical Observatory of Japan (Fig. 1). The workshop was organized by the scientific advisory committee, the scientific organizing committee chaired by Seiji Kawamura (ICRR), and the local organizing committee chaired by Raffaele Flaminio (National Astronomical Observatory of Japan). The purpose of the workshop was to foster the collaboration between Korea and Japan on the development, construction and exploitation of the KAGRA gravitational wave detector.

The workshop consisted of several sessions: the instrument, detector characterization, plenary, multi messenger, theory and data analysis, and discussion about the next step sessions. In the instrument session the progress and future plan of the KAGRA subsystems were presented and discussed. Among them Tai Hyun Yoon (Korea University) gave a talk about the fiber ring cavity for frequency stabilization of master laser of iKAGRA. In the detector characterization session Kazuhiro Hayama (Osaka City University) gave a talk about the status of KAGRA detector characterization. In the plenary session after Masahiko Hayashi (NAOJ, director) gave a welcome speech, Takaaki Kajita (ICRR) and Hyung Mok Lee (Seoul National University) gave a talk about the current status of KAGRA and summary of Korean Activities, respectively. We also heard about the advanced Virgo status from Matteo Barsuglia (APC, Paris), and the gravitational wave background from astrophysical sources from Zhu Zong-Hong (Beijing Normal University). In this workshop a special session was devoted to multi-messengers searches based on coincident analysis between different kind of astronomical observatories and GW detectors. In the multi messenger session after the overview by Nobuyuki Kanda (Osaka City University), many experts in each project/experiment gave a talk about the Korean effort for electromagnetic identification of GW sources, CALET experiment and finding EM counterparts, J-GEM, search for X-ray counterparts of GW events with MAXI, AROMA-W, and extracting broadband spectra from long duration GRBs. In the theory and data analysis session after Hideyuki Tagoshi (Osaka City University) summarized the status of the prepara-on for iKAGRA data analysis, the progress and future plan of the theory and data analysis of KAGRA were presented and discussed. A tour of NAOJ, including a visit to the TAMA300 facility, was also given at the end of the first day of the workshop.

In the discussion session we started discussing the instrument collaboration. We agreed that the fiber ring cavity, which Tai Hyun Yoon has been developing, will be used for the iKAGRA input optics if the system works fine. Also Kyuman Cho (Sogang University) will develop the tilt sensor at ICRR for 7 weeks at the beginning of 2015 as an ICRR visiting professor. For the detector characterization we agreed that we will integrate iDQ into HasKAL, KAGRA detector characterization library, the Korean GW group will lead development of a novel correlation method based on the mutual information, and we will develop and study a new trigger-generation method based on Hilbert-Huang transform. For the data analysis it was agreed that the parameter estimation for KAGRA CBC should be performed to implement the PE library to KAGALI and to demonstrate the parameter estimation by using iKAGRA data. We also decided to have a telecon about once in two weeks. Finally we decided that the next workshop would be held on November 19 - 20, 2014 at the University of Toyama, Japan.

Participants: 49 participants.
Website: http://tamago.mtk.nao.ac.jp/6th_Korea-Japan/index.html

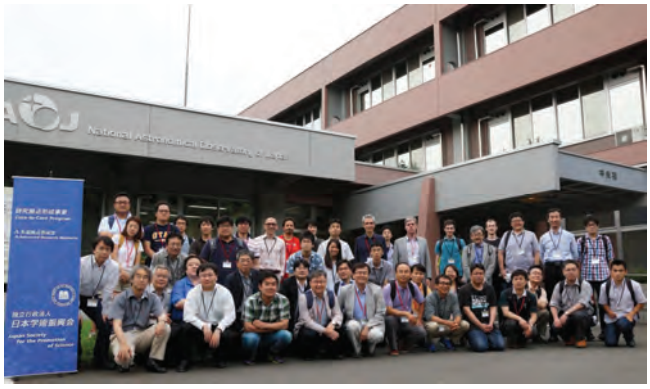

Fig. 1. 6th Korea-Japan workshop on KAGRA.

7th Korea-Japan workshop on KAGRA

Date: December 19-20, 2014
Place: University of Toyama, Japan

Outline: This workshop was the 7th Korea-Japan workshop on KAGRA, and was held at the University of Toyama (Fig. 2). The workshop was organized by the scientific advisory committee, the scientific organizing committee chaired by Seiji Kawamura (ICRR), and the local organizing committee chaired by Fusakazu Matsushima (University of Toyama). The purpose of the workshop was to foster the collaboration between Korea and Japan on the development, construction and exploitation of the KAGRA gravitational wave detector.

The workshop started with the KAGRA tour, and then we had several sessions: the opening, plenary, detector, detector characterization, theory and data analysis, and discussion sessions. In the KAGRA tour sixteen participants including all the Korean participants visited the KAGRA site (Fig.3). They were impressed by the huge space inside the tunnel and also the rapid progress of the installation. After we came back from the tour, Masaaki Shimizu (University of Toyama, Dean of Faculty of Science) and Takaaki Kajita (ICRR) gave an opening talk of the workshop. In the plenary session Yoshio Saito (ICRR) gave a talk about the present status of KAGRA, and Takashi Uchiyama (ICRR) explained the tunnel of KAGRA. In the detector session the current status of the laser, input optics, and intensity stabilization system of KAGRA were presented and discussed. In the detector characterization session after Kazuhiro Hayama (Osaka City University) talked about the status of KAGRA detector characterization, various topics about the detector characterization, such as the non-Gaussian noise characterization System, data analysis of correlated channels in CLIO, and non-stationary large noises of a gravitational wave detector by using non-parametric Bayesian clustering were presented. In the theory and data analysis session Hideyuki Tagoshi (Osaka City University) gave a talk about the status of the KAGRA data analysis system and Hirotaka Yuzurihara (Osaka City University) talked the current status of KAGRA data analysis library, KAGALI, several presentations were given on the various aspects of the theory and data analysis, such as Eccentric BH binaries, F2Amp wave form, and Hilbert-Huang Transform.

In the discussion session we first explained the importance of the shift call to the site and the authorship policy of the KAGRA papers. For the instrument collaboration we verified that Kyuman Cho (Sogang university) will develop the tilt sensor at ICRR for seven weeks in January and February, 2015 as an ICRR visiting professor with his student, Junegyu Park (Sogang University). We will discuss the possibility of using the tilt sensor for the alignment sensing of the KAGRA mirrors. We also agreed that we should start the discussion to find the possibility of collaboration on the tilt sensor for the top part of the vibration isolation system. For the detector characterization we agreed to apply several methods for finding correlation we had proposed to the LIGO GW and PEM data and KAGRA environmental data. For the data analysis it was agreed that the Korean members will test some of KAGALI components in order to get familiar with KAGALI and the Japanese members will visit Inje University in February, 2015 to discuss MCMC and KAGALI. We will continue to discuss iKAGRA plan for CBC parameter estimation. Finally we decided that the next workshop would be held on June 27, 2015 in Gwangju, Korea, right after the Amaldi conference.

Participants: 34 participants.
Website: http://www.sci.u-toyama.ac.jp/phys/kagra-tym/japankorea2014/index.html

Fig. 2. 7th Japan-Korea workshop on KAGRA.

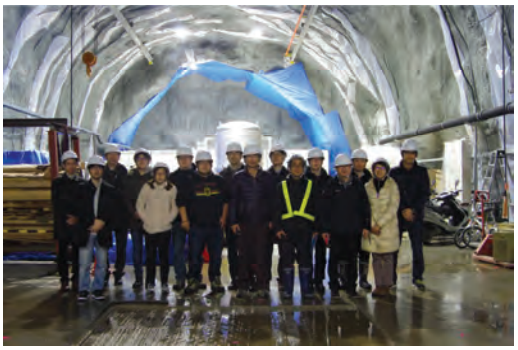

Fig. 3. KAGRA tour.

The Inaugural Symposium of the Hyper-Kamiokande Proto-Collaboration and Signing Ceremony

Date: January 31, 2015
Place: Kashiwa-no-ha Conference Center, Japan

Outline: The symposium was held to commemorate and promote the proto-collaboration to advance the Hyper-Kamiokande project internationally. In addition, a signing ceremony marking an agreement to promote of the project between the Institute for Cosmic Ray Research (ICRR) of the University of Tokyo and the Institute of Particle and Nuclear Studies of the High Energy Accelerator Research Organization (KEK) took place during the symposium.

Participants: 108 participants.

Third general meeting of ELiTES

Date: February 9-10, 2015
Place(First day): Delegration of the European Union to Japan, Tokyo
Place(Second day): Yayoi Auditorium, Hongo campus, UTokyo, Tokyo

Outline: The ELiTES program is conducted both by EU researchers who promote Einstein Telescope project and by KAGRA collaborators for gravitational wave physics since March, 2012. The objective of ELiTES is to develop advanced techniques for cryogenic interferometer by exchanging information and researchers. The funding comes from European Commission under FP7-PEOPLE-IRSES for EU researchers and Japanese side has a matching fund from JSPS. It originally spans four years and will be extended by one year. Under ELiTES, we have a general meeting of two days in Tokyo and a workshop in EU country, every year. The first day of the meeting in this financial year was held at the Delegation of the European Union to Japan (Europa house, Minamiazabu, Minatoku, Tokyo) and the second day meeting was held at Seihoku gallery of the Yayoi Auditorium, Hongo campus of the University of Tokyo. The half part of the morning session of the first day was devoted to an outreach program inviting pupils of Super Science High school in Tokyo. After the welcome talk by Dr. Leonidas Kavapiperis who is the head of Science and Technology session of the Europa house, Prof. K. Somiya (TITECH) gave a lecture on Astrophysics and Gravitational wave physics. After this talk, all pupils left and ELiTES presentations started. The ambassador, Viorel Isticioaja Budura gave a welcome speech at lunch time. As was usual, a reception dinner was served in the evening. On the second day, we listened to scientific products obtained under this ELiTES program and discussed for future prospects.

I would like to thank the EU house and Italian Embassy for their supports.

Participants: 42 participants.
Website: http://www.et-gw.eu/descriptionelites

Fig. 4. The 3rd general meeting of ELiTES in Tokyo. SSH pupils were invited as an outreach activity of Europa house, Tokyo.

B. ICRR Seminars

1. June 4, 2014: Dmitry Khangulyan (JAXA) , "Gamma-Ray Emitting Binary Systems"
2. June 5, 2014: Haruki Nishino (Kavli IPMU) , "CMB B-mode polarization experiments: Recent results from POLARBEAR (and BICEP2)"
3. August 27, 2014: Kazumasa Kawata (ICRR) , "A hotspot of the ultra-high energy cosmic rays observed by the Telescope Array experiment"
4. October 1, 2014: Motohiko Yoshimura (Okayama University) , "SPAN - SPectroscopy of Atomic Neutrino"
5. October 15, 2014: Karsten Berger (University of Delaware) , "Exploring the Extreme Universe with VERITAS"
6. October 29, 2014: Jerome Degallaix (The Laboratoire des Materiaux Avances, Lyon) , "Status of the gravitational wave detector Advanced Virgo"
7. November 12, 2014: Alexander Kusenko (UCLA/Kavli IPMU) , "Higgs relaxation and leptogenesis"
8. November 19, 2014: David Paneque (Max-Planck Institute), "The challenge of studying blazars: the crucial role of gamma-ray astronomy"
9. November 26, 2014: Makoto Miura (ICRR) , "Search for Nucleon decays in Super-Kamiokande"
10. December 17, 2014: Daniel Mazin (ICRR) , "Extragalactic science with CTA"
11. February 25, 2015: Kyuman Cho (Sogang University) , "Novel balanced-path homodyne and heterodyne I/Q-interferometer schemes and their applications: from biosensors to a local sensor for KAGRA"
12. March 26, 2015: Kazuaki Kuroda (ICRR) , "Theory of General Relativity and the detection of gravitational waves (The Last Lecture)"

C. List of Publications

(a) Papers Published in Journals

1. "Test of Lorentz invariance with atmospheric neutrinos", K. Abe et al. (Super-Kamiokande Collaboration), Phys. Rev. D **91**, 052003 (2015).
2. "Measurement of the neutrino-oxygen neutral-current interaction cross section by observing nuclear deexcitation γ rays", Abe, K. et al. (T2K Collaboration), Phys. Rev. D **90**, 072012.
3. "Search for proton decay via p$\rightarrow \nu K^+$ using 260 kilotonEyear data of Super-Kamiokande", K. Abe et al. (Super-Kamiokande Collaboration), PhysRevD. 90, 072005.
4. "Search for Nucleon Decay via $n \rightarrow \bar{\nu}\pi^0$ and $p \rightarrow \bar{\nu}\pi^+$ in Super-Kamiokande", K. Abe et al. (Super-Kamiokande Collaboration), PhysRevLett.**113**, 121802.
5. "Search for Bosonic Superweakly Interacting Massive Dark Matter Particles with the XMASS-I Detector", The XMASS Collaboration (K. Abe et al.), Physical Review Letters, **113**, 121301 (2014).
6. "Search for Trilepton Nucleon Decay via $p \rightarrow e^+\nu\nu$ and$p \rightarrow e^+\mu\nu$ in the Super-Kamiokande Experiment", V. Takhistov et al. (Super-Kamiokande Collaboration), PhysRevLett.**113**, 101801.
7. "Search for Dinucleon Decay into Kaons in Super-Kamiokande", M. Litos et al. (The Super-Kamiokande Collaboration), Phys. Rev. Lett. **112**, 131803.
8. "Supernova Relic Neutrino Search with Neutron Tagging at Super-Kamiokande-IV ", H.Zhang et al. (Super-Kamiokande Collaboration), Astroparticle Physics **60** (2015) 41.
9. "Measurement of the intrinsic electron neutrino component in the T2K neutrino beam with the ND280 detector", K. Abe et al. (T2K Collaboration), Phys. Rev. D **89**, 092003 .

10. “Precise Measurement of the Neutrino Mixing Parameter θ_{23} from Muon Neutrino Disappearance in an Off-Axis Beam”, K. Abe et al. (T2K Collaboration), Phys. Rev. Lett. **112**, 181801.

11. “Measurement of the inclusive charged current cross section on iron and hydrocarbon in the T2K on-axis neutrino beam”, K. Abe et al. (T2K Collaboration), Phys. Rev. D **90**, 052010.

12. “Measurement of the Inclusive Electron Neutrino Charged Current Cross Section on Carbon with the T2K Near Detector”, K. Abe et al. (T2K Collaboration), Phys. Rev. Lett. **113**, 241803.

13. “Search for short baseline e disappearance with the T2K near detector”, K. Abe et al. (T2K Collaboration), Phys. Rev. D **91**, 051102.

14. “Progress and open questions in the physics of neutrino cross sections at intermediate energies”, L Alvarez-Ruso, Y Hayato and J Nieves, New J. Phys. **16** 075015.

15. “Review of Particle Physics (MONTE CARLO NEUTRINO EVENT GENERATORS)”, K.A. Olive et al. (Particle Data Group), Chinese Phys. C **38** 090001.

16. “Search for inelastic WIMP nucleus scattering on 129Xe in data from the XMASS-I experiment”, H. Uchida et al. (XMASS Collaboration), Prog. Theor. Exp. Phys. 2014, **063**C01.

17. “Neutrino Physics (Rapporteur talk) ”, M. Nakahata, Braz.J.Phys. **44** (2014) 465-482.

18. “Development of a high-sensitivity 80 L radon detector for purified gases”, K. Hosokawa et al., Prog. Theor. Exp. Phys. (2015) 2015 (3): **033**H01 .

19. “Limits on sterile neutrino mixing using atmospheric neutrinos in Super-Kamiokande”, K. Abe et al. (Super-Kamiokande Collaboration), Phys. Rev. D **91**, 052019.

20. “The Measurement of Neutrino Properties with Atmospheric Neutrinos”, Takaaki Kajita,, Annu. Rev. Nucl. Part. Sci. 2014, **64**, 343-362.

21. “Recent progress and future prospects with atmospheric neutrinos”, Roger Wendell and Kimihiro Okumura, New J. Phys. **17** (2015) 025006.

22. “Discovery of very high energy gamma-ray emission from the blazar 1ES 0033+595 by the MAGIC telescopes, MAGIC collaboration, Aleksić et al. MNRAS **446** (2015) 217.

23. “MAGIC observations of MWC 656, the only known Be/BH system, MAGIC collaboration et al., A&A **576** (2015) 36.

24. “Multiwavelength observations of Mrk 501 in 2008, MAGIC collaboration, Aleksić et al.; VERITAS collaboration, : et al., A&A **573** (2015) 50.

25. “Probing the very-high-energy gamma-ray spectral curvature in the blazar PG 1553+113 with the MAGIC telescopes, MAGIC collaboration, D’Ammando et al.; Fermi-LAT collaboration, Lähteenmäki et al., MNRAS **450** (2015) 4399.

26. “The 2009 multiwavelength campaign on Mrk 421: Variability and correlation studies, MAGIC collaboration, Aleksić et al.; VERITAS collaboration, : et al., A&A **576** (2015) 126.

27. “Black hole lightning due to particle acceleration at subhorizon scales, MAGIC collaboration, Aleksić et al., Science, **346** (2014) 1080.

28. “First broadband characterization and redshift determination of the VHE blazar MAGIC J2001+439”, MAGIC collaboration, Aleksić et al., A&A **572** (2014) 121.

29. “MAGIC gamma-ray and multifrequency observations of flat spectrum radio quasar PKS 1510-089 in early 2012”, MAGIC collaboration, Aleksić et al., A&A **569**. (2014) 46.

30. “Discovery of TeV gamma-ray emission from the pulsar wind nebula 3C 58 by MAGIC collaboration”, Aleksić et al., A&A **567** (2014) 8.

31. “Search for Very-High-Energy Gamma Rays from the z = 0.896 Quasar 4C +55.17 with the MAGIC telescopes, MAGIC collaboration”, Aleksić et al., MNRAS **440** (2014) 530.

32. “Optimized dark matter searches in deep observations of Segue 1 with MAGIC”, MAGIC collaboration, Aleksić et al., JCAP **02** (2014) 008.

33. “Contemporaneous observations of the radio galaxy NGC 1275 from radio to very high energy gamma-rays, MAGIC collaboration”, Aleksić et al., A&A **564** (2014) 5.

34. “Detection of bridge emission above 50 GeV from the Crab pulsar with the MAGIC telescopes”, MAGIC collaboration, Aleksić et al., A&A **565** (2014) 12.

35. “Discovery of very high energy gamma-ray emission from the blazar 1ES 1727+502 with the MAGIC Telescopes”, MAGIC collaboration, Aleksić et al., A&A **563**. (2014) 90.

36. “MAGIC long-term study of the distant TeV blazar PKS 1424+240 in a multiwavelength context”, MAGIC collaboration, Aleksić et al. , A&A **567** (2014) 135.

37. “MAGIC observations and multifrequency properties of the Flat Spectrum Radio Quasar 3C 279 in 2011”, MAGIC collaboration, Aleksić et al., A&A **567** (2014) 41.

38. “MAGIC reveals a complex morphology within the unidentified gamma-ray source HESS J1857+026”, MAGIC collaboration, Aleksić et al., A&A **571** (2014) 96.

39. “MAGIC search for VHE γ-ray emission from AE Aquarii in a multiwavelength context”, MAGIC collaboration, Aleksić et al., A&A **568** (2014) 109.

40. “MAGIC upper limits on the GRB 090102 afterglow, MAGIC collaboration”, Aleksić et al., MNRAS **437** (2014) 3103-3111.

41. “Multifrequency Studies of the Peculiar Quasar 4C+21.35 during the 2010 Flaring Activity”, MAGIC collaboration, Ackermann et al., ApJ **786** (2014) 157.

42. “Rapid and multi-band variability of the TeV-bright active nucleus of the galaxy IC 310”, MAGIC collaboration, Aleksić et al., A&A **563** (2014) 91.

43. “The Cherenkov Telescope Array potential for the study of young supernova remnants”, CTA Consortium, Acharya et al., Astro. Part. **62** (2015) 152.

44. “Study of Ultra-High Energy Cosmic Ray composition using Telescope Array’s Middle Drum detector and surface array in hybrid mode”, R.U. Abbasi et al. (TA collaboration), Astroparticle Physics **64** (2015) 49-62.

45. “SEARCHES FOR LARGE-SCALE ANISOTROPY IN THE ARRIVAL DIRECTIONS OF COSMIC RAYS DETECTED ABOVE ENERGY OF 10^{19} eV AT THE PIERRE AUGER OBSERVATORY AND THE TELESCOPE ARRAY”, Auger Collaboration & TA Collaboration, The Astrophysical Journal **794**:172 (15pp), 2014.

46. “Indications of Intermediate-Scale Anisotropy of Cosmic Rays with Energy Greater Than 57 EeV in the Northern Sky Measured with the Surface Detector of the Telescope Array Experiment”, R.U. Abbasi et al., Astrophysical Journal Letters, **790**:L21 (5pp), 2014.

47. “Energy spectrum of ultra-high energy cosmic rays observed with the Telescope Array using a hybrid technique”, T. Abu-Zayyad et al., Astroparticle Physics **61** (2015) 93-101.

48. “The hybrid energy spectrum of Telescope Array’s Middle Drum Detector and surface array”, R.U. Abbasi et al., Astropart. Phys.**68**(2015) 27-44.

49. “Gain monitoring of telescope array photomultiplier cameras for the first 4 years of operation”, B.K. Shin et al., Nucl. Instr. and Methods A**768**(2014)96-103.

50. “Performance of the Tibet hybrid experiment (YAC-II+Tibet-III+MD) to measure the energy spectra of the light primary cosmic rays at energies 50-10000 TeV” J. Huang et al., Astroparticle Physics **66** (2015) 18-30.

51. “A balloon experiment using CALET prototype (bCALET-2)”, Tae Niita, Shoji Torii, Katsuaki Kasahara, Hiroyuki Murakami, Shunsuke Ozawa, Yoshitaka Ueyama, Yosui Akaike, Tadahisa Tamura, Kenji Yoshida, Yusaku Katayose, Yuki Shimizu, Hideyuki Fuke, Advances in Space Research Volume **55**, Issue 2, 15 January 2015, Pages 753-760.

52. “Synchrotron Self-Compton Emission by Relativistic Electrons under Stochastic Acceleration: Application to Mrk 421 and Mrk 501”, Jun Kakuwa, Kenji Toma, Katsuaki Asano, Masaaki Kusunose, and Fumio Takahara, Mon. Not. R. Astron. Soc., **449**, 551.

53. “Synchrotron X-ray emission from old pulsars”, Shota Kisaka, Shuta J. Tanaka, Mon. Not. R. Astron. Soc. **443**, 2063.

54. “The Evolution of High Temperature Plasma in Magnetar Magnetospheres and its Implications for Giant Flares”, Makoto Takamoto, Shota Kisaka, Takeru Suzuki, Toshio Terasawa, Astrophys. J. vol **787** 84 (13pp) 2014 May 20.

55. “Neutrino and Cosmic-Ray Release from Gamma-Ray Bursts: Time-Dependent Simulations”, Katsuaki Asano, Peter Meszaros, 2014 ApJ **785** 54.

56. “Mechanical loss of a multilayer tantala/silica coating on a sapphire disk at cryogenic temperatures: Toward the KAGRA gravitational wave detector”, Eiichi Hirose, Kieran Craig, Hideki Ishitsuka, Iain W. Martin, Norikatsu Mio, Shigenori Moriwaki, Peter G. Murray, Masatake Ohashi, Sheila Rowan, Yusuke Sakakibara, Toshikazu Suzuki, Kouichi Waseda, Kyohei Watanabe, and Kazuhiro Yamamoto, Phys. Rev. D **90**, 6 (2014).

57. “A Study of Cooling Time Reduction of Interferometric Cryogenic Gravitational Wave Detectors Using a High-Emissivity Coating”, Y. Sakakibara, N. Kimura, T. Suzuki, K. Yamamoto, D. Chen, S. Koike, C. Tokoku, T. Uchiyama, M. Ohashi, K. Kuroda, Adv. Cryog. Eng. **59**, 1176-1183 (2014).

58. “Progress on the Cryogenic System for the KAGRA Cryogenic Interferometric Gravitational Wave Telescope”, Yusuke Sakakibara1, Tomotada Akutsu, Dan Chen, Aleksandr Khalaidovski, Nobuhiro Kimura, Shigeaki Koike, Tatsuya Kume, Kazuaki Kuroda, Toshikazu Suzuki, Chihiro Tokoku and Kazuhiro Yamamoto, Class. Quantum Grav. **31**, 224003 (2014).

59. “Excavation of an underground site for a km-scale laser interferometric gravitational-wave detector”, T Uchiyama, K Furuta, M Ohashi, S Miyoki, O Miyakawa and Y Saito, Class. Quantum Grav. **31**, 224005 (2014).

60. “Sapphire screws and strength test on them at liquid nitrogen temperature”, Eiichi Hirose, Yusuke Sakakibara, Yukihiko Igarashi and Takashi Ishii, Rev. Sci. Instrum. **85**, 104503 (2014).

61. “Vibration measurement in the KAGRA cryostat”, D Chen, L Naticchioni, A Khalaidovski, K Yamamoto, E Majorana, Y Sakakibara, C Tokoku, T Suzuki, N Kimura, S Koike, T Uchiyama and S Kawamura, Class. Quantum Grav. **31**, 224001 (2014).

62. “Update on development of cryogenic sapphire mirrors and their seismic attenuation system for KAGRA”, E Hirose,T Sekiguchi, R Kumar, R Takahashi, Class. Quantum Grav. **31**, 224004 (2014).

63. “Evaluation of heat extraction through sapphire fibers for the GW observatory KAGRA”, A Khalaidovski, G Hofmann, D Chen, J Komma, C Schwarz, C Tokoku, N Kimura, T Suzuki, AO Scheie, E Majorana, R Nawrodt, K Yamamoto, Class. Quantum Grav. **31**, 105004 (2014).

64. “The gas inflow and outflow rate in star-forming galaxies at $z \sim 1.4$”, Kiyoto Yabe, Kouji Ohta, Masayuki Akiyama, Fumihide Iwamuro, Naoyuki Tamura, Suraphong Yuma, Gavin Dalton, Ian Lewis, ApJ, **798**, 45.

65. “The Subaru high-z quasar survey: discovery of faint $z \sim 6$ quasars”, Nobunari Kashikawa, Yoshifumi Ishizaki, Chris J. Willott, Masafusa Onoue, Myungshin Im, Hisanori Furusawa, Jun Toshikawa, Shogo Ishikawa, Yuu Niino, Kazuhiro Shimasaku, Masami Ouchi, Pascale Hibo, ApJ, **798**, 28.

66. “The Relationship between Stellar Mass, Gas Metallicity, and Star Formation Rate for Halpha-selected Galaxies at $z \sim 0.8$ from the NewHalpha Survey”, Mithi A. de los Reyes, Chun Ly, Janice C. Lee, Samir Salim, Molly S. Peeples, Ivelina Momcheva, Jesse Feddersen, Daniel A. Dale, Masami Ouchi, Yoshiaki Ono, Rose Finn, The Astronomical Journal **149** (2) 79 (2015).

67. “Hubble Frontier Fields First Complete Cluster Data: Faint Galaxies at z∼5-10 for UV Luminosity Functions and Cosmic Reionization”, Masafumi Ishigaki, Ryota Kawamata, Masami Ouchi, Masamune Oguri, Kazuhiro Shimasaku, Yoshiaki Ono, The Astrophysical Journal, **799**:12 (21pp), 2015 January 20.

68. “A First Site of Galaxy Cluster Formation: Complete Spectroscopy of a Protocluster at $z = 6.01$”, Jun Toshikawa, Nobunari Kashikawa, Roderik Overzier, Takatoshi Shibuya, Shogo Ishikawa, Kazuaki Ota, Kazuhiro Shimasaku, Masayuki Tanaka, Masao Hayashi, Yuu Niino, Masafusa Onoue, 2014 ApJ **792** 15.

69. “MOSFIRE and LDSS3 Spectroscopy for an [OII] Blob at $z = 1.18$: Gas Outflow and Energy Source ”, Yuichi Harikane, Masami Ouchi, Suraphong Yuma, Michael Rauch, Kimihiko Nakajima, Yoshiaki Ono, ApJ, **794**, 129.

70. “Constraining dust formation in high-redshift young galaxies”, Hiroyuki Hirashita, Andrea Ferrara, Pratika Dayal, Masami Ouchi, MNRAS (September 11, 2014) **443** (2): 1704-1712.

71. “Large-scale environment of $z \sim 5.7$ CIV absorption systems I: projected distribution of galaxies ”, C. Gonzalo Diaz, Yusei Koyama, Emma V. Ryan-Weber, Jeff Cooke, Masami Ouchi, Kazuhiro Shimasaku, Fumiaki Nakata, MNRAS**442**,946-978 (2014).

72. "Accelerated Evolution of Lyα Luminosity Function at $z >= 7$ Revealed by the Subaru Ultra-Deep Survey for Lyα Emitters at $z = 7.3$", Akira Konno, Masami Ouchi, Yoshiaki Ono, Kazuhiro Shimasaku, Takatoshi Shibuya, Hisanori Furusawa, Kimihiko Nakajima, Yoshiaki Naito, Rieko Momose, Suraphong Yuma, Masanori Iye, 2014 ApJ **797** 16.

73. "Faint Submillimeter Galaxies Revealed by Multifield Deep ALMA Observations: Number Counts, Spatial Clustering, and a Dark Submillimeter Line Emitter", Yoshiaki Ono, Masami Ouchi, Yasutaka Kurono, Rieko Momose, 2014 ApJ **795** 5.

74. "Diffuse Lyα Halos around Galaxies at $z = 2.2 - 6.6$: Implications for Galaxy Formation and Cosmic Reionization", Rieko Momose, Masami Ouchi, Kimihiko Nakajima, Yoshiaki Ono, Takatoshi Shibuya, Kazuhiro Shimasaku, Suraphong Yuma, Masao Mori, Masayuki Umemura, Mon.Not.Roy.Astron.Soc. **442** (2014) 110.

75. "Evidence for a gas-rich major merger in a proto-cluster at $z = 2.5$", Ken-ichi Tadaki, Tadayuki Kodama, Yoichi Tamura, Masao Hayashi, Yusei Koyama, Rhythm Shimakawa, Ichi Tanaka, Kotaro Kohno, Bunyo Hatsukade, Kenta Suzuki,, 2014 ApJ **788** L23.

76. "Identification of the progenitors of rich clusters and member galaxies in rapid formation at $z > 2$", Rhythm Shimakawa, Tadayuki Kodama, Ken-ichi Tadaki, Ichi Tanaka, Masao Hayashi, Yusei Koyama, MNRAS, **441**, L1-L5.

77. "What is the physical origin of strong Lyα emission? II. Gas Kinematics and Distribution of Lya Emitters", Takatoshi Shibuya, Masami Ouchi, Kimihiko Nakajima, Takuya Hashimoto, Yoshiaki Ono, Michael Rauch, Jean-Rene Gauthier, Kazuhiro Shimasaku, Ryosuke Goto, Masao Mori, Masayuki Umemura, 2014 ApJ **788** 74.

78. "When did round disk galaxies form?", Tomoe M. Takeuchi, Kouji Ohta, Suraphong Yuma, Kiyoto Yabe, ApJ, **801**, 2.

79. "Large-scale environment of $z \sim 5.7$ CIV absorption systems -II. Spectroscopy of Lyman-α emitters", C. Gonzalo Diaz, Emma V. Ryan-Weber, Jeff Cooke, Yusei Koyama, Masami Ouchi, Mon. Not. R. Astron. Soc., **448**, 1240-1270.

80. "The spectral energy distribution of the redshift 7.1 quasar ULAS J1120+0641", R. Barnett, S. J. Warren, M. Banerji, R. G. McMahon, P. C. Hewett, D. J. Mortlock, C. Simpson, B. P. Venemans, K. Ota, T. Shibuya, Astronomy&Astrophysics, **575**, A31.

81. "NIR spectroscopic observation of massive galaxies in the protocluster at $z = 3.09$", Mariko Kubo, Toru Yamada, Takashi Ichikawa, Masaru Kajisawa, Yuichi Matsuda, Ichi Tanaka, ApJ, **799**, 38.

82. "First direct implications for the dust extinction and star formation of typical Lyα emitters from their faint infrared luminosities", Haruka Kusakabe, Kazuhiro Shimasaku, Kimihiko Nakajima, Masami Ouchi, ApJL, **800**, L29.

83. "Lower bound of the tensor-to-scalar ratio $r \gtrsim 0.1$ in a nearly quadratic chaotic inflation model in supergravity", Keisuke Harigaya Masahiro Kawasaki and Tsutomu T. Yanagida, Physics Letters B Volume **741**, 4 February 2015, Pages 267-271.

84. "CDM/baryon isocurvature perturbations in a sneutrino curvaton model", Keisuke Harigaya, Taku Hayakawa, Masahiro Kawasaki and Shuichiro Yokoyama, JCAP**10**(2014)068.

85. "Gravitational effects on vanishing Higgs potential at the Planck scale", Naoyuki Haba, Kunio Kaneta, Ryo Takahashi and Yuya Yamaguchi, Phys. Rev. D **91**, 016004.

86. "Q-ball dark matter and baryogenesis in high-scale inflation", Shinta Kasuya and Masahiro Kawasaki, Physics Letters B, Volume **739**, 12 December 2014, Pages 174-179.

87. "Cosmic neutrino background absorption line in the neutrino spectrum at IceCube", Masahiro Ibe, Kunio Kaneta, Phys. Rev. D **90**, 053011.

88. "Thermal Effects and Sudden Decay Approximation in the Curvaton Scenario", Naoya Kitajima, David Langlois, Tomo Takahashi, Tomohiro Takesako, Shuichiro Yokoyama, JCAP **1410** (2014) 10, 032.

89. "Blue-tilted Tensor Spectrum and Thermal History of the Universe", Sachiko Kuroyanagi, Tomo Takahashi, Shuichiro Yokoyama, JCAP**02**(2015)003.

90. "Relaxing Isocurvature Bounds on String Axion Dark Matter", Masahiro Kawasaki, Naoya Kitajima, Fuminobu Takahashi,, Physics Letters B, Volume **737**, 7 October 2014, Pages 178-184.

91. "Vanishing Higgs potential at the Planck scale in singlets extension of the standard model", Naoyuki Haba, Hiroyuki Ishida, Kunio Kaneta and Ryo Takahashi, Phys. Rev. D **90**, 036006.

92. “A solution to the baryon-DM coincidence problem in the CMSSM with a 126-GeV Higgs boson”, Ayuki Kamada, Masahiro Kawasaki and Masaki Yamada, Phys.Rev.D.**91**.081301.

93. “Non-perturbative approach for curvature perturbations in stochastic-δN formalism”, Tomohiro Fujita, Masahiro Kawasaki, Yuichiro Tada, JCAP **10**(2014)030.

94. “Chemical separation of primordial Li^+ during structure formation caused by nanogauss magnetic field”, Motohiko Kusakabe and Masahiro Kawasaki, MNRAS **446**, 1597-1624.

95. “Inflaton potential on a Riemann surface”, Keisuke Harigaya, Masahiro Ibe, Physics Letters B,Volume **738**, 10 November 2014, Pages 301-304.

96. “Affeck-Dine Baryogenesis and Dark Matter Production after High-scale Inflation”, Keisuke Harigaya, Ayuki Kamada, Masahiro Kawasaki, Kyohei Mukaida and Masaki Yamada, Phys. Rev. D **90**, 043510.

97. “Isocurvature perturbations and tensor mode in light of Planck and BICEP2”, Masahiro Kawasaki, Toyokazu Sekiguchi, Tomo Takahashi, Shuichiro Yokoyama, JCAP**08**(2014)043.

98. “Curvaton in large field inflation”, Tomohiro Fujita, Masahiro Kawasaki, Shuichiro Yokoyama, JCAP**09**(2014)015.

99. “Compensation for large tensor modes with iso-curvature perturbations in CMB anisotropies”, Masahiro Kawasaki, Shuichiro Yokoyama, JCAP**05**(2014)046.

100. “High-Scale SUSY Breaking Models in light of the BICEP2 Result”, Keisuke Harigaya, Masahiro Ibe, Koji Ichikawa, Kunio Kaneta, Shigeki Matsumot, Journal of High Energy Physics, July 2014, 2014:**93**.

101. “Dynamical Chaotic Inflation in the Light of BICEP2”, Keisuke Harigaya, Masahiro Ibe, Kai Schmitz, Tsutomu T. Yanagida, Physics Letters B,Volume **733**, 2 June 2014, Pages 283-287.

102. “Probing small-scale cosmological fluctuations with the 21 cm forest: effects of neutrino mass, running spectral index and warm dark matter”, Hayato Shimabukuro, Kiyotomo Ichiki, Susumu Inoue, and Shuichiro Yokoyama, Phys.Rev. D**90** (2014) 8, 083003.

103. “Testing the Minimal Direct Gauge Mediation at the LHC”, Koichi Hamaguchi, Masahiro Ibe, Tsutomu T. Yanagida, Norimi Yokozaki, Phys. Rev. D **90**, 015027.

104. “Peccei-Quinn Symmetric Pure Gravity Mediation”, Jason L. Evans, Masahiro Ibe, Keith A. Olive, Tsutomu T. Yanagida, Eur. Phys. J. C (2014) **74**:2931.

105. “Baryogenesis from the Gauge-mediation type Q ball and the dark matter New type Q ball”, Shinta Kasuyaa and Masahiro Kawasaki, Phys. Rev. D **89**, 103534.

106. “Dark Matter Production in Late Time Reheating”, K. Harigaya, M. Kawasaki, K. Mukaida and M. Yamada, Phys. Rev. D **89**, 083532.

107. “Baryon asymmetry, dark matter, and density perturbation from primordial black holes”, Tomohiro Fujita, Masahiro Kawasaki, Keisuke Harigaya, Ryo Matsuda, Phys. Rev. D **89**, 103501 .

108. “Dynamical fractional chaotic inflation”, Keisuke Harigaya, Masahiro Ibe, Kai Schmitz, Tsutomu T. Yanagida, Phys. Rev. D **90**, 123524.

109. “Phase Locked Inflation. Effectively Trans-Planckian Natural Inflation”, Keisuke Harigaya, Masahiro Ibe, JHEP**1411**(2014)147.

110. “R-symmetric Axion/Natural Inflation in Supergravity via Deformed Moduli Dynamics”, Keisuke Harigaya, Masahiro Ibe, Tsutomu Yanagida, Physics Letters B, Volume **739**, 352-356.

111. “Anomaly Mediated Gaugino Mass and Path-Integral Measure”, Keisuke Harigaya, Masahiro Ibe, Phys. Rev. D **89**, 085028.

112. “Light Higgsinos in Pure Gravity Mediation”, Jason L. Evans, Masahiro Ibe, Keith A. Olive, Tsutomu T. Yanagida, Phys.Rev. D**91** (2015) 5, 055008.

113. “Mass of Decaying Wino from AMS-02 2014”, Masahiro Ibe, Satoshi Shirai, Shigeki Matsumoto, Tsutomu Yanagida, Phys.Lett. B**741** (2015) 134-137.

114. “Gravitational waves as a probe of the SUSY scale”, A. Kamada, M. Yamada, Phys. Rev. D **91**, 063529 (2015).

115. “No quasistable scalaron lump forms after R2 inflation”, N. Takeda, Y. Watanabe, Phys. Rev. D **90**, 023519 (2014).

(b) Conference Papers

1. “Future Long-Baseline Neutrino Oscillations: View from Asia”, Y. Hayato, Proceedings of XXVI International Conference on Neutrino Physics and Astrophysics (Neutrino 2014), June, 2014.
2. “Monte Carlo neutrino event generators”, Y. Hayato, 2014 Review of Particle Physics.
3. “Search for Nucleon Decay in Super-Kamiokande”, M. Miura for the Super-Kamiokande Collaboration, 37th International Conference on High Energy Physics, 2014.
4. “Recent Results from Telescope Array”, M.Fukushima, ISVHECRI 2014, CERN, August 18-22, 2014.
5. “TAx4”, H. Sagawa, UHECR2014, Springdale, Utah, USA, October 12-15, 2014.
6. “Simulations of Ultra High Energy Cosmic Rays propagation”, E.Kido, UHECR2014, Springdale, Utah, USA, October 12-15, 2014.
7. “TA-muon”, T.Nonaka, UHECR2014, Springdale, Utah, USA, October 12-15, 2014.
8. “Hard X-ray observations with Suzaku HXDat the time of giant radio pulses from the Crab pulsar”, R. Mikami, T. Terasawa, S. Kisaka, K. Asano, S. J. Tanaka, M. Sekido, K. Takefuji, H. Takeuchi, H. Odaka, T. Sato, Y. T. Tanaka, and N. Kawai, Suzaku-MAXI 2014: Expanding the Frontiers of the X-ray Universe, 19-22 February 2014, Ehime, Japan, p.180.
9. “Second-Order Fermi Acceleration and Emission in Blazar Jets”, K. Asano, F. Takahara, K. Toma, M. Kusunose, J. Kakuwa, 40th COSPAR Scientific Assembly, 2-10 August 2014, Moscow, Russia Abstract E1.5-13-14.
10. “Evolution of Hot Plasma in Magnetar Magnetospheres and its Implications for Initial Spikes of Giant Flares”, M. Takamoto, T. Terasawa, S. Kisaka, T. Suzuki, 40th COSPAR Scientific Assembly Held 2-10 August 2014, Moscow, Russia, Abstract E1.12-13-14.
11. “Spectral Model of Wind Nebulae Powered by a Magnetar”, S. J. Tanaka, 40th COSPAR Scientific Assembly, 2-10 August 2014, Moscow, Russia, Abstract E1.16-38-14.
12. “Performance of particle identification with the CALET calorimeter expected by CERN-SPS beam tests”, Y. Akaike, and CALET collaboration, 40th COSPAR Scientific Assembly, 2-10 August 2014, Moscow, Russia, Abstract E1.6-88-14.
13. “Time and Space Dependent Stochastic Acceleration Model for the Fermi Bubbles”, K. Sasaki, K. Asano, T. Terasawa, 2014 Fermi Symposium, 20-24 October 2014, Nagoya, Japan eConf C14102.1.

(c) ICRR Reports

1. ICRR-Report-675-2014-1
   “Isocurvature perturbations and tensor mode in light of Planck and BICEP2”
   Masahiro Kawasaki, Toyokazu Sekiguchi, Tomo Takahashi, Shuichiro Yokoyama.
2. ICRR-Report-676-2014-2
   “Curvaton in large field inflation”
   Tomohiro Fujita, Masahiro Kawasaki, Shuichiro Yokoyama.
3. ICRR-Report-677-2014-3
   “Affleck-Dine Baryogenesis and Dark Matter Production after High-scale Inflation”
   Keisuke Harigaya, Ayuki Kamada, Masahiro Kawasaki, Kyohei Mukaida, Masaki Yamada.
4. ICRR-Report-678-2014-4
   “Inflaton potential on a Riemann surface”
   Keisuke Harigaya, Masahiro Ibe.
5. ICRR-Report-679-2014-5
   “History of Cosmic Ray Air-Shower Research ”
   Motohiko Nagano.

6. ICRR-Report-680-2014-6
"Non-perturbative approach for curvature perturbations in stochastic-δN formalism"
Tomohiro Fujita, Masahiro Kawasaki, Yuichiro Tada.

7. ICRR-Report-681-2014-7
"No quasi-stable scalaron lump forms after R^2 inflation"
Naoyuki Takeda, Yuki Watanabe.

8. ICRR-Report-682-2014-8
"Wino Dark Matter and Future dSph Observations"
Biplob Bhattacherjee, Masahiro Ibe, Koji Ichikawa, Shigeki Matsumoto and Kohei Nishiyama.

9. ICRR-Report-683-2014-9
"A solution to the baryon-DM coincidence problem in the CMSSM with a 126-GeV Higgs boson"
Ayuki Kamada, Masahiro Kawasaki, Masaki Yamada.

10. ICRR-Report-684-2014-10
"Relaxing Isocurvature Bounds on String Axion Dark Matter"
Masahiro Kawasaki, Naoya Kitajima, Fuminobu Takahashi.

11. ICRR-Report-685-2014-11
"Gravitational waves as a probe of SUSY scale"
Ayuki Kamada, Masaki Yamada.

12. ICRR-Report-686-2014-12
"Blue-tilted Tensor Spectrum and Thermal History of the Universe"
Sachiko Kuroyanagi, Tomo Takahashi, Shuichiro Yokoyama.

13. ICRR-Report-687-2014-13
"CνB absorption line in the neutrino spectrum at IceCube"
Masahiro Ibe, Kunio Kaneta.

14. ICRR-Report-688-2014-14
"Dynamical Fractional Chaotic Inflation – Dynamical Generation of a Fractional Power-Law Potential for Chaotic Inflation"
Keisuke Harigaya, Masahiro Ibe, Kai Schmitz, Tsutomu T. Yanagida.

15. ICRR-Report-689-2014-15
"Phase Locked Inflation – Effectively Trans-Planckian Natural Inflation"
Keisuke Harigaya, Masahiro Ibe.

16. ICRR-Report-690-2014-16
"Thermal Effects and Sudden Decay Approximation in the Curvaton Scenario"
Naoya Kitajima, David Langlois, Tomo Takahashi, Tomohiro Takesako, Shuichiro Yokoyama.

17. ICRR-Report-691-2014-17
"R-symmetric Axion/Natural Inflation in Supergravity via Deformed Moduli Dynamics"
Keisuke Harigaya, Masahiro Ibe, Tsutomu T. Yanagida.

18. ICRR-Report-692-2014-18
"CDM/baryon isocurvature perturbations in a sneutrino curvaton model"
Keisuke Harigaya, Taku Hayakawa, Masahiro Kawasaki, Shuichiro Yokoyama.

19. ICRR-Report-693-2014-19
"Anomaly Mediated Gaugino Mass and Path-Integral Measure"
Keisuke Harigaya, Masahiro Ibe.

20. ICRR-Report-694-2014-20
"New resonance scale and fingerprint identification in minimal composite Higgs models"
Shinya Kanemura, Kunio Kaneta, Naoki Machida, Tetsuo Shindou.

21. ICRR-Report-695-2014-21
"Coupling Unification and Dark Matter in a Standard Model Extension with Adjoint Majorana Fermions"
Tasuku Aizawa, Masahiro Ibe, Kunio Kaneta.

22. ICRR-Report-696-2014-22
"Axion dark matter from topological defects"
Masahiro Kawasaki, Ken'ichi Saikawa, Toyokazu Sekiguchi.

23. ICRR-Report-697-2014-23
"IceCube potential for detecting the Q-ball dark matter in gauge mediation"
Shinta Kasuya, Masahiro Kawasaki, Tsutomu T. Yanagida.

24. ICRR-Report-698-2014-24
"Affleck-Dine baryogenesis after D-term inflation and solutions to the baryon-DM coincidence problem"
Masahiro Kawasaki, Masaki Yamada.

25. ICRR-Report-670-2014-25
"Consistent generation of magnetic fields in axion inflation models"
Tomohiro Fujita, Ryo Namba, Yuichiro Tada, Naoyuki Takeda, Hiroyuki Tashiro.

D. Doctoral Theses

1. "Study of a cryogenic suspension system for the gravitational wave telescope KAGRA",
Dan Chen,
Ph.D Thesis, Mar. 2015.

2. "A Study of Cryogenic Techniques for Gravitational Wave Detection",
Yusuke Sakakibara,
Ph.D Thesis, Mar. 2015.

3. "Development of Neutron-Tagging Techniques and Application to Atmospheric Neutrino Oscillation Analysis in Super-Kamiokande",
Tristan James Irvine,
PhD Thesis, Sep. 2014

E. Public Relations

(a) ICRR News

ICRR News is a quarterly publication written in Japanese about scientific and educational activities at ICRR. It includes:

1. reports on scientific activities of ICRR staff members and those conducted at one or more of its facilities,
2. reports of international conferences on topics relevant to ICRR's research activities,
3. reports on topics discussed at ICRR's Committees,
4. list of publications published by ICRR [ICRR-Report],
5. list of seminars held at ICRR,
6. announcements, and
7. other items of relevance.

Below lists the main topics in the issues published in FY 2014:

No.89 (June 30, 2014)

- Hubble and ALMA observations of the giant space blob seen close to comic dawn, Masami Ouchi.
- Excavation of the KAGRA Tunnel, Takashi Uchiyama.

- ICRR Spring School 2014 Report.
- Staff reassignment.
- ICRR-Seminar.
- ICRR-Report.

No.90 (September 30, 2014)

- A hotspot of the highest energy cosmic rays observed by Telescope Array, Kazumasa Kawata & Hiroyuki Sagawa.
- Inflation theory and the BICEP2, Shuichiro Yokoyama.
- Report of the KAGRA Tunnel Tour.
- Awards.
- Staff reassignment.
- ICRR-Seminar.
- ICRR-Report.

No.91 (December 31, 2014)

- The current status and future of the XMASS Experiment, Ko Abe.
- Open Campus 2014 Report.
- Awards.
- Staff reassignment.
- ICRR-Seminar.
- ICRR-Report.

No.92 (March 31, 2015)

- The Hyper-Kamiokande Project, Yoshinari Hayato.
- Report of the ICRR Joint-Use Report Workshop, Shinji Miyoki & Kazuhiro Yamamoto.
- Report of the Inaugural Symposimu of the Hyper-Kamiokande Proto-Collaboration.
- Report of the 4th ICRR Graduate Students Workshop.
- Awards.
- Staff reassignment.
- ICRR-Seminar.
- ICRR-Report.

(b) Public Lectures

- "Rikei Saizensen," Aug. 2, 2014, Kavili IPMU, Kashiwa, Chiba, Naoko Ohishi (ICRR, University of Tokyo).
- "Chiba Career Challenge School," Aug. 20-21, 2014, ICRR, Kashiwa, Chiba, Seiji Kawamura (ICRR, University of Tokyo).
- "Hirameki-Tokimeki Science," Aug. 23-24, 2014, ICRR, Kashiwa, Chiba, Seiji Kawamura (ICRR, University of Tokyo).

- “Open Camups Science Cafe,” Oct. 24-25, 2014, ICRR, Kashiwa, Chiba, Seiji Kawamura, Kazumasa Kawata, Yosuhiro Nishimura (ICRR, University of Tokyo).
- “Special Lecture,” May. 24, 2014, Kanazawa-city, Ishikawa, Shoei Nakayama (ICRR, University of Tokyo).
- “Science Cafe,” Jul. 5, 2014, Toyama-city, Toyama, Masayuki Nakahata (ICRR, University of Tokyo).
- “Hirameki Tokimeki Science,” Aug. 1, 4 , 2014, Kamioka-cho, Hida-city, Gifu, Masaki Yamashita & Roger Wendell (ICRR, University of Tokyo).
- “Belle Plus Science Cafe,” Aug. 7, 2014, Tsukuba-city, Ibaraki, Hiroyuki Sekiya (ICRR, University of Tokyo).
- “Science Cafe,” Aug. 30, 2014, Gifu-city, Gifu, Masayuki Nakahata (ICRR, University of Tokyo).
- “Lecture,” Sep. 20, 2014, Toyama-city, Toyama, Roger Wendell (ICRR, the University of Tokyo).
- “Public Lecture in Kashiwa Open Campus,” Oct. 25, 2014, Kashiwa-city, Chiba, Masato Shiozawa(ICRR, the University of Tokyo).
- “Public Lecture in Komaba Campus,” Nov. 15, 2014, Meguro-ku, Tokyo, Masaki Yamashita (ICRR, the University of Tokyo)
- “SSH The Shizuoka-Kita High School”, Apr. 25, 2014, Kamioka-cho, Hida-city, Gifu, Ko Abe (ICRR, the University of Tokyo).
- “SSH The Yoshiki High School”, Jul. 7, 2014, Kamioka-cho, Hida-city, Gifu, Astushi Takeda (ICRR, the University of Tokyo).
- “SSH The Kariya High School”, Jul. 23, 2014, Kamioka-cho, Hida-city, Gifu, Jun Kameda (ICRR, the University of Tokyo).
- “SSH The Momoyama High School”, Jul. 29, 2014, Kamioka-cho, Hida-city, Gifu, Makoto Miura (ICRR, the University of Tokyo).
- “SSH The Gakushuin High School”, Jul. 30, 2014, Kamioka-cho, Hida-city, Gifu, Motoyasu Ikeda (ICRR, the University of Tokyo).
- “SSH The Kumagaya High School”, Jul. 31, 2014, Kamioka-cho, Hida-city, Gifu, Hiroyuki Sekiya (ICRR, the University of Tokyo).
- “SSH The Ashikaga High School”, Aug. 5, 2014, Kamioka-cho, Hida-city, Gifu, Motoyasu Ikeda (ICRR, the University of Tokyo).
- “SSH The Sapporo Nishi High School”, Aug. 7, 2015, Kamioka-cho, Hida-city, Gifu, Yoshinari Hayato (ICRR, the University of Tokyo).
- “SSH The Keio High School”,Aug. 19, 2014, Kamioka-cho, Hida-city, Gifu, Jun Kameda (ICRR, the University of Tokyo).
- “SSH The Senior High School Attached to Kyoto University of Education”, Aug. 20, 2014, Kamioka-cho, Hida-city, Gifu, Atushi Takeda (ICRR, the University of Tokyo).
- “SSH The Nanao High School”, Oct. 6, 2014, Kamioka-cho, Hida-city, Gifu, Ko Abe (ICRR, the University of Tokyo).
- “Kamioka Junior High School”, Oct. 30, 2014, Kamioka-cho, Hida-city, Gifu, Roger Wendell (ICRR, the University of Tokyo).
- “SSH The Doshisya Junior High School”, Dec. 11, 2014, Kamioka-cho, Hida-city, Gifu, Motoyasu Ikeda (ICRR, the University of Tokyo).
- “SSH The Keio High School”, Feb. 18, 2015, Kamioka-cho, Hida-city, Gifu, Yoshinari Hayato (ICRR, the University of Tokyo).
- “Exploring the Edge of the Universe with the Large Telescopes— Mathematics Making the Discovery of the Ancient Object, Himiko,” November 9, 2014, Tokyo International Exchange Center, Odaiba, Tokyo, Masami Ouchi (ICRR, the University of Tokyo).

- "Cosmic History Studied with the Large Telescopes," November 19, 2014, Tokyo Metropolitan Musashi High School, Masami Ouchi (ICRR, the University of Tokyo).
- "Galaxy evolution 10 billion years ago when the universe was young," November 1, 2014, Seishin Gakuen High School, Chiba, Japan, Suraphong Yuma (ICRR, the University of Tokyo).
- "Galaxy evolution in the early universe," November 17, 2014, Engineering-Science classroom, King Mongkutfs University of Technology Thonburi, Bangkok, Thailand, Suraphong Yuma (ICRR, the University of Tokyo).
- "Galaxy evolution in the early universe: recent progress in the field, resent progress in Thailand," November 22, 2014, 7th Thailand-Japan international academic conference, UTokyo, Tokyo, Japan, Suraphong Yuma (ICRR, the University of Tokyo).
- "Astrophysics × Social Science of Hope", June 4, 2014, Kamioka-cho, Hida-city, Gifu, Masatake Ohashi (ICRR, University of Tokyo).
- "Visiting KAGRA's Control Room [KAGRA's future prospects]", April 8, 2014, Kamioka-cho, Hida-city, Gifu, Masatake Ohashi (ICRR, University of Tokyo).
- "SSH Shizuoka-Kita [Observing the Universe with Gravitaional Wave Telescopes]", April 25, 2014, Kamioka-cho, Hida-city, Gifu, Naoko Ohishi (NAOJ).
- "Detecting Gravitational Waves with KAGRA!", May 10, 2014, Shinjuku-ku, Tokyo, Seiji Kawamura (ICRR, University of Tokyo).
- "The Goals of the Large-scale Cryogenic Gravitational Wave Telescope KAGRA", June 27, 2014, Nagaoka-shi, Niigata, Masatake Ohashi (ICRR, University of Tokyo).
- "Science Cafe on a night of Summer", July 25, 2014, Kamioka-cho, Hida-city, Gifu, Masatake Ohashi (ICRR, University of Tokyo).
- "The wonderous Universe!", September 10, 2014, Kita-ku, Tokyo, Seiji Kawamura (ICRR, University of Tokyo).
- "Einstein's Melody from the Universe", November 7, 2014, Sendai, Miyagi, Seiji Kawamura (ICRR, University of Tokyo).
- "Public Lecture [KAGRA-Probing the Universe with Gravitational Waves] at Toyama International Workshop on Higgs as a Probe of New Physics 2015 (HPNP2015)", February 15, 2015, Toyama-shi, Toyama, Seiji Kawamura (ICRR, University of Tokyo).
- "Gravitaional Waves/ On the Road to Detection", October 27, 2014, Hida-shi, Kamioka, Masatake Ohashi (ICRR, University of Tokyo).
- "Constructing the Large-scale Cryogenic Gravitational Wave Telescope KAGRA", November 15, 2014, Kamioka-cho, Hida-city, Gifu, Masatake Ohashi (ICRR, University of Tokyo).
- "Toyama University students' visit [Detecting Gravitational Waves with KAGRA]", October 1, 2014, Kamioka-cho, Hida-city, Gifu, Seiji Kawamura (ICRR, University of Tokyo).

(c) Visitors

KASHIWA Campus (Total: 12 groups, 1,575 people)

- High Schools: total 3 schools
- Kashiwanoha Science Forum
- Open Campus
- Press Session
- Others: 6 groups

KAMIOKA Observatory (Total: 149 groups, 2,680 people)

- Yumeno Tamago Jyuku (Hida Academy for High School Students)

- MEXT Super Science High School (SSH) project: total 14 schools
- Schools and Universities: total 21 groups
- Researchers: total 13 groups
- Others: 102 groups

Gravitational Wave Project Office KAMIOKA (Total: 97 groups, 981 people)

- MEXT Super Science High School (SSH) project: total 1 school
- Schools and Universities: total 6 groups
- Researchers: total 8 groups
- Others: 34 groups

F. Inter-University Research Activities

Numbers of Researchers

	Number of Applications	Number of Adoptions	Number of Researchers
Facility Usage			
Kamioka Observatory	38	38	833
Akeno Observatory	5	5	70
Norikura Observatory	10	10	75
Low-Level Radioisotope Measurement Facility	4	4	34
Cryogenic Laser Interferometer in Kashiwa	22	22	494
Laboratorial Facility in Kashiwa	5	5	87
Computer Facility in Kashiwa	14	14	372
Conference Facility in Kashiwa	10	10	370
Over Sea Facilities	11	11	139
Annual Sums	119	119	2,474

Joint Research			
Neutrino and Astroparticle Research	39	39	839
High Energy Cosmic Ray Research	48	48	1,001
Astrophysics and Gravity Research	24	24	543
Research Center for Cosmic neutrinos	8	8	91
Annual Sums	119	119	2,474

Research Project Titles

1. Study of simulation for atmospheric neutrino
2. Study of atmospheric neutrino flux and neutrino oscillations
3. Study of three flavor oscillation in atmospheric neutrinos
4. Study of flavor identification of atmospheric and beam neutrinos
5. Improving the sensitivity of atmospheric neutrinos with external constraints
6. Study of Solar Neutrino Flux

7. Energy spectrum measurement of solar neutrinos in Super-Kamiokande
8. Precise measurement of Day/Night effect for B8 solar neutrinos
9. Solar neturino measurement at Super-Kamiokande
10. Study for Supernova monitor
11. Study of Supernova Relic Neutrinos
12. Study of proton decay $p \to \nu K^+$
13. Search for proton decay via $e^+\pi^0$ mode
14. Study in upward-going muons and high energy neutrinos
15. Sidereal daily variation of $\sim$10TeV galactic cosmic ray intensity observed by the Super-Kamiokande
16. Tokai to Kamioka Long Baseline Experiment T2K
17. Neutrino interaction study using accelerator data
18. Study for the electron neutrino appearance measurement in the T2K experiment
19. Energy calibration for Super-Kamiokande
20. Development of low concentration radon detection system
21. R&D of a Mton water Cherenkov Hyper-Kamiokande
22. Development of the Hybrid Photodetector for a next-generation neutrino detector
23. Neutrino Workshop
24. Study for double beta decay of 48Ca
25. Calibration study of liquid xenon detector
26. R&D studies of low temperature rubber for XMASS
27. Micro-analysis of gaseous contamination in Xe
28. Study for upgrade of XMASS detector
29. Development of radon detector for purified gases
30. A study on near-ultraviolet emission of liquid xenon scintillator
31. Studies on steady removal of noble gas impurities using laser resonance ionization
32. Direction-sensitive dark matter search experiment
33. Integration of crustal activity observation around the Atotsugawa fault
34. Strain, tilt, seismic measurement in Kamioka-mine
35. The storage of Nuclear Emulsion plates for the E07 experiment in the Kamioka mine
36. Dark Matter Search with double-phase Argon Detector
37. A Search for Dark Matter using Liquid Xenon Detector
38. Study of annual modulation for dark matter search
39. Study for lowering backgrounds of radioisotopes in large volume detectors
40. Multi-Color Imager for Transients, Survey and Monstrous Explosions
41. Observation of Galactic Cosmic Ray Intensities using Large Area Muon Telescopes
42. R&D for a Small Atmospheric Cherenkov Telescope in Akeno Observatory

43. Observation of solar neutrons in solar cycle 24
44. Alpine vegetation study on Mt. Norikura
45. Community of mycorrhizal fungi on seedling establishment in alpine zone
46. Observations of total ozone and UV solar radiation with Brewer spectrophotometer on the Norikura mountains
47. Observation of cosmogenic nuclides concentrations with temporal variability at Mt. Norikura
48. A trial of Lock Ptarmigan conservation by cage
49. Space weather observation using muon hodoscope at Mt. Norikura
50. Dynamics of Abies mariesii forests of forest line of Mt. Norikura
51. Monitoring of secondary cosmic-ray neutrons at Norikura Observatory
52. Study of gamma ray bursts from mountain-top thunderclouds
53. CTA Project R&D
54. CTA-Japan Physics Research
55. Development of the readout system for the CTA large-size telescopes
56. CTA Monte Carlo simulation
57. Development of Foal Plane Instruments for the CTA Large Scale Telescope
58. Development of camera for CTA small-sized telescopes
59. Development of the mirror alignment system for the CTA Large Size Telescope
60. Development of an ultra-fast data acquisition system for the CTA Large Size Telescope
61. Development of advanced photon counter for the future IACT
62. Study of High Energy Gamma-ray Objects with the MAGIC telescopes
63. Study of Extremely-high Energy Cosmic Rays by Telescope Array
64. The observation of abnormal shower event with lightning by TA surface particle detector
65. Study of absolute energy calibration of air shower by a compact electron linac
66. Calibration of TA-EUSO 64ch multi-anode PMT and comparison with CRAYS
67. Reseach and development of the surface detectors for the TALE experiment
68. Study of radio detection of highest energy cosmic rays
69. Research and development of detectors for MBR microwave radiations
70. Development of new surface detector for observation of ultra high energy cosmic ray at Telescope Array site
71. Observation of airshower fluorescence light at the TA FD site by using an Imaging UV telescope
72. Cosmic ray interactions in the knee and the highest energy regions
73. Experimental Study of High-energy Cosmic Rays in the Tibet AS γ Experiment
74. Study of High Energetic Radiation from Thundercloud in Tibet
75. Study of the composition of cosmic-rays at the Knee
76. Sidereal daily variation of $\sim$10TeV galactic cosmic ray intensity observed by the Tibet air shower array
77. A study on variation of interplanetary magnetic field with the cosmic-ray shadow by the sun.
78. Integration of the trigger system for Ashra

79. Observation with the All-sky Survey High Resolution Air-shower detector (Ahsra)
80. R&D of a Compton Camera with a New Concept for Measurement of Astronomical Gamma-Ray Lines
81. BASJE (Bolivian Air Shower Joint Experiment)
82. Study on High Energy Cosmic Ray Sources by Observations in Space
83. The beam test for calibrating the ARA detectors
84. Towards the imaging of the massive black hole in SgrA*
85. Comparative study of astrophysical particle acceleration processes
86. School of Monte Carlo Simulation
87. The extreme Universe viewed in very high energy gamma-rays 2014
88. Gravitational Wave Detector in Kamioka (XIII)
89. Numerical simulation of Electro-Magnetic Wave Propagation in Gravitational wave Detector II
90. Development of noise visualization system for gravitatinal wave detectors
91. Development of optical cavities for ultranarrow stable lasers
92. Data analysis using CLIO data (V)
93. Application of geophysical observations in the Kamioka mine to the dynamics of snow and water
94. Research on ultra-low frequency anti-vibration system for KAGRA
95. Research of Large-scale Gravitational wave Telescope(IV)
96. Research on cryogenic payload for KAGRA
97. Development of Very Low Vibration Cryo-Cooler System
98. Study of 5N high purity tungsten suspension wire for KAGRA
99. Development of a stabilization system for the KAGRA laser source
100. R&D for the intensity stabilization of the laser system in KAGRA
101. Development of beam position monitoring and controlling systems for KAGRA 2
102. Identification of impurities in sapphire mirror for KAGRA using electron spin resonance
103. Development of Sapphire Mirror Suspension for KAGRA (LCGT) (X)
104. Development of precision profiler for mirrors of LCGT interferometer 4
105. Development of KAGRA detector characterization
106. Development of the output mode-cleaner for KAGRA
107. Study for KAGRA data analysis and Research for its System (IV)
108. High sensitivity multiple reflection shadow sensor for Gravitational Waves detection
109. Research and Development for Next-Generation Ultra-High Sensitive Quantum Interferometer in KAGRA II
110. Cosmic Reionization Probed with Large Optical Near-Infrared Telescopes
111. Evolution of the universe and particle physics
112. Detection of time variations for cosmogenic Be-7
113. Observation of global air-mass motion measuring radionuclides of Cs in the air
114. Frontier of the planetary material science

115. Continuous Environment Measurement of the Kashiwa Underground Laboratory
116. Evaluation of the erupted radioactivities into the environment
117. Simulation study for the IceCube Neutrino Observatory
118. Precise calculation of the atmospheric neutrino flux
119. CRC workshop for future plans in cosmic ray research

G. List of Committee Members

(a) Board of Councillors

KAJITA, Takaaki	ICRR, the University of Tokyo
KAWAMURA, Seiji	ICRR, the University of Tokyo
TESHIMA, Masahiro	ICRR, the University of Tokyo
NAKAHATA, Masayuki	ICRR, the University of Tokyo
GONOKAMI, Makoto	The University of Tokyo
MATSUMOTO, Yoichiro	The University of Tokyo
YAMAUCHI, Masanori	KEK
SASAKI, Misao	YITP, Kyoto University
HAYASHI, Masahiko	National Astronomical Observatory of Japan
NAKAMURA, Takashi	Kyoto University
OKAMURA, Sadanori	Hosei University
TORII, Shoji	Waseda University
TSUNETA, Saku	Institute of Space and Astronautical Science
SUGIYAMA, Naoshi	Nagoya University
KOMAMIYA, Sachio	ICEPP, the University of Tokyo

(b) Advisory Committee

KAJITA, Takaaki	ICRR, the University of Tokyo
HISANO, Junji	Nagoya University
SHIBATA, Masaru	Kyoto University
HAZUMI, Masashi	KEK
KISHIMOTO, Tadafumi	Osaka University
YOKOYAMA, Masashi	The University of Tokyo
KANDA, Nobuyuki	Osaka City University
ITOW, Yoshitaka	Nagoya University
OGIO, Shoichi	Osaka City University
MUNAKATA, Kazuoki	Shinshu University
TERASAWA, Toshio	ICRR, the University of Tokyo
KAWASAKI, Masahiro	ICRR, the University of Tokyo
OHASHI, Masatake	ICRR, the University of Tokyo
FUKUSHIMA, Masaki	ICRR, the University of Tokyo
TESHIMA, Masahiro	ICRR, the University of Tokyo
NAKAHATA, Masayuki	ICRR, the University of Tokyo

(c) Inter-University Research Advisory Committee

NISHIJIMA, Kyoshi	Tokai University
YAMAMOTO, Tokonatsu	Konan University
TAJIMA, Hiroyasu	Nagoya University
KUBO, Hidetoshi	Kyoto University
MUNATAKA, Kazuoki	Shinshu University
TAKEUCHI, Yasuo	Kobe University
TOMARU, Takayuki	KEK
MASUDA, Kimiaki	Nagoya University
TERASAWA, Toshio	ICRR, the University of Tokyo
TAKITA, Masato	ICRR, the University of Tokyo
SAGAWA, Hiroyuki	ICRR, the University of Tokyo
MORIYAMA, Shigetaka	ICRR, the University of Tokyo
MIYOKI, Shinji	ICRR, the University of Tokyo

H. List of Personnel

Director KAJITA, Takaaki,

Vice-Director TERASAWA, Toshio,

Kamioka Observatory (Neutrino and Astroparticle Division)

Scientific Staff	ABE, Ko,	HAYATO, Yoshinari,	HIRAIDE, Katsuki,
	ICHIMURA, Koichi,	IKEDA, Motoyasu,	KAMEDA, Jun,
	KISHIMOTO, Yasuhiro,	KOBAYASHI, Kazuyoshi,	MIURA, Makoto,
	MORIYAMA, Shigetaka,	NAKAHATA, Msayuki,	NAKAYAMA, Shoei,
	OGAWA, Hiroshi,	SEKIYA, Hiroyuki,	SHIOZAWA, Masato,
	TAKEDA, Atsushi,	TANAKA, Hidekazu,	TOMURA, Tomonobu,
	WENDELL, Roger Alexandre,	YAMASHITA, Masaki,	YANG, Byeongsu,
Administrative Staff	OIDA, Yoshihito,	TANAKA, Masahiro,	
Technical Staff	FURUTA, Hajime,	HIGASHI, Tetsuji,	NOZAWA, Noriyuki,
	ONOUE, Tatsuya,	TAMORI, Yukio,	
Research Fellow	BAI, Lili,	WILKING, Michael Joseph,	
Secretary	EJIRI, Midori,	OKURA, Yoko,	TANIMURA, Naoko,
	YONEZAWA, Keiko,		

Research Center for Cosmic Neutrinos (Neutrino and Astroparticle Division)

Scientific Staff	KAJITA, Takaaki,	MASUDA, Kimiaki,	NISHIMURA, Yasuhiro,
	OKUMURA, Kimihiro,		
Technical Staff	SHINOHARA, Masanobu,		
Secretary	KITSUGI, Atsuko,	WATANABE, Keiko,	

High Energy Cosmic Ray Division

Scientific Staff	ASANO, Katsuaki,	ENOMOTO, Ryoji,	FUKUSHIMA, Masaki,
	HAYASHIDA, Masaaki,	IKEDA, Daisuke,	KAWATA, Kazumasa,
	MAZIN, Daniil Mihajlovic,	NAKAJIMA, Daisuke,	NONAKA, Toshiyuki,
	OHISHI, Michiko,	OHNISHI, Munehiro,	PANQUE CAMARERO, Daved
	SASAKI, Makoto,	TAKEDA, Masahiro,	TAKITA, Masato,
	TERASAWA, Toshio,	TESHIMA, Masahiro,	TOKUNO, Hisao,
	YOSHIKOSHI, Takanori,		
Technical Staff	AOKI, Toshifumi,	IKEBA, Kiriko,	MATSUBAYASHI, Nobuko,
	NIWA, Hiroki,	OOKI, Kaoru,	TAMURA, Akiko,
Research Fellow	AKAIKE, Yosui,	FUJII, Toshihiro,	HADASCH, Daniela,
	HANABATA, Yoshitaka,	INOUE, Susumu,	KIDO, Eiji,
	NAGAOKA, Yoichi,	SAITO, Koji,	SAKO, Takashi,
	TANAKA, Syuta,		
Secretary	KOKUBUN, Yayoi,	SUGAHARA, Midori,	

Akeno Observatory (High Energy Cosmic Ray Division)

Scientific Staff	SAGAWA, Hiroyuki,		
Tecnical Staff	HONDA, Ken,	OHOKA, Hideyuki,	SHIMIZU, Kanetoshi,

Norikura Observatory (High Energy Cosmic Ray Division)

Technical Staff	AGEMATSU, Yoshiaki,	AWAI, Kyosuke,	ISHITSUKA, Hideki,
	OKAZAKI, Nao,	SHIMODAIRA, Hideaki,	USHIMARU, Tsukasa,

Astrophysics and Gravity Division

Scientific Staff	CHO, Kyuman,	HIROSE, Eiichi,	IBE, Masahiro,
	KAWAMURA, Seiji,	KAWASAKI, Masahiro,	KIMURA, Nobuhiro,
	KOKEYAMA, Keiko,	KUMAR, Rahul,	KURODA, Kazuaki,
	MIYAKAWA, Osamu,	MIYOKI, Shinji,	OHASHI, Masatake,
	OHISHI, Naoko,	ONO, Yoshiaki,	OUCHI, Masami,
	SAITO, Yoshio,	SUZUKI, Toshikazu,	TOMARU, Takayuki,
	UCHIYAMA, Takashi,	YAMAMOTO, Kazuhiro,	YOON, Tai Hyun,
Administrative Staff	TAKAYAMA, Kyouichi,		
Technical Staff	DOI, Kohei,	FURUTA, Kiyoshi,	KAMIIZUMI, Masahiro,
	NOGUCHI, Tsukasa,		
Research Fellow	DUVAL, Florent Marcel Didier,	KANETA, Kunio,	KAWAKAMI, Etsuko,
	KHALAIDOVSKI, Alexander ,	KUBO, Mariko,	MOMOSE, Rieko,
	OHSHIMA, Shin-ichi,	SAITO, Tomoki,	SHIBUYA, Takatoshi,
	YOKOYAMA, Shuichiro,	YUMA, Suraphong,	
Secretary	CHIDA, Ai,	KAWAKAMI, Akiko,	KIKUCHI, Rie,
	MASHIMA, Chieko,	OKINAKA, Mihoko,	

Graduate Students

Doctor	CHEN, Dan,	HAGA, Yuto,	IRVINE, Tristan James,
	IYOGI, Kazuki,	KONNO, Akira,	MIKAMI, Ryo,
	NAITO, Yoshiaki,	NAKAGAWA, Katsuma,	NAKANO, Masayuki,
	NAKANO, Yuuki,	RICHARD, Euan Neil,	SAKAKIBARA, Yusuke,
	SEKIGUCHI, Takanori,	TAKACHIO, Osamu,	TAKEDA, Naoyuki,
	TAKEISHI, Ryuji,	YAMADA, Masaki,	
Master	AIZAWA, Tasuku,	AKUTSU, Ryosuke,	FUJIMOTO, Seiji,
	FUKAMI, Satoshi,	HARIKANE, Yuichi,	HAYAKAWA, Taku,
	HIROSHIMA, Nagisa,	HONG, Jeong Pyong,	ISHIGAKI, Masaufumi,
	ISHIO, Kazuma,	ISHIZAKI, Wataru,	KOBAYASHI, Masatoshi,
	KOJIMA, Takumi,	KONISHO, Shiori,	LIU, Yingtao,
	MIYAMOTO, Takahiro,	NAKAJIMA, Takeo,	NISHIMURA, Tsubasa,
	NORITA, Takayuki,	OGINO, Momoko,	ONO, Kenji,
	ORII, Asato,	SASAKI, Kento,	SHIN, Heungsu,
	SUZUKI, Motoo,	TAKAHASHI, Mitsunari,	TAMAZAWA, Hiroko,
	TANAKA, Hiroki,	TO, Sho,	WATANABE, Atsushi,
	YAMANAKA, Yuji,		

Administrative Division

Administrative Staff	AKIYAMA, Makiko,	ASAKA, Sadako,	FUJIE, Tamiko,
	IRIMAJIRI, Aki,	ISHII, Yoshikazu,	MARUMORI, Yasuko,
	MORITSUBO, Shigeru,	NAKAMURA, Saori,	OCHI, Masashi,
	SAITO, Akiko,	WATANABE, Wataru,	YAMAGUCHI, Akiko,
Research Administrator	SATO, Ritsuko,		
Public Relations Staff	HAYASHIDA, Misato		